Three facets of modern liquid crystal science

The complex phase behavior of chiral thermotropic smectics

Electrospinning of nano-/microfibers with liquid crystals

Dispersing and aligning carbon nanotubes in lyotropic liquid crystals

Jan Lagerwall

January 27, 2011

Curiosity is one of the permanent and certain characteristics of a vigorous intellect.

Samuel Johnson

Three facets of modern liquid crystal science

Habilitationsschrift

zur Erlangung des akademischen Grades

doctor rerum naturalium habilitatus (Dr. rer. nat. habil.)

vorgelegt der

Naturwissenschaftlichen Fakultät II
der Martin-Luther-Universität Halle-Wittenberg

von

Herrn Tekn. Dr. Jan P. F. Lagerwall

geb. am 28.05.1970 in Göteborg, Schweden

Gutachter:

1. Herr Prof. Dr. H. Kitzerow (Universität Paderborn)
2. Herr Prof. Dr. E. Samulski (University of North Carolina at Chapel Hill)
3. Herr Prof. Dr. C. Tschierske (Martin-Luther-Universität Halle-Wittenberg)

Halle (Saale), verteidigt am 23.11.2010.

Preface

This habilitation thesis summarizes my research during the almost eight years that have passed since I gained my Ph.D. The common denominator of this work is liquid crystals, which have played a central role in almost all my research work. During the last five-six years I have however combined liquid crystal research with aspects, materials and techniques from quite different research areas. Therefore, of the three main chapters of this thesis only the first deals purely with liquid crystals. The two latter are devoted to polymer fibers containing liquid crystals— produced by the technique of coaxial electrospinning—and composites of liquid crystals and carbon nanotubes, respectively. Considering this quite broad scope I hope that a readership comprising also non-liquid crystal researchers can find the thesis interesting.

In order to render the thesis understandable also for these readers, working perhaps mainly with electrospinning or carbon nanotube research, I have included an introductory chapter that is relatively comprehensive, aiming to introduce also scientists with little or no background in liquid crystals into this fascinating materials class and its study. While liquid crystal researchers often focus strongly on one of the two main liquid crystal classes, thermotropics or lyotropics, both of them actually play very important roles in my research and I therefore discuss the two classes on equal par in the introduction. This approach is quite rare, hence I believe that the introductory chapter may in fact have some novelty value even for many a liquid crystal expert. I hope that the comparison of the two classes, highlighting their similarities as well as their differences, can stimulate interesting new research ideas. The topics that are specific to the three main chapters of the thesis—spontaneous polarization in chiral smectics, electrospinning and carbon nanotubes—are introduced concisely at the beginning of each respective chapter.

My research would not have been possible without the input and help from many other scientists. In particular, my entrance into the fields of carbon nanotube and electrospinning research would have been very much more difficult without the generous and open attitudes of the friends and colleagues from these communities that I have come to know in the last few years. Giusy Scalia was the one who got me interested in carbon nanotubes and initiated me into their study together with liquid crystals. I owe a great deal of my understanding about these particles to her. Giusy's support has however reached well beyond the field of carbon nanotubes. Via Giusy I was also fortunate enough to come to know the carbon nanotube research group of Siegmar Roth at the Max-Planck-Institut für Festkörperforschung in Stuttgart. Through him and his colleagues, foremost Ursula Dettlaff-Weglikowska, Viera Skakalova, Miro Haluska, Monica Jung de Andrade and Marcio Dias Lima, I learnt invaluable things not just about carbon nanotubes, but the spectrum ranged from Slovak cooking via etymology to other scientific fields.

For my achievements in the field of electrospinning I am much indebted to Jesse McCann, Eric Formo and Younan Xia. It was Jesse's inspiring talk at a one-day conference on electrospinning, that I attended more or less by coincidence, that attracted me to this field and gave me the basic ideas for my research on the topic. I then got my first practical experience with electrospinning during a three week visit to the Xia group at the University of Washington in Seattle in May 2007.

Not only did Jesse and Eric help me with the practical work of conducting the first experiments on electrospinning of fibers with liquid crystalline cores during this visit, but with their open and enthusiastic attitude they also shared many vital tips and tricks with me on how to succeed with the preparation and characterization of the fibers.

My interest in liquid crystals is much older, in fact introduced to me by my father, Sven Lagerwall, when I was a child by showing the colorful and dynamic textures of liquid crystals between crossed polarizers. My fascination for liquid crystal polarizing microscopy textures has never ended, and neither has the support of Sven throughout my journey to explore the secrets of liquid crystals. Although he is now officially retired, he is still active in liquid crystal research and his input on any idea of mine has always been extremely valuable. My advisors from my doctoral time at Chalmers, Bengt Stebler and Per Rudquist, have also been very important for my continued scientific career. Still today, although it is now some eight years since we lived in the same country, the interaction with Per and Bengt is both inspiring and joyful. Bengt has also always been very helpful in many practical issues, even when I gave him extremely little time to prepare.

The most important person in teaching me the physical chemistry of liquid crystals has been Frank Gießelmann. My stay as a post-doc in his group at the University of Stuttgart from 2003 to 2007 was a period of fascinating research and at the same time, great fun. Frank is generous not only in sharing scientific understanding, but also good wines and food were often enjoyed in the company of him and his family. I first met Frank when he stayed as visiting professor in the Chalmers group when I did my doctoral studies. In the group at that time was also his previous fellow doctoral student from the Technical University of Clausthal, Ingo Dierking, then conducting a post-doc at Chalmers. The interaction with Ingo, since a couple of years at the University of Manchester, has been very inspiring, his broad approach to liquid crystal research being a good model to follow. While it was Giusy who in practice introduced me to carbon nanotubes, it was the team of Ingo and Giusy that did some of the seminal work on CNT liquid crystal composites.

Between my Ph.D. and my post-doctoral stay in Germany I spent a brief time as a post-doc at the University of Colorado at Boulder, working together with the groups of Noel Clark and Dave Walba in the physics and chemistry departments, respectively. Although very short, this was a fantastically intense stay from which I learnt a lot and got plenty of inspiration for how to develop my own independent research. Still today, I learn something new every time I meet Dave and Noel at conferences or other occasions and their approach to liquid crystal research certainly demonstrates how rich this research field is. When starting in Germany I did not go to Frank right away but I first spent a few months in the group of Gerd Heppke at the Technical University of Berlin. Although again very short, also this stay was most rewarding, the pleasant atmosphere in this lab inspiring to many new ideas. In fact, I had come to know the Heppke group during a shorter stay in Berlin a few years earlier, where a long-lasting friendship with several students in the group started. In particular I wish to mention Daniel Krüerke, Hans Sawade and Mario Müller, with whom I am still interacting actively.

Since 2007 I have been working at the Martin-Luther-Universität Halle-Wittenberg, surrounded by many scientists who have helped me very much in developing my research these years. Wolfgang Weissflog and Carsten Tschierske were my first contacts here, already prior to moving to Halle, and their support and enthusiasm set the stage for a very pleasant working environment. I have also learnt a great deal about thermotropic liquid crystal chemistry from them and Carsten's enthusiasm and active involvement in our current joint project on developing a new class of materials for aiding nanotube dispersion in thermotropic liquid crystals has been instrumental for its success. Another greatly enthusiastic person in Halle is Ute Baumeister, whose expertise in x-ray scattering and willingness to collaborate with my group have been of

great value for our research.

While I had acquired good experience in surfactant-based lyotropic liquid crystals during my time in Stuttgart, my knowledge in this field was greatly improved thanks to the discussions with Annette Meister and Alfred Blume, in particular regarding the lamellar phases formed by phospholipids. Prof. Blume as well as Prof. Jörg Kressler are both thanked also for their kind welcome to me at the institute. Many questions about DNA and biophysical chemistry were clarified by Andreas Kerth who has also been of great help in setting up various lab equipment. Invaluable practical support was also provided during my time in Halle by Andreas Lonitz, always available when a computer needs to be convinced about something or when a particular cable arrangement is needed. Equally important is the incredibly professional help of Herr Reese in the mechanical workshop of the chemistry institute. Our work on electrospinning and microfluidics would have been a great deal more difficult without his ingenious designs. I am also grateful to Prof. Goerg Michler and his group for their efforts to help us with transmission electron microscopy imaging of our electrospun fibers.

My position in Halle is financed by the Cluster of Excellence *Nanostrukturierte Materialien* of the Land Sachsen-Anhalt. I would like to thank all members of the Cluster through its leader, Prof. Ingrid Mertig. For her generous and always enthusiastic support I would like to express my deep gratitude. Helping me with all administrative issues related to my group is Daniela Lemke. Her professionalism, readiness to help out and ways of always finding a solution around a problem have really been fantastic.

Finally, I thank my faithful doctoral students, Eva Enz, Stefan Schymura, Sarah Dölle, Martin Kühnast and Hsin-Ling Liang, who together form a fantastic group, both in terms of research and atmosphere. The research that I conducted in Halle would not have been possible without them, and much of the data in this thesis has been produced by them.

There are so many other people who have been important in the development of my research but this preface would breach all boundaries if I would mention you all by name. Thus, I collectively express my deep gratitude to all you who have not been mentioned above but nevertheless helped me at one stage or another in my work.

Halle, April 2010

Jan Lagerwall
jan.lagerwall@lcsoftmatter.com

Contents

Chapter 1

A concise introduction to the characteristics of liquid crystals important for this thesis

1.1 Liquid crystal classes and phases

1.1.1 Foundations: long-range order, the nematic phase and the director concept

What makes liquid crystals unique is that they exhibit long-range order despite being fluid. With long-range order we mean that either the orientation or position, or both, of a building block is correlated with the orientation or position of building blocks a long distance away. More formally, we require that the orientational or positional **correlation function** $G(r)$ is either independent of the distance r between the blocks considered (true long-range order) or falls off algebraically (quasi-long-range order), $G(r) \propto r^{-\eta}$ where η is small and positive. Ordinary isotropic liquids, in contrast, are short-range ordered and characterized by a correlation function that falls off exponentially, $G(r) \propto e^{-r/\xi}$ where ξ is defined as the correlation length.

In the simplest and best studied liquid crystal phase, the **nematic**[1] (abbreviated N), the long-range order is of purely orientational type, the positions of the building blocks being as dynamic and disordered as in ordinary isotropic liquids. Consequently, a lattice cannot be defined. Instead, the description of the orientational order takes place via the introduction of the **director**[2], one of the most central concepts in liquid crystal science. The director, abbreviated **n**, is a sign-invariant (**n** = -**n**) unit vector indicating the average direction of the principal symmetry axis of the building blocks, as illustrated in Fig. 1.1. Reflecting the continuity of the fluid phase, **n** varies smoothly throughout a sample without discrete changes (except in defects), hence one often speaks of the **director field** **n**(**r**), where **r** is the space coordinate.

In order to have a well-defined principal symmetry axis, the building block must obviously be anisometric (having unequal size in different directions). Indeed, liquid crystal phases are

---

[1]The name, which was introduced by the French mineralogist GEORGE FRIEDEL [1], comes from the Greek adjective νηματικός (*woven*), in turn derived from the Greek word for *thread*, νῆμα. It refers to the threadlike defects which are typical of the phase when observed through a polarizing microscope, cf. Fig. 1.14.

[2]The concept of the director was introduced by the Swede CARL-WILHELM OSEEN while the name was introduced by FRANK LESLIE and JERALD ERICKSEN, of British and American nationality, respectively [1].
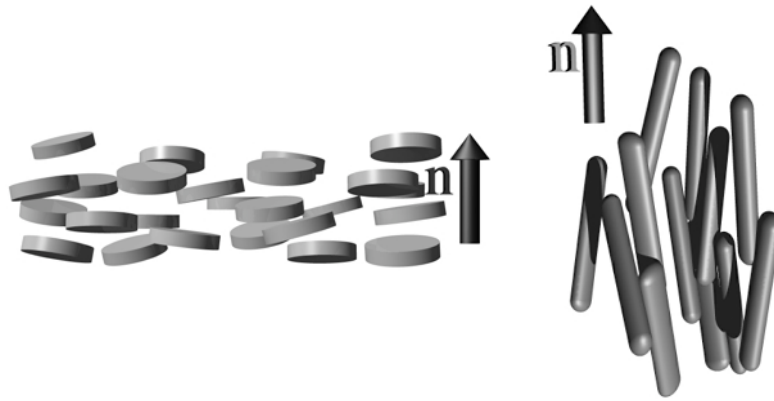
Figure 1.1: Two cartoons of a nematic phase built from disc- and rod-shaped building blocks, respectively, drawn with a vertical director **n**.

most often built up by units that are effectively either rod- or disc-shaped. When one wants to emphasize the shape of the building blocks one often speaks of **calamitic**[3] and **discotic** liquid crystals for these two cases, respectively. It can however be rather misleading to speak of calamitic or discotic *phases*; many liquid crystal phases can be formed by rod- as well as disc-shaped building blocks and the phase itself of course has no particular shape.

The achiral nematic phase is generally uniaxial, that is it has full cylindrical rotational symmetry around **n** (point group $D_{\infty h}$ in Schönfließ notation). The symmetry of any **chiral** liquid crystal phase is reduced by the absence of mirror planes (the index h in the symmetry notation signifies a horizontal mirror plane), a reduction that has several important consequences for the physical properties of the phase, as we will see in Chapter 2. For simplicity, I consider only achiral versions of the phases in this introduction. A biaxial nematic phase is however not fundamentally impossible and, indeed, the first example of a biaxial nematic phase was identified in the 1980's among the class of lyotropic liquid crystals [2,3]. Very recently biaxial nematic phases seem to have been found also among thermotropics [4].

1.1.2   Thermotropics and lyotropics: the two liquid crystal classes

I have so far deliberately avoided speaking of liquid crystal molecules, instead discussing phase building blocks. The reason is that I in my research work with both main classes of liquid crystal, thermotropics and lyotropics, on an equal footage. The fundamental difference between them is the nature of the building blocks and their surroundings. **Thermotropic** liquid crystals are generally unassociated liquids[4], that is the building block is a single molecule and no further molecular species (specifically solvent molecules) are required for the liquid crystal phase formation. The name thermotropic reflects the fact that temperature is the fundamental thermodynamic control parameter determining the phase. Two temperatures are particularly important, namely those defining the beginning and end of the liquid crystalline regime, cf. Fig. 1.2. The **melting point** is, as for other materials, the temperature where the solid crystal melts, only

---

[3]This term (which is disliked by some researchers who prefer the simpler term *rod-like*) has its origin in the Greek καλάμη, meaning *stem* or *reed*.

[4]Associated thermotropic liquid crystal phases do exist, typically formed by 'half-mesogens' linking pairwise via e.g. hydrogen bonding into 'dynamic dimers' [5]. These are still counted to the thermotropic class, since no addition of solvent is required.
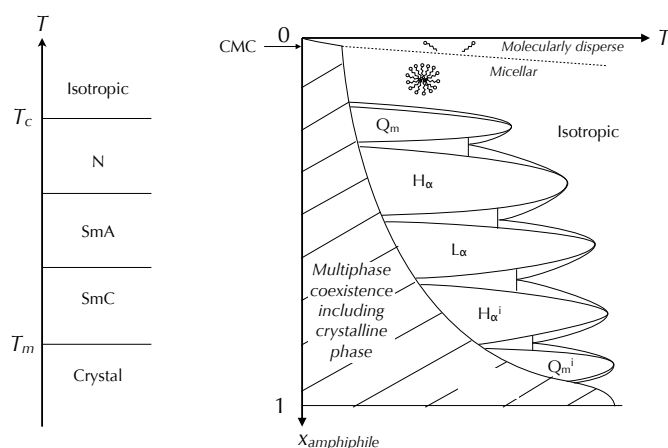
Figure 1.2: A comparison between a generic phase sequence of thermotropic calamitic liquid crystals (left) and a generic phase diagram of lyotropic liquid crystals (right), both highly simplified. The vertical axis of each diagram corresponds to the main thermodynamic control parameter, *temperature T* for thermotropics and *amphiphile concentration x* for lyotropics. In the former case the liquid crystalline regime is bounded by the melting point T_m and the clearing point T_c, in the latter it is located between the water-free crystalline solid at $x = 1$ and the isotropic liquid (this can be molecularly disperse as well as micellar) at low x. For lyotropics the temperature (horizontal axis) acts as a secondary control parameter. Its influence can be very small and the system is then said to be 'athermal'.

for liquid crystals it is not into an isotropic liquid but into a liquid crystalline state. Unique to liquid crystals is the definition of the second special temperature, the **clearing point**. This is the temperature at which the highest-temperature liquid crystal phase turns into an isotropic liquid. It owes its name to the fact that a bulk liquid crystal scatters light and thus looks turbid whereas the isotropic liquid state of the same material is clear.

Being intermediate between the completely ordered crystal state and the disordered isotropic liquid, the liquid crystalline states are sometimes collectively referred to as **mesomorphic**[5] and molecules capable of forming thermotropic liquid crystal phases are often called **mesogenic** molecules or **mesogens**. In addition to the anisometry, the mesogenicity typically has its origin in a combination of a stiff core and flexible terminal chains, cf. the representative examples in Fig. 1.3. Although a few extreme cases of very high-temperature thermotropic phases formed by molecules without terminal chains (e.g. *p*-quinque- and sexiphenyls [6]) are known, one generally needs the combination of order-promoting rigid cores and disordering flexible moieties (without which the tendency for crystallization is strong) to allow for the subtle balance between regularity and randomness that is the hallmark of liquid crystals. Rod-shaped mesogens typically consist of a more or less straight 2- to 4-ring rigid core structure and two flexible terminal chains (noncyclic aliphatics), attached to each of the core rod's two ends. A discotic mesogen also has a multi-ring core but with a flat circular geometry, e.g. as in triphenylene, and it has multiple (typically six) flexible terminal chains, symmetrically distributed around the core perimeter.

Lyotropic liquid crystals form only upon addition of a solvent, most often water[6]. Moreover, the building block of a classic lyotropic liquid crystal is not one but many molecules (typically on

---

[5]Again a term introduced by FRIEDEL [1], derived from the Greek words $\mu\acute{\epsilon}\sigma o\varsigma=$ *intermediate*, and $\mu o\rho\varphi\acute{\eta} =$ *shape*.

[6]The term lyotropic is derived from the Greek $\lambda\acute{\upsilon}\omega$, which can be translated as *dissolve* or *melt*. It refers to the action of the solvent, the presence of which is a prerequisite for lyotropic behavior.
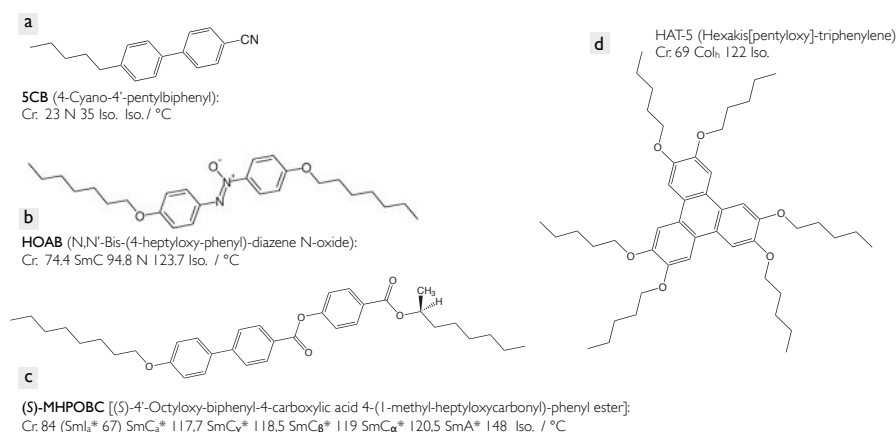
Figure 1.3: A few characteristic examples of thermotropic mesogens, calamitic (a-c) and discotic (d).

the order of 100), organized into an aggregate called a **micelle** (diminutive of the Latin word for crumb, *mica*). Such lyotropic liquid crystals thus belong to the category of associated liquids. The micelle formation is a result of the amphiphilic[7] character of the constituent molecules, that is they have one end that likes the solvent and one that does not. Typical examples are surfactants[8] found in commercial soaps and detergents, which have a polar and thus hydrophilic (water-liking) head group and a nonpolar hydrophobic (water-fearing), alternatively referred to as lipophilic (fat-liking), tail. Another very important example is given by the amphiphilic lipids (e.g. phospho-, glyco- and sphingolipids) that build up the membranes of the cells in our own bodies. Here each polar head group normally has two non-polar end chains, extending next to each other in the same direction. There are also many examples of block co-polymers that may form liquid crystal phases in a similar way as low molar mass amphiphiles. Examples of some important surfactants will be given in Chapter 4.

When an amphiphilic molecule is placed in an aqueous environment[9] the head group is easily accommodated but the nonpolar end chain disrupts the hydrogen bond network of the surrounding water molecules, reducing their options for interacting favorably with their neighbors, thereby decreasing the entropy of the water [7]. This **hydrophobic effect** has the consequence that beyond a limiting amphiphile concentration, the entropy of the whole system is actually increased by ordering the amphiphiles into aggregates in which the nonpolar tails are directed inwards, protected from contact with the water by the polar head groups which together form a 'shell' around the hydrophobic 'core', cf. Fig, 1.4 (these cartoons haver for simplicity been drawn with a totally unrealistic degree of chain order). These aggregates are the micelles and the concentration where association begins is consequently called the **Critical Micelle Concentration**, abbreviated **CMC**. Typical CMC values lie in the 1-10 mM range (or, in terms of mass ratio amphiphile to water, typically about 0.01-0.1 wt.-%)[10] . Note that the CMC does

---

[7]From Greek $\alpha\mu\varphi\acute{\imath}$, here having the meaning of *both*, and $\varphi\acute{\imath}\lambda o\varsigma$ which can be translated as *friend*.

[8]Surfactant is short for *surf* ace-*act*ive ag*ent*, the name reflecting the fact that they reduce the surface tension of water considerably.

[9]Amphiphilicity must not necessarily refer to liking/disliking water (they may for instance have one fluorocarbon- and one hydrocarbon-liking side) but this case is so totally dominating, and so important, that I disregard other possibilities in the following.

[10]The corresponding values of amphiphilic block co-polymers, generally not forming normal micelles but rather larger structures sometimes referred to as 'polymersomes', may be quite different. We will however hardly consider such systems in this book.
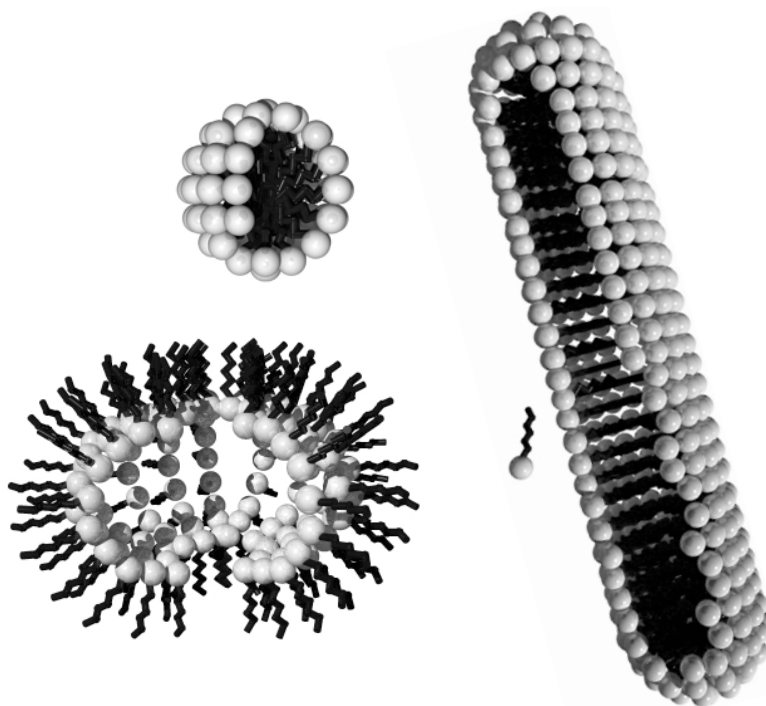
Figure 1.4: Highly simplified cartoons of a spherical and a rod-shaped micelle of normal type (top left and right), as well as of an inverse micelle (bottom left). In order to reveal the micelle interior a sector of amphiphiles has been left out in each case. In reality the hydrated polar head groups (depicted as white balls) constitute an essentially complete shell around (normal) or within (inverse) the non-polar chains (black zigzags). Note that the order is grossly exaggerated in all three drawings.

not constitute the onset of liquid crystalline order: the micellar phase at amphiphile concentrations in the vicinity of the CMC and quite a substantial regime beyond is isotropic in all properties. This isotropic micellar phase can in some sense be compared to the isotropic phase of a thermotropic material heated above its clearing point; the building blocks are there and they may be anisometric but they are not long-range ordered. We thus see here that the main thermodynamic control parameter for lyotropics is not the temperature (it is often the secondary control parameter) but the amphiphile concentration, low concentrations corresponding to high temperatures of thermotropics, cf. the comparative phase diagrams in Fig. 1.2.

If rather than water oil is added as a solvent (generally, both solvents are required but with oil in large excess) then obviously the reverse micelle structure is favorable. Indeed, under such circumstances one observes inverted lyotropic phases, where the micelles have a polar interior and non-polar exterior. For indicating inverted structures I follow one of the more commonly used notation schemes, adding a superscript i to the shorthand for the basic structure. However, the nomenclature of lyotropics is unfortunately rather non-uniform, several parallel notation schemes still being in use, none of which can be regarded as free of problems.

Often the micelles are spherical and thus rather unsuitable for building liquid crystal phases (they may build up cubic phases), but with the right concentration of the right amphiphile, sometimes with the aid of an appropriate co-surfactant, the micelles may take a rod- or disc-like shape. The full details regulating the micelle shape are outside the scope of this thesis but,

in brief, it is the relationship between the effective sizes of the hydrophilic and hydrophobic molecule parts, respectively, that dictates the final shape of the micellar aggregate (this relationship can be compactly described using the so-called 'packing parameter', introduced by JACOB ISRAELACHVILI). An in-depth treatment of these issues can be found in many treatises, e.g. [8].

Although actually a very dynamic and fairly flexible construct, the micelle in lyotropic liquid crystals plays the part of the rigid core in thermotropics, whilst the isotropic solvent takes the role of the thermotropic mesogen's flexible end chains. Anticipating what is to follow below a bit, I would like to point out that also the columns and bilayers of columnar and lamellar lyotropic phases, respectively, can in fact be regarded as micellar aggregates in the extreme limit; in the first case the aggregate is a rod micelle with quasi-infinite length, in the second it is a disc micelle with quasi-infinite diameter.

Building block anisometry is one requirement for lyotropic liquid crystal formation, another is that there is a sufficient number of blocks present. The latter means that the amphiphile concentration must generally be some 100 - 500 times the CMC before an anisotropic fluid arises. When this happens, it may be—as often in thermotropics—because the anisometric micelles become long-range ordered in their orientation without losing their liquid-like short-range positional correlation. Such a lyotropic nematic phase is however relatively rare among lyotropics, where the columnar and lamellar phases, exhibiting positional as well as orientational order, strongly dominate.

Before ending this section, I should add that there are also examples of unassociated lyotropic liquid crystals. These are formed by colloidal suspensions of anisometric non-amphiphilic particles or macromolecules such as polymers, viruses or inorganic rods or discs in solution. This subclass of lyotropics, which is often ignored in basic discussions of lyotropic liquid crystals, is attracting more and more interest today [9–12]. Polymers that form liquid crystals of this type may be synthetic such as carbon nanotubes or the polyaramide chains that are processed via a liquid crystalline state into Kevlar® fibers, or they may be biological, e.g. DNA. A somewhat intermediate position is taken by the chromonic class of lyotropic liquid crystals [13], where the constituent molecules do not aggregate into micelles but instead stack up into columns of varying lengths. The molecules forming chromonic liquid crystals, which are generally dyes (hence the name), are amphiphilic but of somewhat different type than the classic examples: the main surface of a chromonic molecule is hydrophobic (thus forming the interior of the stack) whereas its border is water soluble.

1.1.3   The smectic and lamellar phases

The nematic is the simplest liquid crystal phase and it therefore often serves as a first model for describing what is meant by the term liquid crystal. There are however many other mesomorphic phases. In fact, considering thermo- and lyotropic liquid crystals together, well over 100 different thermodynamically stable liquid crystalline phases have been identified to date, and reports of new phases appear every now and then. The nematic phase is unique, however, in the sense that it is the only liquid crystal phase that exhibits no long-range positional order and thus the only anisotropic 3D liquid[11]. All other liquid crystal phases exhibit quasi-long-range positional order in one, two or three dimensions. I will now discuss the most important positionally ordered phases briefly, starting with the family of phases with one-dimensional (1D) positional order: the **smectic** (in thermotropics) and **lamellar** (in lyotropics) phases.

---

[11]One may also speak of the nematic phases, in plural, if one distinguishes between the normal uniaxial nematic and the very rare biaxial nematic phase, or between nematics with different building block shape and/or different signs of the diamagnetic anisotropies. While the former distinction undoubtably is justified, the latter is more questionable.
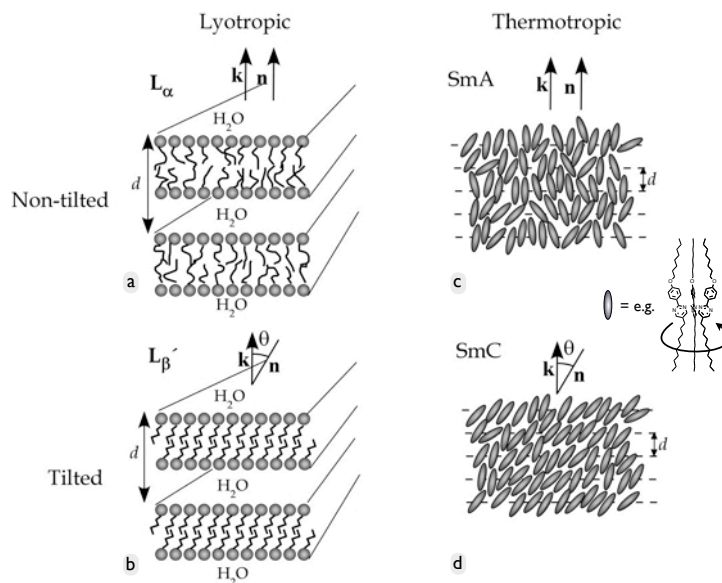
Figure 1.5: Schematic drawings of the most important lamellar and smectic phases, the amphiphiles of the former drawn with a ball for the polar head group. The mesogens in the smectic phases are drawn as ellipsoids reflecting their fast rotation around the main axis of inertia, effectively averaging out the details of the molecular structure in many respects. The distance d along the layer normal $\mathbf{k}$ is the repeat distance in each phase.

Common to smectic and lamellar phases is a layered structure. In the lamellar case, for which the basic shorthand notation L is used, we have a periodic stack of parallel molecular bilayers separated by water, cf. Fig. 1.5 a-b. Within each bilayer the hydrophobic chains can be in a liquid-like state (a), being highly flexible with many *gauche* conformers and very dynamic in their orientation, or they can be 'frozen' in an extended all-*trans* conformation with a common well-defined orientation throughout the bilayer (b). This difference is the distinguishing factor between the two most important categories of lamellar lyotropic polymorphism. In the modern notation for lamellar phases the status of the chains is represented by a Greek letter appended as an index to the basic L shorthand: α indicates liquid-like disordered chains and β is used when the chains are in a stiff ordered state.

The fluctuations of the disordered chains in the L_α phase are unbiased with respect to directions in the lamellar plane, hence their average direction is simply along the layer normal. Such a phase thus has the same uniaxial (cylindrical) $D_{\infty h}$ symmetry as the nematic phase, with the director $\mathbf{n}$ parallel to the bilayer normal $\mathbf{k}$ (I use this letter for the layer normal throughout this thesis, but there is no standard convention in this case). The L_α phase is of great biological importance, because it is the natural state of our cell membranes, the main component of which is phospholipids. If our body would fail to keep the right temperature, allowing the cell temperature to cool down a few degrees, the membrane could undergo a transition to the lamellar state with stiff chains, denoted L_β if the cylindrical symmetry is retained or $L_{\beta'}$ for the more common case of uniformly tilted chains that break the rotational symmetry. This situation would be fatal to the cell function and consequently to life, hence it does not occur naturally in living systems[12]. The L_β and $L_{\beta'}$ phases are often referred to as **gel phases**, reflecting their low degree

---

[12]Poikilothermic organisms, whose body temperature varies with environment, have a different composition of
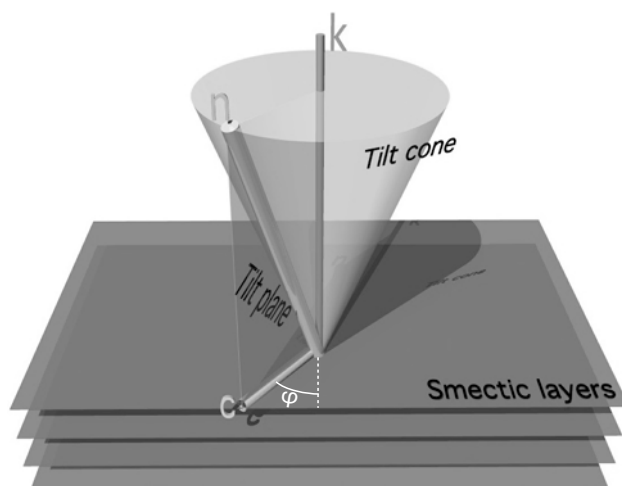
Figure 1.6: The geometry of the SmC phase calls for the definition of many new help concepts, such as the tilt plane, the tilt cone and the C-director **c**.

of fluidity. While many surfactants do not develop gel phases, their sole lamellar phase being L_α, amphiphilic lipids normally form both phases, the transition between them largely being thermally controlled. The transition temperature is then often called the 'main transition'.

In many respects one can regard L_β and $L_{\beta'}$ as one and the same phase, the key characteristic being the rigidity of the apolar chains and the consequent well-defined chain orientation throughout each bilayer. Whether this direction is along the layer normal (L_β) or tilted by some angle from **k** ($L_{\beta'}$) is essentially determined by how the molecules can best pack closely together. In the vast majority of cases a certain non-zero tilt (independent of temperature) is the promoted situation, that is most lipids exhibit no L_β phase but only $L_{\beta'}$ on cooling from L_α. In the following I will thus for simplicity use only $L_{\beta'}$ as representative of the lamellar gel phase. A number of additional variations of lamellar lyotropic type have been identified (e.g. the $P_{\beta'}$ 'ripple' phase) but these are outside the scope of this thesis.

It is important to be aware of the fact that the chain tilting direction in the $L_{\beta'}$ phase is long-range correlated only *within* each bilayer; between adjacent bilayers the direction of tilt changes randomly. Thus, although the molecules are everywhere tilted by the same angle, the lack of directional correlation along **k** yields an averaging-out on a global scale, rendering the *phase* uniaxial with its principal symmetry axis parallel to **k**. Just like L_α, the point group symmetry of the bulk $L_{\beta'}$ phase is thus $D_{\infty h}$. It is however not obvious that one should always consider the bulk properties when discussing the $L_{\beta'}$ phase, the definition of the director being a particularly tricky issue. Rather than representing the global symmetry, i.e. being along **k** as in the L_α phase, the director could equally be chosen to describe the order within one single bilayer, a choice that means that the director changes randomly at every layer of water. While both options can be well justified, I prefer the latter in the interest of coherence with the director definition in the case of thermotropic smectics, as will be further discussed in a moment. When using this definition, considering each bilayer separately, the symmetry of an achiral lamellar system is reduced from $D_{\infty h}$ to C_{2h} at an L_α to $L_{\beta'}$ transition, that is the bilayer is biaxial with a single two-fold rotation axis and a mirror plane perpendicular to it. The mirror plane is the 'tilt plane', spanned by **n** and **k** (Fig. 1.6), and the two-fold rotation axis thus its normal.

In thermotropics the analog to L_α is the smectic-A phase, abbreviated SmA[13]. It (generally)

---

lipids in their membranes, rendering L_α stable over a wider temperature range [14], hence also in their case the phase transition does not take place.

[13]The letters A, B, C etc. in the smectic nomenclature simply signify the historical order of discovery. This

has the same uniaxial cylindrical $D_{\infty h}$ symmetry with the director **n** along the layer normal **k**. As the molecules are not amphiphilic and as there is no solvent, we here do not have bilayers but monolayers. Furthermore, they are normally not as well-defined as in the lyotropic case (where the solvent 'seals off' adjacent bilayers from each other), cf. Fig. 1.5c. In fact, it is in many respects more appropriate to speak of a 1D periodic electron density modulation along **k** than of distinct layers. The mesogens can diffuse considerably along **k** and they may 'stick out' (interdigitate) a fair amount outside their current 'home' layer. The electron-rich aromatic cores are found mainly in the centers of the layers, such that we again may compare the core of the thermotropic mesogen with the micelle (extended into a bilayer in the lamellar phase) of the lyotropic analog, and the more disordered flexible end chains with the solvent. In fact, long end chains can enhance smectic order because their tendency toward entanglement, contrasting with the aromatic cores' tendency for regular packing, promotes a microphase segregation between disordered chain and ordered core regimes. Considering the positions on the molecule of the terminal chains, it is thus understandable that smectic phases generally are formed by rod-like molecules, but there are in fact also a few examples of smectic phases from discotics, then requiring a strongly asymmetric folding of the terminal chains [15].

While the SmA phase is almost always uniaxial a few examples of biaxial SmA phases have recently been identified [16,17]. Much more important as biaxial smectic is however the family of smectic-C-type phases, characterized by a tilted director and in this respect thus a thermotropic relative of the lyotropic $L_{\beta'}$ phase. The tilt angle, generally given the symbol θ, is however in the smectic case usually temperature dependent, often approaching zero on heating towards the SmA phase, while it at lower temperatures normally saturates in the range 20 - 30°. An important difference from the lyotropic $L_{\beta'}$ analog is that the tilt direction in smectics is correlated over macroscopic distances in all three dimensions[14], thereby giving rise to the biaxiality of the phase.

There are several versions of the basic smectic-C-type structure, distinguished by different interlayer tilting direction correlation schemes (these will be discussed in some detail in Chapter 2). In the fundamental SmC phase the tilt in adjacent layers is in the same direction, rendering the C_{2h} symmetry not only local but global. One often defines the ***SmC tilt plane*** as the plane spanned by the director **n** and the layer normal **k**, cf. Fig. 1.6. In addition, when considering the physics of the SmC phase PIERRE-GILLES DE GENNES realized [18] that it is convenient to define an additional vector field, closely related to the director. Reflecting the phase in which it finds use, it is called the ***C-director***, abbreviated **c**, and it is defined as the projection of the actual director **n** onto the smectic layer plane, cf. Fig. 1.6. As we will see demonstrated below, the C-director turns out to be very helpful in the description of the structure and behavior of SmC and analog phases.

If we want to define a SmC state completely, it is not sufficient to give the value of the tilt angle θ, we must also tell in which direction **n** tilts. This is generally done by defining some (arbitrary) reference axis in the smectic layer plane and then stating the angle φ between this reference axis and the tilting direction, cf. Fig. 1.6. However, while the *magnitude* of tilt θ critically influences the free energy of a SmC phase (θ is in fact the primary order parameter of the SmA-SmC transition), explaining its typical strong temperature dependence, φ is what is referred to as a *gauge variable*, meaning that it is required for defining the phase structure but its value has no impact on the energy. More formally expressed: it does not enter the expression

---

naming scheme was introduced by the Martin-Luther-Universität physical chemists DIETRICH DEMUS and HORST SACKMANN [1]. When indices are added these sometimes have physical meaning.

[14]The possibility of a tilted smectic phase without long-range correlation in tilt direction along the layer normal, a 'random SmC phase', is currently a hot topic in thermotropic liquid crystal research, cf. Paper 6. Such a (possibly hypothetical) structure is one of the options for what is referred to as a 'de Vries smectic', after the crystallographer who first considered this possibility. Apart from the differences in chain orientational order and temperature dependence of the tilt angle, this would be a true thermotropic equivalent to $L_{\beta'}$.

of the Hamiltonian. The symmetry of the SmC phase structure is thus lower than that of its Hamiltonian, a situation often referred to as 'broken symmetry'. The same situation arises in a ferromagnetic material below the transition from the para- to the ferromagnetic state. The material will get magnetized but we don't know in which direction, because any direction results in the same energy. As a result we get domains with opposite magnetization if we cool a magnet down into its ferromagnetic phase without poling it with an external magnetic field. The same holds for a SmC phase formed on cooling from a SmA phase: any value of φ is equally good so we will spontaneously get domains with different tilting directions.

At any temperature at which a sample not influenced by external forces is in a SmC phase, we thus have not one stable state but a whole range of stable states, defined by a specific value of θ but full degeneracy in φ. Together this range of possible states defines a cone with opening angle 2θ and symmetry axis along the layer normal **k**. One thus often says that the director must be somewhere on the **SmC tilt cone** when discussing the SmC phase and its analogs, cf. Fig. 1.6. The fact that all states on the tilt cone have equal energy means that fluctuations on the cone surface cost no energy apart from what is lost in overcoming the dissipative forces that counteract molecular reorientation. In the limit of infinitely slow variation in φ, the fluctuation indeed costs no energy at all, and the advanced reader may recognize that φ variations in the SmC phase thus constitutes an example of a so-called *Goldstone mode* [19–21]. As the thermal energy at typical SmC temperatures is more than sufficient for overcoming the dissipative forces experienced in the phase even at non-zero variation speed, a SmC phase is characterized by rather strong fluctuations, provided it is not influenced by external forces that break the φ degeneracy of the energy, e.g. surfaces or a magnetic or electric field.

From a symmetry point of view, all these aspects about tilting direction should apply also to the lyotropic $L_{\beta'}$ phase and one could thus imagine directional fluctuations also in this phase. However, the much higher degree of order within the lamellae compared to a SmC phase renders the dissipative costs of φ variations prohibitive, hence fluctuations in tilt direction can only be expected if they are indeed close to infinitely slow. Moreover, the lack of long-range correlation in tilting direction makes it very difficult, if not impossible, to actually study any such fluctuations experimentally.

In case of a SmC phase containing chiral molecules, a situation I will come back to below, a helical precession of the director along **k**, incommensurate with the layer spacing, arises spontaneously. Considering this helical geometry as well as the more or less complex φ correlation schemes in the other smectic-C-type phases, one may again discuss if the director should be defined globally or on a single-layer scale; the rotational symmetry of the *phase* can obviously be quite different from that of a single layer. It turns out that a consistent description of the physical properties of the different SmC-type phases, in particular their behavior in an electric field, requires the definition of the director on a single-layer scale [22], and this is thus unanimously adopted throughout the thermotropic liquid crystal community. For consistency, the same definition should be applied to the lyotropic case of $L_{\beta'}$.

In lamellar as well as smectic phases the (bi-) layer thickness is a function on the one hand of the effective average length of the amphiphiles or mesogens, on the other of the average inclination that the molecules exhibit with respect to the layer normal (see Paper 6). Basically, the smectic layer thickness is the projection of the average mesogen length on **k**, whereas the thickness of the lamellar bilayer is twice the corresponding projection of the average amphiphile length. Four parameters can be considered for estimating the layer thickness: the molecular structure, the conformational freedom of the molecules, the orientational order, and the equilibrium direction of **n** with respect to **k** (tilted or not). The average molecule length is a function of the structure and conformational freedom of the molecules, whereas the average inclination depends both on the director tilt and on the orientational order in a rather complex fashion. Finally, I should

point out that the bilayer thickness is not the periodicity of the lamellar phase: its period is the sum of the bilayer thickness and the thickness of the water layer separating two adjacent bilayers. This means that the translational periodicity in lyotropic lamellar phases is a function of water content.

In the smectic and lamellar phases the quasi-long-range positional order is one-dimensional, along **k**. Within the layers of SmA, L_α and SmC phases the molecule positions have only the randomly fluctuating short-range order of isotropic liquids. The layers of these phases can thus be regarded as two-dimensional liquids. In case of the $L_{\beta'}$ lamellar phase [23] and in the so-called higher-ordered smectic phases (e.g. SmB, SmI and SmF) so-called hexatic order prevails within the layers [24]. This means, on the one hand, that a somewhat extended but still relatively short-range (correlation length on the order of 100 molecules) hexagonal close-packed positional order exists. On the other hand, the orientation of the corresponding hexagonal unit cell is long-range correlated within the layer, a special type of orientational order that is referred to as bond orientational order[15].

1.1.4 The columnar phases

The next step in long-range positional order in liquid crystal phases is encountered among the columnar phases. Now the building blocks are positioned on a 2D lattice, but in the third direction there is no long-range positional correlation, cf. Fig. 1.7. In the thermotropic case the columnar order is typically formed by discotic mesogens, the aromatic cores stacking up as in piles of coins, each pile being located on a point of a lattice that is hexagonal (Fig. 1.7a) or very close to hexagonal (Fig. 1.7b). Within a pile the molecule positions are normally not long-range correlated (the stack is internally disordered), hence the structures can be regarded as 1D liquids. Moreover, the peripheral chains of each mesogen are rather flexible and disordered, putting the interstitial volume 'between the columns' in a state with very low degree of order, an aspect that has been ignored in the cartoons in Fig. 1.7.

The average orientation of the disc is most often flat, that is **n** is along the column axis, giving the phase D_{6h} symmetry with a C_6 axis along the columns and six C_2 axes perpendicular to them. The positional lattice is truly hexagonal. The discs may however also be more or less uniformly tilted within the columns. If there is correlation in the tilting direction between adjacent columns the phase loses its D_{6h} symmetry, the hexagonal lattice shrinking along the tilting direction into a rectangular one. The phase instead becomes one of three types of rectangular columnar phase, one of which is sketched in Fig. 1.7, or even a columnar phase with an oblique lattice. Note that the single remaining symmetry element in Fig. 1.7b is a C_2 rotation axis perpendicular to the columns and to the tilting direction: there is no longer any rotational symmetry around any axis along the columns. Reflecting their respective symmetries the three possible main cases of columnar mesomorphology are denoted Col_h, Col_r and Col_{ob}, respectively[16]. The details of the rectangular and oblique phases can be quite complex [15].

In the lyotropic columnar phases we have 'infinitely' long rod-shaped micelles positionally correlated on a 2D lattice in a plane perpendicular to the rods, that is perpendicular to **n**, cf. Fig. 1.7c. The disorder of the system is mainly found in the water (or other solvent) found between the columns, just like the disordered peripheral chains of discotic mesogens in thermotropic columnar phases. In addition, the amphiphilic molecules diffuse within each column (=micelle)

---

[15]The term is somewhat misleading as it has nothing to do with chemical bonds. The interested reader is referred to standard liquid crystal textbooks or handbooks [24] for more information.

[16]Sometimes an additional index *o* (ordered) or *d* (disordered) is added, referring to the presence or absence of a medium-range positional correlation along the column axis. The IUPAC recommendation is *not* to use these indices [25], as in both cases the positional order along the column is liquid-like, only with different correlation lengths.
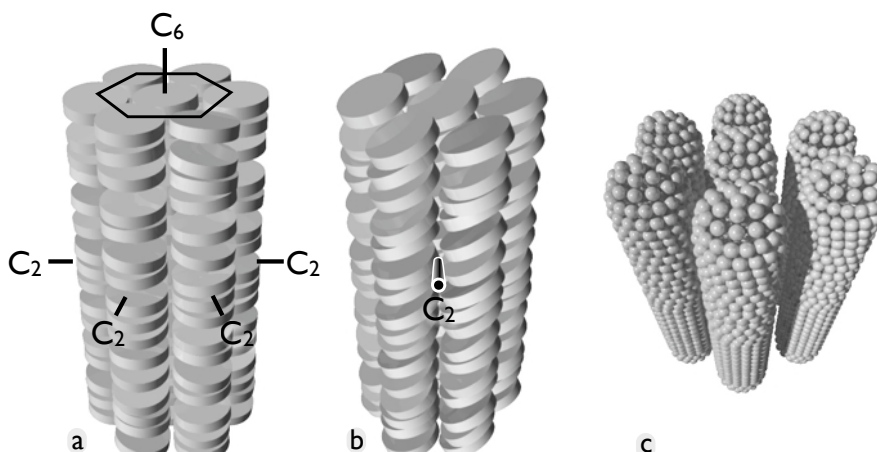
Figure 1.7: Cartoons of three different columnar phases. Parts *a*) and *b*) both depict thermotropic phases, the columns being formed by disc-shaped mesogens stacking with their cores on top of each other. If the cores are non-tilted or randomly tilted the phase has hexagonal point group symmetry D_{6h} (a) but if they are tilted in a well-defined common direction the symmetry gets reduced to rectangular (b). The lyotropic hexagonal columnar phase (c) is formed by uniformly aligned rod micelles positionally organized on a hexagonal lattice in the plane perpendicular to the micelle long axis (defining **n**).

much better than between columns, leading also here to a lesser degree of positional order along **n**. Most often the packing of the rod micelles in the plane perpendicular to **n** is hexagonal and the normal columnar phase is then labelled H_α. Of course, we can also have a hexagonal columnar phase of inverted micelles (water inside, oil between the micelles) which, following the notation chosen above, gets the label H_α^i. For the normal as well as the inverted columnar phases the packing is not restricted to being hexagonal but rectangular as well as square lyotropic columnar phases also occur, denoted R and C, respectively [26].

As already mentioned, lyotropic nomenclature is not very consistent and not without problems. For hexagonal columnar phases a relatively commonly occurring alternative to the notation used in this thesis is H_1 and H_2 for the normal and inverted structures, respectively. I find H_α and H_α^i much better since this notation is congruent with the notation for lamellar phases: in the hexagonal columnar phases the apolar chains of the amphiphiles are, just like in L_α, in a liquid-like disordered state. To complicate the nomenclature situation further, some researchers still use a totally different older terminology for lyotropics, in which lamellar phases are referred to as *neat* and columnar as *middle* phases.

1.1.5   Chiral liquid crystal phases

With the introduction of chirality into liquid crystals, another fascinating as well as useful aspect of this class of ordered soft matter arises. In most cases, chiral liquid crystals are a result of chiral molecules being present, either as chiral dopants in an achiral host phase or by the use of mesogens that are themselves chiral. In both cases the presence of stereoisomerically enriched[17] chiral molecules, leading to a sample that is unichiral on the macroscopic scale (the full bulk sample has the same handedness), is for the case of thermotropic liquid crystals indicated by

---

[17]Racemates, where all stereoisomers of a chiral species are present at equal amounts, are effectively non-chiral in their physical properties. The star is thus used only when one stereoisomer dominates over the other(s).

Figure 1.8: Cartoons of the helical director modulation in the chiral nematic (or cholesteric) phase for the case of rod- and disc-shaped building blocks, respectively. Each rod or disc represents either a mesogen (thermotropics) or micelle (lyotropics) with the corresponding shape. Note that, for clarity, the pitch has been drawn orders of magnitude smaller than in reality and the local degree of order is much too high.

adding a star to the shorthand of the fundamental corresponding achiral phase, e.g. N* for a chiral nematic phase. In lyotropics the same convention is used for chiral nematics but for lamellar phases no star is used, despite the amphiphiles often being unichiral (e.g. in naturally occurring phospholipids). In terms of the symmetries of the different phases, the definition of chirality tells that no mirror planes are present, regardless of how the liquid crystal has become chiral. This means that the index h in all symmetries mentioned so far must be removed for the chiral version of a phase.

The chiral nematic phase (often referred to as the ***cholesteric*** phase[18]) is the best studied chiral liquid crystal, a result of its simplicity, ubiquity, beauty as well as applicability. The molecular chirality here expresses itself macroscopically in the phase as a helical modulation of the director along an axis perpendicular to **n**, cf. Fig. 1.8, giving rise to spectacular optical properties which will be discussed in section 1.6.

When the helical twisting power is low the N* phase behaves very much like a non-chiral nematic, but when the twist is strong enough that the helical modulation has a pitch on about the same scale as the wavelength of light—or even less—new phenomena appear. First of all the director configuration can no longer be regarded as spatially uniform even on an approximative level. It is periodic in space along the helix axis, giving the material new features and properties that are not present in the non-chiral nematic. For instance, short-pitch cholesterics acquire a new elasticity along the helix axis equivalent to that of a weak solid[19] and their optical properties are characteristic of a one-dimensional photonic crystal (section 1.6).

The cholesteric helix is a result of the interaction between chiral molecules that confers a certain twist in the orientation of any neighbor molecule. With a twist along a single direction, as in the N* phase, the material can continuously fill space without any defects. The tendency to twist however applies along *all* directions perpendicular to any local director, so the single-helix situation of a cholesteric is not the energy-minimizing state if we consider only a very local scale. Instead the minimizing structure would be one where the director twists along any radius perpendicular to a certain central director, as schematically drawn in Fig. 1.9a. Although this configuration, referred to as double-twist, locally minimizes the elastic energy in the chiral

---

[18]The term 'cholesteric' has historical origin: the phase was first discovered in a sample of cholesteryl benzoate, exhibiting BP* and N* phases. In fact, the sample in question, synthesized by the Austro-Hungarian biochemist FRIEDRICH REINITZER in 1888 from cholesterol (that he had initially extracted from carrots), was the first compound ever recognized as a liquid crystal. Reinitzer's initial observations of a strange two-step melting behavior were shortly afterwards followed by a much more thorough characterization of the compound and its relatives by OTTO LEHMANN, a German specialist in polarizing microscopy. As a result of the discovery, Lehmann became the first great promoter of the idea of a liquid crystalline state [1].

[19]Some researchers make a distinction between 'cholesteric' and 'chiral nematic', reserving the first term for materials with such short pitch that this solid-like elasticity appears.
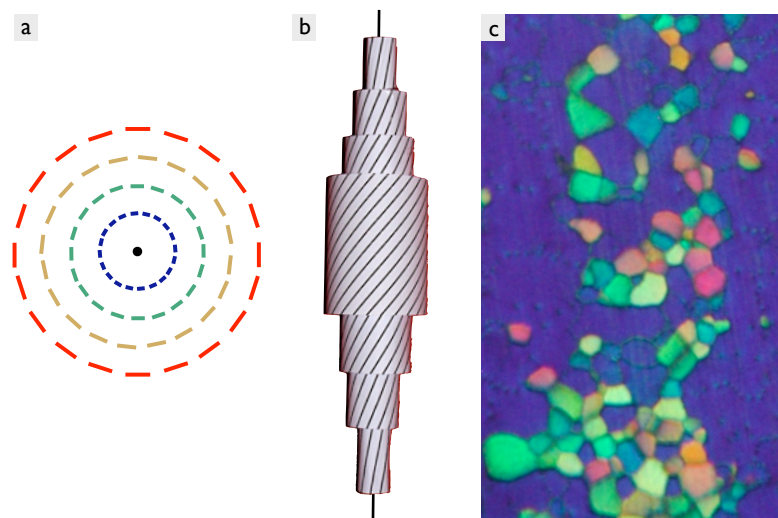
Figure 1.9: *a*: The interactions between adjacent chiral molecules in a phase with nematic-like order promote twisting along all directions perpendicular to a certain starting director (here going out of the paper plane as illustrated with the central black point). The director rotation around axes in the paper plane is indicated with a color coding, black for **n** perpendicular to the paper plane, red for director 45° out of the paper plane. *b*: A simple paper model of the double-twist cylinder structure that is the basic building block of BP I* and BP II* blue phases. Lines printed on each sheet represent the director field at that distance from the central vertical director. The drawing in *a* corresponds to a horizontal cut through the center of the model. *c*: Example of the multi-colored platelet polarizing microscopy texture characteristic of BP I* and BP II*.

system, it cannot fill three-dimensional space without generation of a network of defects or voids. The concept 'local scale' here means within a distance from the central director where the twist has reached about 45° as illustrated in Fig. 1.9b where the multiply twisting director field in *a* has been extended along the central director into what is called a *double-twist cylinder* unit.

It turns out that when the twisting power is sufficiently high, rendering the elastic energy of a local defect-free regime markedly lower for double- than single-twist, and the temperature is close enough to the clearing point, such that the energetic cost of defects is much less than when the nematic order is very well developed (see below for a discussion of the temperature dependence of the nematic order parameter), then three new liquid crystal states, related to but not equal to the chiral nematic phase, may become energetically stable. In these **blue phases** [27–30], abbreviated[20] BP*, double-twist cylinder units indeed develop in a thermodynamically stable state.

The subtle and fascinating blue phases can be seen as successive melting steps of the cholesteric towards the isotropic phase. First the N* phase melts to BP I*, then eventually to BP II* (less stable than BP I*) and sometimes even to BP III*. The latter phase, also called the 'blue fog' phase, has been found to be amorphous but its local structure is still not conclusively elucidated. In the BP I* and BP II* phases, in contrast, the double-twist cylinders have been confirmed to develop along three perpendicular directions, building body-centered cubic and simple cubic

---

[20]In the literature one finds the blue phase acronyms either with or without the asterisk for chirality. Although the latter option is more common I here use the former for the sake of consistency with the asterisk usage for thermotropic liquid crystals in the rest of this thesis.

structures, respectively, combined with a regular network of defect lines (called disclinations). In the first case the lattice constant corresponds to one pitch of the helix, in the latter case to half a pitch. These blue phases are thus in essence soft solids so how can we regard them as liquid crystals? The answer is that the molecules do not have any positional order. Within the cubic structure, that has a lattice constant of about a micrometer instead of a nanometer as in usual solid crystals, the molecules move freely while observing the orientational order defined by the position in the lattice.

Having cubic symmetry or being amorphous, all blue phases are optically isotropic in that they show no linear birefringence, but they show optical activity and reflect circularly polarized light. For BP I* and BP II* the reflected wavelength is not unique (and not necessarily blue) but depends on the orientation in space of the cubic lattice. These phases show a characteristic platelet texture (Fig. 1.9c), each platelet corresponding to one lattice orientation. The color arises from Bragg reflection from the 'crystal planes' of the structure, different orientations yielding constructive interference for different wavelengths, hence the multitude of colors.

The temperature range of blue phases is normally so small (often less than 1 K) that they are difficult to study and applications of them long seemed totally unrealistic. In 2002, however, this situation changed thanks to an important breakthrough by Hirotsugi Kikuchi and co-workers [31]. By polymerizing a non-mesogenic monomer dispersed in a blue phase, the temperature range of the phase was expanded by almost two orders of magnitude. The polymer chains aggregate within the defect lines of the host phase since they are in an isotropic state, allowing the polymer chains to adopt a random coil conformation instead of the entropically unfavorable stretched-out state that the ordered liquid crystal between the defects would require. In this way the lattice of defects is made permanent, stabilizing the blue phase over a temperature range of some 60 K, including room temperature! As a result, the company Samsung recently introduced the first prototype for a blue phase liquid crystal display, utilizing the Kerr effect in a polymer-stabilized BP I* phase.

In smectic phases, a helical director modulation perpendicular to $\mathbf{n}$ would break the layers and is thus not admitted[21]. The SmA* phase therefore has the same structure as an achiral SmA phase. Its physical properties are however quite different from its achiral analog, as will be described in Chapter 2. It is therefore important to recognize that the phase is still chiral, despite the absence of a helix. In contrast to SmA*, the chiral SmC* phase does allow a helical superstructure, but it applies to the C-director rather than the normal director. In other words, $\mathbf{n}$ in SmC* does not twist as in N*, but $\mathbf{c}$ does, i.e. the tilting *direction* precesses helically along the smectic layer normal, as illustrated in Fig. 1.10.

While cholesteric phases exist among thermotropic as well as lyotropic liquid crystals, the chirality effects typical of stratified structures (cf. Chapter 2) have so far been found almost exclusively among thermotropic smectics. Although some reports of their observation in lyotropic SmC*-like phases exist [32–36] the evidence is not straightforward. Moreover, the most convincing data were produced by replacing water as solvent by ethylene glycol [36]. The lack of correlation in tilting direction φ between adjacent lamellae in the ordinary aqueous $L_{\beta'}$ phase at least rules out the formation of a helix in this system. It is a very interesting but still open question if other chirality effects can be detected with certainty in lyotropic lamellar phases.

The pitch p (periodicity of the helix) can be anywhere from a few hundred nanometers to infinity, for cholesterics as well as SmC*-type phases. It depends on the one hand on the so-called 'helical twisting power' (HTP) of the chiral molecule (in other words, it is structure-specific), on

---

[21]Nevertheless, this may in fact happen for very high twisting power but the phase is then not categorized as a normal smectic. In these *Twist Grain Boundary* (TGB*) phases, the structure can be described as finite blocks of smectic order, each block rotated a specific angle around an axis in the smectic layer plane with respect to its neighbor blocks, thereby forming a discrete helical structure.

the other on its enantiomeric enrichment ('enantiomeric excess', *ee*), third on the temperature. The typically rather strong temperature dependence of the pitch, which can give rise to a color that changes on heating or cooling, is the basis for the common use of N* liquid crystals in temperature sensors. The handedness of the helix depends on which stereoisomer builds up the phase or is added to the achiral host phase. If more than one stereoisomer is present, the surplus stereoisomer will determine the handedness, and the pitch will be longer than for a unichiral sample. Quantitatively, the *inverse* pitch depends linearly on *ee*, going from 0 (infinite pitch) at the racemate to p_0^{-1} at 100% *ee*, where p_0 is the pitch of the unichiral material.

Whereas the discovery of the N* phase is as old as the discovery of liquid crystals[18] the awareness of the SmC* phase is somewhat younger, but it has still been known for some 50 years. More recent is the discovery of the variations of the basic chiral SmC-type structure (Paper 6), as well as the class of chiral smectic liquid crystals forming from achiral bow-shaped molecules [37–39]. Although the latter liquid crystal class, discovered in the mid 1990's, will play only a marginal role in this thesis, no modern account of chiral liquid crystals would be complete without mentioning the possibility of chiral mesophases forming without molecular chirality. It can arise in smectic phases formed by molecules with a strongly bent core because such molecules can only pack efficiently if the bend direction is uniform over large distances. If in addition the director is now tilted (as is often the case in these systems), we have three non-parallel directions describing quasi-long-range order: the layer normal, the tilting direction and the bend direction. Together, these three vectors span a Cartesian coordinate system, thus exhibiting a handedness. In other words, although no chiral molecules are present, the phase is locally chiral, with a handedness L or R that is randomly generated [40]. In practice, macroscopic L and R chiral domains exist next to each other with equal coverage in a typical sample. The nomenclature for designating this class of phases is still not totally uniform (although a system now seems to win general acceptance) but in contrast to ordinary chiral smectic phases, a star is not added, signifying the absence of global chirality. The phase *as a whole* (the full bulk sample) is not chiral: there are as many L as there are R domains, so considered as a single phase the sample is racemic. A macroscopic preference for one handedness over the other would require the addition of a (uni-) chiral dopant and then a star would of course be added to its shorthand.

φ=0

φ

φ=180°

molecule (director)
helix
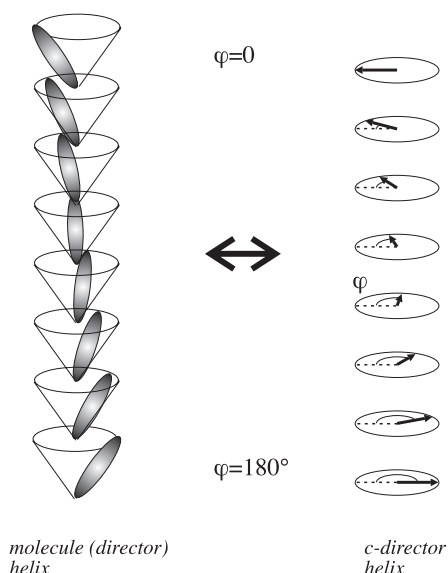
c-director
helix

Figure 1.10: The helical modulation of the chiral smectic-C (SmC*) phase applies to the director tilting direction φ or, equivalently, to the C-director **c**. To the left a cartoon of the molecular order is shown, each layer being represented by a tilt cone on which the actual director is indicated with an ellipse. The right drawing shows the corresponding modulation in **c** (represented by the black arrow) and φ. Half a period of the helical structure is drawn, the twist greatly exaggerated for reasons of clarity. A real short-pitch SmC* phase has a helical pitch on the order of 100 smectic layers.

In columnar phases, the requirement for a macroscopic chiral superstructure reflecting molecular chirality is, just like in smectics, a non-zero director tilt of the molecules with respect to the column axis. If the director is along the columns, a chiral superstructure would require a breaking of the hexagonal 2D lattice, a situation that to the best of my knowledge has not yet been reported[22]. If **n** on the other hand is tilted, we can again imagine a helical modulation of the tilt direction, this time along the column axis.

1.1.6 Further liquid crystal polymorphism

Fig. 1.2 summarizes what has been stated above about calamitic thermotropic[23] and lyotropic liquid crystals, respectively, in highly simplified generic phase diagrams. In reality the phase diagrams are generally more complex and they often include several more phases. Moreover, the details of the typical multi-phase regions occurring at low temperatures in lyotropic systems are ignored in the right diagram. The polymorphism of liquid crystals is incredibly rich and encompasses many phases that I cannot discuss here, at least not in detail. I will just mention a few further examples of liquid crystal polymorphism in extreme brevity.

Cubic phases (which by symmetry have to be optically isotropic) are rare among thermotropics but relatively common in the lyotropic realm [26]. They may be formed by micelles packed on a cubic lattice with medium-range 3D positional order, in which case the phase is often denoted Q_m. Another variant of cubic lyotropic mesomorphism is given by the bicontinuous phases, where amphiphiles are organized in infinitely extended but highly curved bilayers, leading to a complex cubic structure where a continuous water phase is everywhere separated from another continuous oil phase. An amphiphilic molecule in a bicontinuous phase can diffuse through the whole sample without ever needing to leave its bilayer environment, a situation which is obviously quite different from lyotropic phases with finite micelles. A non-cubic (in fact, it has no long-range order and its classification as liquid crystal phase can thus be discussed) bicontinuous phase is the sponge phase, denoted L_3. Finally, in lyotropic phase diagrams a number of intermediate phases may appear, often as transition structures between two larger realms of e.g. lamellar and columnar phases.

Also among thermotropics several further phases exist, in many cases as more or less subtle modifications of the basic smectic, columnar and nematic structures defined above. In addition to the cholesteric BP* phases introduced above, chirality may lead to similar frustrated states based on a smectic structure, e.g. Twist-Grain-Boundary (TGB*) phases[21] or smectic blue phases, again rarely appearing and generally with small temperature ranges.

One final pair of terms should be defined in this discussion of liquid crystal phases. Some thermotropic substances show a greater number of liquid crystalline phases on cooling than on heating, the reason being that some of them may occur only as metastable supercooled phases, when cooling the substance past its melting point. If crystallization then does not set in immediately (generally because of kinetic hinderance of some kind), a phase transition into a new liquid crystalline state may instead take place, the new phase being referred to as a ***monotropic*** phase of the substance in question. Sooner or later the supercooled phase will however be replaced by the crystalline state corresponding to the global energy minimum.

---

[22]A related situation can however be induced by dissolving a chiral thermotropic columnar phase in an aliphatic solvent, e.g. dodecane [41]. The discotic molecules may then still stack in columns, of medium length, that are roughly parallel but no longer exhibit positional order. In other words, the phase effectively becomes a chiral nematic, allowing it to develop a macroscopic helical modulation.

[23]The phase diagrams of thermotropic discotics are more difficult to generalize, columnar and nematic phases rarely appearing in one and the same compound [42]. When they do, the surprising result is that the nematic phase may appear at temperatures below the columnar ones [43]!

When heating the substance from the crystalline state the monotropic liquid crystal phase will not develop, but the substance will melt directly into the first **enantiotropic** liquid crystal phase of the compound, that is the first thermodynamically stable liquid crystal phase, forming on heating as well as on cooling. The term 'enantiotropic' of course applies to any thermodynamically stable liquid crystal phase, regardless of whether the compound exhibits monotropic phases or not, but the distinction is generally called upon only when discussing substances exhibiting metastable phases on cooling.

When stating the phase sequence of a substance with monotropic phases these are enclosed in parentheses, together with the transition temperatures into each phase (which must obviously refer to a cooling run). A compound with a monotropic SmC phase underneath an enantiotropic SmA phase could thus have the phase sequence:

Cr. 31 (SmC 28) SmA 40 Iso.

Note that the melting point (31°C) is higher than the SmA-SmC transition (28°C). Furthermore, all enantiotropic transition temperatures are generally given on heating, since transition temperatures can be determined with greater accuracy in this direction.

1.2   The orientational order parameter

The definition of the director provides a first qualitative description of the long-range orientational order of a nematic phase and enters as the natural variable in what is referred to as the *elastic continuum description* of the free energy of a nematic, in the context of which it was introduced[2]. But apart from the *direction* of the anisotropy axis in space, one often desires also a quantitative measure of the anisotropy, or degree of orientational order. In other words, we are looking for a number that tells us to what extent the building blocks align along the common direction, or how large the fluctuations around this direction are. The parameter filling our needs is nowadays often called 'the nematic order parameter' S, even when applied to non-liquid crystalline systems (such as assemblies of carbon nanotubes) and despite the fact that it was originally developed not for liquid crystals but for describing the chain orientation in polymer fibers. For three-dimensional systems this parameter, introduced in 1939 by P.H. Hermanns and P. Platzek [44] and adopted for liquid crystals in 1942 by Viktor Tsvetkov [45], has the form:

$$S = \frac{1}{2} < 3\cos^2\beta - 1 > \tag{1.1}$$

Here we have introduced the angle β, describing the deviation in orientation away from **n** of a particular building block at a particular moment in time, cf. Fig. 1.11. The deviation is averaged over the ensemble of building blocks constituting the phase considered. In the figure we again use the angle φ to define the tilting direction, this time of the molecule with respect to **n**. While not directly entering the definition of the order parameter it is important to be aware of the degeneracy in φ (all *directions* of deviation from **n** can occur with equal probability), affecting any statistical description of liquid crystal order (this issue is discussed in detail in Paper 6).

The order parameter (1.1) has the desirable property of being zero for total disorder, since in three dimensions $< \cos^2\beta >= 1/3$ for a random orientational distribution, and 1 for perfect order (in which case $< \cos^2\beta >= 1$)[24]. The expression is identical to the second Legendre polynomial

---

[24]The minimum value of Eq. (1.1) is not zero but -1/3. However, the negative values describe a physically irrelevant state of building blocks preferentially aligning *perpendicular* to the director (in conflict with its definition), hence this regime can be ignored.
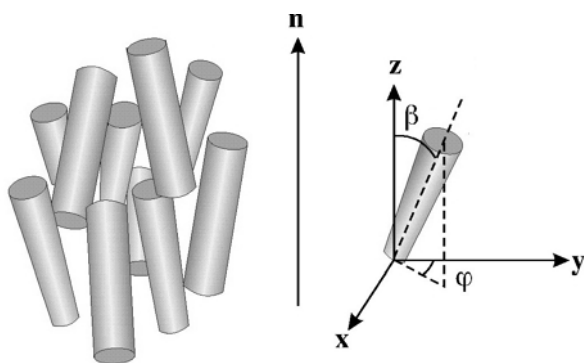
Figure 1.11: Graphical depiction of the concepts required for defining the orientational order parameter. The building blocks of the liquid crystal phase are depicted as rods, on the average oriented along **n** but each deviating by some angle β in a direction φ.

and the order parameter is therefore often referred to as $< P_2 >$ to emphasize this equivalence[25], but in this thesis I will use the simpler shorthand S. In fact, the full scalar orientational order parameter is a series of Legendre polynomials, the first term of which is $S =< P_2 >$, but for many considerations it suffices to use this first term.

It has been empirically as well as theoretically established that the thermotropic isotropic-nematic transition is first-order, that is the order parameter jumps discretely at the phase transition from zero to a non-zero value, typically around $S = 0.4$. On cooling a thermotropic nematic, S increases, initially fast but rapidly approaching saturation around $S = 0.6 - 0.7$, cf. Fig. 1.12. If smectic phases develop on further cooling the orientational order may increase discretely by a small amount at that phase transition as well, but inter-smectic transitions like SmA-SmC generally do not affect S markedly. In thermotropic liquid crystals, the orientational order rarely increases beyond $S \sim 0.8$, columnar phases being an exception.

In lyotropic liquid crystals one can basically distinguish two subclasses as far as the orientational order is concerned. Among surfactant-based lyotropics, the hexagonal phases have very high order parameters in the range of $S \approx 0.9$ [46]. The same holds for nematic phases formed not by surfactant micelles but by colloidal suspensions of more or less hard anisometric particles (viruses, carbon nanotubes, bentonite platelets, ...). In both cases the order parameter

---

[25]Actually, the IUPAC recommendation is to use $< P_2 >$ as shorthand for the scalar orientational order parameter [25] but S is still very commonly employed.
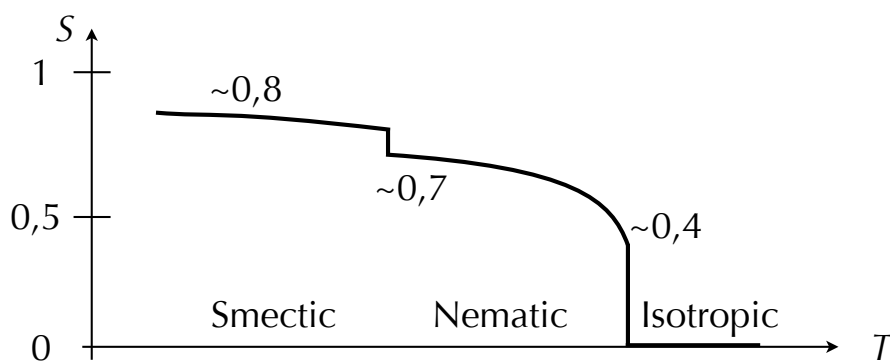
Figure 1.12: Typical temperature dependence of the orientational order parameter in a thermotropic material exhibiting a nematic-smectic phase sequence.

is largely insensitive to temperature so these lyotropic systems are in many respects athermal. Micellar nematic phases, on the other hand—much more rarely observed as they generally require a smart mixture of surfactant and co-surfactant— generally have a strong temperature dependence of the order parameter, often looking qualitatively similar to Fig. 1.12. Moreover, the value S_{NI} at the transition point (which can here by defined either as a temperature or as a concentration) can here be very low, sometimes substantially lower than S_{NI} of thermotropic liquid crystals. It is typically $S_{NI} \approx 0.3$ [47–50] but some experimental works report values as low as $S_{NI} \approx 0.1$ [48, 49].

For a two-dimensional ensemble, e.g. rods restricted to a single plane such as a substrate or thin flat film, the average $< \cos^2 \beta >= 1/2$ for a random distribution, hence the corresponding expression for S in 2D is:

$$S_{2D} =< 2\cos^2 \beta - 1 > \tag{1.2}$$

1.3   The anisotropic physical properties of liquid crystals

The macroscopic anisotropy of liquid crystals, a property shared with no other fluid, is the basis for their successful commercial exploitation. The anisotropy takes on several faces, the most important ones of which will be discussed in the following.

1.3.1   Optical anisotropy

The anisometry of the building blocks and the presence of long-range orientational order together generally render liquid crystals optically anisotropic, that is their refractive index $n_{||}$ parallel to **n** is different from that perpendicular to the director, $n_\perp$. For a uniaxial material, these two indices are the extreme refractive index values and the director is equivalent to the optic axis of the liquid crystal. The magnitude of anisotropy, the birefringence, is defined as $\Delta n = n_{||} - n_\perp$. Consequently, if $n_{||}$ is the maximum refractive index, $\Delta n > 0$ and we call the liquid crystal positive uniaxial (this is the general case for rod-shaped mesogens), whereas if it is the minimum the phase is negative uniaxial (this is the standard case for discotics).

A birefringent material can affect the polarization of light, changing the ellipticity continuously between linear and circular polarization as well as changing the main oscillation direction or reverse the rotation handedness. This is the basis for the use of liquid crystals in most electrooptic devices like displays, where the substance is placed between crossed polarizers. In the bright state the director/optic axis is oriented such that the polarization of the incident light changes in a way that it after passage through the liquid crystal is again linear but with the electric field oscillations in the direction transmitted by the exit polarizer (the analyzer). Light thus passes through. In the dark state the director is instead reoriented such that no birefringence effect takes place. The polarization of the light then remains unchanged, linear, with oscillations of the optical electric field along the transmission direction of the polarizer but perpendicular to that of the analyzer, leading to its absorption by the latter. The function of liquid crystal displays is well described in numerous books and I thus refer the reader to other sources for a more complete explanation of their operation.

The dark state just described is usually achieved by establishing a so-called ***homeotropic*** director geometry (Fig. 1.13, left), a term used when **n** and consequently the optic axis is perpendicular to the sample plane. Light passing through the sample at normal incidence (the light ray is perpendicular to the sample plane) thus propagates exactly along the optic axis, rendering the apparent birefringence zero[26]. In contrast, the maximum effective birefringence is experienced

---

[26]While the exact origin of the term *homeotropic* is obscure, it may be understood as a condensed form of
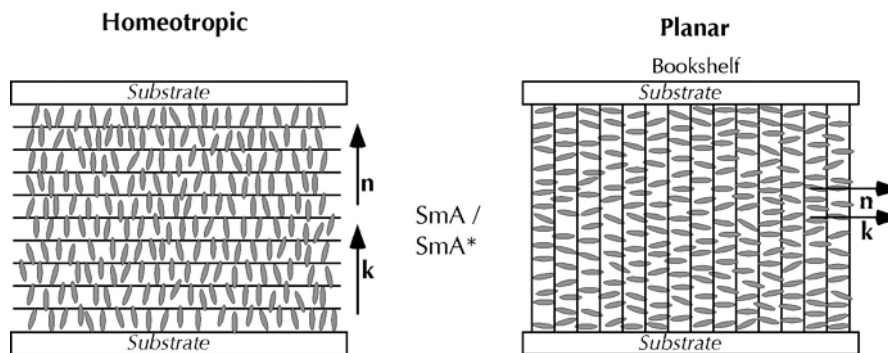
Figure 1.13: Schematic drawing of homeotropic and planar alignment, respectively, here illustrated for the case of an SmA phase. Normal light incidence means that the light beam is propagating vertically in the picture. Note that the drawing is not to scale: a smectic layer is some three orders of magnitude thinner than the distance between the sample substrates.

when the propagation direction is perpendicular to the optic axis. Again considering the case of normal incidence, this corresponds to **n** being in the sample plane. In liquid crystal science this geometry is referred to as **planar** alignment[27].

In Fig. 1.13 the two principal alignment types are illustrated for the case of a smectic-A phase. Note that hometropic alignment corresponds to smectic layers in the plane of the cell whereas the planar alignment is equivalent to a geometry where the layers are standing up. The latter geometry is therefore often called *bookshelf geometry*, referring to the layers standing as books in a shelf. The nematic case is identical to the SmA case apart from the absence of layers, but the SmC case is somewhat different. Here one usually maintains the *layer* geometries in Fig. 1.13 in the definition of the concepts homeotropic and planar, although the director is then not along the viewing direction in the former case and not necessarily in the sample plane in the latter. The substrates surrounding the liquid crystal in bookshelf geometry can however be treated such that the director is anchored in one of its two possible truly planar alignments (defined by the cross section of the SmC cone and the sample plane), hence the term planar alignment is indeed appropriate also in SmC. For the case of horizontal layers, however, one should in principle use the term **quasi-homeotropic** to acknowledge the fact that light at normal incidence is not propagating along the optic axis (a quasi-homeotropic SmC sample is consequently not dark in the polarizing microscope, an issue I will soon come back to).

In a planar-aligned nematic sample where **n** has no restriction to any particular direction in the sample plane (I refer to this geometry as degenerate planar alignment), the random variations of **n(r)** result in the same random variations of the optic axis throughout the sample area. When observing the sample between crossed polarizers, all locations where **n** is parallel to one of the polarizers will appear black. Since these locations are continuously connected with each other via randomly curving 'threads' or 'streaks' we get a texture that is very characteristic for the nematic phase, cf. the example in Fig. 1.14. This texture is called a **schlieren** texture after the

homeoisotropic meaning *like isotropic*, referring to the fact that the birefringence effectively vanishes for light propagating along the optic axis.

[27]An older term sometimes encountered is *homogeneous alignment*. There are many reasons to avoid this term which is not only obsolete but also grossly misleading: *homeotropic* alignment is *homogeneous* in the proper sense of the word and a *planar* sample without a well-defined direction of **n** in the sample plane (the normal result when using alignment layers for planar alignment that have not been rubbed, cf. section 1.4) is an example of a highly *inhomogeneous* director field.

German word for streak; *Schliere*.

The magnitude of the birefringence of a phase with uniform director depends on the degree of orientational order S and the polarizability anisotropy $\Delta\alpha$ of the building blocks of the phase, according to:

$$\Delta n \propto S\Delta\alpha \qquad (1.3)$$

It is thus a linear function of the nematic order parameter and the difference in polarizability along and perpendicular to the principal symmetry axis of the building block. While $\Delta\alpha$ is largely temperature independent the order parameter generally changes strongly at temperatures close to the transition to the isotropic phase, as discussed above, hence Δn decreases rapidly as a thermotropic liquid crystal is heated towards its clearing point, cf. Fig. 1.15. Of course any other influence on the degree of order, e.g. the addition of particles that disturb the nematic organization, will have the same type of very visible influence on Δn.

The linear aromatic core commonly found in calamitic thermotropic mesogens results in a high value of $\Delta\alpha$, hence thermotropic calamitics belong to some of the strongest birefringent materials known. The circular core structure of discotic mesogens yields somewhat lower $\Delta\alpha$ although its high degree of aromaticity still allows for reasonably high values. Lyotropic liquid crystals, in contrast, are most often formed by molecules without aromatic moieties, making $\Delta\alpha$ rather small. Consequently, a lyotropic nematic has orders of magnitude smaller birefringence than its thermotropic counterpart, although $S(T)$ is similar for the two cases.

If we cool a nematic-forming material down from its isotropic into its nematic phase, the isotropic refractive index will split up in $n_{||}$ and $n_\perp$ at the phase transition, cf. Fig. 1.15. At that temperature, these three refractive indices are related as:

$$n_{iso}(T_{NI}) = \frac{n_{||} + 2n_\perp}{3} \qquad (1.4)$$

a result of the geometrical averaging taking place in the isotropic phase. This holds regardless of whether the material has positive (Fig. 1.15a) or negative (b) optical anisotropy. As a result, the isotropic refractive index at the phase transition is closer to the greater nematic refractive index for a negative uniaxial material, whereas it is closer to the smaller one for a positive material. The decrease in n_{iso} upon heating through the isotropic phase is a result of the dependence of the refractive index on the density of the phase, which decreases on further heating.

The visible effect of birefringence is generally not simply one of bright or dark, but one of color. The exact change in polarization that light undergoes on passage through the liquid crystal depends on its wavelength, or color. Therefore, a liquid crystal between crossed polarizers
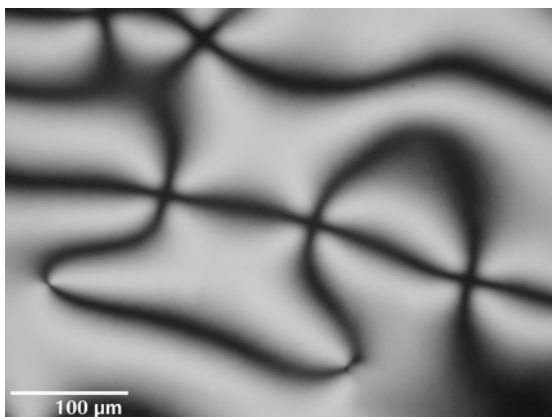
Figure 1.14: An example of the characteristic schlieren texture exhibited by nematic liquid crystals in degenerate planar alignment. The micrograph is of a lyotropic nematic formed by disc-shaped micelles, but exactly the same type of texture can be formed by any type of achiral nematic in the right geometry.
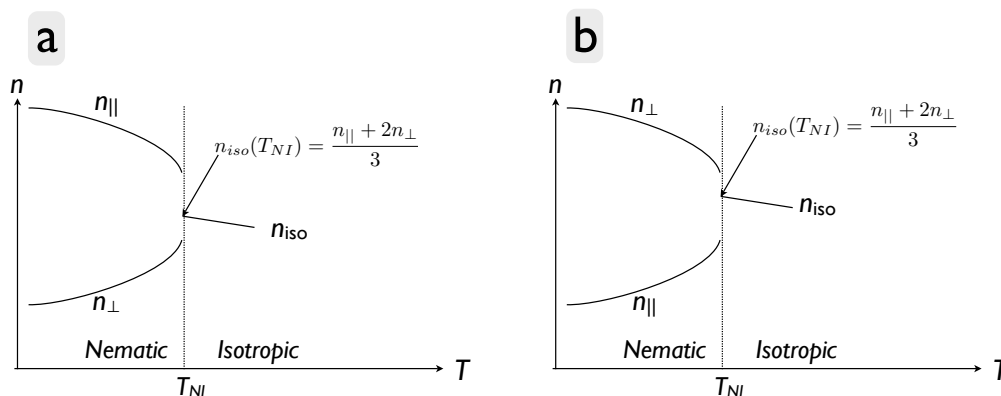
Figure 1.15: Typical temperature dependencies of the refractive indices of a positive (a) and negative (b) uniaxial nematic, below and above the clearing point.

illuminated by white light (this is the typical situation when studying liquid crystals in a polarizing microscope) will often appear strongly colored. The color depends on the magnitude of Δn and the thickness of the sample, as is graphically summarized in a *Michel-Lévy* chart[28], cf. Fig. 1.16. This chart is an invaluable aid to the polarizing microscopist and thus has a very good place on the wall in any lab where liquid crystal investigations are a major theme.

The horizontal axis of the diagram corresponds to the phase shift introduced by the birefringent sample and the vertical axis corresponds to the sample thickness. The behavior of a sample with a particular value of birefringence can thus be determined by drawing a straight line from the origin. Such lines are normally drawn for a large number of Δn values, allowing one to quickly locate the line roughly corresponding to the sample presently under study. The Michel-Lévy chart shown in Fig. 1.16 is actually rather unique because it has been drawn on a scale optimized for thermotropic liquid crystals. The diagrams provided by e.g. microscope manufacturers or that are available on the internet are generally drawn with inorganic crystals in mind, typically having about an order of magnitude lower birefringence than thermotropic liquid crystals. In many cases, therefore, only the two or three final lines are of interest for liquid crystal researchers.[29] In Fig. 1.16, in contrast, a typical thermotropic sample will follow a line close to the central line, extending from the lower left to the upper right corner. For lyotropic liquid crystals, on the other hand, a standard Michel-Lévy chart may be more appropriate as their birefringence is smaller.

In the chart one can immediately find the color that a sample of a certain thickness and birefringence will have when viewed between crossed polarizers. For typical thermotropic birefringence values of $\Delta n \approx 0.1$ one finds that a regime of strong colors (varying quasi-periodically over two - three orders) for sample thicknesses in the range $d \approx 3\mu$m to $d \approx 20\mu$m, is surrounded by a grey-white regime for very thin cells ($d \approx 1-2\mu$m) and a regime with an ill-defined and uninformative pallid appearance for very thick cells. The latter is one of the reasons why thermotropic liquid crystal samples are rarely much thicker than some tens of microns (cf. sec-

---

[28]It is named after the French 19th century mineralogist Auguste Michel-Lévy, who introduced it.

[29]The colors of a standard Michel-Lévy diagram may however be more accurate if the print is of high quality, because the colors in Fig. 1.16 are good estimates but not quite correct. The diagram has been created using the software Pro Fit by calculating the intensity after the sample (placed between crossed polarizers) of each wavelength of incident white light and summing all contributions. While the result thus far is exact, the translation from light wavelengths to the RGB values used by computers to display color is only approximate.
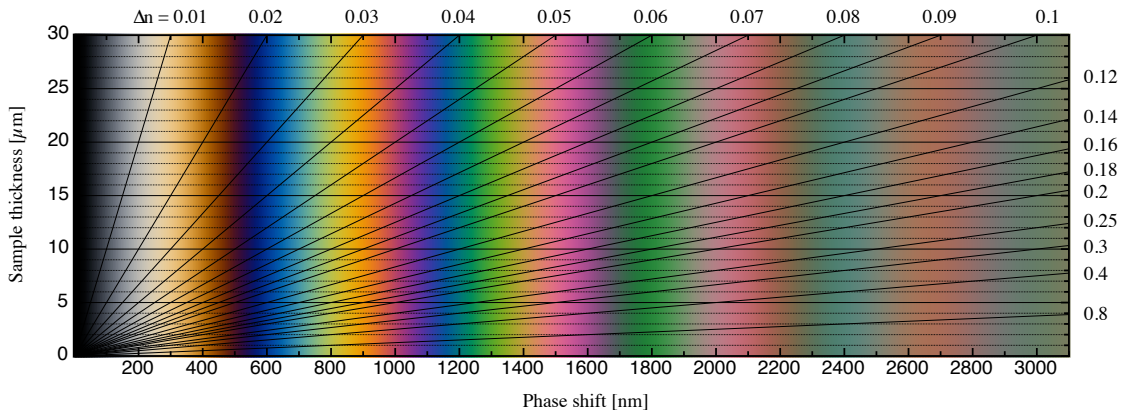
Figure 1.16: Calculated Michel-Lévy diagram optimized for typical birefringence values of thermotropic liquid crystals. The colors are only approximately correct (in particular, the true color at about 530 nm phase shift is in fact a deep violet).

tion 1.4). Conversely, if we know the sample thickness, one can use the chart to estimate Δn or at least track changes in birefringence. Indeed, if you place a planar-aligned thermotropic nematic sample of about 5 μm thickness in a polarizing microscope equipped with a hot stage and start heating it towards its clearing point, you can verify the behavior sketched in Fig. 1.15 simply by looking at the color changes and comparing with a Michel-Lévy chart.

This very brief discussion of the optical anisotropy of liquid crystals has been done using the simplest case of uniaxial birefringence. The optical situation gets more complicated in case of a biaxial phase, which has two optic axes and three extreme values of refractive index n_1, n_2 and n_3. In fact, the definition of the director is a rather intricate issue for biaxial phases. The way that it is usually defined as an axis of rotational symmetry, renders it a strictly uniaxial concept. When working with liquid crystals we often deal with uniaxial phases (N, SmA, L$_\alpha$, ...), however, and even the biaxial phases (SmC, ...) are often very weakly so, such that we in a first approximation can neglect the biaxiality and use the director concept almost as usual. In the case of SmC, for instance, one often takes the bisector of the two optic axes (this is also referred to as the *slow axis* since it is the direction of highest refractive index) as the director.

1.3.2   Dielectric, conductive and magnetic anisotropy and the response to electric and magnetic fields

While the optical anisotropy is responsible for the function of a liquid crystal in a device in its bright state(s), it is normally the dielectric anisotropy that allows us to change the state; to 'switch' the director field between different defined geometries, giving different transmission. Obviously, this dynamic aspect is a requirement for the operation of any display or related type of electrooptic device. It is also highly useful, and gives rise to many fascinating phenomena, when doing research on liquid crystals.

If an electric field **E** is applied over a dielectric medium such as a liquid crystal, the field will polarize the medium, that is an electric dipole moment will be induced, proportional to the field strength and to the dimensionless electrical susceptibility χ^e of the medium:

$$\mathbf{P} = \epsilon_0 \chi^e \mathbf{E} \tag{1.5}$$
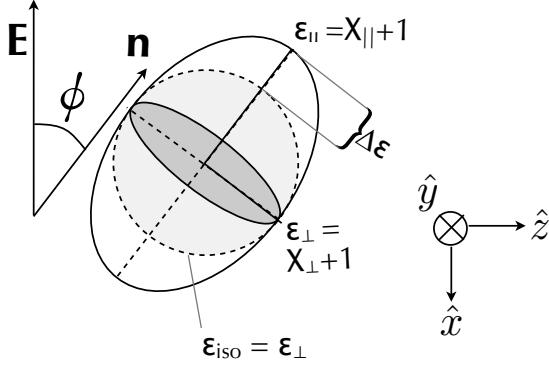
Figure 1.17: When an electric field is applied over an anisotropic dielectric medium like a liquid crystal, a polarization is induced that may be non-parallel to the field. This results in a torque which, in case of the highly fluid nematic, reorients the director until the induced polarization is along the electric field.

The vacuum permittivity $\epsilon_0 \approx 8.85 \cdot 10^{-12}$ C/Vm is required to get the dimension of a polarization. In an isotropic medium χ^e is independent of direction and can be represented by a scalar. The resulting polarization will thus always be exactly parallel to $\mathbf{E}$. In anisotropic media, in contrast, the susceptibility depends on the direction of the field and its full description requires a tensorial χ^e. We will here consider only the simplest uniaxial nematic case, for which we only require the two scalar susceptibility values $\chi^e_{||}$ parallel and $\chi^e_\perp$ perpendicular to $\mathbf{n}$. Analogously to the optical anisotropy we can now define the susceptibility anisotropy as $\Delta\chi^e = \chi^e_{||} - \chi^e_\perp$.

The important consequence of the susceptibility being anisotropic is that the induced polarization $\mathbf{P}$ is not necessarily directed along $\mathbf{E}$. Field application thus generally results in a local torque $\mathbf{\Gamma}_\epsilon = \mathbf{P} \times \mathbf{E}$ on the director, acting to align $\mathbf{n}$ along ($\Delta\chi^e > 0$) or perpendicular ($\Delta\chi^e < 0$) to the field, allowing us to quickly and easily modulate the director orientation with the field. The electrical susceptibility is rarely considered in practice, as the quantity that is typically known (or measured) is the dielectric permittivity $\epsilon = \chi^e + 1$. However, as the one quantity is just the other rescaled by the addition of a constant, their anisotropies are numerically identical, $\Delta\epsilon = \epsilon_{||} - \epsilon_\perp = \Delta\chi^e$.

Consider the situation depicted in Fig. 1.17: an electric field $\mathbf{E}$ is applied vertically (in $-\hat{x}$ direction as defined in the figure) over a uniaxial nematic with positive $\Delta\epsilon$, the director of which is inclined an angle ϕ from the vertical direction. The anisotropic permittivity is represented graphically by a rotationally symmetric ellipsoid, the distance between its center and its surface in each point being equal to ϵ in that particular radial direction. It turns out to be convenient to separate the permittivity in an isotropic component $\epsilon_{iso} = \epsilon_\perp$ (graphically represented by the dotted sphere) and an anisotropic addition $\Delta\epsilon$. The former component can be analyzed as for any isotropic system so the resulting polarization is parallel to the field and has the magnitude $P_{iso} = \epsilon_0 \chi^e_\perp E = \epsilon_0(\epsilon_\perp - 1)E$. More interesting is the anisotropic component, which generates a polarization along the director but is driven only by the component of the field along $\mathbf{n}$, $E_{||} = E \cos\phi$.

We can now calculate the dielectric torque $\mathbf{\Gamma}_\epsilon = \mathbf{P} \times \mathbf{E}$ imposed on the nematic director by the electric field, writing it as the sum of the torques corresponding to the isotropic permittivity and the anisotropic addition, respectively (using that the anisotropic addition of the susceptibility is $\Delta\chi^e = \Delta\epsilon$):

$$\mathbf{\Gamma}_\epsilon = \epsilon_0(\epsilon_\perp - 1)\mathbf{E} \times \mathbf{E} + \epsilon_0 \Delta\epsilon E \cos\phi (\mathbf{n} \times \mathbf{E}) = 0 - \epsilon_0 \Delta\epsilon E^2 \cos\phi \sin\phi \hat{y} \qquad (1.6)$$

In the last step I have specifically indicated that the cross product of $\mathbf{E}$ with itself is zero, resulting in a vanishing torque related to the isotropic permittivity component (as was perhaps obvious from the beginning), and we have evaluated the cross product between the director and field, amounting to $|\mathbf{n} \times \mathbf{E}| = E \sin\phi$ and directed out of the paper, in the $-\hat{y}$ direction. We can

finally rewrite the product of cosine and sine as sine for the double angle to get a compact final expression:

$$\mathbf{\Gamma}_\epsilon = -\frac{1}{2}\epsilon_0\Delta\epsilon E^2 \sin 2\phi \hat{y} \qquad (1.7)$$

Applying this expression to the situation we see that the torque turns the director into the field direction, that is the field switches **n** until it lines up with the electric field. At that point $\Phi = 0$ and the torque disappears. While the same torque would arise in the corresponding situation with an anisotropic crystalline solid instead of a nematic, the only mechanical result that can be expected is that the whole crystal, in one piece, rotates until the maximum permittivity is along the field direction, a freedom that the sample does not necessarily have. In the nematic liquid crystal, on the other hand, the sample as such is not rotated at all since its fluidity allows it to reorient its *internal* structure; only the director ligns up with the field. This switching process is fundamental for the use of liquid crystals in the displays of your computer, mobile phone, handheld electronic devices etc.

A curious thing is that in display devices the starting alignment is typically planar, that is **n**$||\hat{z}$ in Fig. 1.17 and $\phi = 90°$. If you enter that angle into Eq. (1.7) you will obtain the result that there is no torque at all on the director. From Eq. (1.7) alone one might thus get the impression that the director would stay planar despite the presence of the field. What Eq. (1.7) does not show is that the $\phi = 90°$ situation is an unstable state of maximum energy in the presence of the field, hence the director will not remain planar. The situation may be recognized from mechanics as Euler buckling, where a force is applied along e.g. a column or rod, having no effect if the force is weak since it exerts no torque on the object. But above a threshold value of the force the column becomes unstable and will buckle in some direction perpendicular to the column. In Chapter 3 we will encounter yet another analogous instability, of great importance for the process of electrospinning. In all cases it is a fluctuation that initiates the response. Although the zero-field ground state in most displays is indeed planar (a situation ensured by adequate treatment of the surfaces encapsulating the liquid crystal, cf. section 1.4) thermal fluctuations constantly turn the local director out of the display plane, by randomly varying small amounts. The angle ϕ is thus not simply $90°$ but it fluctuates around this value, any deviation resulting in a non-zero dielectric torque from the applied field trying to enhance the fluctuation and turn the director away from the electrostatically energy-maximizing planar state. The operation of displays thus relies not only on our ability to control the steady-state alignment and to apply electric fields at will, but also on the spontaneous thermal fluctuations in the director field.

Had there been no influence on the director except the electric field we would be able to reorient **n** with an arbitrarily weak field. In a display (or in a typical test cell used for research on thermotropic liquid crystals, see section 1.4) there is however a strong influence from the sample substrates, often imposing planar anchoring, i.e. the director is essentially locked in an orientation parallel to the sample plane at the bounding surfaces. Because of the elastic properties of the nematic (to be discussed below) this surface-imposed alignment is propagated through the liquid crystal in order to minimize deformations in **n(r)** which would increase the energy. This is what allows us to control the steady-state alignment of the sample in the first place. When an electric field is applied we thus get a competition between the dielectric contribution to the free energy, promoting a reorientation of the director, and the elastic contribution, counteracting any change from the initial planar-aligned state. At weak fields the elastic contribution 'wins' and the director remains unaffected by the field, at strong fields it is the other way around and the sample is switched. The borderline case is called the **Frederiks threshold** after the Polish-Russian physicist VSEVOLOD FREDERIKS, who was the first to study the switching phenomenon in detail [1]. The switching process is nowadays called the **Frederiks transition**.

The anisotropy of liquid crystals is also reflected in their magnetic and conductive properties.

As for the former, the diamagnetic anisotropy $\Delta\chi^m = \chi_{||}^m - \chi_{\perp}^m$ of a thermotropic liquid crystal most often has the same sign as its dielectric anisotropy. It is positive for calamitic and negative for discotic mesogens. In lyotropics, on the other hand, this relation as well as the reverse one occurs and lyotropic nematic phases are therefore often denoted with one of the shorthands N_C^+, N_C^-, N_D^+ or N_D^-. The index C or D refers to calamitic (or cylindrical) and discotic micelle shape, respectively, and the $+$ or $-$ superscript to the sign of the diamagnetic anisotropy.

As with dielectric anisotropy and electric fields, the non-zero diamagnetic anisotropy means that we can exert a torque on the director by applying a magnetic field. The same type of analysis as done above for electric fields yields analogous results, including the definition of a (magnetic) Frederiks threshold. While it is thus perfectly possible to build a magnetically controlled liquid crystal device (a magnetooptic device) this is rarely done, mainly because of the greater practical ease in using electric fields to control the orientation of a thermotropic liquid crystal. The influence of magnetic fields on the director orientation can be quite important in the research on lyotropics, however, since the water normally used as solvent rules out the use of electric fields for reorienting the director. The diamagnetic anisotropy is however often not large enough to allow a reorientation of higher-ordered lyotropic phases like the lamellar and columnar phases, hence field alignment in lyotropics is a realistic option essentially only when working with nematic phases.

Just like the optical anisotropy, the dielectric and diamagnetic anisotropies depend on the orientational order and anisotropy in the molecular origins of the susceptibilities, and the type of behavior sketched in Fig. 1.15 for Δn is seen also for these parameters. The numerical relations are however somewhat more complex than Eq. (1.3) since we are here considering electric and magnetic fields of frequencies much lower than those of light, extending down to the static case[30]. At optical frequencies, the electronic polarizability is the only contribution to the polarization of the material, hence it is the only molecular property appearing in Eq. (1.3). But if the field is static, or oscillating but with a relatively low frequency (kHz - MHz), permanent dipoles in the molecules contribute strongly, as they are (partially) aligned by the applied field, resulting in a much stronger induced macroscopic dipole than what would result from the electronic polarization alone (corresponding to α). Thus, while the dielectric and diamagnetic susceptibility anisotropies will still be linearly proportional to the order parameter, becoming exactly zero for $S = 0$ in the isotropic phase, the various low-frequency contributions to the macroscopic polarization or magnetization must also be considered.

The molecular origin of the macroscopic dielectric susceptibility anisotropy is thus the molecular polarizability anisotropy and the molecular dipole moment. Among most thermotropics, the latter is in fact the dominating factor. This dipole moment (as well as the molecular polarizability anisotropy) is of course present whether or not we have a liquid crystal phase, so, we might expect that we can align the molecules by applying an electric field over a sample even if it is in its isotropic state. A typical mesogen dipole moment is on the order of 5 D or about $17 \cdot 10^{-30}$Cm so the energy of interaction with a typical applied electric field (say 10 V/μm = 10 MV/m) is on the order of $-\mathbf{p} \cdot \mathbf{E} \approx 2 \cdot 10^{-22}$J. This should now be compared to the thermal energy, $k_B T$, which at room temperature is about $4 \cdot 10^{-21}$J, thus about an order of magnitude larger than the electrical interaction energy. Hence, it is clear that the alignment induced by a reasonable electric field applied over a mesogenic compound in its isotropic phase is negligible. Only because of the long-range order prevailing in the liquid crystalline phases, resulting in some 10^{23} molecules responding together in unison to applied fields, do we get the strong response

---

[30]The frequency is indeed the distinguishing factor between dielectric/diamagnetic and optical properties. In both cases, we are considering the interaction of matter with electric and magnetic fields but the oscillation frequency of optical fields is in the range of hundreds of THz, whereas it ranges from the static case up to a few GHz when we discuss dielectric/diamagnetic properties.

to relatively weak electric fields that is the hallmark of liquid crystals. While this example was worked out for the case of electric fields, an analogous estimation for the magnetic field response yields the same results, see e.g. Ref. [18].

While the dielectric and diamagnetic anisotropies are not too much affected by an inter-liquid crystal phase transition, the situation can be radically different for the electrical conductivity anisotropy $\Delta\sigma$, which typically changes sign at the transition between a nematic (having maximum σ along $\mathbf{n}$) and a smectic phase. This is because the appearance of long-range positional order greatly influences the charge carrier mobility μ, the smectic structure increasing μ (and thus σ) along the layers but decreasing it perpendicular to them. Also in columnar phases the translational order greatly affects the conductivity σ, the greatest value appearing along the columns. In most cases, this direction coincides with the director, hence there would be no change in sign of $\Delta\sigma$ expected in case of a nematic-columnar phase transition. The high conductivity along $\mathbf{n}$ in discotic columnar phases has rendered these phases particularly interesting for organic electronics. However, the fluctuations in columnar liquid crystal phases are still sufficiently large that scattering prevents the conductivity from reaching values that are truly competitive with alternative materials. When considering discotics for organic electronics, the typical desired route is to use the liquid crystal phase for achieving a columnar geometry without the differently oriented domains and the boundaries between them that pester the corresponding crystalline phases, and then vitrifying the system (it should undergo a glass transition) to get rid of the fluctuations without losing the desired boundary-free columnar geometry [15].

1.3.3   The viscoelastic properties of liquid crystals

Just like in any other fluid, flow in a liquid crystal is counteracted by a non-zero shear viscosity. In contrast to isotropic liquids, however, a liquid crystal has not one but several shear viscosities, reflecting the importance of the direction in which the flow occurs relative to the director. Moreover, a liquid crystal exhibits a type of viscosity that has no counterpart in isotropic fluids, namely reorientational viscosity: during the use of a liquid crystal display there is no bulk flow but there is collective molecular reorientation whenever the director is being switched. I will here give only a very simplified description of the most important aspects of liquid crystal hydrodynamics, considering first the viscous response to shear flow of a nematic, then looking at the reorientational viscosities of nematics and smectics.

Fig. 1.18a shows a classic set-up for defining shear viscosity: a fluid is encapsulated between a stationary bottom plate and a top plate that moves with velocity v, as indicated by the long thick arrow. Since the fluid at each plate is at rest with respect to that plate, the fluid velocity as measured in the external reference frame increases continuously from zero at the bottom plate to v at the top plate, as illustrated by the arrows increasing in length from bottom to top. The resulting shear flow is counteracted by dissipative forces described by the shear viscosity of the fluid. So far everything holds for any fluid experiencing shear flow. But we are here considering a liquid crystal, the orientational order of which must also be taken into account. It makes a great difference if the flow is along or perpendicular to $\mathbf{n}$, and for the latter case it also makes a difference if the flow velocity gradient is along or perpendicular to the director. In the 1930's these three situations, depicted by three orthogonal director orientations in Fig. 1.18a, were for the first time successfully realized for measuring the three corresponding viscosities, η_1, η_2 and η_3, by the Polish physicist MARIAN MIĘSOWICZ. In his classic experiment the flow cell was oriented in three orthogonal directions relative to a strong external magnetic field, controlling the direction of $\mathbf{n}$. Consequently, these three special viscosity values of a nematic (corresponding to an artificial situation of blocked director) are nowadays referred to as the ***Mięsowicz viscosities***.

It is probably intuitively obvious that the lowest of the three shear viscosities is η_2, corre-
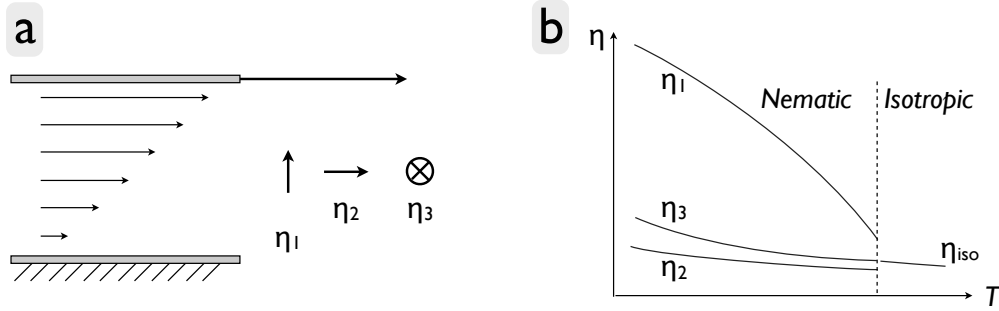
Figure 1.18: a) The three Mięsowicz viscosities are defined by considering a classic shear flow experiment, except that **n** is blocked by an external magnetic field, giving three different orthogonal director orientations with respect to the flow direction. b) The isotropic viscosity splits into the three Mięsowicz viscosities below the transition to the nematic phase, η_3 often essentially following the isotropic viscosity value, whereas η_1 is higher and η_2 lower than the viscosity in the isotropic phase.

sponding to flow along the director. The largest viscous resistance is obtained when the director is perpendicular to the flow but parallel to the velocity gradient, so η_1 is the largest Mięsowicz viscosity. The η_3 value, finally, is of intermediate magnitude, generally considerably closer to η_2 than η_1. A typical temperature dependence is sketched in Fig. 1.18b.

In a very approximate way the Mięsowicz viscosities are sufficient for understanding the basic viscous behavior of liquid crystals. For instance, if we make no particular effort to control the director orientation during flow, the flow will align the director for minimum dissipation, that is **n** will be more or less along the flow[31]. This also means that if one attempts to measure the viscosity of a nematic with a standard viscometer, one will generally measure a viscosity not far from η_2, obtaining a value on the order of a Poise (0.1 Pa s) for thermotropics. Flow alignment can be very useful, sometimes even essential, for achieving uniformly aligned samples of liquid crystals that are difficult to align by means of field application or surface action (see section 1.4), e.g. when dealing with lyotropic columnar or lamellar liquid crystals (however, for liquid crystals with positional order the minimum dissipation is along the layers or columns, thus not necessarily along **n**).

While the three Mięsowicz viscosities η_1, η_2 and η_3 bear a close resemblance to the scalar viscosity η in an isotropic liquid there are in a nematic also new types of viscosity that have no correspondence in an isotropic liquid. If the director is free to reorient, two such viscosity coefficients appear. Consider, for instance, that a magnetic field **B** has aligned the sample homogeneously with an initial director $\mathbf{n}_0$ along **B** in the xy plane. This is the minimum energy situation and there is no flow. If we now rotate the field slowly some angle Φ around the z axis the director will everywhere (except at the boundaries) reorient, following the field with a certain phase lag such that the magnetic torque balances a viscous torque that counteracts the reorientation. The phase building blocks simply rotate everywhere around an axis perpendicular to **n** without any bulk flow. The viscous torque is:

$$\Gamma = -\gamma_1 \cdot \frac{d\phi}{dt} \tag{1.8}$$

where the change in azimuthal direction ϕ is counteracted by a viscosity γ_1. This viscosity is

---

[31] In reality the situation is more complicated since the director **n** and the flow velocity v are strongly interacting. If **n** is perpendicular to the flow lines, it suffers a large torque. But even if **n** is along the flow lines it suffers a (smaller) torque and will tend to form an angle with v [18].

a Nematic

*Rotation of **n** counteracted by rotational viscosity* Υ_l

b SmA

*Rotation of **n** (induction of tilt* θ*) counteracted by rotational viscosity* Υ_θ

c SmC

*Azimuthal rotation of **n** at constant tilt* θ *counteracted by rotational viscosity* Υ_φ
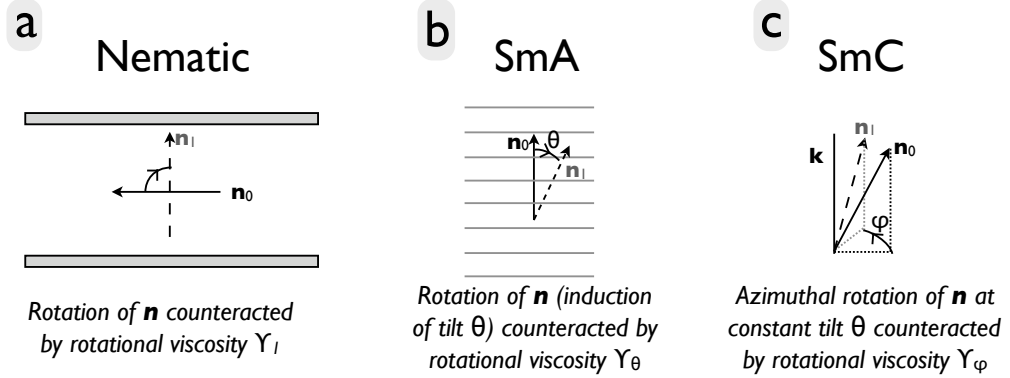
Figure 1.19: Three main rotational viscosities are considered in the study of liquid crystals, not related to bulk material flow but to reorientation of the director. In the nematic phase the most important rotational viscosity γ_1 (a) relates to director reorientation in the liquid crystal at rest (no shear flow). In SmA and SmC a related viscosity is denoted γ_θ, corresponding to an induction (in SmA) or variation (in SmC) of a director tilt θ (b). As this motion involves strong elastic forces, due to a change of layer thickness, it is only to a first approximation viscous. Finally, because the steady-state tilt in SmC is non-zero, there is a rotational viscosity γ_φ describing the (weak) resistance against azimuthal rotations at constant tilt angle (c).

called the **rotational viscosity**. An analog case occurs if we have a uniformly planar-aligned nematic phase ($\mathbf{n}_0$ along one direction in the xy plane) with positive dielectric anisotropy over which we apply an electric field in the z direction. As described above the director will now tend to reorient until it is aligned along $\hat{z}$. This rotation of the director around a perpendicular axis is again counteracted by the same rotational viscosity γ_1, cf. Fig. 1.19a. The coefficient γ_1 also determines the speed of back relaxation of the director when we take the field away (assuming that the surfaces promote the original planar alignment $\mathbf{n}_0$). It is a technically very important characteristic as it influences the maximum frequency at which a nematic device can be driven. The second coefficient of the same nature, γ_2, regards the rotation of the director in a shear velocity gradient, that is the reorientation that would be the result if we took the magnetic field away during the Mięsowicz experiment. It describes the coupling between the orientation of $\mathbf{n}$ and the shear flow.

Five independent viscosity coefficients have now been introduced for the nematic phase. Indeed, the hydrodynamics of nematics requires five independent viscosities for its general description [18] as worked out by Ericksen and Leslie. I will not discuss this description but only mention that the fundamental five viscosity coefficients $\alpha_1, ..., \alpha_5$ in this theory are very different from the viscosities introduced above. Among other things some of them can even take negative values. However, $\eta_1, \eta_2, \eta_3, \gamma_1$ and γ_2 can be expressed in these coefficients and vice versa when convenient.

In smectics the viscosities are essentially different in character. A rotation of $\mathbf{n}$ that induces a director tilt in SmA or changes the SmC tilt angle θ is normally coupled to a layer contraction [51]. Such a motion is thus very limited (if it nevertheless occurs at large magnitude it will induce a layer reorientation) but for small tilts it is useful to define a so-called 'soft mode' viscosity γ_θ for this motion, cf. Fig. 1.19 b. In the SmC phase we have another characteristic rotational viscosity, different from γ_1 and γ_2 of the nematic. Because the director is naturally tilted with respect to the layer normal we now have the possibility of reorientation of the tilting direction

φ around the tilt cone, cf. Fig. 1.19c. The corresponding viscosity is denoted γ_φ and in contrast to γ_θ it is generally very low. This is because the reorientation in question has no impact on the smectic structure and, at least in the absence of external boundary conditions, it corresponds to a change between energetically equivalent states.

1.4 How liquid crystals are studied: alignment control, field application and some other practical issues

The fluidity of liquid crystals generally requires the encapsulation of a sample for experimental studies, e.g. in a polarizing microscope. For thermotropics, the standard container is referred to as a 'cell' and it consists of two planar glass substrates assembled in parallel with a well-defined distance, often somewhat displaced laterally to one another in one direction (to allow for electric connections), cf. the left drawing in Fig. 1.20. The substrate distance (the 'cell gap') is typically in the range $1-100\mu m$. Thinner cells are very difficult to realize with accuracy, thicker are generally not very useful as the thermally induced fluctuations render thick samples scattering. Further, the director tends to become non-uniform in thick samples.

A uniform director field, preferably with a selectable direction of **n**, is of great importance to the study of liquid crystals, since the physical properties of liquid crystals to such a great extent are linked to the director. In a standard cell filled with a calamitic thermotropic this is achieved by coating the inner substrate surfaces with an appropriate alignment agent, typically polyimide or nylon for planar alignment or a surfactant for hometropic alignment[32]. The two former polymers render the surface in contact with the liquid crystal hydrophobic and the aromatic cores of the mesogens like to be in close contact with them, leading to the planar alignment. Normally one also requires a selected direction in the plane for **n** and this is most commonly achieved by mechanically rubbing the coated substrates, giving the alignment layer a uniformly grooved structure. When the cell is filled with the liquid crystal, the mesogens tend to align along the grooves, giving the uniform director orientation. If the substrates are instead coated with a surfactant, its polar (hydrophilic) head group tends to stick to the glass surface while its non-polar (hydrophobic) tail extends essentially perpendicular out from the surface. The surface will have the character of a 'forest of trees' to the liquid crystal filled into the cell and the mesogens will generally line up along the surfactant tails, ensuring the homeotropic alignment.

The above mentioned alignment layers work well for most calamitic thermotropics (although there are several exceptions). For discotic materials alignment is a much trickier issue. A clean surface may induce homeotropic alignment in some substances, but others will exhibit a random alignment. The only alignment layer known to me that can ensure a uniform planar alignment of discotic thermotropics is teflon, but such alignment layers are not easily realized and they also often do not work reliably. An alternative is to shear the substrates back and forth against each other, but this method can be difficult to apply to the highly viscous columnar phases and it requires a rather special cell construction (normally the substrates are glued together, ruling out any shearing).

For lyotropic liquid crystals the standard container is a capillary with rectangular cross section (the surfaces are 'optically flat', meaning that they are flat enough to induce no apparent distortion of the optical image), cf. the right drawing in Fig. 1.20. It is typically substantially thicker than the cells used for thermotropics (reflecting the much lower birefringence of lyotrop-

---

[32]A word of warning may be appropriate here. Commercially available cells made for homeotropic alignment sometimes have ionic surfactants as the alignment layer. While they work very well for ensuring the alignment, they will also have disastrous consequences for the ionic content of the sample, rendering investigations in electric fields difficult.
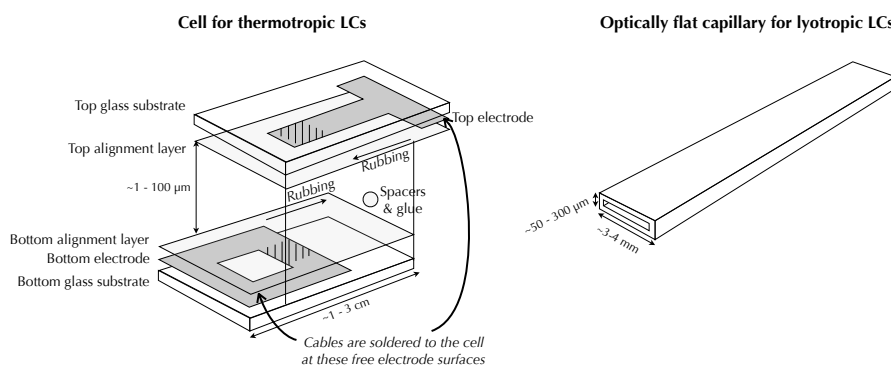
Figure 1.20: Drawings of a cell typically used for studying thermotropic liquid crystals (left) and a flat capillary used for studying lyotropic samples (right). The active area in the cell is the hatched area, defined by the overlap of the top and bottom electrodes.

ics), often in the range 50 - 300 μm. Alignment layers for control of the director in lyotropics unfortunately do not exist, a lack that makes many investigations of lyotropic samples difficult. Most often, the polar glass substrates induce a steady-state alignment that is homeotropic but this may vary from phase to phase and from amphiphile to amphiphile. While some lyotropic phases may prefer to align planarly, I know of no surface that ensures a stable *uniform* planar director orientation. Such a surface is however not *a priori* an impossibility; the current lack of it probably reflects the historical differences in the study of lyotropics and thermotropics. While the application of thermotropic liquid crystals in displays made reliable alignment control an absolute necessity, resulting in years of very strong research into thermotropic liquid crystal alignment all over the world, the types of experiments typically done in the lyotropic community have often been largely insensitive to director alignment, hence this has not been an issue with priority. Hopefully this situation is soon to change.

When uniform planar director alignment is required in a lyotropic sample, this may often be achieved by application of a strong magnetic field or by shear flow. I personally find the latter to be quite effective, although the alignment achieved is not necessarily a steady-state situation; during the course of a day or two it will often have been replaced by homeotropic alignment. The easiest way to shear-align the lyotropic phase in the capillary is to suck the liquid crystal into the capillary with relatively high speed, e.g. by attaching the capillary to a syringe via rubber tubing and sucking vacuum with the syringe until the capillary is filled.

It is often important to be able to apply an electric or magnetic field over the sample, in experiments as well as in applications. While magnetic field application is often done simply by placing the whole sample in the field of an external magnet, permanent or electrical, electric field application is generally achieved by equipping the cells with transparent electrodes, which are then connected to an external voltage source. The standard electrode material is indium tin oxide (ITO), the best compromise known until today in terms of transparency and electrical conductivity. While there are many reasons for finding replacements (especially the growing indium shortage) none of the alternative materials that have been developed so far has been able to match the performance of ITO and this is thus the electrode material used in cells as well as in any display device on the market. For quantitative measurements it may be important to know the exact effective electrode area (the 'active area') and the ITO layer is therefore usually patterned on the top and bottom substrates such that a well-defined area of overlap results, typically about 20 mm^2 in size, cf. Fig. 1.20.

The study of liquid crystals is not always done in cells or capillaries or in any other confining container. One can rather easily draw free-standing films [52] of smectic or lamellar phases (the latter however requires humidity control since otherwise the water in the lamellar film will quickly evaporate [53]) which offer some quite unique possibilities to study liquid crystals. Typically, one places a drop of the substance on a substrate next to a small hole that has been drilled through it, and then pulls it over the hole for instance with an inclined cover slip. Another very interesting container-free geometry that has been applied to study smectics is one of bubbles, achieved by blowing gas into a smectic sample until a bubble forms [54, 55]. In Chapter 3 I will describe another geometry that I have introduced myself, namely with the liquid crystal encapsulated in very thin electrospun fibers. This provides a close to one-dimensional cylindrical sample with many peculiar properties.

1.5 Liquid crystal elasticity

From solids we know the concept of elastic deformation as a non-permanent shape change and (in case of crystalline solids) a distortion of the crystal lattice. Because the interatomic or intermolecular distances in the crystal are then no longer at their equilibrium energy-minimizing value, there is a restoring force acting to reestablish the original shape as soon as the deforming force is released[33].

An ordinary liquid, in contrast, shows no shape elasticity and it can be expanded or compressed only with difficulty. It is one of the defining properties of liquids that under normal gravity they take the shape of their containers, i.e. they have no equilibrium shape and will show no resistance to shape change other than dissipative viscosity[34]. Nematics share these properties, and smectics do to a large extent. But a liquid crystal is not an ordinary liquid and it additionally exhibits elastic behavior of a new kind. While it is probably no surprise that liquid crystal phases with long-range positional order can exhibit solid-like elasticity as a response to mechanically induced changes in a lamellar, smectic or columnar structure, it may seem more mysterious at first that elastic deformation and restoration exist also in nematics. However, this is not the standard solid-like elasticity related to shape change, but an orientational elasticity connected to deformations in the director field. I will in this introductory chapter discuss only this type of elasticity, which is quite unique to liquid crystals[35]. It is the only type of elasticity existing in nematics, but it is just as important also in smectics and lamellar phases. In columnar phases the 2D lattice makes director field distortions somewhat more complicated, but also there they play a role.

1.5.1 Deformations in the director field

The undeformed elastic ground state of an achiral nematic is one where the director field is totally uniform, that is **n** points in the same direction everywhere throughout the sample. An elastic deformation in the case of a nematic results from a *local* reorientation δ**n** of the director, leading to a director field distortion transmitted over a larger scale. Since distortions in the director field cost energy, the nematic tries to reestablish the uniform director field, not by a force as in solid elasticity but by an elastic *torque*. The strength of the torque can be calculated by

---

[33]In case of amorphous solids the reason can be quite different, the most extreme being rubber, where the restoring force is of entropic origin, striving for maximum disorder of the polymer chains

[34]In free space they will actually take an equilibrium spherical shape but this has nothing to do with elasticity; it is the surface tension that strives to minimize the bounding surface of the liquid.

[35]While orientational elasticity can be defined also in solid crystals, reorientations cannot take place without also distorting the lattice, hence its weak contribution can be completely ignored compared to the ordinary elasticity.

Splay   Twist   Bend

$K_1 \left(\nabla \cdot \mathbf{n} \right)^2 \neq 0$ $K_2 \left(\mathbf{n} \cdot \nabla \times \mathbf{n} \right)^2 \neq 0$ $K_3 \left(\mathbf{n} \times \nabla \times \mathbf{n} \right)^2 \neq 0$
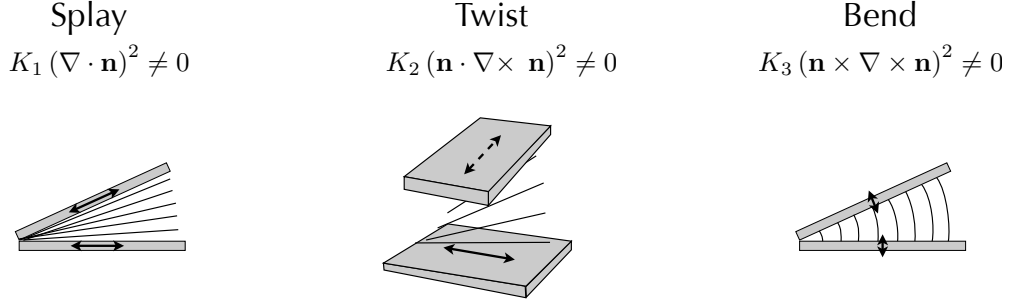
Figure 1.21: Graphical definitions of the three elementary director field deformations splay, twist and bend, together with their corresponding terms in the elastic free energy and their respective elastic constants K_1, K_2 and K_3. The drawings illustrate how each deformation can be produced in practice by encapsulating a nematic between flat substrates, the insides of which are prepared such as to ensure uniform planar or homeotropic director orientation at the substrate (the preferred director is indicated with a thick double-headed arrow). Redrawn after de Gennes and Prost [18].

differentiating the elastic free energy. The starting point for analyzing elastic deformations and their consequences in a nematic is thus to establish the mathematical expression for the elastic contributions to the free energy. This was first done successfully by Oseen in 1928, followed by the Englishman Sir CHARLES FRANK who in 1958 introduced the notation and terminology that is still used today [1]. Consequently, the result is nowadays referred to as the **Oseen–Frank theory.**

I will not go into the details of the work of Oseen and Frank here but simply state the results and discuss the meaning. The main conclusion of Oseen's work was that, neglecting surface effects, *any* generic deformation of the nematic director field can be described as a linear combination of three elementary elastic deformations: **splay**, **twist** and **bend** (the English names were coined by Frank). These three fundamental distortions, defined graphically in Fig. 1.21, are independent of one another: a twist can only be compensated by a twist of opposite handedness, not by any combination of splay and bend, and analogously for the other deformations. As a result the full elastic free energy of a bulk nematic can be written as a sum of three terms, each giving the total elastic free energy contribution due to splay, twist and bend deformations in the sample, respectively:

$$G_{deform.} = \frac{1}{2} K_1 \left(\nabla \cdot \mathbf{n} \right)^2 + \frac{1}{2} K_2 \left(\mathbf{n} \cdot \nabla \times \mathbf{n} \right)^2 + \frac{1}{2} K_3 \left(\mathbf{n} \times \nabla \times \mathbf{n} \right)^2 \qquad (1.9)$$

Each deformation is described by the appropriate combination of the vector operators divergence and curl squared (the handedness or direction of a deformation cannot play a role in an achiral system, hence linear terms are ruled out) and the energy cost for a certain deformation is proportional to the respective elastic constant, K_1 for splay, K_2 for twist and K_3 for bend[36]. These constants are very important material parameters, critically dictating the behavior of a nematic, e.g. in a display device or as a host for creating regular patterns of colloidal inclusions [56]. They have the dimension of a force, the magnitude typically in the pN range, and they must be positive (required for stability). Often K_1 and K_2 have about the same value whereas K_3 is

---

[36]Because the three elastic constants in a way represent diagonal elements in the elastic energy, they are sometimes written K_{11}, K_{22} and K_{33}. Oseen also introduced a fourth constant, K_{24}, named saddle-splay by Frank, which can be ignored far from the boundaries but is of importance e.g. in membranes.

about twice that value. It can be convenient to approximate them all equal to a single value K, an approximation referred to with the fitting term the 'one-constant approximation'.

Some aspects of the meaning of Eq. (1.9) can be made clearer by making some simplifications. First, since divergence and curl essentially are two types of spatial derivatives of a vector field, we may see each term in (1.9) as proportional to $\delta\mathbf{n}^2$, rendering an analogy with Hooke's law for solid elasticity obvious: for solid and nematic elasticity alike the energy is proportional to the square of the deformation magnitude. Second, since a spatial derivative gives us an inverse length, we see that each term in (1.9) is proportional to $1/R^2$, where R is the characteristic length of each particular deformation. This means that the energy of the deformation gets negligible if it is not strongly localized. The characteristic length is the pitch in case of a twist deformation, the radius of curvature of a bend deformation, and the distance to the 'source' of a splay deformation. Note that the former is independent of location: the energy cost of a twist deformation depends on how tightly twisted $\mathbf{n}(\mathbf{r})$ is but not on which point in the sample we consider. In contrast, the characteristic length of bend and splay is only defined once we have chosen a location, and it is not uniform. This means that the energy cost of a bend or splay deformation varies throughout the sample (which is natural, since a bend or splay locally gets less and less apparent the further away from the 'source' we are).

The $1/R^2$ dependence and the small magnitude of the elastic constants means that elastic deformations cost very little energy if their characteristic length is not very small, so little in fact that large-scale deformations are all the time thermally generated in a nematic liquid crystal. It is these constantly generated random large-scale deformations that yield the non-uniformity in $\mathbf{n}(\mathbf{r})$ of a bulk nematic, giving rise to its characteristic turbidity: since $\mathbf{n}(\mathbf{r})$ changes randomly over distances that are large (but not too large) on an optical scale, so does the effective refractive index for a light beam going through the sample, and strong scattering results.

The expression of the elastic free energy (1.9) is a most important result and it is also very useful in practice. Probably the most common use is to find the equilibrium state under a certain set of boundary conditions by minimizing the free energy, which of course must contain any other relevant terms, e.g. electric field terms. If only the elastic energy terms are present it is clear that the ground state will be one of a uniform, or at least minimally deformed director field (compatible with the boundary conditions) throughout the sample. This is the foundation for our ability to control the ground state director orientation in a simple manner, an absolute prerequisite for using nematics in devices such as displays. By using substrates prepared for inducing planar or homeotropic anchoring, in the former case with one direction in the substrate plane being the preferred direction of $\mathbf{n}$, we can control the director configuration throughout the sample. By assembling the substrates with their preferred direction non-parallel we can even induce a well-defined twist, as is the case in the classic *Twisted Nematic* display configuration.

1.6 Optical properties of chiral liquid crystals

As mentioned in Section 1.1.5 the chiral nematic, or cholesteric, phase features a helical director modulation, that is the director field is spontaneously twisted along an axis perpendicular to $\mathbf{n}$. In the chiral smectic-C-type phases the helix axis is instead perpendicular to the C-director $\mathbf{c}$, thus along the smectic layer normal. Since it is here the tilting direction that is helically modulated the SmC* director field exhibits a bend as well as twist. Obviously, both helical structures are incompatible with Eq. (1.9) which predicts a totally uniform ground state director field. As was pointed out by Frank in 1958 the expression for the elastic contribution in the free energy must be slightly modified for the case of a chiral nematic. The standard achiral twist

term is replaced by a slightly extended term that expresses the spontaneous twist:

$$G_{twist}^{N*} = \frac{1}{2}K_2\left(\mathbf{n} \cdot \nabla \times \mathbf{n} + q_0\right)^2 \tag{1.10}$$

The added term $q_0 = 2\pi/p_0$ is the wave vector of the cholesteric helix, p_0 being its natural pitch. It is a straight-forward exercise to show that (1.10) indeed gives a minimum for the helical ground state. By parametrizing a cholesteric director field with an arbitrary helical wave vector q as $\mathbf{n} = (\cos qz, \sin qz, 0)$, where we have taken the $\hat{z}$ direction as the helix axis, we find that the curl of the director, $\nabla \times \mathbf{n}$, becomes simply $-q\mathbf{n}$. Since the director is a unit vector, $\mathbf{n} \cdot \mathbf{n} = 1$, the content of the parenthesis in Eq. (1.10) becomes $-q + q_0$ and the equation can alternatively be written:

$$G_{twist}^{N*} = \frac{1}{2}K_2(q - q_0)^2 \tag{1.11}$$

In other words, the twist term of the free energy is minimized not by a uniform director field but by a twisted one, for which q is equal to the natural wave vector q_0. When the natural twist is very weak, q_0 is small and the term in Eq. (1.10) does not add significantly in case of a non-twisted director field to the energy Eq. (1.9) for a non-chiral nematic with the same $\mathbf{n}(\mathbf{r})$. For strong natural twist, however, typically with the pitch on the same order as the wavelength of visible light or smaller, the added term in Eq. (1.10) or Eq. (1.11) means a new contribution to the elastic energy that can be dominant. As Eq. (1.11) shows, if we compress or dilate the helix, the elastic energy is a quadratic function of the deviation from the natural wave vector. This means that the cholesteric helix acts as an elastic spring trying to keep the pitch equal to the natural (spontaneous) pitch p_0. Indeed, Eq. (1.11) is nothing else than Hooke's law for cholesterics, fully analogous to the well known equation of basic mechanics. This very much resembles the elasticity of smectics, keeping the layer distance constant. Although in the cholesteric case this elasticity is much weaker, it is of the same nature as in a smectic or a solid and is responsible for the fact that short-pitch cholesterics show very similar textures (e.g. focal conic defects) to those of smectics.

Chirality has several important consequences for the physical properties of liquid crystal phases, sometimes related to the helical modulation, sometimes simply to the loss of mirror symmetry. In Chapter 2 I will discuss the latter effects in some detail. Among helix-related effects in nematics can be mentioned strong optical activity and that the characteristic textures and defects of the non-chiral phases are replaced by other defects characteristic of the helical structure. If the helix pitch is short, on the order of 300 nm, then the optical anisotropy of the phase reverses compared to the non-helical analog, the helix axis becoming the effective optic axis. Moreover, the substance may show so-called ***selective reflection*** of visible light, a striking phenomenon that is both useful and beautiful. It will play a key role in the discussion in Chapter 3.

1.6.1   Optical activity and selective reflection

Few liquid crystals are as immediately fascinating as a short-pitch cholesteric. Placed on a dark background and observed by the naked eye, it can exhibit striking iridescent colors, ranging from deep violet to dark red. If the observer tilts the sample, s/he will notice that the color changes with the angle at which the sample is observed, shifting towards shorter wavelengths (more towards the violet) for more oblique angles. Moreover, the color will often also change as a result of variations in temperature, generally towards longer wavelengths on cooling. The origin of these striking colors is selective reflection. A somewhat more elaborate examination will reveal that the selectively reflected light is circularly polarized if the sample is viewed at

normal incidence, elliptical if it is tilted. Sometimes the cholesteric will not be colored because it is so strongly twisted that the reflected wavelength is below the visible region, but a careful investigator might then find that plane polarized light sent through the sample along the helix axis gets its polarization plane strongly rotated: the cholesteric is optically active, in some cases extremely strongly so.

The complete derivation of the optical properties of cholesterics is a rather advanced optics exercise, involving the solution of Maxwell's equations in the helically modulated medium (see e.g. chapter 11 of *Introduction to Liquid Crystals* by Preistley and Wojtowicz [57] where a very readable account of the procedure can be found). I will here simply state the results, beginning with the fact that we must distinguish three regimes of different behavior, depending on the ratio of the light wavelength inside the cholesteric, λ_{N*} and the pitch of the cholesteric helix, p_0:

- **$p_0 \gg \lambda_{N*}$ (*Mauguin limit*):**
  For very long helix pitch, light propagates along the helix of the chiral nematic essentially as two orthogonal linearly polarized eigenmodes (they are slightly elliptic), their planes of polarization following the rotation of the local optical indicatrix in the structure. In the $\lambda_{N*}/p_0 \to 0$ limit the formal optical 'rotatory power' $|\alpha|$ (the magnitude of the polarization plane rotation) for each mode is simply equal to $2\pi d/p_0$ (see the left diagram in Fig. 1.22), where d is the sample thickness. For a sample of thickness $d = p_0$ the polarization plane is thus rotated one full turn. This is not optical activity in the normal sense, the rotation is just given by the helix and is independent of λ. It is thus *achromatic* (a useful property of the old twisted nematic displays based on this phenomenon) but requires that the incident light is polarized according to one of the eigenmodes of the cholesteric structure in order to work. This long-pitch regime is often called the Mauguin limit, in recognition of the first analysis of the situation by CHARLES MAUGUIN [1].

- **$p_0 \approx \lambda_{N*}$:**
  As the light wavelength in the cholesteric approaches the helix pitch from the short-wavelength side the ellipticity e of eigenmode 1 grows from zero (vertical linear polarization) to near 1 (circular polarization) and then back to zero at the band edge. At the same time eigenmode 2 goes from horizontal linear polarization (infinite ellipticity) to circular. The medium becomes truly optically active, with a rotatory power that diverges, $|\alpha|$ becoming extremely high in the direct vicinity of the selective reflection band. Since optical activity can be regarded as birefringence of a medium with circularly polarized eigenmodes ('circular birefringence') the process can alternatively be described as the refractive index of one circular mode diverging, i.e. this circular polarization experiences increasing difficulties to propagate through the medium. The point of divergence is the edge of the reflection band, defined by $\lambda_{N*} = p_0 \pm \frac{1}{2}\Delta n p_0$, where Δn is the birefringence the sample would have had if the helix were unwound. Within the reflection band the light is truly separated into two circularly polarized components, the one with the same handedness as the cholesteric helix no longer being accepted by the medium and thus fully reflected, the other one fully transmitted. The attribute 'selective' refers to the rather narrow width of the reflection band. In modern terminology, the cholesteric liquid crystal has a natural *photonic band gap*. On the long-wavelength side of the selective reflection band the cholesteric is again strongly optically active, just as on the short-wavelength side, but the sign of the optical rotation has changed. While the rotation of the polarization plane was in the same sense as the helix for $\lambda_{N*} < p_0$, it is now in the opposite sense.

- **$p_0 \ll \lambda_{N*}$:**
  All light is again transmitted through the sample but both eigenmodes are now very nearly
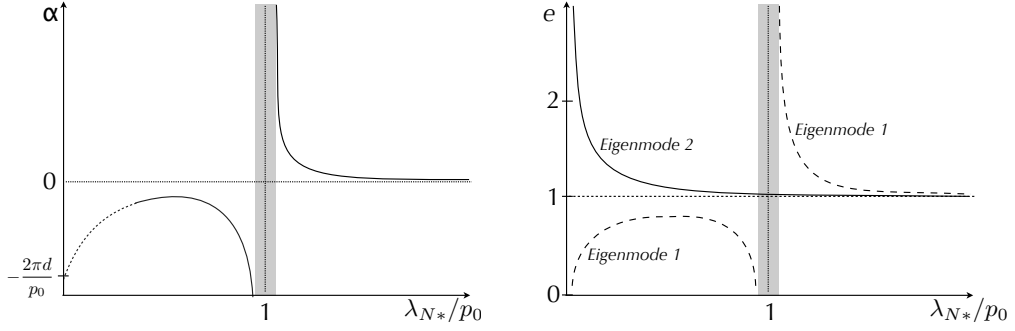
Figure 1.22: Generic sketches of the optical rotatory power α (left; $\alpha > 0$ defined as right-handed rotation) and the ellipticity e of the eigenmodes (right) of a left-handed cholesteric liquid crystal along its helix axis, as a function of the ratio of the light wavelength in the cholesteric medium to its helix pitch, λ_{N*}/p_0. The handedness in eigenmode 1 is the same as in the helix, in mode 2 it is opposite.

circularly polarized. In this regime the optical rotatory power decreases with increasing wavelength as $\alpha \sim \lambda_{N*}^{-2}$, like in other common optically active media, e.g. quartz.

These results are summarized graphically in Fig. 1.22.

The origin of the selective reflection is the optically periodic structure resulting from the helical modulation. Although the periodicity of the helix is p_0 the optical periodicity is half of this, since already a 180° turn of the director takes us back to an optically equivalent situation. Based on this periodicity we can apply the standard geometrical method well known from the analysis of x-ray diffraction from crystals to, in a simple way, obtain an expression for the relation between the selectively reflected color and the viewing angle. Not surprisingly, we thereby obtain a result that is identical to Bragg's law, but for cholesterics we must add some restrictions.

Consider the schematic cholesteric structure drawn in the left part of Fig. 1.23. The sample is aligned with its helix axis vertical and it is illuminated by light coming from the left in the picture at some arbitrary angle θ. Just as in the analysis of Bragg scattering in crystals the rays entering the cholesteric are reflected at a periodic set of planes, the spacing here being the optical period $p_0/2$. These virtual planes are defined by the local optic axis having a certain angle with respect to the plane of incidence (the paper plane in Fig. 1.23). Basic optics tells us that the reflection angle is equal to the angle of incidence (we are here not considering the path of light outside the liquid crystal). Looking at the figure we see that the lower of the two depicted reflected rays has gone a slightly longer path than the upper one, the difference being exactly $2 \cdot (p_0/2) \sin \theta = p_0 \sin \theta$. These two rays will interfere to produce the effective reflected light and the interference will be constructive if the path difference is equal to a multiple of a full wavelength. In other words, we obtain for the reflected light the result:

$$p_0 \sin \theta = m \lambda_{N*} \tag{1.12}$$

where m is an integer. We recognize this from crystallography as Bragg's law. In cholesterics Eq. (1.12) is however fully correct only for oblique incidence ($\theta \neq 90°$). For normal incidence (along the helix) all higher-order reflections are absent, leaving only the fundamental reflection ($m = 1$). Basically, the reason is the perfectly sinusoidal modulation in the N* phase: higher-order reflections represent higher harmonics of the periodic structure but a sinusoidal modulation has no harmonics, only the fundamental. For oblique incidence the modulation is no longer perfectly sinusoidal since we are not following the helix, hence higher harmonics are present in the structure and we get higher-order reflections (albeit weak).
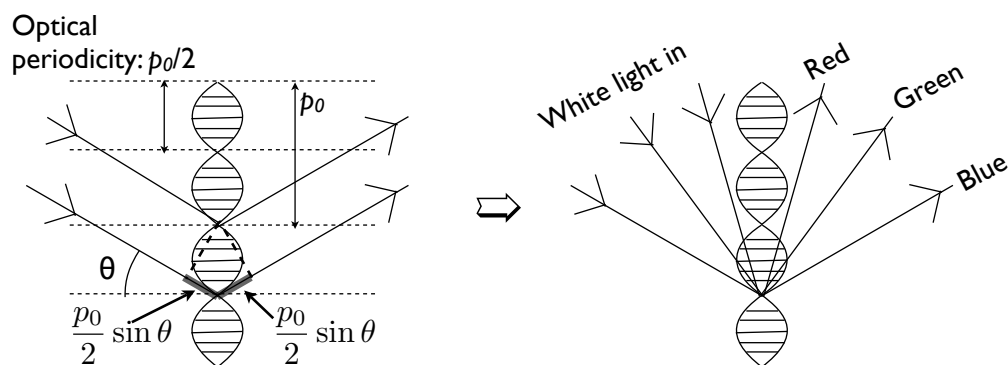
Figure 1.23: The viewing angle dependence of the color of a cholesteric liquid crystal, summarized to the right, can be understood following a simple graphical procedure, sketched to the left. See text for further explanations.

For the normal incidence case, $\theta = 90°$ and $m = 1$, Eq. (1.12) gives us the result stated previously, namely that the selectively reflected light has a wavelength equal to the cholesteric pitch. The light wavelength in the medium is shortened with respect to the wavelength in vacuum by a factor equal to the average refractive index. For typical chiral thermotropics this is about 1.5, so we can immediately estimate the helix pitch of a cholesteric that looks green ($\sim$550 nm wavelength in air) when we observe it straight on as roughly 370 nm. A decrease in the angle of incidence θ of the light leads, according to Eq. (1.12), to a decreased wavelength of the selectively reflected light. This immediately explains the observation that the color changes towards shorter wavelengths (in the direction from red to blue) if we tilt a cholesteric sample away from us, as schematically summarized in the right part of Fig. 1.23.

Since the helical modulation imposed on **n** in cholesterics applies to **c** in chiral smectic-C-type liquid crystals, also these chiral phases exhibit the special optical properties described above, including the optical activity (with sign and magnitude depending on the relation between light wavelength and helix pitch) and selective reflection. For the basic SmC* phase the quantitative results derived above regarding the selective reflection—Eq. (1.12) complemented with the restriction that $m = 1$ for normal incidence—are directly valid. For more complex chiral smectic-C-type structures the situation may be slightly different.
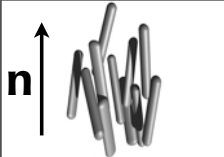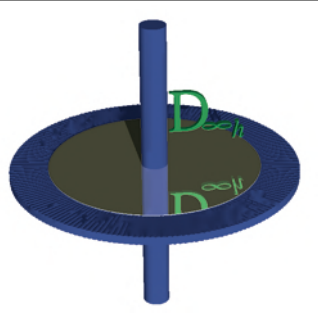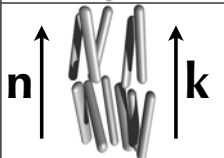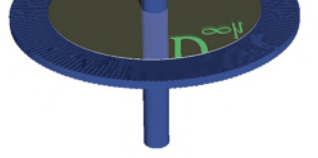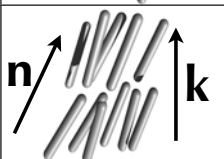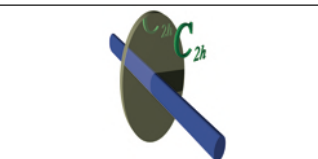
Chapter 2
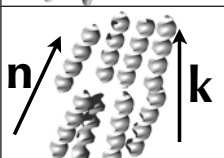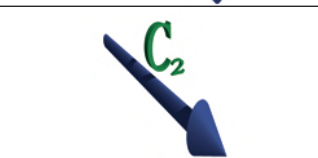
The complex phase behavior of chiral thermotropic smectics

2.1 The spontaneous polarization of chiral tilted smectics

As recognized by ROBERT MEYER in the mid 1970's [58], chirality in a layered mesophase with a non-zero tilt angle θ between the layer normal $\mathbf{k}$ and the director $\mathbf{n}$ has a quite dramatic impact on the dielectric properties of the phase. As mentioned in section 1.1.3 and as schematically illustrated in Fig. 2.1, the monoclinic symmetry prevailing in tilted smectics like the SmC phase contains only one axis of rotational symmetry, namely a C_2 axis lying in the plane of the smectic layers and directed perpendicular to the tilt plane. In an achiral SmC phase the tilt plane is also a mirror plane, hence the point group symmetry of SmC is C_{2h}. By introducing chirality, however, we remove the mirror plane and we are left with the two-fold rotation axis as only symmetry element. The symmetry of the SmC* phase is thus, on a local scale, C_2. The C_2 axis is now a polar axis (it is allowed to have a specific direction; we can draw it with an arrow head at one end) since there no more is a mirror plane perpendicular to it that would reverse a vector along C_2.

Meyer realized that, as a result of this low symmetry, the SmC* phase is spontaneously polarized, with the polarization $\mathbf{P}_s$ fixed along the C_2 direction (Fig. 2.2). Obviously, for this spontaneous polarization to appear, the mesogen must also exhibit a permanent dipole moment with a component perpendicular to the long molecular axis. This is however almost always the case. As the underlying physics is a general symmetry argument, the conclusion applies not only when the mesogen is chiral, but just as much to the case that chiral dopant molecules are added to an achiral SmC matrix. In fact, it applies even (as was realized much later [40]) to the case of *achiral* but bent-shaped molecules forming a locally chiral phase because the three directions layer normal, tilt direction and bend direction form a Cartesian system that is either right- or left-handed (see Section 1.1.5).

The direction of the polarization, parallel or antiparallel to $\mathbf{k} \times \mathbf{n}$, is a characteristic of each molecular species and opposite enantiomers of the same species have opposite directions of $\mathbf{P}_s$. The same is true for opposite bend direction at constant tilt direction in case of bent-core smectics. The magnitude is proportional to the tilt angle through $\mathbf{P}_s \propto \mathbf{k} \times \mathbf{n} = \mathbf{k} \times \mathbf{c}$, reducing to $P_s \propto \sin\theta$. For chiral smectics exhibiting a SmA*-SmC* tilting transition the magnitude of the spontaneous polarization, P_s, thus becomes a secondary order parameter of the transition, the primary being the tilt angle θ.

Phase	Molecule' organization	Symmetry
Nematic (N)		
Smectic A (SmA)		
Smectic C (SmC)		
Chiral smectic C (SmC*)		

Figure 2.1: Local symmetries of the N, SmA, SmC and SmC* phases. In the center column, the organization of the phase building blocks, drawn as straight rods or spirals, is shown in a very schematic way, in order to define the director **n** and layer normal **k**. The symmetry illustrations on the right, where the axes are axes of rotational symmetry, are drawn to correspond to the geometry of the center column. This means that the two-fold rotation axis defining the 'vertical' direction in C_{2h}, is drawn horizontal, while the 'horizontal' mirror plane is drawn vertical. The infinite number of two-fold axes in the mirror plane of $D_{\infty h}$ are represented by a large number of two-fold axes.
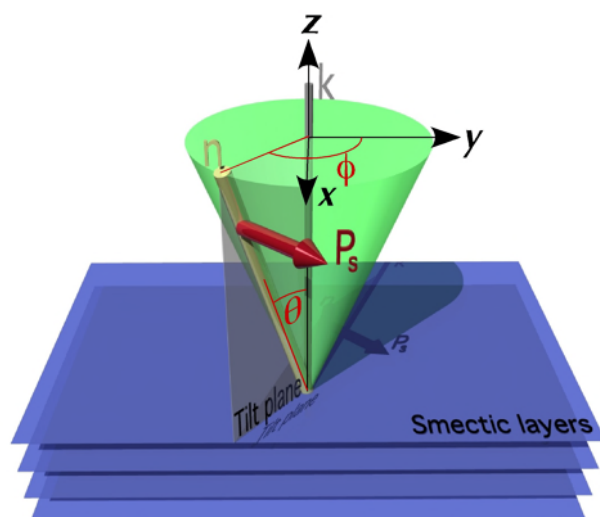
Figure 2.2: The symmetry of the chiral smectic-C phase (SmC*) allows the appearance of a spontaneous polarization $\mathbf{P}_s$. From Paper 6. (Copyright Wiley-VCH Verlag GmbH & Co. KGaA. Reproduced with permission.)

The spontaneous presence of polarization is one of the characteristics of ferroelectricity, and Meyer therefore called compounds exhibiting the SmC* phase *Ferroelectric Liquid Crystals* (FLCs). Strictly speaking, this terminology is only partially correct, an issue we will return to in Section 2.5. In order to call a medium **ferroelectric** a non-zero *macroscopic* polarization should exist in absence of a field and it should be switchable between two stable directions by an applied field [22,59]. The bulk SmC* samples studied by Meyer and co-workers in their early experiments did not quite fulfill this requirement, because of the spontaneous helical superstructure of the SmC* phase. This gives the bulk SmC* phase the *global* symmetry D_∞, not C_2. The natural SmC* phase thus has the same global symmetry as the non-polar N* or SmA* phases and all three phases are optically uniaxial (in case of SmC* assuming that the pitch is not much longer than optical wavelengths).

With $\mathbf{c}$ rotating continuously as we travel along $\mathbf{k}$, also $\mathbf{P}_s$ will rotate around $\mathbf{k}$ with the same periodicity, due to the fixed directional relationship between $\mathbf{c}$ and $\mathbf{P}_s$. This results in a complete cancellation of polarization on a macroscopic scale. Bulk SmC* samples are thus not ferroelectric in the true meaning of the word, but rather *helielectric* or *helical antiferroelectric* [22,60,61]. The term antiferroelectric refers to systems with a non-zero *local* spontaneous polarization but zero macroscopic polarization, the latter due to a cancellation on a mesoscopic scale. It is important to be aware that it is irrelevant *how* this cancellation arises. The term does not specify a particular structure of the system, only that it leads to zero polarization in the absence of field. By applying an electric field above a threshold value, antiferroelectrics are switched to a 'ferroelectric state' of uniformly aligned dipoles, such that they become macroscopically polarized, but this state is not stable upon field removal. In the case of helical SmC* a sufficiently strong field 'unwinds' the helix (typically rather weak fields suffice), resulting in the uniform non-helical ferroelectric state as long as the field is applied.

2.2   Antiferroelectric liquid crystals: anticlinic and beyond

At the end of the 1980s it was discovered that several variants of the basic smectic-C-type structure exist, in particular for mesogens with a biphenyl-ester-phenyl core and a chiral 1-methylheptyloxycarbonyl terminal chain, or its close cousin 1-(1,1,1 trifluoromethyl)heptyloxycarbonyl, on one side. The typical difference between the different variants was eventually identified to be different correlation schemes in tilt direction, given by $\mathbf{c}$, across layer boundaries. While the original SmC phase (which is still called so) has *synclinic* tilt order, that is with tilt in the same direction in adjacent layers (disregarding the slight shift resulting from the helical superstructure in case of SmC*) it now turned out that the correlation could be also *anticlinic* (opposite tilt direction in adjacent layers). This occurs in the phase that is now labelled SmC_a or SmC_a* (achiral and chiral, respectively). It can be even more complex as in the SmC_β* and SmC_γ* phases, appearing only with chiral mesogens. While there has been a vivid discussion on the number of smectic-C-type phases possible and claims of many 'new' phases appearing every now and then, to date we can regard the existence of five different variants being confirmed beyond doubt. (We here do not include the phases of bent-core mesogens, which form a very rich polymorphism distinctly different from ordinary smectic-C-type phases from linear mesogens.) The structures of the different tilted chiral smectic phases are summarized graphically in Fig. 2.3.

While the four smectic-C-type phases mentioned so far are distinguished by their different $\mathbf{c}$ correlation schemes, the fifth phase, SmC_α*, is a special case. As can be seen in Fig. 2.3 this phase is actually identical to a small-tilt and extreme short-pitch SmC* phase. It is identified as a phase of its own mainly by the fact that one finds a phase transition between SmC_α* and SmC* in several materials. Structurally, there is no distinguishing difference between the two
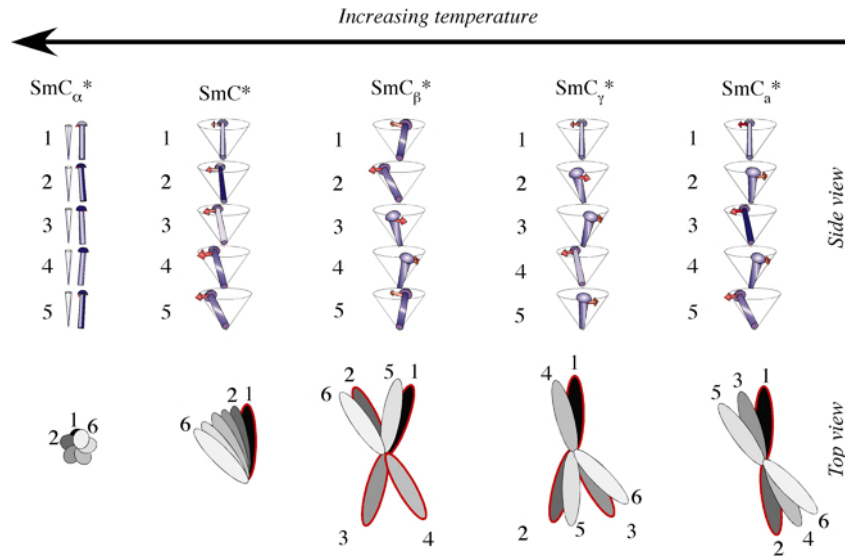
Figure 2.3: Schematic drawings of the tilt correlation schemes in the five chiral smectic-C-type phases identified beyond doubt. From Paper 6. (Copyright Wiley-VCH Verlag GmbH & Co. KGaA. Reproduced with permission.)

phases but the difference is rather one of magnitude (in pitch). In this sense the SmC_α^*- SmC^* phase transition is reminiscent of the liquid - gas transition and, just like this transition, it must be of first order due to the lack of symmetry change.

SmC_α^* is a comparatively rare phase requiring the presence of chiral mesogens. When it forms, it always does so directly below a second-order transition from the high-temperature untilted SmA^* phase and its temperature range is never more than some $5°C$. This means that the tilt angle θ in the phase is very small, never greater than about $5°$, and it changes continuously from zero at the border to SmA^* to this maximum value at the low-temperature boundary of SmC_α^*. The phase is essentially synclinic although this is pretty much at the limit of the word's meaning, since the strong helical modulation leads to a substantial variation in **c** from layer to layer, typically on the order of $60°$. It is however important to note that this does *not* mean that the phase would be characterized by great discontinuities in the normal director **n** from layer to layer: because the tilt is so small the effective angle between directors of adjacent layers is approximately equal to the tilt angle, that is no more than $5°$ at most (see a more extensive discussion of this issue in Paper 5).

Because the spontaneous polarization is linked to the tilt direction through $\mathbf{P}_s \propto \mathbf{k} \times \mathbf{c}$ any type of correlation in **c** between adjacent layers in chiral tilted smectics automatically leads to the same correlation in polarization direction. We can thus speak of the SmC^* phase as synpolar and the SmC_a^* phase as antipolar. An antipolar structure means that the spontaneous polarization is cancelled out on the scale of just two layers, rendering the macroscopic polarization zero in the absence of field. By applying a sufficiently strong electric field, however, the interaction of the spontaneous polarization with the field eventually leads to every second layer switching its polarization/tilt direction into a synclinic, synpolar structure. As mentioned above, such a ground state and such a response to electric fields is the hallmark of antiferroelectricity and the SmC_a^* phase is typically the phase we refer to when we discuss antiferroelectric liquid crystals,
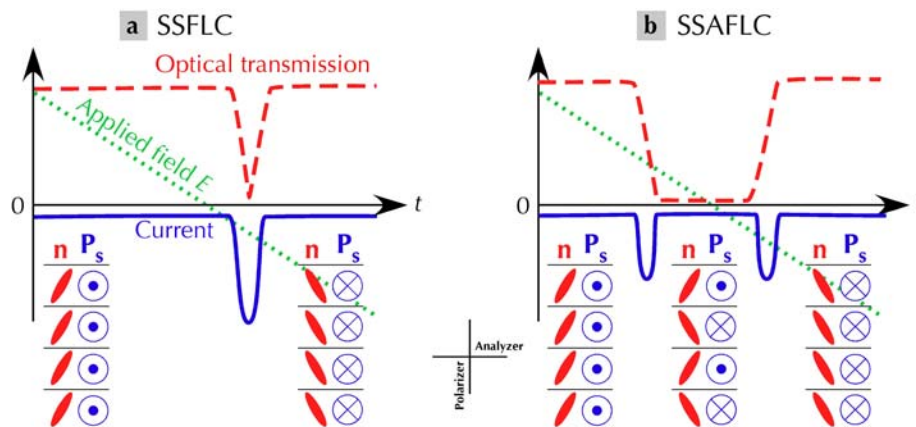
Figure 2.4: Switching non-helical (surface-stabilized) SmC* and SmC$_a$* phases with an electric field yields distinctly ferro- and antiferroelectric response curves, respectively. They can thus be called *surface-stabilized ferroelectric* and *antiferroelectric liquid crystals* (SSFLC, SSAFLC), respectively. From a book chapter by myself and F. Giesselmann [62].

or AFLCs. As a convention, however, the label AFLC is typically given to any liquid crystal forming a SmC$_a$* phase, even if this liquid crystal in addition has ordinary SmC* or other versions of smectic-C-type order in its phase sequence. Despite helical SmC* also being a special kind of antiferroelectric as mentioned above and further discussed below, materials exhibiting *only* this polar phase are today referred to as FLCs, following Meyer's original terminology. This is motivated from a practical point of view because FLCs are typically used in a structure which indeed is ferroelectric, as will now be explained.

2.3 Surface-stabilization and electric field response

Among the five members of the chiral smectic-C family, the two important ones are SmC* and SmC$_a$*. This is first because they strongly dominate the phase sequence, the others—if at all present—normally having a stability range of only a few degrees. Second, only these two phases can be usefully applied. Both have strong potential for electrooptic applications where fast response is of essence, the SmC* phase today being used in niche applications like microdisplays and portable projectors. A number of impressive prototypes of SmC$_a$*-based devices have been presented but until now none has reached commercial production. The potential, challenges and possible ways forward for applications of chiral smectics (FLC and AFLC devices, respectively) is discussed in depth in Paper 6.

When one wishes to apply FLCs or AFLCs the helical superstructure is normally a problem. The way to resolve it is to introduce the liquid crystal between closely spaced substrates inducing planar alignment. The strong surface influence leads to the helix being suppressed, as the planar alignment at the surface is not compatible with the helical modulation. Thus, **n**, **c** and **P**$_s$ are essentially uniform throughout the sample. This gives the SmC* liquid crystal in such a geometry a spontaneous *macroscopic* polarization and the structure is thus called a *Surface-Stabilized Ferroelectric Liquid Crystal* (SSFLC). Usually, the geometrical constraint for achieving the SSFLC state is that the thickness of the device (or cell, in the case of academic research) is of the order of the helical pitch. Unlike the natural helical SmC* phase this constrained structure is

optically biaxial and its slow axis (along **n**) can be switched between the two directions compatible with planar alignment by an external electric field pulse. The two directions correspond to polarization up and polarization down, respectively. If no field is applied both geometries are equally probable[1] and domains of each type can be seen to appear spontaneously as a result of the surface stabilization [60].

If one applies a triangular wave electric field over an SSFLC cell placed between crossed polarizers one will see a typical ferroelectric electrooptic response, as shown in Fig. 2.4a. Starting in the polarization UP state, in this figure corresponding to **n** being inclined in a 1-to-7 o'clock direction, the applied field is continuously decreased, passing zero without any change occurring since each SSFLC state is a stable ground state. But as the field turns negative (DOWN) a threshold level is eventually reached where the polarization of the cell is also turned downwards, resulting in **n** rotating to a 5-to-11 o'clock direction. Since the optic slow axis is along **n** both states are optically equivalent in case of the configuration of Fig. 2.4, where the polarizer and analyzer are set parallel and perpendicular, respectively, to the smectic layer normal, but during the switching a dip in optical transmission (red dashed curve) will be seen. At the same time a peak will be seen in a curve obtained by measuring the current through the cell (blue curve) because the reorientation of the dipoles corresponds to a current of $2P_s$ (from $+P_s$ to $-P_s$). While surface-stabilization is imperative for FLC devices, it is generally not required to see an electrooptic response like in Fig. 2.4a, because the rewinding of the helix once it has been unwound by applying an electric field is often a relatively slow process. During the continuous switching experiments that one typically conducts to establish the electrooptic response of a sample it rarely has time to reform and the switching is thus directly between the two ferroelectric states although the cell is too thick to suppress the helix in the ground state.

This typical ferroelectric response is easily distinguished from an antiferroelectric one, most easily achieved by surface-stabilizing the SmC_a^* phase (surface-stabilized antiferroelectric liquid crystal, or SSAFLC), sketched in Fig. 2.4b for the same experimental configuration. The starting point is the same but since the ferroelectric state is now not a stable but a field-induced one the sample will relax to the anticlinic antipolar ground state before the applied field reaches zero. Because the anticlinic variation of **n** occurs on the scale of just two smectic layers the optical effect is an average, meaning that the slow axis is along the smectic layer normal, thus along the polarizer in the experiment, and the sample will turn dark. The relaxation is again accompanied by a current peak but now only of magnitude P_s, as we are switching from $+P_s$ to zero. Only when we reach a threshold value of the negative field will the sample switch again, this time to the other ferroelectric state, again giving a peak of magnitude P_s and again rendering the sample bright, as the slow axis is no longer along one of the polarizers.

In summary, electrooptic switching studies may allow us to distinguish a ferroelectric from an antiferroelectric sample. The former has a two-state bistable switching, yielding one current peak per half cycle of the applied triangular waveform field, the latter ideally has a tri-state but monostable switching, with two current peaks per half cycle.

2.4   Induced polarization in SmA*: the electroclinic effect

In case of a chiral SmA* phase a spontaneous polarization is not allowed by the high symmetry of the phase (D_∞ does not admit polarity). The absence of mirror planes ensured by chirality is not sufficient, also a director tilt is required. However, any fluctuation of **n** away from **k**

---

[1]This is slightly idealized: in practical work with surface-stabilized SmC* samples one often has the situation that one tilt/polarization direction is slightly preferred. It requires a person skilled in the art to achieve a truly symmetric response.

obviously breaks the full rotational symmetry around **k**, temporarily and locally giving the phase C_2 symmetry. This means that a polarization in the absence of field is allowed even in SmA*, albeit only in this off-equilibrium state caused by the fluctuating director. A fluctuation $\delta\theta$ in the director orientation therefore leads, in the chiral case, also to a fluctuation $\delta\mathbf{P}$ in the polarization.

Via **P** the tilt angle thus couples to an electric field **E** in the smectic layer plane, allowing us to bias the fluctuations in θ by applying a field **E** perpendicular to **k**. The result is that we can field-induce a non-zero director tilt $\theta_{ind} \neq 0$ in the SmA* phase, in a direction $\mathbf{c}_{ind} \perp \mathbf{E}$, an effect referred to as the **electroclinic effect** (also discovered by Meyer [63]). However, since we rely on the spontaneous fluctuations in θ and **P** to do this, and since such fluctuations are generally very small as they disturb the smectic layer geometry (see section 1.3.3), the electroclinic effect is often negligible in magnitude. Often but not always: the exception is when we get close to a phase transition to a tilted (smectic-C-type) phase. It is a general property of second order phase transitions that the magnitude and relaxation time of the order parameter fluctuations out from the equilibrium value diverge on approaching the transition temperature from either side ('critical behavior'), the temperature dependence being characterized by a critical exponent [64]. The SmA*-SmC* transition (or variants where the tilting transition is to another chiral smectic-C-type phase) is no exception and, as a result, the magnitude of the electroclinic effect gets important close to this transition, which most often is second order or weakly first order. The angle θ_{ind} that we can achieve in a sample aligned in bookshelf geometry is a linear function of the electric field strength up to a saturation value. Close to the tilting transition this can be quite high, often $10°$ - $15°$.

2.5   Do we need to bother about helielectricity?

The terms ferroelectric, antiferroelectric and helicoidal antiferroelectric are taken over from the research on ferroelectricity and antiferroelectricity in solids, where these phenomena have a much longer history than polar phenomena in liquid crystals. In the field of chiral smectics it i not uncommon that this history and the established definitions are ignored, helical SmC* often simply being referred to as an FLC, or ferroelectric liquid crystal. In most cases this is perfectly fine from a practical point of view, since the phase can produce a ferroelectric response if surface-stabilized, but one should be aware of the approximation that one does when using this terminology and that there are cases when it really cannot be applied. In trying to understand the complex electrooptic response of an unusual chiral tilted smectic with very short helical pitch (Paper 1) I realized that this was such a case. When the pitch gets very short the antiferroelectricity of the helical structure is really not just a semantic issue but it must be explicitly taken into account in order to correctly interpret experimental data.

To demonstrate this in a convincing way I prepared a binary mixture of chiral smectics that produced an ordinary SmC* phase with the required very short pitch (here around 300 nm), and studied this by means of dielectric spectroscopy and switching studies (Paper 5). The dielectric spectra clearly proved that the phase was SmC*.The antipolar nature of a SmC_a* phase renders the dielectric response of that phase very weak, whereas that of SmC* can be strong, as was indeed the case here, with a dielectric susceptibility of about 90 in the temperature range of interest, cf. Fig. 2 in Paper 5. Yet a distinct antiferroelectric electrooptic switching curve could be detected in thick cells, as shown in Fig. 2.5. While the current response was not the ideal antiferroelectric curve shown in Fig. 2.4b, mainly due to the effect of the cell surfaces that delay the relaxation into the helical structure, dual peaks per half-cycle are easy to recognize. With a simple numerical simulation I showed in the paper that the double-peak current response from
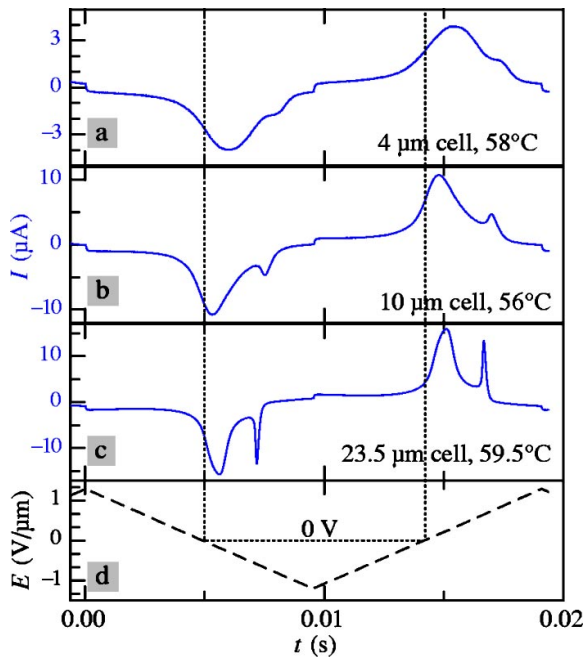
Figure 2.5: Current response of a very short-pitch SmC* phase in cells of three different thicknesses. Two peaks per half cycle can clearly be distinguished in the thicker cells, demonstrating the antiferroelectric aspect of the helical superstructure, and even in the thinnest cell a remnant of the second peak renders the current response atypical for ferroelectric samples. © 2005 American Physical Society.

the helielectric SmC*structure can become very close to that of a non-helical antipolar SmC_a* phase (Fig. 5 in the paper and the related discussion). The helix unwinding/rewinding is capable of generating a peak with a magnitude of about $0.8P_s$.

This observation is important because it very clearly demonstrates that an antiferroelectric switching response is not necessarily a sign of an *antipolar* structure, it only indicates that the sample that in one way or another is antiferroelectric, but this includes helical SmC*. . Very often in smectic liquid crystal research, however, antiferroelectric switching has been taken as a 'proof' of anticlinic/antipolar local structure. One exotic example where this understanding becomes important has already been mentioned, namely the material studied in Paper 1 (to be discussed in more detail below), but another example of much more general relevance is given in the second part of Paper 5, which I now wish to briefly summarize.

As mentioned in Section 2.2 the SmC_α* phase is structurally equivalent to an extreme short-pitch SmC* phase. From the above reasoning we thus understand that one can expect an antiferroelectric electrooptic response from the phase, which is indeed what is seen and what had created a substantial confusion about the nature of the phase over some 15 years of research efforts. Specifically, the phase was often reported to show an antiferroelectric response at high temperatures whereas it became more complex on cooling [65] stimulating researchers to propose a number of complex models for how the local tilt direction correlation would vary on cooling. This is however in contradiction with the dielectric response of the phase (Fig. 6 in Paper 5), which is a fingerprint of an extreme short-pitch SmC* phase (as it should be). But since the antiferroelectric aspect of the helical modulation was ignored these complex models resulted.

In Paper 5 I studied the AFLC compound MHPOCBC [4'-Nonanoyloxy-biphenyl-4-carboxylic acid 4-(1-methyl-heptyloxycarbonyl)-phenyl ester] by dielectric spectroscopy and electrooptical switching. This compound is very convenient because it exhibits a relatively broad SmC_α* phase and no SmC* phase. The phase directly following SmC_α* on cooling is instead the antipolar SmC_a*. As the electrooptic response was monitored on continuous cooling from SmA*, through SmC_α* into SmC_a*, the SmC_α* phase was easily recognized by a clear antiferroelectric response
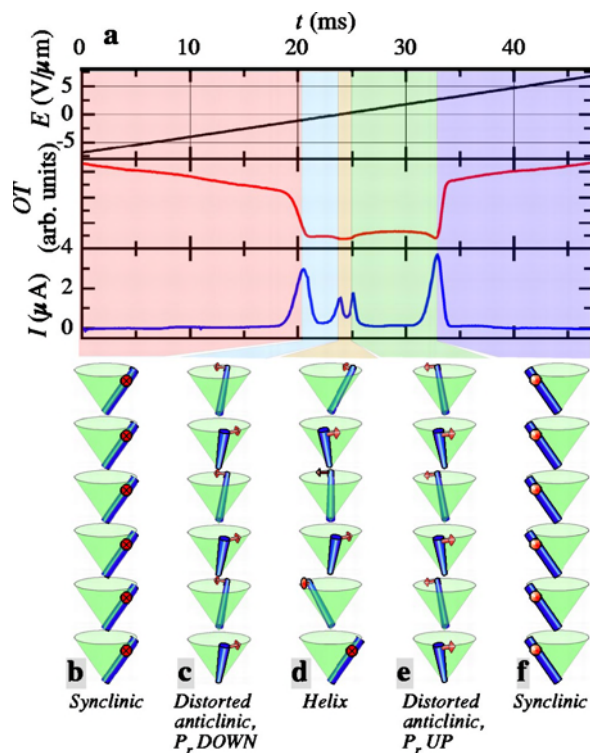
Figure 2.6: Current I (lower curve) and optical transmission OT (middle curve) at λ=633 nm through a 10 μm MHPOCBC sample between crossed polarizers (parallel and perpendicular to the layer normal), during an increasing half period of the applied 10.5 Hz triangular wave field (top curve), at 99 °C. At the bottom schematic cartoons illustrate the five different states gone through during the switching process. From Paper 5. © 2005 American Physical Society.

(Fig. 7 in the paper) with two distinct peaks that grew in magnitude on cooling, reflecting the increasing value of P_s. Only very close to the transition to SmC_a^* did the response become more complex, reflecting some degree of phase coexistence. The dielectric spectroscopy as well as the electrooptic switching signatures of MHPOCBC can be perfectly explained by considering the response of a helielectric phase to weak (dielectric spectroscopy) and strong (switching studies) electric fields. The combination of the data rules out any locally antipolar order. The previously reported complex switching behavior in the low-temperature range can easily be understood as a result of phase coexistence with the phase following on cooling. If this is SmC*, as is most often the case, then phase coexistence can indeed produce very complex-looking switching data, but these should be understood simply as artifacts from a mixture of phases.

How can we be so sure that SmC_α^* is not locally antipolar? The phase shows, after all, an antiferroelectric electrooptic response that is very similar to that of the ordinary, antipolar SmC_a^* phase. There are two features of the experimental data from MHPOCBC that clearly shows that the local order is not antipolar. First, as already mentioned the dielectric spectroscopy data are perfectly described by a model for an extreme short-pitch SmC* phase (Paper 5, Fig. 6 and the related discussion) whereas a locally antipolar structure, as in SmC_a^*, would give the same very low dielectric permittivity as seen in the latter phase. The difference is very clearly seen in Fig. 6 of the paper. Second, MHPOCBC is particularly interesting because the helical pitch is unusually short also in the SmC_a^* phase (below 300 nm) such that we actually see *both* types of antiferroelectric switching, helielectric and antipolar, simultaneously! Had the SmC_α^* phase had a locally antipolar structure, we should have had the same response in this phase, but there we have a simple antiferroelectric response.

The double antiferroelectric switching in the SmC_a^* phase of the material is best understood by looking at Fig. 2.6, containing the optical and current response from MHPOCBC in the SmC_a^*

phase, a few degrees below the transition from SmC_α^*. Four peaks are clearly seen in the current response and also the optical response shows five different regimes, a result of the twin-scale antiferroelectric switching. Starting at the fully switched, synclinic state for maximum negative applied voltage (red regime, first cartoon) at the left of the figure, letting the applied voltage increase continuously, we will before reaching zero voltage have a relaxation of the synclinic structure into one that is almost anticlinic (blue regime, second cartoon). This gives rise to the first current peak and the optical transmission strongly decreases as the optic slow axis is now almost along the polarizer. But the helix has not yet been reformed and the liquid crystal is thus not in its ground state. Moreover, the field, albeit below threshold for the synclinic state, distorts the anticlinic structure such that a small non-zero polarization exists even on a local scale [66]. In MHPOCBC the helix is so short that the tendency to rewind it when the electric field disappears is very strong (the helix has a 'large spring constant'), such that it in fact does rewind during the switching process in the experiment. When this happens, it gives rise to the second current peak and a slight further decrease of optical transmission, as the optic axis is now really along the polarizer, and we get the structure shown in the third cartoon, corresponding to the beige regime in the upper panel. The current peak is much smaller because the polarization that is at its origin is only the small residual polarization that resulted from the slightly distorted anticlinic structure.

As the applied voltage continues to increase, now reaching non-zero positive levels, the helix again gets unwound, this time with the resulting residual polarization pointing in the opposite direction. Again we get a small current peak, a slight increase in optical transmission, and we get the fourth cartoon structure, essentially stable throughout the green regime. This is then replaced by the other synclinic, ferroelectric state drawn in the fifth cartoon once the voltage reaches the threshold level, producing the final current peak and again increasing the optical transmission substantially.

This is the way a structure that is antiferroelectric on two mesoscopic scales, on the local bilayer scale and on the helical superscale, responds to an electric field of varying magnitude. Since such a response is not seen in SmC_α^* we can safely assume that the only type of antiferroelectric order prevailing in this phase is the helical modulation, with exceptionally short pitch.

2.6   Is there life between syn- and anticlinicity?

Although SmC and SmC_a are two closely related variants of the same family of smectic phases their difference in C-director correlations render their structures clearly incompatible. It is not at all obvious what one should expect upon mixing the two phases with each other (more correctly, mixing a material forming no smectic-C-type phase other than SmC/SmC^* with one where SmC_a/SmC_a^* is the only smectic-C-type phase), creating a frustration as a tendency towards synclinic ordering is overlaid with one towards anticlinic. How will the system go from syn- to anticlinic order as the mixing ratio is varied? This question was the starting point for a series of investigations I took on at the University of Stuttgart in 2003-2004 in a project funded by the Alexander von Humboldt foundation, resulting in five main publications (Papers 2, 3, 4, 6 and 7). Two related papers were published in 2007 (Paper 8) and 2009 (Paper 9) but these had slightly different starting points and main themes.

The mixtures were investigated mainly by optical microscopy texture studies and dielectric spectroscopy, together giving enough data to determine the phase diagram. Contact samples between the materials played a particularly important role as, due to the distinctly different quasi-homeotropic textures of the different chiral smectic-C-type phases (related to very different pitch lengths), they allow a good estimate of the phase sequence across the whole mixing ratio
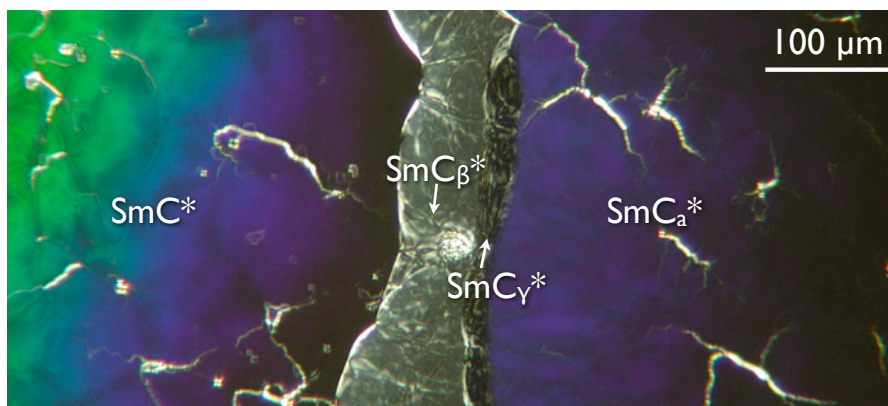
Figure 2.7: A contact sample between the synclinic material (S)-DOBAMBC (left side) and the anti-clinic (S)-TFMHPBC-11 (on the right) in quasi-homeotropic alignment viewed at $66.5°$C in transmission polarizing microscopy with slightly decrossed analyzer. The SmC* and SmC$_a$* phases are recognized by their strong colors, originating in their helix pitch being in the right range for giving visible selective reflection/transmission, whereas the intermediate phases have defect-rich pure grey-scale textures (ranging from bright white to dark black) since the helix pitch in these phases is very long. The molecule structures are given in Paper 4.

at a single glance, cf. Fig. 2.7.

From single-component AFLCs we know of two paths between syn- and anticlinic. Either there is a direct transition (which must be first order [62]) or there is a transition via the two phases SmC$_\beta$* and/or SmC$_\gamma$* (Fig. 2.3). Their location between SmC* and SmC$_a$* early on led to the natural suggestion that these phases appear as a result of the frustration between syn- and anticlinic order, somehow mediating the conflicting structures, and they are often called the 'intermediate' phases.

These two paths were thus more or less what we expected to encounter during our mixture experiments, although previous experience had indicated that the intermediate phases were very sensitive to sample purity, optical [67] as well as on a more general level [68], suggesting that the route via SmC$_\beta$*/SmC$_\gamma$* would be rather rare. The conclusions from our large and systematic mixing experiment study (Paper 4) were thus in two respects somewhat surprising. First, the path via intermediate phases turned out to be the most common path encountered, even when one mixture component was achiral, discarding the idea that mixing *per se* would destabilize these phases and making the requirements on molecular chirality less clear. Second, these two paths were not the only possibilities for passing from syn- to anticlinicity. Three different paths were in fact identified during the course of the study:

1. direct transition from SmC* to SmC$_a$*,

2. transition via induced 'intermediate' phases SmC$_\beta$* and/or SmC$_\gamma$*,

3. separation of syn- and anticlinic order by an extension of the non-tilted SmA* phase downwards in temperature.

The third option apparently occurs when the incompatibility between the two types of SmC-type order is so strong that the mixture system escapes the frustration entirely by removing its source: the director tilt. The extension of the temperature range without tilt could in these cases be

quite impressive, typically more than 50 K, rendering Sm-A^* stable at temperatures where both pure components are crystalline. The tendency to decrease the director tilt was actually observed also in the systems following the other paths (including cases where neither single component featured SmA/SmA* in its phase diagram), but the effect was then much less dramatic.

While the transition via intermediate phases was the most common path, the least common was the direct transition from SmC* to SmC$_a$*. For the combinations investigated (five different anticlinics, all chiral, and nine synclinics, seven of which were chiral) we could not see any pattern regarding the choice of anticlinic and the path followed, possibly because the anticlinics were too similar to each other (anticlinic-forming rod-shaped smectogens are much less common than those forming synclinic tilted phases). In terms of the synclinics we could identify certain trends, first and foremost that the path via subphases seems to require a second-order SmA-SmC transition or the absence of SmA phase of the synclinic component. Experiments with synclinics with a first-order SmA-SmC transition in most cases resulted in the path via extended SmA* phase, but in a few cases also direct SmC*-SmC$_a$* transitions were observed.

The most important observation in this study is the dominance of the path via SmC$_\beta$* and/or SmC$_\gamma$*, confirming that these phases are indeed intermediate in character, with structures resulting from the frustration that arises when the tendencies for syn- and anticlinicity are almost perfectly balanced. This balance is extremely sensitive; as soon as one clinicity dominates slightly over the other the intermediate phases disappear, explaining why they in single-component AFLCs exist over only some 1-5 K. In this case it is a variation of temperature that shifts the system from predominantly synclinic to predominantly anticlinic, and the frustrated situation cannot be extended much in temperature. Our alternative approach where we induce the phases via mixing has the benefit that we are at liberty to tune the balance almost independently of temperature. This allowed us to extend the temperature range of these phases by an order of magnitude, finding mixtures where either the SmC$_\beta$* or SmC$_\gamma$* phase was present over more than 50 K! Obviously this greatly facilitates the study of these phases.

In Paper 8 we presented an unexpected complementary experiment to the above study. While the main purpose of this work was to investigate the effect of single-wall carbon nanotubes (see Chapter 4 for a detailed discussion about these fascinating particles and why they are interesting to add to liquid crystals) on chiral smectics, we discovered that both intermediate phases were induced when we mixed a certain AFLC mesogen, exhibiting SmC* and SmC$_a$* in its phase sequence, with a *nematic* mixture, having no smectic phases at all and being essentially non-chiral (it had one tenth of a percent of a chiral dopant added). The complex phase diagram arising in this mixture was quite unexpected, corroborating our previous conclusion that neither the sample purity nor the chiral interactions must be exceptional to see the intermediate phases. Mixing in fact appears as a means of stabilizing rather than destabilizing the intermediate phases, and it can be done with a large share of achiral mesogens, the chiral ones not being in any sense extraordinary in terms of their stereogenic centers.

The result of mixing however strongly depends on which components are mixed. In this study the fluorinated tail of the AFLC mesogen, and the lack of perfluorinated mesogens in the nematic mixture, were probably key to the result. This combination is likely to induce a microphase segregation that greatly enhances the smectic order. When adding the nanotubes, on the other hand, they were strongly destructive for the phase sequence. Even 0.002 wt.-% CNTs was sufficient to destroy all smectic-C-type phases but SmC*.

An interesting side track to this project, devoted to the helix handedness in SmC* and SmC$_a$*, respectively, was a collaboration with the theoretical physicist Mikhail Osipov at the University of Strathclyde, Glasgow, UK (Paper 7). It had long been known empirically that the handedness of the helical superstructure always reverses at a transition between SmC* and SmC$_a$*, alternatively within the intermediate phase range if these appear in between, but until our collaboration the

phenomenon had never been investigated in detail. The discrete phenomenological theory worked out by Prof. Osipov, demonstrated and confirmed by my mixture experiments, showed that the helical twisting changes sense as a consequence of a transition between syn- and anticlinic order, hence the empirical observation of helices with opposite handedness on the two sides of this transition is indeed to be expected.

Apart from giving a formal explanation to this phenomenon, we could draw some further interesting conclusions from this work. First, an unanticipated result of the theory was that an effective elastic constant governing the helical twisting can get very close to zero in case the switch from syn- to anticlinic preference occurs in a regime of low director tilt angle, as is the case close to the SmA* phase. The result would be an extremely short pitch, much shorter than is known from usual SmC* phases. Extremely short pitch helix, low tilt and vicinity to an anticlinic phase are the hall marks of SmC_α*, hence the theory in principle gives a very simple explanation to the appearance of this phase.

Second, since the helix handedness must change at a transition between syn- and anticlinic order we could induce a very interesting frustrated situation by mixing a chiral synclinic with a chiral anticlinic, both having the *same* helix handedness on their own. The only way for the system to resolve this conflict is to remove the helix in some way, either by removing the tilt (extending the SmA* phase) or by letting the pitch diverge to infinity, where left- and right-handed become degenerate. The experimental result was the latter solution, although the former might of course happen for other choices of mixture components. In any case, this is an observation of considerable practical relevance, because it is of great importance for devices based on FLCs and AFLCs to keep the helical pitch long, such that the structures can be reliably surface-stabilized at cell gaps compatible with large-scale production technology. This has turned out to be very difficult for AFLCs in particular. Simply mixing with an achiral mesogen or with the opposite enantiomer does not solve the problem, as this also reduces the spontaneous polarization and may have other adverse effects. Based on our study we could suggest the alternative approach to mix chiral synclinics and anticlinics with the same helix handedness. Because the helix must diverge at the clinicity transition, without any reduction in spontaneous polarization, it should be easy to prepare FLC or AFLC mixtures with very long pitch in this way.

2.7 Nematics and AFLCs: can we have both?

A challenge when it comes to applying smectic liquid crystals is that they are more difficult to align uniformly in a well-controlled way than nematics. A standard approach in FLC device production is to use a mixture that exhibits a SmC* phase over the full device operating temperature range but a nematic (or, more precisely since the mixture is chiral, cholesteric) phase at higher temperature, allowing the liquid crystal to be well aligned at high temperature before cooling down the device to room temperature. This solution has unfortunately turned out not to be applicable to AFLC devices because until this day there are no smectics from rod-shaped mesogens that combine the SmC_a* phase with a cholesteric phase at higher temperatures. This can be understood relatively easily in terms of the requirements on smectic order imposed by the anticlinic structure. Low smectic order, that is strong fluctuations of molecules between adjacent layers, would place a large share of the molecules in an undefined state, where their tilt direction is not well defined since they are located at the boundary between two layers with opposite C-directors. Thus we can expect that anticlinic phases appear only in case of high smectic order, but this is of course very far away from a nematic, exhibiting no positional order whatsoever. A system that should combine a nematic phase with a SmC_a* phase must allow large positional

fluctuations at higher temperatures but provide high smectic order at low temperatures. Can any mesogen provide such a combination?

In the light of this situation it came as a great surprise when Isa Nishiyama and co-workers in 2002 published the first observation of an AFLC with a cholesteric phase. This article obviously triggered a large interest in the smectic liquid crystal community. The reaction of the synthetic chemist Michael Wand, at the time at the microdisplay development company Displaytech Inc. in Longmont, USA, close to Boulder where I was staying in the end of 2002 for my first post-doctoral research stay, was to resynthesize the compound and he was kind enough to give me a sample for investigation. Somewhat foolishly, I thought this would be a more or less 'routine' investigation, testing for the typical characteristics of a nematic phase on the one hand and SmC_a^* on the other. Very soon I realized, however, that this compound—code-named BMHBOP-8—is truly unique and that it would not reveal its secrets so easily. Several months of intense investigations later I had understood that this exotic compound represents something entirely new in liquid crystal research. Thanks to its symmetric structure with two identical chiral mesogenic moieties linked via a flexible central octylene spacer (Fig. 2.9) the compound acquires a chameleon-like behavior: it seems to change conformation between rod- and bent-shape at the cholesteric-smectic transition. As a result, the behavior of the material combines characteristics of ordinary rod-shaped mesogens with the peculiar properties of bent-core smectics. While Dr. Nishiyama had not quite solved the problem of finding a useful AFLC with a cholesteric phase in designing BMHBOP-8, he had produced a compound presenting a new type of phase transition between nematic and smectic, providing a striking demonstration of how difficult it can be to guess the molecular conformation of a mesogen. Moreover, it proved a perfect illustration of how important it is to recognize helical antiferroelectricity, as discussed in Chapter 2.5.

I first spent considerable time behind the polarizing microscope, continuously discovering new unexpected textures as I varied sample thickness, cooling rate, electric field treatment, etc., cf. Fig. 2.8 and 2.10 - 2.11. Regardless of sample thickness the cholesteric phase was black in planar-aligned samples and insensitive to rotation of the sample on the microscope table, suggesting that it formed with the helix along the viewing direction and that this helix had a very short pitch, giving it colors neither from selective reflection (the pitch is too short) nor from birefringence (we are looking along the optic axis). At the transition to the smectic phase a transitional texture typically formed, exhibiting brightly colored domains reminding of the texture of a blue phase (Fig. 2.8e) but this was soon replaced by a planar smectic texture in thin cells or a combination of homeotropic and planar areas in thick cells. The loss of planar alignment was at first very bewildering but once the unusual conformational change behavior of the molecule was accepted also this could be explained, as described below.

Although BMHBOP-8 doesn't have a distinctly bent core, its planar smectic textures (Fig. 2.8 d-f shows some representative examples) very much resemble the characteristic 'myelinic' textures that are often observed in phases formed by bow-shaped mesogens [39] and this was the first clue that BMHBOP-8 adopts a bent shape in the smectic phase. On the other hand, the fact that it exhibits a cholesteric phase at high temperatures suggests that the molecule is rod-shaped in this phase since the bent shape promotes smectic ordering, hence it seemed there was a change of conformation at the nematic to smectic transition. Such a conformational change is unusual in liquid crystals and would require that the two conformations are very close in energy. That this is indeed the case for BMHBOP-8 was confirmed by MOPAC/AM1 computer modeling for variations of the torsional angle around the bond at the center of the octylene spacer, revealing three energy minima. As expected, the global minimum corresponds to the linear molecule shape with an all-*trans* spacer, but there are in fact two bent conformations giving local energy minima almost as low as for the linear conformation, cf. Fig. 2.9. The balance between bent and straight molecule shape is thus very subtle and it is not surprising that it can be biased by the drastic
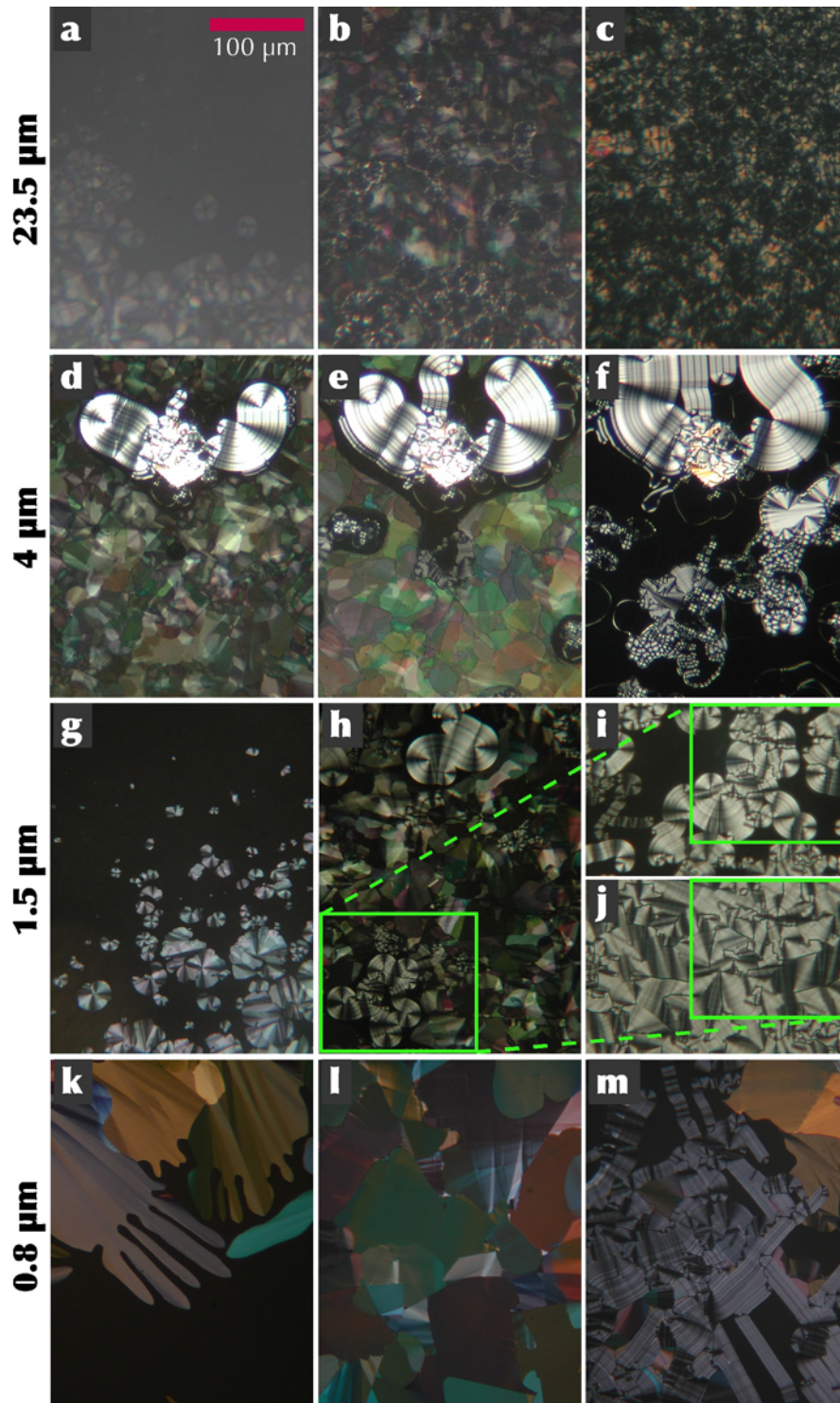
Figure 2.8: An overview of the textures forming in the 'chameleon' liquid crystal BMHBOP-8, as a function of cell gap. Pictures a, b, d, e, g, h and k are all taken at the temperature T_0 of the N*-SmC$_s$P$_F$* transition, those in the first column at the beginning and those in the second 10-30 s later. The other pictures are taken at (l) $T_0 - T = 0.8$ K, (f), (i) and (m) $T_0 - T = 1$ K, (j) $T_0 - T = 3$ K and (c) $T_0 - T = 4$ K. Reprinted with permission from Paper 1. Copyright 2004 American Chemical Society.
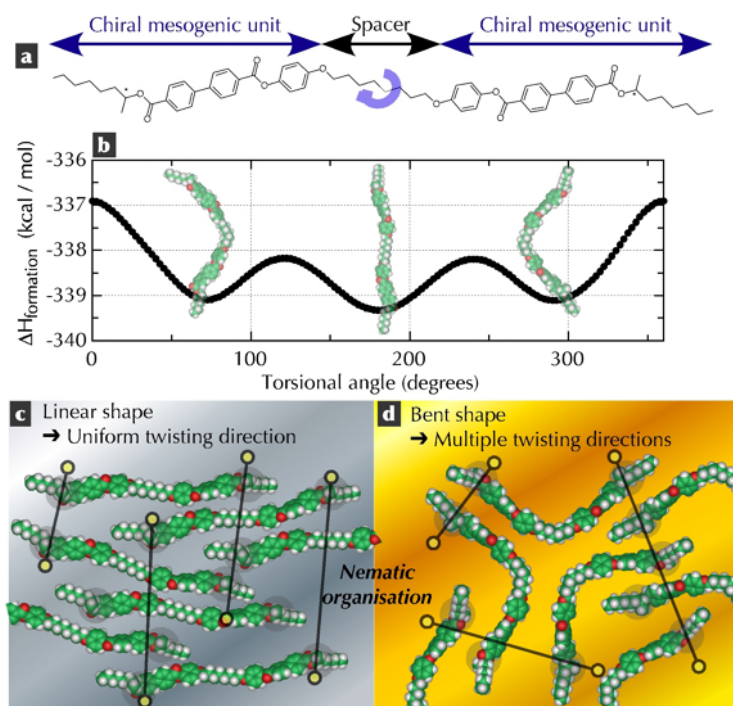
Figure 2.9: (a-b) The energies of rod- and bent-shaped conformations of BMHBOP-8 are very similar, making conformational switching as a result of a phase change and the corresponding change of molecular environment plausible. (c-d) A change between rod- and bent-shaped conformations also has strong implications for the chiral interactions of this molecule, with a stereogenic center at each end, possibly explaining the transitional 'blue phase-like' texture seen at the N*-SmC$_s$P$_F$* transition. Reprinted with permission from Paper 1. Copyright 2004 American Chemical Society.

change of environment that a nematic-smectic transition entails.

With this assumption it became possible to tie together all of the unique textural observations as well as some other peculiar effects seen in this compound. For instance, apart from explaining the myelinic smectic textures as a result of the bent molecule shape, the change in conformation also provided an explanation to the colorful transitional texture and the unexpected change from planar N* alignment to homeotropic smectic alignment in thick cells. As the molecules start bending at the transition to the smectic phase (which typically starts at the cell substrates, where the positional order is the highest) the two stereogenic centers in each molecules suddenly do not act in concert, but rather in directions close to perpendicular to each other. In other words, a complex situation arises where the director field can twist in all directions. In such a case we will have domains with very different helix axis directions, and the pitch is likely to be longer as both stereogenic centers cannot contribute constructively to the same helix formation. These two phenomena can explain the colorful transitional texture, present until the last remnants of cholesteric ordering are gone. The simultaneous twisting in all directions also leads to the loss of uniform planar alignment in thick cells, explaining the combination of homeotropic and planar domains in these cases. In thin cells the substrate influence is strong enough to promote planar ordering also in the smectic phase, hence the smectic phases becomes planar-aligned throughout these samples.

With smectic phases formed by bent molecules we concluded that these could not be the ordinary smectic-C-type phases but must rather belong to the class of phases formed by bent-core smectogens, with the addition that the molecule here is chiral, hence they were classified as SmC$_s$P$_F$* and SmC$_a$P$_A$*, respectively. Only the former is enantiotropic and it is actually synpolar (the index 'F' stands for 'ferroelectric', which is here not quite correct due to the helical modulation). The second is in all respects antiferroelectric but it is only monotropic and thus difficult to investigate. Most of our work was thus focused on the SmC$_s$P$_F$* phase.
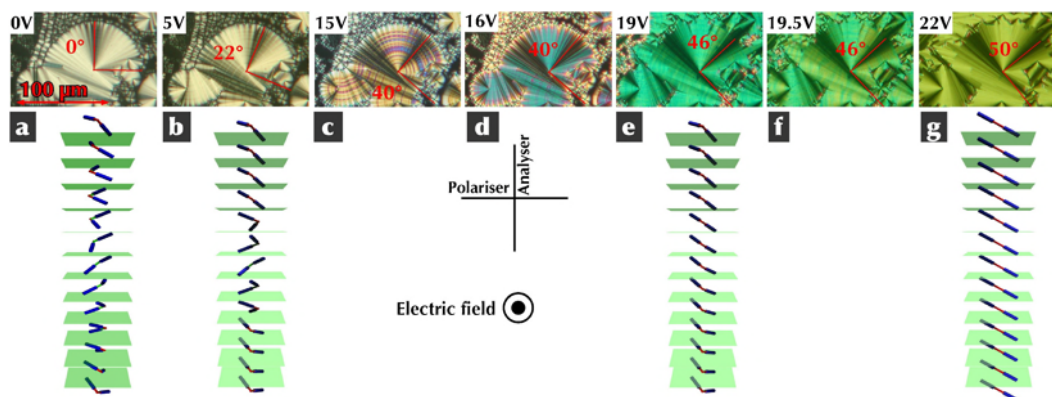
Figure 2.10: The four-stage switching observed in the $SmC_sP_F^*$ phase of BMHBOP-8, in a 4 μm planar-aligning sample. The cartoons in the lower row illustrate how the superstructure as well as the molecular conformation responds to the applied electric field. Reprinted with permission from Paper 1. Copyright 2004 American Chemical Society.

When applying an electric field to the $SmC_sP_F^*$ phase in planar alignment, it responded in a complex four-step process, cf. Fig. 2.10. Initially an analog response was detected, the optical tilt angle increasing continuously up to about 20° and the birefringence increasing slightly. Then a discontinuous jump of tilt angle up to about 40° took place, during which the birefringence increased strongly. This jump took place in a 'finger-like' switching process along the smectic layers, cf. Fig. 2.10c, reminding much of typical antiferroelectric switching (current response curves confirmed that the response was antiferroelectric, cf. Fig. 3 in Paper 1) although the analog low-voltage response is clearly incompatible with AFLC behavior. The explanation is the very short pitch of the helix in this phase. As described in Section 2.5 a very short-pitch SmC* phase *is* antiferroelectric, albeit of the helielectric type. The same holds for the $SmC_sP_F^*$ phase of BMHBOP-8, where the analog low-voltage regime corresponds to helix distortion whereas the threshold at which the apparent tilt angle jumps by about 20° corresponds to helix unwinding.

The switching process in BMHBOP-8 however had another peculiarity: if the voltage was further increased, a second threshold could be distinguished at which the tilt angle again increased discretely, this time to the rather uniquely high value of 50°, and the birefringence also increased. We explained this by assuming that the field now switched the conformation of the molecule from bent to rod-shaped. This raises the birefringence as all mesogenic moeities are now aligned and it would require greater tilting since the effective molecule length has increased, while the smectic layer thickness is fixed at the value determined as the smectic phase was formed by bent molecules. The reason why the field would induce a conformational switch to linear shape is that the dipole of each mesogenic unit is then pointing along the field, whereas this is not possible in a bent conformation. Again, the small energy difference between the conformations is what makes the change possible in the first place.

Accepting that an electric field can switch the molecule conformation from bent to rod-shaped, and acknowledging that bent shape works well with smectic order while rod-shape fits nematic ordering better, we can now understand the next spectacular behavior of BMHBOP-8, shown in Fig. 2.11. If the electric field application experiment described above is performed at a temperature just below that of the N*-$SmC_sP_F^*$ transition in the absence of field, the response is similar up to the first threshold but then a completely different process takes over. Surprisingly, a typical nematic *schlieren* texture appeared temporarily (Fig. 2.11c), the smectic
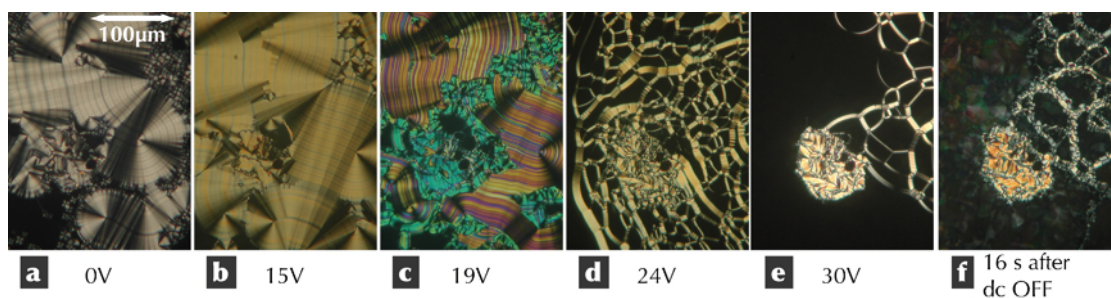
Figure 2.11: The development of the texture of a 4 μm sample of BMHBOP-8 at a temperature just below the field-free transition from N* to SmC$_s$P$_F$* as an electric field of increasing amplitude is applied (a-e), inducing the cholesteric phase, as well as after switching it off (f), the smectic phase reentering. Reprinted with permission from Paper 1. Copyright 2004 American Chemical Society.

texture disappeared, and eventually a texture of a cholesteric phase with 'oily streaks' on a black background was stabilized (Fig. 2.11d-e). The cholesteric phase had thus been field-induced from the smectic. If the field was removed the transition back to the smectic phase followed after a few seconds (Fig. 2.11f). Obviously the electric field shifts the balance between nematic and smectic ordering at this temperature, such that the cholesteric phase prevails at high field, whereas the smectic dominates in the field-free state. As rod-like molecules promote nematic ordering whereas a bent shape promotes smectic ordering, this very unusual behavior can be understood in terms of the field-induced change of molecule conformation.

The bottom line of this study is that the change in molecule shape at the nematic–smectic transition of BMHBOP-8 explains why it can form both nematic and anticlinic smectic phases (the latter albeit only as a monotropic phase). The high degree of smectic order required for an anticlinic arrangement is provided by the bent molecule shape prevailing in the smectic phases, whereas the large translational freedom necessary to give a nematic phase is made available by the conformational change to linear shape. It is interesting to note that in Dr. Nishiyama's original study of several BMHBOP-n homologs he found an odd-even effect regarding the presence of the cholesteric phase: only the homologs with even-numbered spacers had this phase, the others formed smectic phases directly from the isotropic liquid. This is now easy to understand: with an odd-numbered spacer a BMHBOP-n molecule is *always* bent, promoting smectic but not nematic ordering. Likewise it is very interesting from his study that there was no odd-even effect in the smectic layer spacing, instead this always corresponded to the value you can expect for the bent conformation. This confirms that the molecules bend in the smectic phase regardless of spacer length, but the freedom to switch to linear conformation at higher temperatures allows the members with even-numbered spacers to also exhibit the N* phase.

Admittedly, all evidence for the conformational change in BMHBOP-8 at the nematic-smectic transition is indirect, made plausible by the conformational energy balance resulting from computer modeling, but not unequivocally proven. Yet, there are so many independent indications that all fit with this scheme that the full picture in my opinion is quite convincing. A complete proof could be provided by subjecting a deuterated version of BMHBOP-8 (each mesogenic unit must have e.g. a deuterated phenyl ring) to NMR investigations, an interesting challenge that remains to take on for the synthetic chemists and NMR spectroscopists...

2.8 Outlook: where is research in chiral smectics heading?

The structural variation possibilities in liquid crystals is truly astonishing, strategically designed molecules—chiral or non-chiral—giving rise to highly complex phase diagrams [37, 69], with or without chirality. The systems I have described in this chapter constitute a very limited selection, yet the flora of phases they produce is already so rich that it is still far from fully understood. Clearly, the variety of structures and phenomena arising in liquid crystals makes these materials very worthwhile to study, but at the same time the vast breadth calls for an effort to focus the research. I believe this is also what is happening in the community dealing with the study of these phases today, a number of issues appearing as particularly pertinent to study deeper, and certain phases appearing as more rewarding to work with than others. But we should not just continue going deeper in the study of thermotropic smectics, we should also look around us to see where the knowledge and understanding developed in this research may find new uses.

One example of such a broadening that I believe is very worthwhile is the study of macro-/mesoscopic chirality effects in lyotropic lamellar liquid crystals. Since the L_α phase is the natural phase of living cell membranes and since biological matter is unichiral, there is good reason to expect interesting synergetic effects by applying the physicochemical understanding obtained via the study of chiral smectics to biomembranes. It is important to note that the foundation of these phenomena is a symmetry argument which is entirely robust and it therefore must apply also to lamellar liquid crystal phases with tilted director (permanently or during fluctuations) in biological systems.

Only very few researchers from the thermotropic liquid crystal community have yet ventured in this direction but this has already produced some interesting results. For instance, Antal Jakli and co-workers measured a high spontaneous polarization in the $L_{\beta'}$ phase of unichiral dipalmitoylphosphatidylcholine (DPPC) in ethylene glycol, and they saw clear indications of a macroscopic helical director modulation along the layer normal [36]. On the one hand, this confirms that chirality yields a spontaneous polarization also in lyotropic phases from phospholipids, on the other hand it raises an important question: why is there long-range order in the C-director between lamellae (such order is required for the development of the helical modulation) when using ethylene glycol as solvent, whereas this seems to be absent in the biological case of aqueous phospholipid phases? Apparently one solvent allows information to be transmitted between double layers, whereas the other does not. Other interesting issues to consider are the impact of the broken director sign invariance of a single monolayer in a lamellar phase (the polar head group is always towards the water, the apolar chain always in the opposite direction) and what type of correlation in tilt/polarization one might expect between the monolayers. Both syn- and antipolar structures might be expected, the latter clearly more difficult to detect experimentally due to the threshold in reacting to an external field. If a bilayer of $L_{\beta'}$ is synpolar the lack of **c** correlation when water is the solvent renders this phase essentially a 'random SmC*' phase, one of the structures that is often being discussed in terms of 'de Vries smectics', a hot topic in today's smectic liquid crystal research (Paper 6).

Regrettably, I have found it difficult to raise enthusiasm in these issues among researchers from the lyotropic liquid crystal/biology community. It is not made easier because the communities largely speak different languages (as an example, the director concept is rarely if ever used by biomembrane researchers and even the term 'liquid crystal' is used in a somewhat different way than what I am used to). Moreover, the awareness that chiral lamellar liquid crystal phases with tilted molecules should be spontaneously polarized by symmetry is probably not very well spread outside the thermotropic liquid crystal community. One issue that is vividly debated among biomembrane researchers today is that of lipid rafts [70]: fluctuating patches in a cell membrane with locally different composition and increased order, giving rise to a distinction

between 'liquid ordered' and 'liquid disordered' phases. While I am but a curious layman in this field, it seems to me that the liquid ordered phase, with higher order than L_α yet without the rigidity of the $L_{\beta'}$ gel phase, could be the perfect membrane liquid crystal phase for searching for spontaneous polarization, electroclinic effect etc. in living systems.

The earliest attempt that I know of to apply the understanding of chiral smectics on chiral lipid membranes was the proposal by Pierre-Gilles de Gennes to explain an unexpected morphology change between spherical vesicle and tubular shape of certain lipids based on the appearance of a spontaneous polarization [71]. While he was later proven wrong experimentally in this case—the ions dissolved in the water screen out any polarization such that this could not explain the process—the basic theoretical arguments were perfectly valid. Even if ions screen out the polarization over large distances and over long times (making it challenging to study the phenomenon experimentally), one should note that the lipid tails in the L_α phase are fluctuating strongly: symmetry says that if these fluctuations are in any sense collective, even within a small ensemble of molecules, a fluctuating spontaneous polarization should be the result as long as the molecules have a non-zero transverse dipole moment (the electroclinic effect). Conversely, a local in-membrane electric field should induce a uniform tilt of the surrounding lipids. Have such fluctuations and their consequences ever been considered by membrane biophysicists? If Jakli's data are correct the fluctuating polarization can be strong and this should certainly play a role in the function of the biological membrane.

Another interesting area to combine with the research in chiral smectics is research in solid state ferro- and antiferroelectrics. Not only could the physical combinations of FLCs or AFLCs on a solid state ferroelectric substrate be of practical interest but it is also interesting to study how phenomena common to the two classes of spontaneously polarized materials differ or are similar. For instance, how do the characteristic size and structure of domain boundaries compare between the classes and does the switching occur following similar or different processes? The similarities, differencies and synergies between liquid crystal and solid state ferroelectrics certainly constitute an interesting research field to explore.

Chapter 3

Electrospinning of nano-/microfibers with liquid crystals

3.1 What is electrospinning?

Electrospinning is a special technique for spinning very thin fibers, the driving force being of electrostatic origin. The physics and chemistry involved in the process are truly fascinating, making the study of electrospinning very worthwhile from a basic scientific point of view. In addition, the materials produced have considerable application potential, often exhibiting properties that are quite unique, hence there is also an applied reason for doing research on electrospinning and the materials produced by means of the process.

Although the first patents related to electrospinning are now more than a century old [72,73], with the crucial patent by Anton Formhals appearing some 30 years later [74], there has been a strong revival of the interest in this technique in recent years. This is because it offers a number of attractive features which fit very well with today's focus on nano-, micro- and biotechnology and advanced materials research. First, the technique allows easy fabrication of exceptionally thin continuous fibers with diameters down to some 3 nm, difficult if not impossible to achieve with standard spinning techniques. Second, by using different variations of the basic set-up a range of different fibers with varying functionalities can be produced, including composite fibers with different materials in the core and in the sheath, and they can be collected aligned or unaligned, the latter resulting in non-woven textiles. Third, the equipment needed is very small-scale and—compared to the equipment for standard spinning techniques—inexpensive, such that an electrospinning set-up can easily be incorporated in a standard research lab. Finally, the understanding of the electrospinning process has dramatically improved during the last 10-20 years, largely due to seminal works e.g. from the groups of Darrel Reneker (University of Akron), Alexander Yarin (University of Illinois at Chicago), Joachim Wenndorf and Andreas Greiner (Universität Marburg), Gregory Rutledge (MIT), Seeram Ramakrishna (National University of Singapore) and Younan Xia (Washington University of St. Louis). The modern development of electrospinning was recently well summarized by Reneker and Yarin [75]:

> *Electrospinning has rapidly changed fiber making from a capital intensive, large scale process to a low cost, broadly applicable method that manufactures fibers on a labora-*
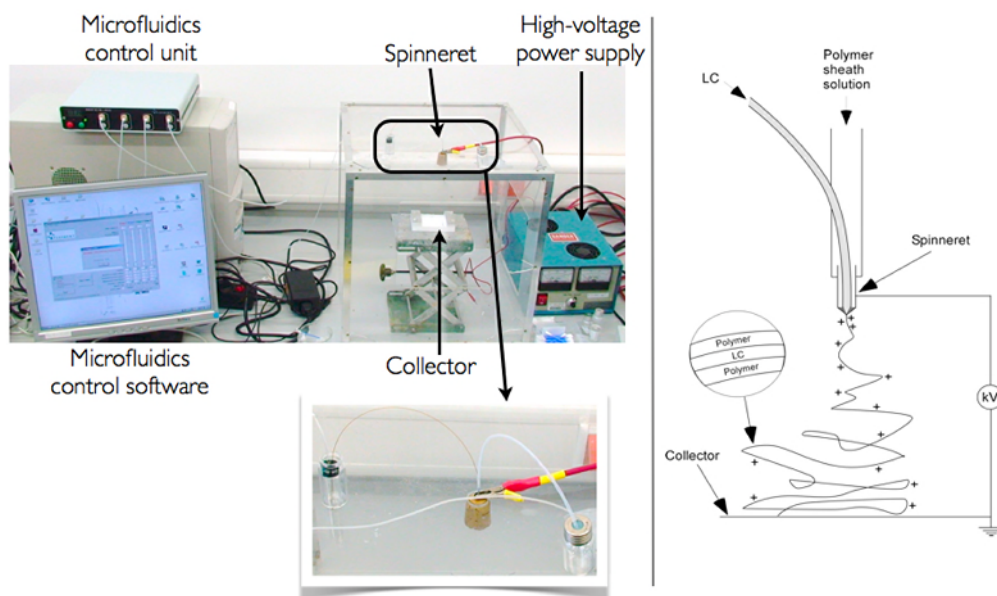
Figure 3.1: Our set-up for coaxial electrospinning (left) and a schematic drawing illustrating the process.

tory bench, to serve diverse needs ranging from materials science and technology to life sciences and clinical medicine.

The two main components of an electrospinning set-up are a syringe pump or microfluidics control unit (we use the latter) and a high-voltage DC power supply. One further needs containers and tubing for the fluids to be spun (when a syringe pump is used a syringe can basically fill both purposes), a metal capillary that acts as the spinneret (the nozzle through which the fluid to be spun is ejected), a target electrode or combination of electrodes on which the fibers can be collected (while this is often referred to as the *collector*, fiber collection is in fact often done on an object inserted between the spinneret and the target electrode) and a construction for varying the distance between spinneret and target electrode. Finally, one generally closes off a volume of air in which the spinning takes place using e.g. a plexiglass box, in order to have some control over the atmosphere in which the fibers are spun. Fig. 3.1 shows a picture of what our electrospinning set-up looks like as well as a scheme of the fundamentals of the process.

3.1.1 Polymers and solvents convenient for electrospinning

As will be explained below the fluid to be spun needs to be non-Newtonian, the typical choice being a polymer solution, although also polymer melts can be spun successfully. The solvent evaporates during the spinning process, leaving the polymer or polymer blend to form the solid fiber. Also non-polymeric fluids or particles can be incorporated within the polymer fiber by using variations of the basic technique, something I will discuss in more detail once the basic electrospinning process has been introduced.

While many different polymers have been electrospun (some examples are presented in Table 3.1), using a variety of solvents, water-soluble polymers such as poly(ethylene glycol) (PEG/PEO), poly(vinyl pyrrolidone) (PVP) and poly(vinyl alcohol) (PVA) are highly convenient to work with from a practical and environmental point of view. Fibers of poly(styrene)

Table 3.1: Examples of polymers and solvents (the list is nonexclusive, solvent mixtures often being used) commonly employed in electrospinning.

Polymer	Abbreviation	Formula	Solvent	References
Poly(ethylene glycol/oxide)	PEG/PEO		water, ethanol	[76–78]
Poly(vinyl pyrrolidone)	PVP		water, ethanol	[79–84]
Poly(vinyl alcohol)	PVA		water, ethanol	[85–91]
Poly(styrene)	PS		DMF, THF, CHCl$_3$, toluene	[92–98]
Polycarbonate	PC		THF, DMF, CHCl$_3$	[99–101]
Poly(acrylonitrile)	PAN		DMF, DMSO	[102–106]
Poly amides	PA		formic acid	[107–109]
Poly(methyl methacrylate)	PMMA		formic acid, DMF, CHCl$_3$	[92, 110–112]

(PS), poly(acrylonitrile) (PAN) and polyamides (PA) are also commonly produced by electrospinning, of course requiring organic solvents that may be less pleasant to work with. Molecular weights are typically in the range 100 000 to several million and the polymer concentration is often around 5% - 30%, giving the spinning fluid a zero-shear viscosity similar to that of honey, about 3 Ns/m^2 [75].

3.1.2 The first zone: formation of the Taylor cone

In contrast to ordinary spinning processes, the pressure on the spinning fluid is weak and the flow consequently very slow in electrospinning. If no electric field is applied there will be a drop of the spinning fluid leaving the spinneret perhaps every 10-20 s. Thus, the flow is not at all a driving force in the spinning process, it is only required to constantly replenish the spinning solution at the spinneret. The driving force is instead the electric field applied to the fluid, typically by attaching the metal capillary to the hot pole of the DC power supply, whereas the ground is connected to the collector. The voltage applied to the capillary is very high, in the

range 10 - 20 kV, hence the power supply must be a rather special one (in fact, most groups doing electrospinning use the same brand of power supply: Gamma High Voltage Research). The current should however be very low (if not there is a short-circuit and something is severely wrong), hence the power supply will deliver only some hundred μA, rendering the set-up quite safe (an electrical shock from an electrospinning set-up is certainly unpleasant, but it will not kill you). The distance between the spinneret and the collector is typically around 10 cm, so the applied field is on the order of kV/cm.

The electric field leads to a separation of charges in the spinning fluid, e.g. the positive charges accumulating at the surface of the drop protruding from a positively charged spinneret (or negative charges for a negative spinneret voltage), as illustrated in Fig. 3.2b. The charges in question are typically ions dissolved in the spinning solution, in some cases deliberately added in order to ensure sufficient charge density. With the application of the electric field a conflict between surface tension and electrostatic forces arises: while the former promotes a spherical droplet shape in order to minimize the surface of the liquid, the latter promotes a movement of the positive ions closer to the collector. The result is a deformation of the droplet into a cone shape (Fig. 3.2c), referred to as the *Taylor cone* after the British physicist and mathematician Sir GEOFFREY INGRAM TAYLOR. He was one of the first to seriously study the deformation of fluids in electric fields, in his case the primary interest being jets of conductive liquid in thunder storms. Once the electric field is sufficiently strong the electrostatic repulsion between the ions at the cone tip, and the attraction of the ions towards the collector, are so strong that they overcome the surface tension, leading to a liquid jet shooting out from the Taylor cone [75], as illustrated in Fig. 3.2d. This is the basis of electrospinning (the region with the capillary orifice and the Taylor cone can therefore be called the first zone of electrospinning) as well as of a technique/process referred to as *electrospray*. We will say a few words about electrospray and the distinction from electrospinning below.

There is a certain delay between field application and jet formation, which depends on the viscous properties of the spinning solution. Under typical electrospinning conditions it is less than a second but with a highly viscoelastic spinning fluid such as a polymer melt the jet ejection can be delayed by as much as 90 s [75]. The size of the orifice has little impact on the jet diameter as it leaves the Taylor cone, as long as it is not so small that it leads to viscous flow restriction [75]. The optimum pumping flow rate is the one exactly equal to the rate at which the jet carries the fluid away from the capillary during spinning. As this increases with the applied electric field, also the pumping flow rate must be increased accordingly if the voltage is raised.

3.1.3 The second zone: jet formation or electrospray

If the spinning solution would be water or another ordinary Newtonian liquid, the jet would soon break up into droplets as a result of the Rayleigh instability[1], also referred to as a capillary instability, minimizing the surface energy of the liquid. When this happens we have electrospray, a technique that has become very important at the sample preparation stage of mass spectrometry, in particular in the study of large biomolecules like proteins. In fact, the introduction of 'electrospray ionization' into the field of mass spectrometry by John B. Fenn was awarded with the 2002 Nobel prize for chemistry. The division into droplets leads to rapid evaporation of liquid and a consequent strong increase in charge density within each droplet, quickly becoming so high that the initially formed droplets break up into much smaller ones, a process often referred to as

---

[1]After Lord RAYLEIGH, who among so many other ground breaking achievements in various fields of physics contributed greatly to the understanding of fluid flow. The instability is also often referred to as the Plateau-Rayleigh instability, acknowledging the initial experimental contribution by the Belgian physicist JOSEPH PLATEAU, another intellectual giant in the study of the physics of fluids, in particular their surfaces and interfaces.
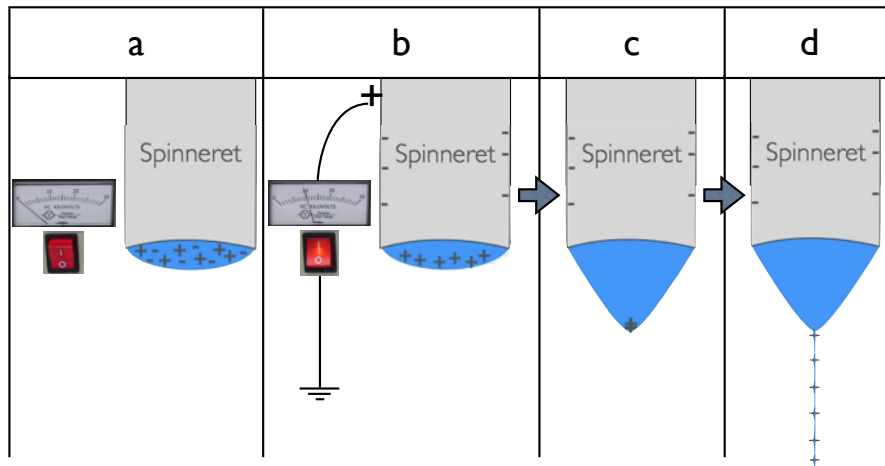
Figure 3.2: The different steps in the formation of the Taylor cone, the first stage of electrospinning. *a*) The spinning fluid is slowly pumped through a capillary (the spinneret) until it protrudes slightly from the capillary orifice. *b*) As the electric voltage is applied to the spinneret the ions in the fluid of charge opposite to the voltage are attracted to the capillary wall, those with the same charge instead being repelled towards the boundary of the protruding drop. *c*) These charges are attracted so strongly towards the collector that the drop deforms into a cone. *d*) Eventually the self repulsion between the accumulated charges and their attraction towards the collector overwins the surface tension of the fluid, leading to the ejection of a thin jet of highly charged fluid from the cone tip towards the collector.

'atomization' (it is physically analogous to the initial formation of the Taylor cone).

Electrospray is something we wish to avoid in electrospinning and we do this by using non-Newtonian liquids as spinning solutions, as mentioned above most often polymer solutions or sometimes polymer melts. The viscoeleastic properties of the polymer solution/melt counteracts the separation into drops due to the Rayleigh instability and stabilizes the jet, which thus stays intact and moves towards the collector. Nevertheless, the Rayleigh instability may be partially effective, producing a chain of regularly spaced drops along the fiber. This beaded morphology is normally not desired and one must then modify the spinning parameters to regain continuous, smooth fibers. To some extent beading can be counteracted by increasing the feed rate of the spinning solution but more effective is to modify the composition of the solution. One can either raise the polymer concentration, although this will also give thicker fibers, or increase the conductivity of the solution e.g. by salt addition. Since thin fibers are typically desired the latter option is often to prefer. The situation is graphically summarized in Fig. 3.3.

3.1.4 The third zone: bending instabilities and fiber stretching

On the way from the spinneret to the collector the jet is longitudinally stretched due to the repulsion between the like-charged ions that it carries with it but it also repeatedly experiences a second instability, which is of great importance for the electrospinning process and the resulting fibers [75, 113]. This is a bending instability, also fundamentally resulting from the electrostatic repulsion between like-charged elements along the jet, but now in conjunction with a lateral fluctuation. As illustrated in a highly simplified way in Fig. 3.4, considering only three charges distributed along a certain length of the jet, the electrostatic self repulsion will lead to no net force on the central element as long as the jet is absolutely straight: all forces are then along
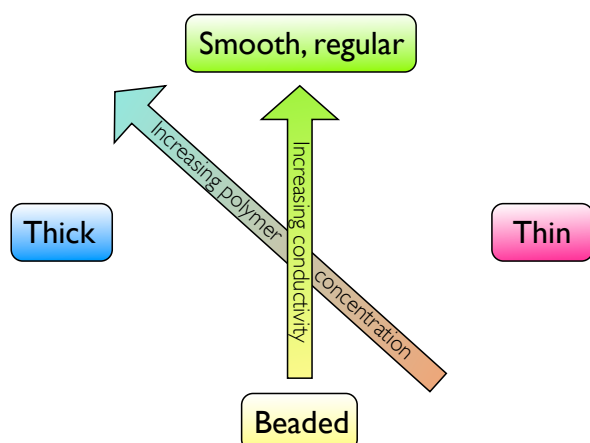
Figure 3.3: The character of the produced fibers can be tuned between 'beads on a string' and constant thickness smooth fibers by varying the composition of the spinning solution, changing the polymer concentration (thereby also influencing the fiber thickness) and/or the conductivity solution (e.g. by salt addition).

the jet in opposite directions. But as soon as we have a slight perturbation sideways of the jet there will be a net lateral force on the element diverging the most from the linear path (here the central element). The instability arises when this force is strong enough to overcome the elastic and viscous forces promoting the linear jet path (which is the shortest) such that the fluctuation is amplified and a strong lateral excursion of the jet results. The process is analogous to the Euler buckling process in mechanics (and thus also to the Frederiks transition, at the core of most electrooptic applications of liquid crystals), where a pillar compressed along its axis eventually breaks with a lateral movement, as a lateral fluctuation is amplified by the axially applied force.

The bending instability gives rise to a spiral-shaped continued path of the jet with a conical envelope, cf. Fig. 3.5, first with a long pitch and relatively large (and increasing) spiral diameter. Eventually a second bending instability will however appear, resulting in a smaller diameter spiral modulation of the jet, and this can go on to a third and fourth or even fifth hierarchical instability [75, 113]. The reason for the multiple bending instabilities is the continuously increasing charge concentration during the flight of the jet: although one might at first think that the substantial stretching would reduce the local charge density in the jet one must remember that the rapid evaporation of the solvent reduces the total jet volume, generally leading to a net increase in charge density. As a result of the multiple bending instabilities the jet follows a very complex path from the spinneret to the collector, with a path length that is orders of magnitudes greater than the actual spinneret-collector distance, and the continuous stretching along this path renders the
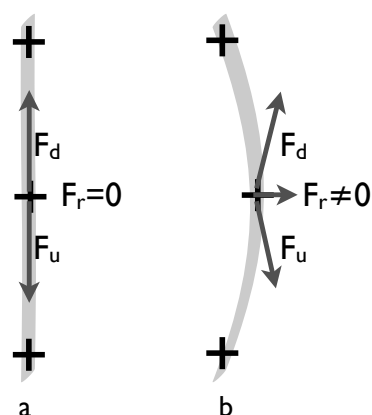
Figure 3.4: A simplified model for explaining the bending instability at the core of the exceptional stretching of the jet during electrospinning. Rather than the real continuous charge distribution along the jet we consider charges at three subsequent points in a small section of the jet and the forces experienced by the central charge from the upper and lower ones (F_u and F_d, respectively, with d for 'down'). As long as the jet is absolutely straight (a) all forces compensate each other resulting in a net resulting electrostatic force $F_r = 0$. But with a slight lateral fluctuation (b) the forces are no longer balanced, yielding a non-zero lateral F_r, amplifying the fluctuation and thus eventually giving rise to the bending instability.
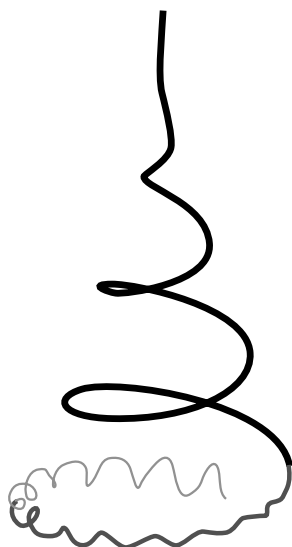
Figure 3.5: A simple cartoon of the envelope of the jet during electrospinning, characterized by multiple superposed spiral modulations due to subsequent electrostatically induced bending instabilities. The first bending instability initiates at the top of the blue section, the second at the transition from the blue to the green. Several further bending instabilities can follow. Redrawn from [75].

jet very much thinner at the end of the process than at the beginning. This is what allows such exceptionally thin fibers to be produced by electrospinning.

The elongation of the jet due to the multiple bending instabilities will normally continue until it hits the collector (or an object inserted in the spinning path) or until the polymer solidifies due to solvent evaporation or, in case of melt spinning, to cooling. During the elongation stage the jet experiences stretching ratios in the range of 10^5 and stretching rates up to 10^5/s, values which are unmatched by other methods like fiber extrusion followed by mechanical stretching [114].

3.1.5 The fourth and final zone: fiber collection

Just before the jet reaches the collector its translational speed is very high, on the order of 40m/s [114]. As it hits the collector the motion is abruptly stopped although the impact is not necessarily quite that which one would expect considering the speed. Because of the bending instabilities during the jet flight the motion is largely in the horizontal plane and the fiber can therefore be deposited as a relatively straight fiber. Depending on the vertical position of the collector, the impact of the jet may however be more or less head on, and in that case the buckling instability arising upon impact will lead to a characteristic small-diameter spiral pattern of the deposited fibers [75].

Normally one tries to optimize a set-up such that the jet solidifies just before or just after it hits the collector. If it is too wet the fiber morphology is not stable and deposited fibers will merge as a result of flow after deposition. If it is entirely dry then the decharging of the fiber via the contact with the grounded collector takes longer time. Since the fiber is still highly charged when it lands on the collector it repels the jet that approaches from above, which therefore moves laterally towards a different collection spot. As long as the charge on the deposited fiber is quickly neutralized this is fine; it results in a criss-cross deposition of fibers producing a characteristic open network mat structure, cf. Fig. 3.6a. But if the decharging takes too long the repulsion of the incoming jet may be so strong that the fibers are instead distributed in an uncontrolled way around the target area, building bridges between various surfaces around the collector.

In many cases an aligned collection of fibers is desired and a number of approaches have been developed to achieve this. The most obvious, but practically more involving, solution is to collect
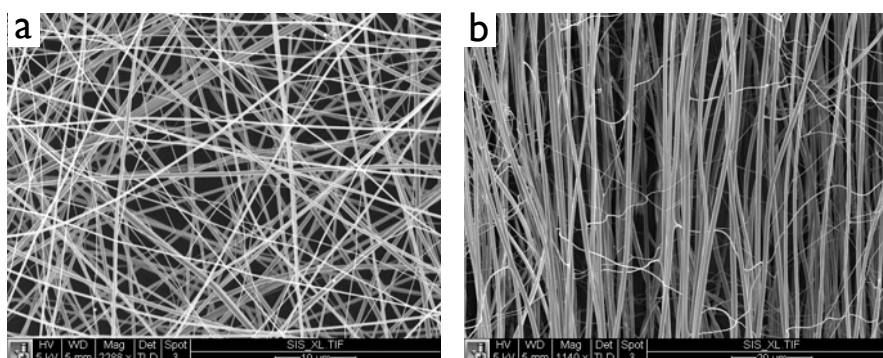
Figure 3.6: Scanning Electron Microscopy images of coaxially electrospun fibers with a nematic liquid crystal core and a composite sheath of PVP and TiO_2. The fibers were collected as a random non-woven mat (a) and aligned between the arms of a tweezer (b).

the fibers on a quickly rotating drum [115, 116], leading to fibers aligned perpendicular to the rotation axis. Quite well aligned fibers can however be achieved in a much easier way, simply by splitting up the collector electrode in two parallel grounded plates or wires [79, 109]. The electric field profile now has a horizontal component that promotes stretching of the fibers across the gap between the electrodes. Together with the repulsion between fibers that are suspended between the electrodes, thus only slowly discharged, this leads to an alignment of the fibers across the gap that can be quite good. The simplest way of realizing this type of alignment is to put a pair of metal tweezers on top of a flat collector electrode, resulting in the fiber jumping back and forth between the arms of the tweezers. The aligned fibers in Fig. 3.6b were obtained in this way.

An interesting variation of this alignment technique was introduced recently by Yan et al. [117]. Rather than splitting up the target electrode in two, they placed two parallel blocks of a high permittivity dielectric material on top of the single grounded target electrode, again resulting in a lateral component of the electric field that stretches the fibers across the gap between the dielectric blocks. They demonstrated the concept with PVA spun from aqueous solution onto blocks of wood, water containers or ferrite, the latter yielding the best results.

3.1.6 Coaxial electrospinning

In our work we use a special version of electrospinning in which one fluid is spun inside another one: coaxial electrospinning [118, 119]. As illustrated in Fig. 3.1 a thin capillary is introduced inside the main tubing through which the polymer solution flows. This inner capillary runs almost coaxially with the main capillary until the orifice where the two capillaries should end at the same height. They must be well centered at this point in order for the Taylor cone to form symmetrically, with the fluid pumped through the inner capillary uniformly surrounded by a layer of polymer solution. Since the introduction of the inner capillary through the wall of the main tubing prevents perfect coaxial alignment of the capillaries, one may need to slightly bend the metal capillary close to the orifice, such that they are well centered at the exit point of the spinneret.

The beauty of coaxial electrospinning is that any fluid with sufficiently low viscosity that is immiscible with the polymer solution (jets produced with miscible fluids do not maintain the coaxial geometry throughout the electrospinning process [118]) can be spun into fibers by pumping this fluid through the inner capillary. The polymer forms a protective and containing

cylindrical wall around the inner fluid. In other words, coaxial electrospinning produces fibers with a core-sheath structures, and because the sheath is a solid polymer the core can be a low-molar mass liquid (it can of course also be a polymer), in our case a thermotropic liquid crystal. The inner fluid gives the composite fiber new functionality, e.g. special optical properties from a liquid crystal core (to be discussed in detail below). But even simple alkanes inside the fibers can functionalize the produced non-wovens into phase change materials useful for temperature stabilization [82].

Directly after leaving the Taylor cone the acceleration of the fluid in the electric field is so strong that the jet acquires translation velocities of about 5 m/s [75]. This should be contrasted with the typical drift speeds of the ions in the solution on the order of 0.1 m/s [120] and the very slow flow rate of the fluid(s) involved. This means that translational flow as well as charge translation within the jet can essentially be neglected from the point where the jet leaves the Taylor cone.

Although we could in principle charge both or either liquid in coaxial electrospinning by using a metal capillary at the end of the *inner* tubing, connecting this to the hot pole of the power supply rather than the outer capillary (which in this case could be made of glass, for instance), the usual configuration is one where only the outer fluid is in direct contact with the electrode (the outer capillary made of metal) and thus only this fluid gets charged. The inner fluid then does not experience the electrostatic forces that drives the electrospinning process, these being active only in the outer fluid. The jet core is instead stretched only by mechanical means as a secondary effect from the electrostatic stretching of the sheath [114]. This is advantageous when spinning living matter, such as cells, which may not survive the strong electrical charging, but it may also be a means of spinning highly conductive solutions, e.g. carbon nanotube suspensions or conductive polymers. These would short-circuit the set-up and thus terminate spinning as soon as the jet makes contact with the collector if spun as the outer (or only) fluid.

3.2 Liquid crystals inside electrospun fibers

The practical usefulness of liquid crystals has been very convincingly demonstrated through the fantastic success of liquid crystal flat panel displays, such that the concept *liquid crystal* is now known by essentially everyone in the developed parts of the world. In displays and in most other applications of thermotropic liquid crystals the liquid crystal is present as a flat film. Liquid crystals being fluid, they are however compatible with a variety of geometries, many so far little explored, in which their functionality may be put to use in new ways, possibly with unique features. One example is the cylindrically symmetric geometry that arises by placing the liquid crystal in a capillary or a fiber. The exploration of the possibilities of using electrospinning for achieving this situation in a fast and cheap manner, with feature sizes in the micron or sub-micron range, has been one of my main research foci during the last few years.

By coaxially electrospinning composite fibers with a liquid crystal core inside a polymer sheath we obtain systems that constitute an entirely new configuration for studying—and applying—liquid crystals, opening possibilities very different from standard liquid crystal device configurations. The liquid crystal gives the fibers new functionality and responsiveness and the encapsulation of the liquid crystal in the narrow cylindrical fiber core allows easy investigation of 1D confinement effects. The fibers also have large application potential. While we are still at the very beginning of the research on and development of liquid crystal-containing electrospun fibers and non-wovens (I was in fact the first one to incorporate low molar mass liquid crystals inside electrospun fibers) one can envisage applying the liquid crystal-functionalized fibers in fields ranging from full spatial resolution temperature sensing, via dynamic camouflage clothing

to wearable electronics.

3.2.1 Practical requirements for electrospinning fibers with liquid crystal cores

While both main classes of liquid crystal can be electrospun as a core of composite fibers I have initially concentrated on thermotropics. This means that the basic electrospinning set-up should be extended with temperature regulation, allowing us to choose the phase adopted by the liquid crystalline material at the onset of spinning. While we may expect nematics to be easily spun, the relevant viscosity η_2 in fact being even lower than the viscosity of the material heated to its isotropic phase, higher-ordered liquid crystal phases like smectics or cholesterics could be expected to be more challenging to spin. It may be difficult to achieve continuous and smooth flow to the spinneret of a highly viscous fluid and a large difference in elongational viscosity between inner and outer fluids complicates the spinning process, such that a continuous filling of the fibers may be impossible. It is thus highly desirable to have the possibility to heat the material well into its isotropic phase if we wish to prepare fibers with a core that eventually is in a high-ordered liquid crystalline state.

It is however not entirely trivial to realize a precise and versatile temperature control for an electrospinning set-up, since the liquid crystal is spatially distributed over the full length of the tubing, the access for a heating system being very difficult in certain places. The simplest solution is to heat the whole system up to the spinneret with a heat gun, a method we used during our very first attempts to spin the short-pitch cholesteric **mixture 1** in Fig. 3.7e, which at room temperature is too viscous to allow electrospinning. This method is readily accessible but obviously lacks precision, preventing true control of the spinning parameters and making repeatability challenging, and it also heats many components that would better stay at room temperature. In the next step we therefore added a heating block for the vial from which the liquid crystal is pumped. This proved generally inadequate, however, since the large surface area of the tubing through which the liquid crystal flows renders temperature equilibration with the surrounding air very rapid, such that the fluid is too cold once it reaches the spinneret. In a recently realized new version of our set-up, designed and realized with the help of the very professional team around Herr Reese at the mechanical workshop at the Chemistry Department of the Martin-Luther-Universität Halle-Wittenberg, a heating block for the liquid crystal vials is combined with a heated air flow along the tubing. We believe that this construction will allow temperature control on the level we need to spin also quite complex liquid crystal phases into the fibers.

In our experiments with various liquid crystals we were however pleasantly surprised by the observation that the inner fluid can in fact sometimes be in a cholesteric or even smectic phase during spinning, allowing the short-pitch cholesteric formed by doping the nematic mixture RO-TN 403/015 S with the chiral dopant CB15 (**mixture 2**, cf. Fig. 3.7d) to be spun at room temperature. This mixture is much less viscous than **mixture 1** although both have about the same very short pitch of the director helix at room temperature. Likewise, 8CB (Fig. 3.7a) could be spun at room temperature where the liquid crystal is in a SmA phase, however close enough to the second-order N-SmA transition that the material still flows reasonably easily.

3.2.2 External morphology of the liquid crystal-containing fibers

Our first experiments (Paper 10) were carried out with an outer spinning solution containing not just polymer but also a $Ti(OiPr)_4$ sol-gel precursor, resulting in a polymer-TiO_2 composite sheath that is particularly stable. The exact composition of the sheath solution was 3% PVP,

a

8CB (4-Cyano-4'-octylbiphenyl):
Crystal 21,5 SmA 33,5 N 41,5 Iso. / °C

b

CB15 [(S)-4-Cyano-4'-(2-methylbutyl)biphenyl]:
Chiral dopant, isotropic at room temperature.

c RO-TN-403 / 015 S
Multi-component nematic mixture with 0.1 wt.-% of cholesteryl nonanoate as chiral dopant.
Crystal <0 N 81,5 Iso / °C

d Cholesteric **mixture 2**
Binary mixture of **b** and **c** at a 50/50 mass ratio.
N* 28.5 BP* 30.2 Iso. / °C

e Cholesteric **mixture 1**
*with color play from red to blue
in the range 20°C to 25°C.*

66.7% Cholesteryl oleyl carbonate

23.8% Cholesteryl nonanoate

9.5% Cholesteryl benzoate

**Figure 3.7:** Key substances used for preparing the liquid crystal core materials in our electrospun composite fibers.

29% Ti(OiPr)$_4$, 48% ethanol and 19% acetic acid, yielding a sheath where the polymer is in fact just a minority (27%, the rest TiO$_2$). While this gave very stable fibers with well-defined morphology (Fig. 3.6) the fact that the sheath consists mainly of TiO$_2$ makes characterization of the liquid crystal core more challenging, and the optical properties of the liquid crystal are inaccessible behind this strongly scattering and birefringent sheath. The verification of the director alignment as well as the investigation of the phase sequence was therefore done with polarized Raman spectroscopy in these fibers (see the following section).

In subsequent work, where we focused very much on investigating (and eventually utilizing) the optical properties of the liquid crystal core we therefore spun fibers with a pure PVP sheath that is largely non-birefringent[2]. This generally worked very well, fibers produced using a 12.5% PVP in ethanol solution as outer fluid appearing quite uniform in optical microscopy and the liquid crystal optical properties being easily detectable (these will be discussed below).

The outer fiber morphology was investigated by scanning electron microscopy (SEM) by Dr. Giusy Scalia and Mr. Enzo Calò at ENEA Portici (Naples), Italy, the results shown in Fig. 3.8. It is important to note that the samples were not metallized prior to investigation, as is often the case in SEM investigations, hence the true fiber surfaces were studied. This allowed the fiber texture to be established with great detail, revealing e.g. a high degree of porosity in some cases. Fibers without liquid crystal inside turned out not to be quite cylindrical, the sheath seeming to have collapsed onto itself after spinning (Fig. 3.8a). With liquid crystal inside the morphology was generally cylindrical, at least up to 0.36 mL/h liquid crystal flow rate (the samples with higher liquid crystal content and pure PVP sheath were unfortunately damaged in the transport between Halle and Naples, hence we lack SEM images of these fibers), although some examples of essentially flat ribbons were also found, see e.g. Fig. 3.8d.

The tendency to form flat ribbons was greatly enhanced by increasing the spinneret – collector distance, to the extent that *all* fibers had flat ribbon character when produced with 15 - 20 cm spinning distance, cf. Fig. 3.9. The polarizing microscopy photos in this figure prove that the

---

[2]PVP is generally said to be an amorphous polymer but some degree of crystallinity is detectable in the electrospun fibers as a non-zero birefringence of fibers containing only PVP. The very strong stretching of the polymer chains during the spinning process is most likely the reason for this unusual state of PVP.
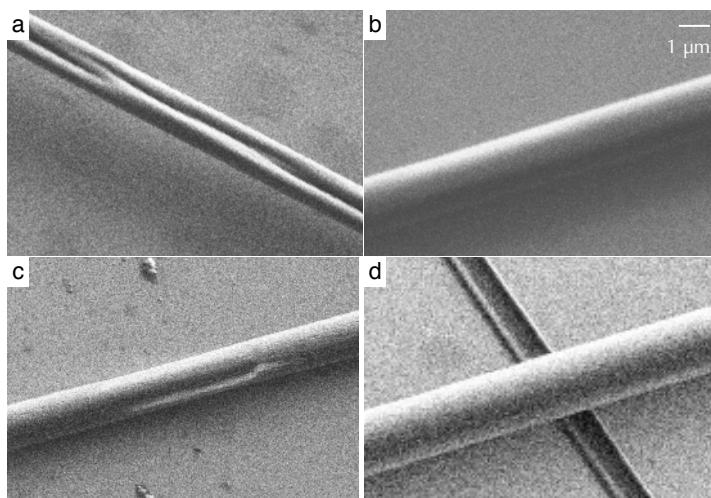
Figure 3.8: Scanning electron microscopy images (courtesy of Dr. G. Scalia) of pure PVP fibers, empty (a) and with liquid crystal core (b-d). The scale is constant throughout all images (scale bar in *b*). All samples were spun (by E. Enz) at room temperature, with 25-35% relative humidity, 10 cm spinneret – collector distance and 10 kV spinning voltage, with a 12.5% PVP in ethanol solution as the outer fluid. This was pumped at a flow rate of 1.8 mL/h in all samples. The inner fluid was **mixture 2** (Fig. 3.7d), cholesteric at room temperature, and this was pumped at flow rates of 0.14 mL/h (b), 0.26 mL/h (c) and 0.36 mL/h (d). Fibers were also prepared with 0.48, 0.63 and 0.80 mL/h liquid crystal flow rate but these were unfortunately damaged in transport prior to SEM characterization.

liquid crystal was still contained inside the ribbons in these samples. In other cases, where flat ribbons were found as more exotic species, these were typically empty, see e.g. Fig. 3.20a. Ribbon morphology in electrospun fibers has been explained as a result of the sheath solidifying before all solvent has evaporated, resulting in a sheath that is larger than the core and that therefore collapses into a flat ribbon after fiber deposition [121]. In our case the ribbon morphology is clearly undesired, hence we avoided such long spinning distances in future experiments. Moreover, the collapsing of the fibers seems to have partially ruptured the sheaths, the close-ups of the fibers revealing fiber surfaces with a large number of cracks along the ribbons (Fig. 3.9d and h).

We were very pleased to see that coaxial spinning with liquid crystal core and pure PVP sheath worked out, but in fact also somewhat surprised. The reason is that earlier attempts by Li and Xia to spin mineral oil coaxially inside a PVP ethanol solution failed due to structural breakdown of the coaxial jet, resulting in complete separation into oil droplets and solid fibers of pure PVP [118]. In this case the addition of the $Ti(OiPr)_4$ sol-gel precursor in the outer fluid was required to stabilize the sheath, that is they used the same outer solution as I did in the very first experiments with liquid crystal core fibers (Fig. 3.6).

In our case with a liquid crystal in the core the situation is somewhat different because also the inner solution is non-Newtonian. Relatively long filaments can be drawn from liquid crystals, in contrast to isotropic Newtonian fluids where the Rayleigh instability more rapidly destabilizes a filament and separates the fluid into droplets. It thus seems that this property of the liquid crystal is beneficial for coaxial electrospinning, allowing us to use a simpler and in many respects practically preferable sheath solution than had the inner fluid been isotropic. This means that heating a liquid crystal into the isotropic phase for spinning is in fact not necessarily desirable: the nematic phase ought to be the optimum phase for spinning but unfortunately not all materials
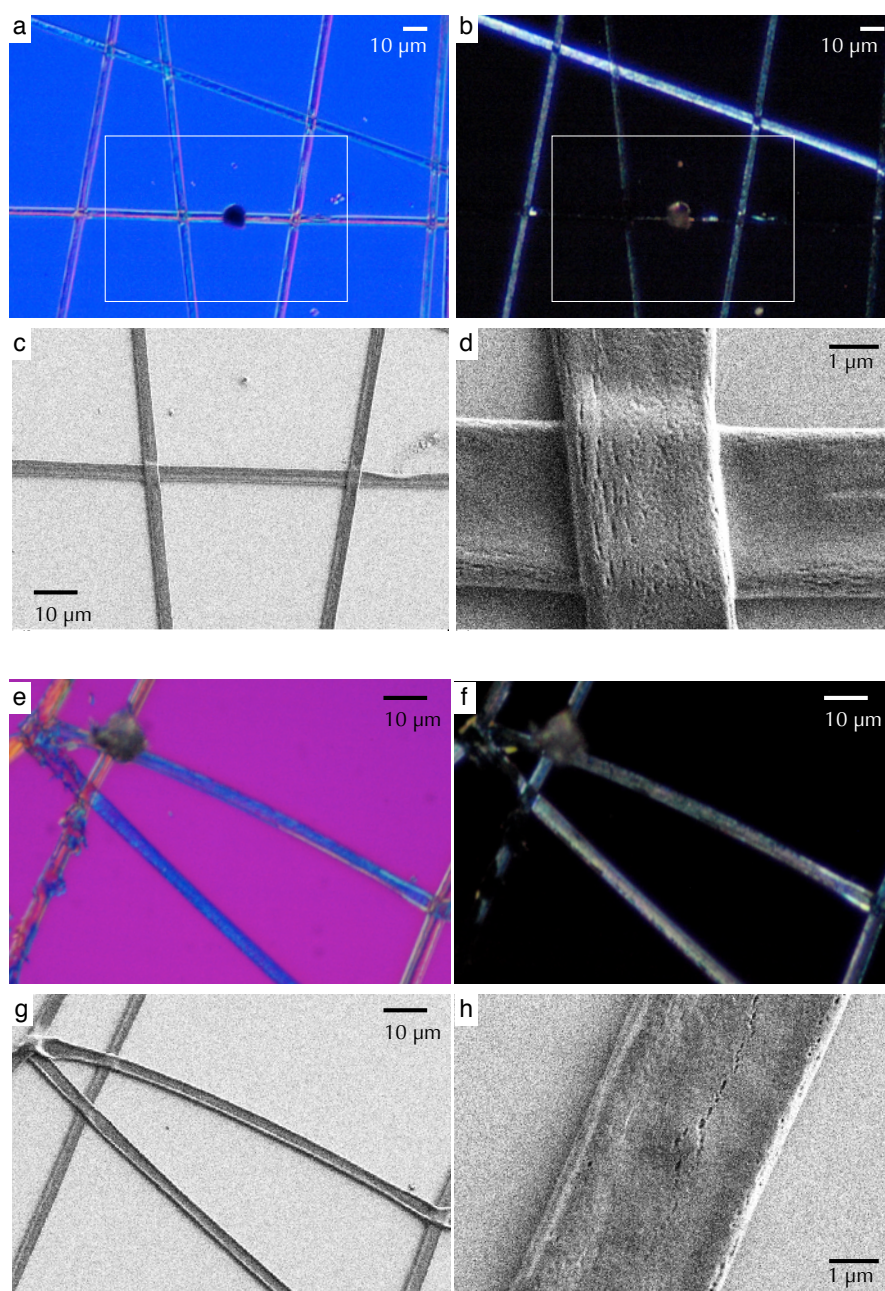
Figure 3.9: Core-sheath fibers electrospun coaxially (by E. Enz) with **mixture 2** as inner fluid and 12.5% PVP in ethanol solution as outer fluid (same fluid combination as in Fig. 3.8). The flow rates for sheath and core fluids were 1.8 mL/h and 0.80 mL/h, respectively, and the spinning voltage was 13 kV. The atmosphere had a relative humidity of 25 - 35%. The distance spinneret-collector was 15 cm for the sample in (*a - d*) and 20 cm for the sample in (*e - h*). Each sample was viewed by differential interference contrast optical microscopy (*a* and *e*), polarizing optical microscopy (*b* and *f*) and scanning electron microscopy (SEM, courtesy of Dr. G. Scalia) (*c - d* and *g - h*). The white frame in *a* and *b* corresponds to the area of the SEM image in *c*. For the second sample, pictures *e - g* have the same scale.

exhibit this phase.

The results of Li and Xia suggest that when encapsulating non-nematic materials a mechanically stronger sheath solution may be required to stabilize the coaxial jet. We therefore also explored variations of the sheath solutions in this direction, still keeping the requirement that the sheath should be at least largely non-birefringent. First we increased the polymer concentration somewhat (Fig. 3.10a-b), leading to fibers that were mainly cylindrical and intact, even at the rather high liquid crystal flow rate of 0.8 mL/h, although a few flat ribbons were also detected. In fact, there was a quite strong variation in the fiber character. The example in Fig. 3.10a-b is quite illustrative, as it shows an area where three fibers were subsequently deposited on top of each other. Zooming in (b) reveals that the first deposited fiber was a flat ribbon, the second a smooth cylindrical fiber, and the final one a very highly porous cylindrical one. Such variations in the resulting fiber morphology without changing the spinning conditions are clearly problematic if one wishes to achieve reproducible results.

Porous fiber textures similar to the fiber labeled α in Fig. 3.10b have been reported from electrospinning in a very humid atmosphere, resulting in water condensing on the fiber surface due to its low temperature (resulting from the rapid solvent evaporation) and leaving small holes after the final evaporation [93, 95]. In our case the atmosphere was basically rather dry during the spinning experiment (25 - 35% relative humidity), hence this explanation is not immediately applicable. On the other hand, it is notable that it was the final deposited fiber that had the porous morphology, whereas the first deposited fiber had a flat ribbon character, indicative of a dry atmosphere that allows the polymer to solidify before the jet hits the collector (see the above discussion of flat ribbons obtained at large spinning distances). It could thus be that the solvent content in the small volume of air in which the spinning takes place actually increases during spinning, due to the solvent that has been evaporated from the jet at the early stage of spinning, to the extent that solvent condenses on the cold surface of fibers deposited later in the process, producing the porous surface.

The next modification was the addition of a small amount of $Ti(OiPr)_4$ sol-gel precursor giving a final fiber with 9% TiO_2 in the sheath (Fig. 3.10c-h). While the fibers formed with this sheath solution were truly excellent in terms of uniformity and cylindrical shape, the small amount of TiO_2 in the sheath did not prevent the liquid crystal from being visible through the fibers (the liquid crystal did appear slightly different in these fibers as well as in the increased polymer content fibers, however, as will be discussed in section 3.2.5). A further interesting observation was that the TiO_2-PVP composite fibers were substantially thinner than those without TiO_2, cf. the comparison of Fig. 3.10b and h, depicted with the same scale and obtained with the same liquid crystal flow rate (if the spinning solutions are kept constant it is the flow rate of the inner fluid that has the greatest impact on the thickness of core-sheath fibers [118]). A systematic increase in fiber thickness can be seen as the liquid crystal flow rate was increased. For the fibers with the greatest liquid crystal loading (Fig. 3.10g-h) a modulation of the diameter along the length of the fiber can clearly be detected in the SEM images. This may suggest a separation of the core fluid into droplets, a situation which would fit well with the optical properties of the fibers, as discussed in section 3.2.5.

While the above described SEM investigation of fibers produced under systematically varied spinning conditions was carried out only for chiral nematic liquid crystal core, it seems likely that the conclusions will apply at least as a first approximation also to other liquid crystal systems. Nevertheless, similar investigations should be done in the future for fibers with non-chiral nematic core as well as with smectic core. It would obviously be of great interest to know also the *internal* structure of the fiber, the inner diameter being the most important parameter to establish. This is however not trivial to realize experimentally and our attempts so far to image the inner structure have failed. One can either carry out SEM on the fractured end surface of

10 μm   1 μm
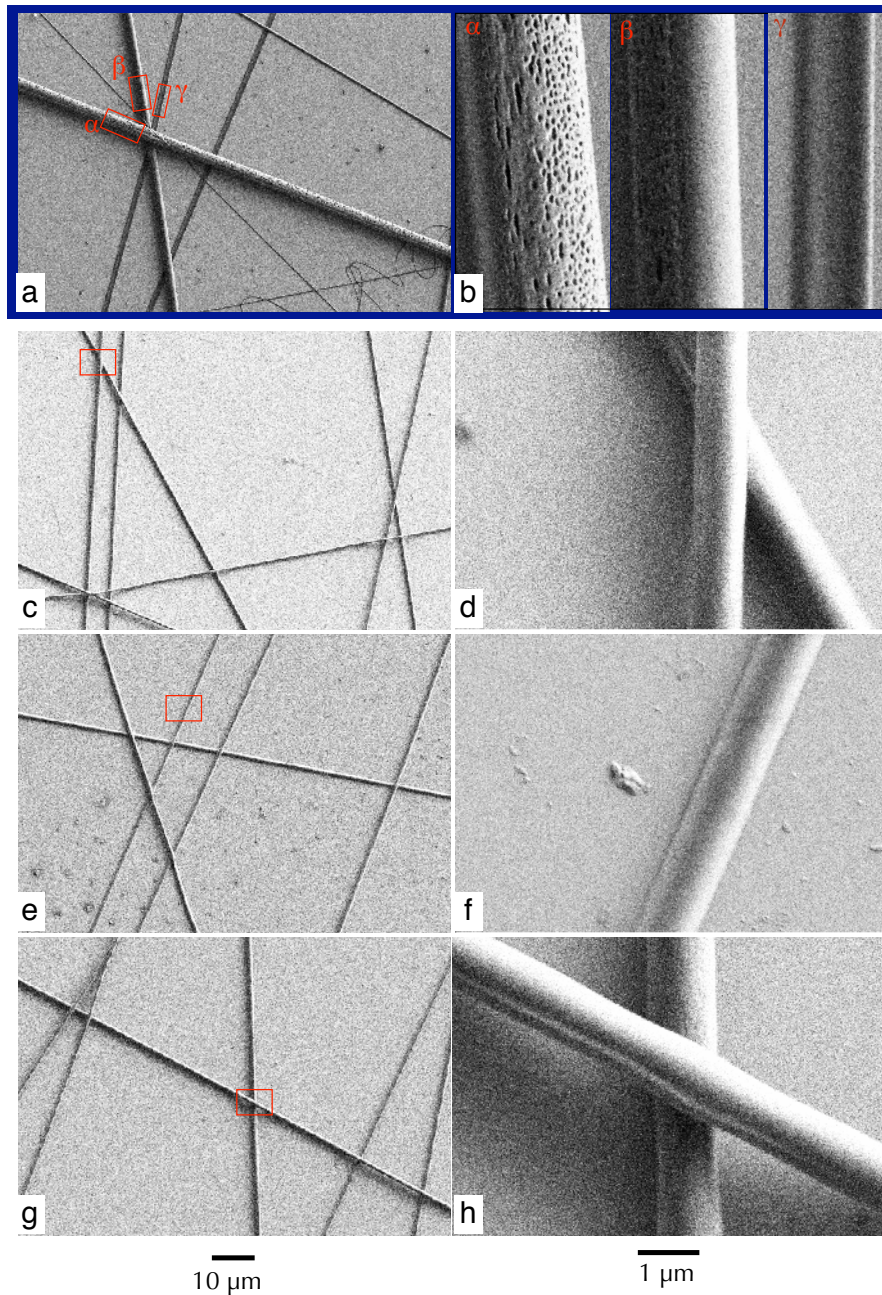
Figure 3.10: Scanning electron microscopy images (courtesy of Dr. G. Scalia) of core-sheath electrospun fibers (prepared by E. Enz) with **mixture 2** in the core. For each row the right image is a magnification, corresponding to the red square(s) in the left image. Within a column all images have the same scale (scale bar below). The sheath solution was a 15% PVP in ethanol mixture for (a) - (b) (pumping pressure 30 mbar; the corresponding flow rate has not yet been measured but is probably around 2 mL/h) whereas the samples in (c) - (h) were spun with an outer 10% PVP in ethanol solution containing also a sol-gel precursor (pumping pressure 10 mbar, also probably corresponding to about 2 mL/h flow rate), yielding a final sheath composition of 91% PVP and 9% TiO_2. The spinneret - collector distance was 10 cm, the spinning voltage was 10 kV and the air humidity was in the range 25-35%. The inner (liquid crystal) fluid was pumped at a flow rate of 0.80 mL/h for samples (a - b) and (g -h), 0.26 mL/h for (c - d) and 0.48 mL/h for (e - f).
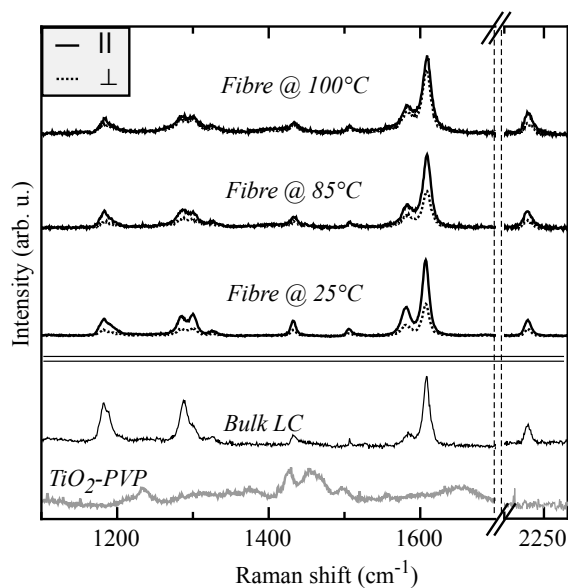
Figure 3.11: The Raman response from RO-TN 403/015 S as a bulk sample (directly below the twin horizontal lines) and in electrospun fibers with a PVP-TiO$_2$ composite sheath (Fig. 3.6) at different temperatures, for polarization parallel and perpendicular to the fiber. At the very bottom the spectrum of the pure sheath material is shown, the response greatly magnified since it is much weaker than that of the liquid crystal. From paper 10. Reproduced by permission of the Royal Society of Chemistry.

fibers that have been broken in two sections, at best after having dissolved the core fluid with a suitable solvent that does not affect the sheath, but this requires that the fiber sheath does not collapse during the fracture. In our case, the sheath closed up entirely regardless of how we broke the fibers (including fracturing the sample in liquid nitrogen) giving no clue of the fiber interior.

An alternative approach is to do transmission electron microscopy (TEM), but this has two other difficulties. First, our fibers are far too thick to be transparent to the electron beam, hence they have to be embedded in an epoxy resin which is then microtomed to slices suitable for TEM characterization. Obviously it can be challenging to find the fibers in this slice. Second, since the electron density contrast between PVP and liquid crystal is too low to yield a contrast in TEM, only fibers with sheaths of TiO$_2$-PVP composite could be considered. Together with the group of Prof. G. Michler, Martin Luther University Halle-Wittenberg, we have done a few attempts to obtain data on the inner diameter but so far without success.

3.2.3   How does the liquid crystal align inside the fiber?

The cylindrical symmetry of the fiber (for simplicity I consider here only fibers with the desired morphology) would intuitively suggest a director alignment along the fiber for a nematic phase but perpendicular for a SmA phase. The perpendicular alignment would allow the smectic layers to form concentrically along the fiber, compatible with easy flow. The former assumption turns out to be correct (even for chiral nematics), the latter not: even in the smectic phase planar alignment prevails, resulting in a stack of smectic layers along the fiber, each layer with a lateral extension no greater than the fiber diameter.

The alignment of the nematic phase in the fibers was investigated using polarized Raman spectroscopy on the first liquid crystal-containing fibers that we produced, with a PVP-TiO$_2$ composite sheath, cf. Fig. 3.11. Raman spectroscopy was here required since the TiO$_2$-dominated sheath did not allow polarizing microscopy characterization of the liquid crystal core. First, the presence of the liquid crystal was verified by comparing the spectrum of the bulk liquid crystal,

that of the pure TiO$_2$-PVP sheath, and that of the core-sheath fiber. The pure sheath material had a very weak spectrum, with no peak coinciding with the much stronger liquid crystal peaks. All of the latter could indeed be recognized also in the coaxially spun fibers, proving that the liquid crystal was inside the fibers. Moreover, the response was distinctly stronger for polarization parallel to the fibers than perpendicular, showing that the director **n** was aligned preferentially along the fiber axis, as expected for the nematic phase.

When we later on spun PVP fibers with the smectogen 8CB in the core, these fibers were investigated by x-ray scattering by Dr. Ute Baumeister at the Martin-Luther-Universität Halle-Wittenberg, giving clear evidence of the director alignment inside the fibers. An aligned and relatively dense fiber mat was rolled up into a scroll either along or perpendicular to the fiber axis and this was then introduced into an x-ray capillary, cf. Fig. 3.12. While the former scroll geometry gave inconclusive results the latter clearly showed small-angle smectic layer diffraction peaks along an axis perpendicular to the rolling direction, along the fiber axis. This means that the smectic layers were in fact not concentric as we had expected but instead flat and perpendicular to the fiber. Obviously the fiber sheath imposes a strong planar director alignment at the boundary between liquid crystal and fiber sheath, stabilizing this smectic geometry. Most likely there must have been a realignment of the liquid crystal after fiber formation because, first, the much greater viscosity for flow along than perpendicular to the layer normal ought to ensure that the liquid crystal was pumped with concentric layers into the Taylor cone. Second, a smectic is easily stretched in the plane of the layers, in which it is a fluid, but it is very difficult to stretch it along the layer normal, since in this direction it behaves like a solid. Thus, also throughout the various stretching processes during spinning the coaxial smectic geometry should have been promoted. The fact that we eventually see the opposite geometry means that the interaction between the PVP fiber sheath and the liquid crystal is so strong in promoting director alignment along rather than perpendicular to the sheath that the liquid crystal geometry (presumably) adopted during spinning is unstable, quickly being replaced by the geometry with layers perpendicular to the fibers.

The lateral extension of the smectic layers is very small with this geometry, only the $\lesssim 1\mu$m diameter of the confined space inside the fiber. This size is smaller than the thickness of the thin cells typically used for preparing planar surface-stabilized FLC samples of very short-pitch SmC* materials. Also in that case a geometry with small lateral smectic layer extension (here only in one dimension) is secured by means of strong director anchoring at the sample boundaries, hence it is in this sense perhaps not so surprising that strong director anchoring at the fiber sheath can counteract the concentric layer geometry inside the fibers, at least for the SmA phase. The polymer chains are stretched along the fiber through the spinning process, most likely leading to a situation similar to that achieved by rubbing the polymer alignment layer used in standard liquid crystal cells. Moreover, at least for the smectic phase the cylindrical symmetry prohibits planar alignment perpendicular to the fiber axis, as this would require a radial smectic layer configuration, incompatible with the requirement of constant layer spacing.

For SmC or SmC* the situation is dramatically different. While the geometry with **n** along the smectic layer normal of SmA does not render the cylindrical symmetry of the fiber problematic, the tilted director of SmC/SmC* leads to frustration. The requirement that each smectic layer should have uniform director tilting direction is incompatible with the circular boundary of the layer (unless the anchoring is so weak that it does not influence the tilting direction at the boundary, but all experimental evidence suggests strong anchoring). It is thus a very interesting question for our on-going experiments to establish how a SmC or SmC* phase resolves this frustration. One may consider a number of scenarios. First, the SmC geometry may be replaced by SmA in order to avoid the problem. Second, a modulation of the tilt magnitude may occur from the layer perimeter to its center, the tilt disappearing at the center (in essence a disclination
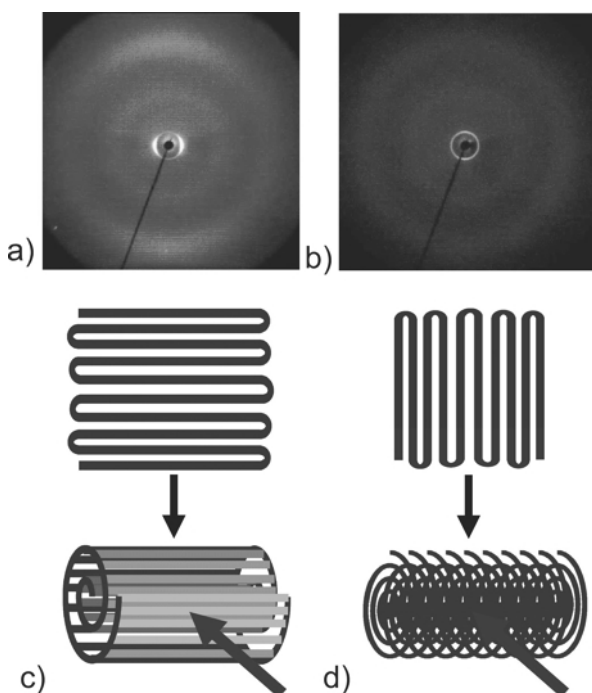
Figure 3.12: a-b: X-ray diffraction patterns (courtesy of Dr. U. Baumeister) from 8CB inside coaxially electrospun PVP fibers (prepared by Ms. E. Enz), rolled into a scroll and placed into a Mark capillary. c-d: Schematic illustration of the fiber rolling geometry and the direction of the incoming x-ray beam. From paper 11.

in the C-director field along the fiber axis). The opposite configuration is of course also possible as a third scenario, a SmA geometry prevailing at the border to the fiber sheath whereas the larger part of the interior of each layer is in SmC geometry with a well-defined tilt direction. Fourth, this interior geometry of each layer may instead be coupled to a relatively rapid rotation around the cone surface taking place on approaching the perimeter, to allow for the circularly varied tilting direction. Of course other scenarios are possible. In case of the chiral SmC* phase the influence of the spontaneous polarization on which scenario prevails may be quite strong since the director field under confinement has been shown to be strongly influenced by high polarization values in case of planar cells [122].

3.2.4 Phase sequence and phase transitions of liquid crystals inside electrospun fibers

It has been experimentally well established that strong encapsulation of liquid crystals can have dramatic consequences for their phase sequence [123–127], particularly sensitive phases such as the chiral smectic-C intermediate phases even disappearing completely already at relatively large surface spacings, like some 10 μm [124]. As the inner sample spacing in this latter case was an order of magnitude larger than the *outer* fiber diameter in our coaxially electrospun fibers, we can clearly expect to see an influence from the encapsulation, even on more robust phases like nematic and SmA. Moreover, the cylindrical symmetry may have a particular effect, as already speculated above for SmC phases and as will be further discussed for the case of chiral nematics and blue phases below.

It was thus not entirely surprising when the Raman characterization of the PVP-TiO$_2$ sheath fibers containing the standard nematic mixture RO-TN 403/015 S revealed a dramatic increase of the clearing temperature for the nematic phase inside the fibers. The anisotropic state was detected by comparing the liquid crystal peak strength for polarization parallel and perpendicular
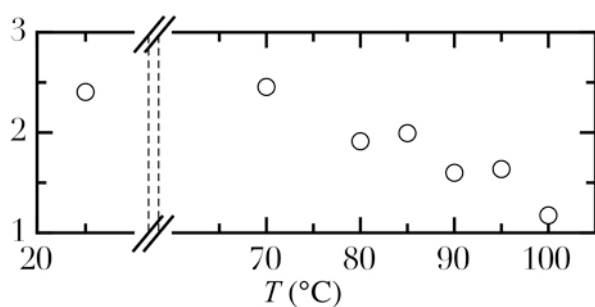
Figure 3.13: The ratio of the intensities of the aromatic ring stretching Raman mode from RO-TN 403/015 S inside the electrospun fibers of Fig. 3.6 for polarization parallel and perpendicular to the fiber axis, as a function of temperature. From paper 10. Reproduced by permission of the Royal Society of Chemistry.

to the fibers, their ratio being greater than 1 for the nematic phase and 1 for the isotropic. While the bulk nematic phase of the mixture clears at 81.5°C, the peak strength ratio for fibers in which it was contained was not much smaller at 85°C than at room temperature, decreasing only gradually on further heating, cf. Fig. 3.13. This figure shows that not only was the nematic temperature range expanded upwards by no less than 20°C, the first-order character of the nematic-isotropic transition also disappeared as a result of the strong confinement, as evidenced by the ratio going seemingly continuously to 1 on heating.

As the ratio is only moderately high at room temperature this suggests that the liquid crystal is not very well aligned with **n** along the fiber axis. As will become clear in the description below of the optical characterization of fibers with less TiO_2 in the sheath, containing chiral nematic liquid crystal, this may well be related to a break-up of the liquid crystal core into droplets, somewhat elongated along the fiber. This process is less apparent when using pure PVP in the core, allowing more complete and continuous filling of the fibers and thus a better definition of the liquid crystal director, but in these fibers with a greatly TiO_2-dominated sheath a droplet formation may be expected, explaining the low effective anisotropy of the nematic phase.

The smearing-out of the clearing transition induced by the confinement has been observed previously, for nematic liquid crystals filled into random-network glass matrices with a pore size of just 7 - 30 nm [123]. While we do not yet know for certain the inner diameter of our fibers it is probably an order of magnitude larger. Once a reliable method of characterizing the inner diameter of the electrospun fibers has been identified (see the above discussion about problems related to this) it will be interesting to study the phase transition behavior of liquid crystals while varying the spinning conditions such that the inner diameter is tuned from a few nanometers to about a micron. This should allow a determination of the critical confinement size for influencing the character of the phase transition.

A more detailed characterization of the effect of confinement on the phase sequence was carried out with coaxially electrospun fibers of 8CB inside a pure PVP sheath, cf. Paper 11. Relatively thick fiber mats were spun, containing a sufficient amount of liquid crystal to give a response in differential scanning calorimetry (DSC) experiments, allowing us to see how the SmA-N and N-isotropic phase transitions were affected by the encapsulation. As expected, the phase transition peaks became weaker and more smeared out than for a bulk sample, and the two transitions approached each other upon increasing confinement, until they could no longer be resolved in a fiber spun with 5μL/hour liquid crystal flow rate, cf. Fig. 3.14. The increase in clearing point is much less pronounced than in the previous study, most likely because the encapsulation is not as strong in the pure PVP sheaths as in case of the TiO_2-PVP composite sheath.

The strong effect on the smectic-nematic transition temperature essentially seems to have its origin in an encapsulation-induced kinetic stabilization (superheating and -cooling, mainly the latter) of whatever molecular arrangement that is presently in place. In the thinnest fibers
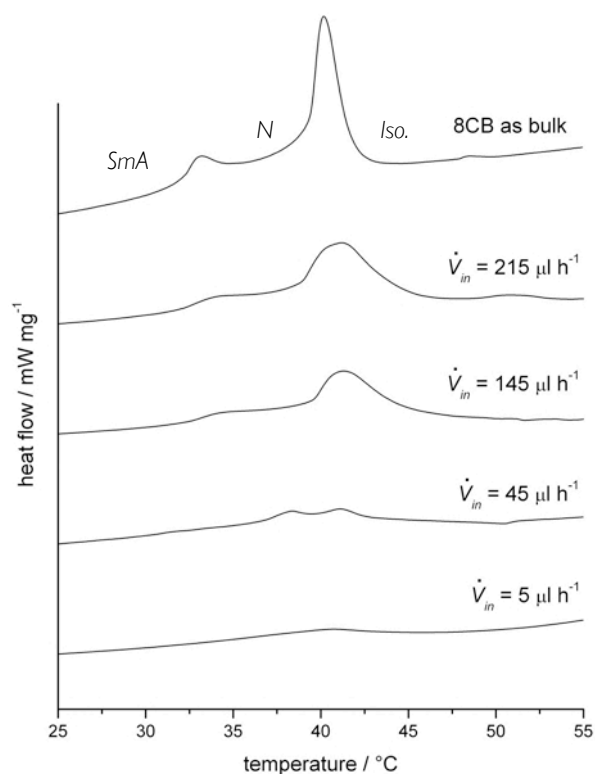
Figure 3.14: Differential scanning calorimetry curves on heating for 8CB in electrospun PVP fibers, as a function of liquid crystal flow rate (lower rate yielding thinner fibers, with stronger confinement). From paper 11.

both liquid crystal transitions could be detected during the first heating from room temperature (where the liquid crystal is in the SmA phase), by DSC as well as in polarizing microscopy. But on subsequent cooling only the isotropic-nematic transition was found and it was shifted to lower temperature; the smectic phase seemed to have been suppressed. However, after storing the samples several weeks at room temperature, the SmA phase was again found in the fibers and the SmA-N transition was detected and distinguished from the clearing transition upon heating these fibers, just as during the initial heating experiment.

Most likely, the mesogens are rather strongly anchored to the inner surface of the polymer sheath, with the order given by the liquid crystal phase prevailing. If the temperature is changed this surface-stabilized cylindrical layer of molecules will counteract reorganization into a less or more ordered phase even if the transition temperature to another phase for a bulk sample is passed. In other words, the DSC data in Fig. 3.14, obtained on heating experiments, should not be interpreted as a sign that the nematic phase is squeezed out of the phase diagram, rather that the smectic phase—once formed—is kinetically stabilized by the confinement such that it may persist all the way to the clearing point of the heating experiment. But on cooling, it is the nematic phase that is stabilized for the same reason, the smectic phase this time having seemingly 'disappeared'.

A somewhat different type of modification of the phase sequence was observed when the chiral **mixture 2** was encapsulated in fibers. Here the phase transition between N* and BP* truly disappeared, on heating as well as on cooling. This was thus not simply an example of kinetic stabilization and supercooling/-heating but in fact a result of the two phases becoming degenerate in the cylindrical confinement. This rather subtle issue will be discussed in the following.

3.2.5   The optical properties and phase behavior of cholesteric and blue phases inside electrospun fibers

The strongly colored selective reflection from short-pitch cholesteric and blue phase liquid crystals renders these phases most attractive and the temperature dependence of the N* pitch makes it straightforward to apply cholesterics as temperature sensors. Generally one uses films with polymer-dispersed cholesteric phase for such purposes, e.g. in simple wine thermometers etc. If the selective reflection appears also from cholesterics encapsulated in electrospun fibers this would immediately render the produced non-wovens useful in various temperature sensing situations (provided that the fibers are rather thick, a requirement I will explain below) where the more common polymer-dispersed cholesterics are less practical. One could for instance spin a web of cholesteric-containing fibers over an apparatus of arbitrary shape, giving it a surface that continuously reveals the temperature at every part, with full spatial resolution. Alternatively, pipes or tubes can be coated with the fibers to monitor the temperature of liquids or gases flowing through a complex system in a cheap and efficient way, useful for monitoring the performance of a cooling water system. Finally, with the right type of polymer sheath the cholesteric phase could be incorporated into synthetic textiles that could find use in cloathing. Not only could one get a temperature read-out of from the textile, but with a porous sheath and adequately prepared cholesteric mixture the textile could function as a chemical sensor [128, 129], useful for people working in hazardous environments.

There is thus good reason to investigate the possibilities of encapsulating N* or BP* liquid crystals in electrospun fibers and to study their optical properties. This has been a major goal of one of my students (Eva Enz) and myself the last year and we have now come to the stage where the concept is proven and several requirements for engineering-style optimization have been identified in order to take it to the stage where a product can be realized. At the same time many new interesting fundamental scientific questions have appeared, most of them still unanswered. Our observations and present understanding regarding coaxial electrospinning of fibers with chiral liquid crystals are summarized in this section and in a manuscript soon to be submitted to *Journal of Materials Chemistry*.

We have worked mainly with two cholesteric mixtures in our experiments so far. In part we have used the three-component cholesteryl ester mixture in Fig. 3.7e (**Mixture 1**), a bulk sample exhibiting selective reflection changing from red via green to blue on heating in the range 20-25°C. Outside this temperature range the mixture is colorless. But our standard cholesteric was **Mixture 2** (Fig. 3.7d), exhibiting blue-green selective reflection at room temperature. At 28.5°C a transition to a blue phase occurs, and on further heating the mixture turns isotropic at a temperature of 30.2°C. Here I will limit the discussion to the results obtained using this mixture.

Mixture 2 is convenient for our purposes because it combines a short enough pitch at temperatures around room temperature (the pitch does not change much with temperature in this mixture) to give blue-green selective reflection with reasonably low viscosity, such that it can easily be pumped by our microfluidics device. We can thus work with this mixture without any need for heating. As mentioned above, it could be encapsulated in fibers with pure PVP sheath as well as in PVP-TiO_2 composite fibers. I begin by discussing the results in the former case.

We prepared a series of PVP sheath fibers containing **Mixture 2**, varying the liquid crystal flow rate as well as that of the sheath solution. With increasing liquid crystal flow rate the fiber core, and thus the fiber, is expected to get thicker and the sheath thinner (since the same volume of sheath solution must now surround the larger-diameter liquid crystal core), an expectation that we could basically verify experimentally, as illustrated in Fig. 3.15. What was also apparent
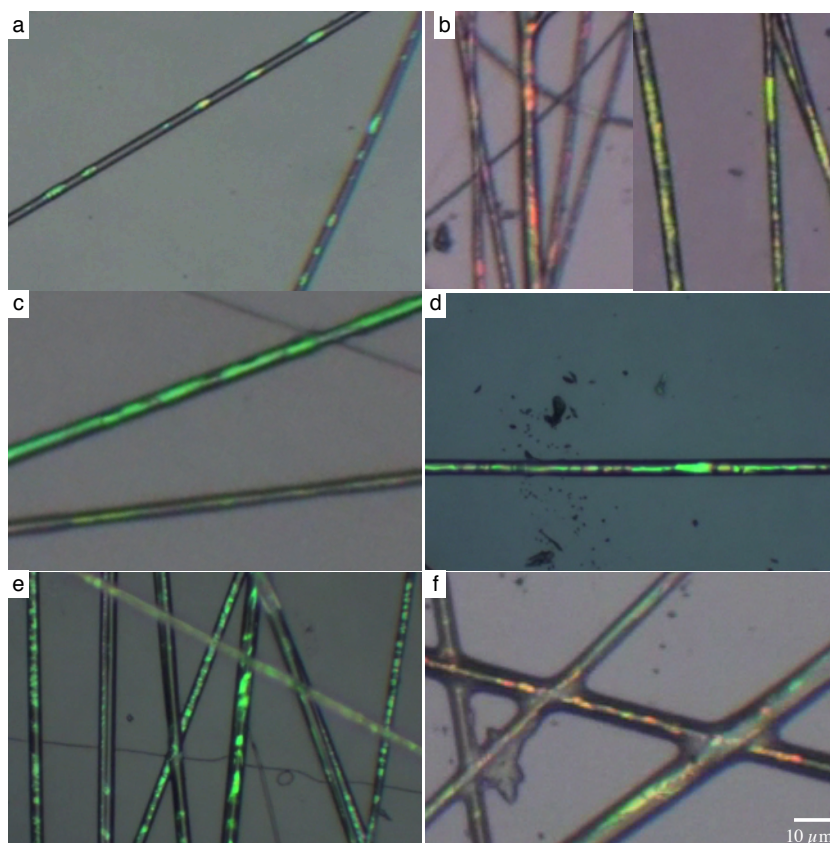
Figure 3.15: Optical microscopy images (reflection, polarized illumination but no analyzer) of core-sheath electrospun fibers (prepared by E. Enz) with the chiral nematic **mixture 2** in the core (SEM images of some of these fibers are shown in Fig. 3.8). The sheath consists of pure PVP (prepared from a 12.5% PVP in ethanol solution, pumped at 1.8 mL/h in all cases but (e) where it was pumped at 3.0 mL/h), and the liquid crystal was pumped at 0.14 (a), 0.36 (b), 0.48 (c), 0.63 (d and e) and 0.80 mL/h (f), respectively.
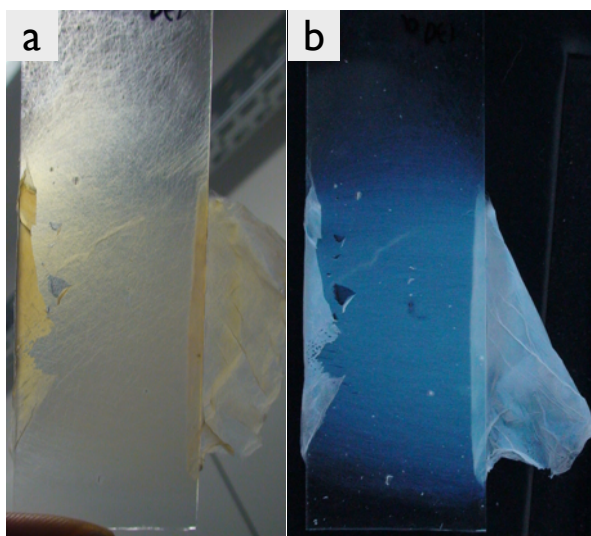
Figure 3.16: A coaxially electrospun mat with pure PVP sheath and a large amount of the cholesteric **mixture 2** inside, viewed in transmission (a) and reflection (b).

was that the degree of liquid crystal filling depended strongly on the flow rate. At low flow rates the fibers were not only thinner but the liquid crystal was also distributed in elongated drops along the fiber (a), rather than forming a continuous thin core. The most uniform filling was obtained at intermediate flow rates (b-e), as too high flow rate resulted in poorer general fiber morphology and again more uneven filling (f).

It is very pleasing that the selective reflection color is clearly visible in the fibers. In fact, with high liquid crystal flow rate the whole fiber mat viewed by eye against an opaque background actually obtains the color reflected by the liquid crystal, cf. Fig. 3.16. If instead viewed in transmission the mat acquires the complementary color, as expected. In fibers produced with lower liquid crystal flow rate, thus with smaller inner diameter, it was quite striking that the color was generally not the natural blue color of the liquid crystal. In many cases the color varied between blue-green and yellow but in certain locations it could even reach the red end of the spectrum, cf. Fig. 3.15b showing two different locations of the same mat. With the highest flow rate, on the other hand, there were also locations like in Fig. 3.15 f where all colors existed right next to each other in the same single fiber.

When viewed in transmission most of the selectively reflecting fibers showed the same color as in reflection, irrespective of fiber alignment with respect to the polarizer, that is we had 'selective transmission' of the color being reflected but for the opposite circular polarization, passing through the linear analyzer. In many cases there was however an orientation sensitive birefringent light transmission superimposed, in contrast to when a flat cholesteric sample is viewed in planar alignment. Finally, fibers showing no selective reflection/transmission but standard birefringence were also observed. Both phenomena will be explained below.

When heating and cooling the fibers we noted first that, as in the fibers with non-chiral liquid crystal, the clearing point went up, the more so the thinner the fiber. In the thinnest the clearing point was about 15 K higher than in the bulk liquid crystal. We also noticed that the transition between blue phase and cholesteric phase could no longer be detected. This held for polarizing microscopy as well as DSC investigations, on heating as well as on cooling. There was simply no sign of phase transition until the core turned isotropic. At first we thought that the blue phase had thus been expanded dramatically in temperature range downwards by the encapsulation, a model that could explain the play in color (randomly oriented domains each reflecting a different color) as well as the lack of an inter-liquid crystal phase transition, but with time we realized that
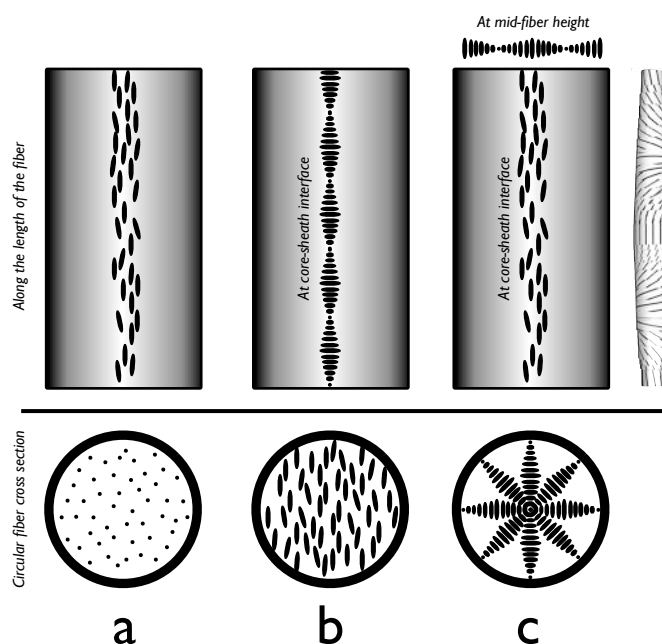
Figure 3.17: Schematic illustrations of how the director field of a cholesteric liquid crystal may be inside an electrospun fiber, considering in *a* and *c* the imposed cylindrical confinement with planar anchoring.

the cylindrical geometry of the fibers with very small diameter actually has a profound influence on the balance between cholesteric and blue phase, such that the two phases essentially become degenerate in case of a sample that uniformly adopts the alignment imposed by the cylindrical boundary. The lack of phase transition is then in fact to be expected. In case of the thicker fibers with multiple colors (Fig. 3.15f) there may, however, indeed be an expanded regular cubic defect lattice blue phase, as motivated below.

In order to understand the different optical characteristics of the fibers as well as the unexpected change in phase sequence we need to consider briefly what the cholesteric director field may do when confined in very narrow cylindrical space. As illustrated schematically in Fig. 3.17, we consider three distinctly different cases. First, the helix could be unwound (case *a*), a scenario one might expect for strong surface anchoring and extremely thin fibers and/or long pitch (but we know that the latter certainly is not our case). However, if the inner fiber diameter is on the order of half the natural pitch length of the cholesteric or greater the same director alignment at the interface to the polymer sheath allows a helical structure with the helix axis perpendicular to the fiber (case *c*). Since our fibers fulfill this thickness condition there thus seems to be no reason to expect the unwound configuration and we therefore rule out the case of Fig. 3.17a, finding case c much more likely.

A third possibility is that the helix develops along the fiber as in Fig. 3.17b. Compared to case c this would be favorable in the sense that the helix has its natural pitch regardless of fiber diameter but it would require degenerate director alignment at the polymer-liquid crystal interface, or a region close to the sheath through which the director rotates by a 90° angle. This would be expected only in case of very weak surface anchoring of the director or for very thick fibers. As seen in the sketch of the perpendicular cross section in Fig. 3.17b this scenario violates the cylindrical symmetry locally (the drawing is done for degenerate boundary but the violation

holds for either solution), but globally it is recovered over a fibre length of half the pitch.

While Fig. 3.17c is the only model fitting with selectively reflecting fibers, which is what we have seen experimentally in most cases, the texture category with strong birefringence but no selective reflection could in principle be explained by the configuration in Fig. 3.17b. Since we are looking perpendicular to the helix of a short-pitch N* phase we have a birefringent material with its optic axis along the fibre axis, fitting the experimental observations well. The case of unwound helix (a) would give the same optical behavior but as motivated above the helix unwinding is very unlikely in our fibers. However, also case Fig. 3.17b is rather unlikely considering our previous findings with nematics and smectics in PVP fibers, demonstrating that the director prefers to align along the fiber axis, not perpendicular as would in this case be necessary. We will see in a moment that also case c can be compatible with lack of selective reflection and, in contrast to N* phases in standard planar alignment, it will give some birefringence. This is because of the cylindrical symmetry: at mid fiber height the helix is in the plane of our sample slide, so this flat section of the fiber will give only birefringence, no selective reflection. The complete optical response of case c should thus be a combination of selective reflection with weak birefringence, which is indeed the texture we observed the most often. We can immediately rule out the option that the phase might be an ordinary BP* in any fiber exhibiting (linear) birefringence, since BP* is optically isotropic. In the cases where no birefringence could be detected the BP* phase could be a plausible explanation, but it could also be that the fiber is so thin that the birefringence is difficult to detect.

Note that case c, which is the most likely scenario for our fibers, requires the director at the center of the fiber to be along the fiber axis since this is the only central director orientation that is compatible with the cylindrical symmetry and allows a director distribution without a singular core (i.e. a disclination in which the core would be isotropic). While a structure with singular core cannot be excluded, it would represent a configuration with much higher energy. In order to also fulfill the external boundary conditions, where the liquid crystal meets the polymer sheath, the inner diameter of the sheath must thus be a multiple of the helix pitch. Because we have a certain variation of fiber diameters we therefore expect a variation in color, as the pitch must adjust to the actual fiber diameter (like in the classic experiment of a Cano wedge cell). Note that the cylindrical geometry is twice as restrictive on the helical pitch as the flat geometry of standard cells. While the substrate distance of the latter must be a multiple of half the pitch, the cylindrical fiber diameter must be an integer number of the *full* pitch, since also the central boundary condition must be fulfilled. This gives a strong quantization of color, to the extent that in a thin fiber it is the fiber inner diameter that effectively determines the color, cf. Fig. 3.18.

This quantization effect is shown quantitatively in Fig. 3.18a, where the effective selective reflection wavelength is plotted (it has been calculated for the case of an effective refractive index $n_{\text{eff}} = 1.5$) as a function of natural pitch, for a few different fiber diameters. This graph is very important because it demonstrates that for thin electrospun fibers the color is almost entirely defined by the inner fiber diameter: the natural cholesteric pitch is close to unimportant. This means that fibers spun for temperature sensing applications must be spun at least some 5 μm thick in order to give any kind of temperature resolution. Fibers with inner diameter in the 1 micron range will clearly not allow any important temperature variation of the helical pitch.

An experimental demonstration of the phenomenon is given in Fig. 3.19, albeit for a planar-aligning cell rather than a fiber. This cell is 1.7μm thick and its substrates have alignment layers inducing planar alignment with collinear director at each substrate. The cell is filled with the cholesteric **mixture 1** and it is being quickly heated from 20°C, where its natural reflection wavelength is just outside the visible range, in the IR, through the temperature range of visible selective reflection, the pitch rapidly decreasing in the process. Regardless of natural
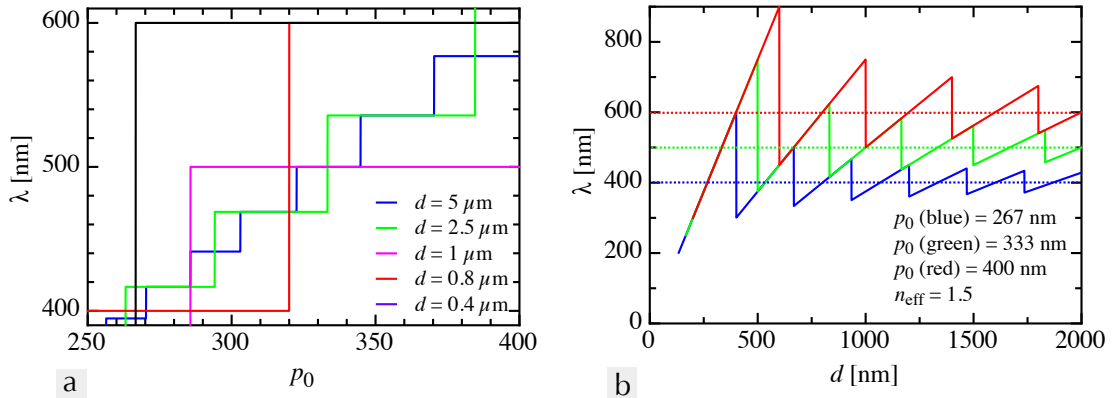
Figure 3.18: Selective reflection wavelength λ from a cholesteric confined in a cylindrical fiber as in Fig. 3.17c, as a function of natural pitch for five different inner diameters (a), and (b) as a function of inner diameter d, calculated for three different natural pitch lengths p_0 corresponding to blue, green and red selective reflection from the cholesteric in its natural undistorted state. In (b) the three curves have been plotted in the color of their respective natural reflection and as guide for the eye this wavelength has been indicated with a horizontal line in the same color. Note that the vertical parts of these curves are plotting artifacts: each vertically drawn segment should in fact be a discontinuity in the curve.

pitch the confinement in the cell requires that an integer number of half pitches match up with the 1.7μm cell gap. The blue color in b) is the last color that can be seen, the next step in the process being areas with black textures, revealing a pitch too short to give visible selective reflection. Considering the reduction of light wavelength in the medium we may assume that the optical periodicity of the helix reflecting this color could be around 300 nm (corresponding to an effective refractive index $n_{\text{eff}} \approx 1.5$), i.e. the pitch would be 600 nm. But considering the boundary conditions we must adjust this value to 283 nm, corresponding to six half periods of a helix with a pitch of 566 nm fitting in the cell. In the adjacent green area the helix must have one quantum (or half-pitch) less, i.e. here the half pitch is 340μm (giving selective reflection at a wavelength of about 500 nm) which fits five times between the boundaries. In the red-orange area four half pitches fit, corresponding to a half-pitch of 425 nm (reflection at 629 nm) and in the black area in a, finally, the pitch is so long that only three half-pitches fit, resulting in a half-pitch of 567 nm (reflection in the IR). Again, the central boundary condition acting in the *cylindrical* fibers renders the quantization twice as strong as in this case of flat geometry. As our fibers produced so far have outer diameters in the range 1-2 μm we can thus expect only one color to be allowed in a particular fiber (Fig. 3.18a), any variation of the natural pitch of the cholesteric having no effect.

While we would thus not see any color variation with temperature in our thin fibers, even if we would have filled them with the temperature sensitive **mixture 1**, we do see a rather strong variation in color between fibers, and sometimes even within one and the same fiber. At least the former can also be explained by the requirement on the pitch to adjust to the confinement, since we have a certain polydispersity in fiber diameter. The color variation as a function of fiber diameter is plotted in Fig. 3.18b. Here one can see that variations across the full visible spectrum, what we in fact see in our fibers, can only occur at very small inner fiber diameter. In fibers with an inner diameter of about a micron or thicker the distortion away from the natural pitch will never be sufficient to account for the most extreme color changes, red reflection appearing from
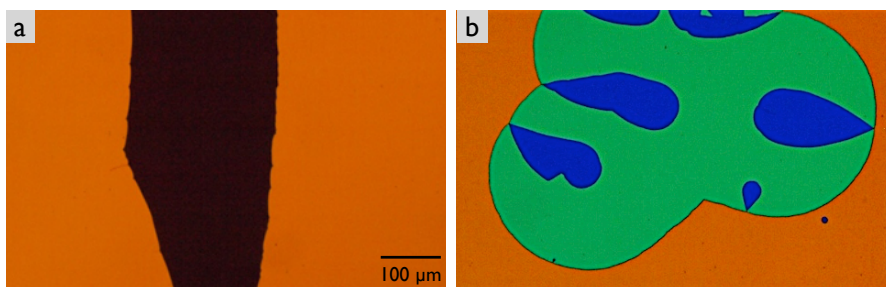
Figure 3.19: Reflection polarizing microscopy photos of the cholesteric **mixture 1** in a 1.7 μm thick planar-aligning cell with substrates prepared for director anchoring along the same direction (up in the picture, the same as the light polarization), as the temperature is quickly increased from 20 to ~26°C. The helix pitch shrinks from a value giving rise to reflection in the IR to one where the reflected color is in the UV. Photo *a* is taken at the beginning, photo *b* in the middle of the process, as the pitch is rapidly decreasing but not yet in equilibrium everywhere, resulting in different areas having different pitch lengths. For further explanations, see main text.

our cholesteric that is blue in its natural state. With a natural pitch p_0 of 333 nm (blue natural color, $\lambda_0 = 400$ nm) we see in Fig. 3.18b that red selective reflection would arise only if the inner diameter is some 400 nm, allowing exactly one very extended helical pitch to fit in the fiber. This means that the fibers where we see this color must in fact have an inner diameter of about this value. The majority of fibers are however more yellow-green, requiring an inner diameter that is either even thinner or around 650 nm. Even larger inner diameters would provide too little constraint, such that the color would be essentially the natural blue one. Having a most common inner diameter lower than some 400 nm in our fibers seems rather unlikely, considering that the outer diameter is in the 1-2 μm range. Thus we can from the selective reflection colors estimate that our fibers that show selective reflection have inner diameters in the range 300 - 650 nm, most of them at the higher value. Thus, although we have not been able to carry out direct electron microscopy imaging of the inner fiber structure the peculiar optical properties of an N* phase in very thin fibers actually provides us with an indirect measure.

We also have many fibers that do not show any visible selective reflection color and it is important to realize that this does not mean that they are unfilled or have the liquid crystal in a non-helical structure. Fig. 3.18b shows that a cholesteric material with $\lambda_0 = 400$ nm, naturally reflecting in the blue, will reflect in the UV when confined in an electrospun fiber of certain thickness, that is they will not reflect *any* visible color. All fibers with thickness yielding a compression of the helix will look colorless. This is not in any sense an extreme case but in fact something we would expect for half of the fibers if we linearly increase the inner diameter through the range 400 nm to 2 μm, as seen in the figure. We thus conclude that fibers not giving any color in reflection are most likely not unfilled; they may simply have an inner diameter that distorts the liquid crystal to reflect in the UV. Should the pitch be just below the limit for selective reflection we should however have strong optical activity (see Fig. 1.22) and it will also be birefringent, hence this situation may be the origin of many of the non-reflection-colored but birefringent fibers that we encountered during the fiber characterization.

For the regions where the color varies very strongly over small distances, e.g. in Fig. 3.15f, another explanation to the color change must however be sought, because the required rapidly changing inner fiber diameter seems unlikely. Here it might be that the ordinary cubic lattice BP* structure in fact develops, differently oriented domains giving rise to the different colors.

This seems likely since the observations were done in the fibers spun with the greatest liquid crystal flow rate, thus with the greatest inner diameter. In case of a cholesteric phase Fig. 3.18b tells us that these fibers should look blue (as in Fig. 3.16), not red or green.

The configuration in Fig. 3.17c is unusual for a cholesteric phase, in which the director normally twists only along a single direction. In the fiber confinement there is instead a helical director twist in *all* directions perpendicular to the fiber axis, imposed by the cylindrical symmetry. This director configuration that the N* phase is now forced to adopt is in fact nothing else than the double-twist cylinder configuration that is the basic building block for blue phases (see model on the far right of Fig. 3.17 and section 1.1.5). The same situation was achieved by Heinz Kitzerow and co-workers [130] by filling cholesteric liquid crystals into glass capillaries, albeit on an order of magnitude larger scale. Both the cholesteric pitch and the capillary diameter were typically in the range tens of microns. Rather than seeing selective reflection from their capillaries with director aligned parallel to the capillary they thus saw a fingerprint texture, reflecting the variation of the director in the capillary center plane (see sketch at the top of Fig. 3.17c). The double twist cylinder was thus in their case structurally analogous to that of blue phases but the scale was entirely different. Moreover, the liquid crystal mixtures used in those studies did not exhibit a blue phase in their phase sequence, only the N* phase.

Considering the blue phase-like director configuration imposed onto the N* phase by the cylindrical confinement, and the fact that the structural scale here is the same as that in bulk blue phases, we can now understand why we no longer see any N*-BP* transition for our **mixture 2** in the fibers: the cylindrical confinement of the N* phase with strong surface director anchoring gives the N* phase a BP*-type structure, hence the two phases have become degenerate. For very thick fibers it should be possible to have a phase transition again, since multiple double-twist cylinders could then build up a cubic network in the BP* phase once the cylindrical confinement is less strong. As discussed above, the regular BP* phase indeed seems to appear in our thickest fibers, although we did not see the phase transition even here. It may thus be that these fibers are not thin enough to make the N* and BP* phases degenerate, but they may prevent the phase transition (possibly kinetically), as was the case in our earlier fibers spun with non-chiral liquid crystals.

The selective reflection of **mixture 2** was observed also in the fibers with slightly sturdier sheath, achieved either by increasing the polymer concentration or by adding the Ti(OiPr)$_4$ sol-gel precursor to the outer spinning solution, but the liquid crystal appeared somewhat different compared to the pure PVP sheath fibers, cf. Fig. 3.20. Here continuous filling was never seen but the cholesteric was separated into small and quite regularly spaced droplets throughout the sample. The main reason for the different encapsulation of the liquid crystal here, compared to the earlier described fibers, is most likely the higher viscosity of the sheath solution. The increase in polymer concentration obviously increases the viscosity of the outer fluid used for producing the fibers in Fig. 3.20a whereas the outer solution used in cases b-e was initially actually much less viscous, due to the lesser polymer content. However, as the gelation starts when the sol-gel precursor is hydrolysed by water from the air during spinning the viscosity of the jet increases dramatically in flight.

From experiments in the Xia group with coaxial electrospinning of mineral oil [118] and octadecane [82], respectively, inside a PVP + Ti(OiPr)$_4$ sheath solution it is known that a change in viscosity of one of the fluids can have a dramatic impact on the continuity of the core. With the rather viscous mineral oil (viscosity about 70-80 mPa s) continuous and uniform filling of the fibers could easily be achieved with this sheath solution but in case of the much less viscous octadecane (heated to the liquid state prior to spinning, giving it a viscosity in the range 2-4 mPa s) varicose break-up occurred inside the coaxial jet, resulting in regularly spaced drops of octadecane in the produced fibers. By increasing the feed rate of the inner fluid its content in
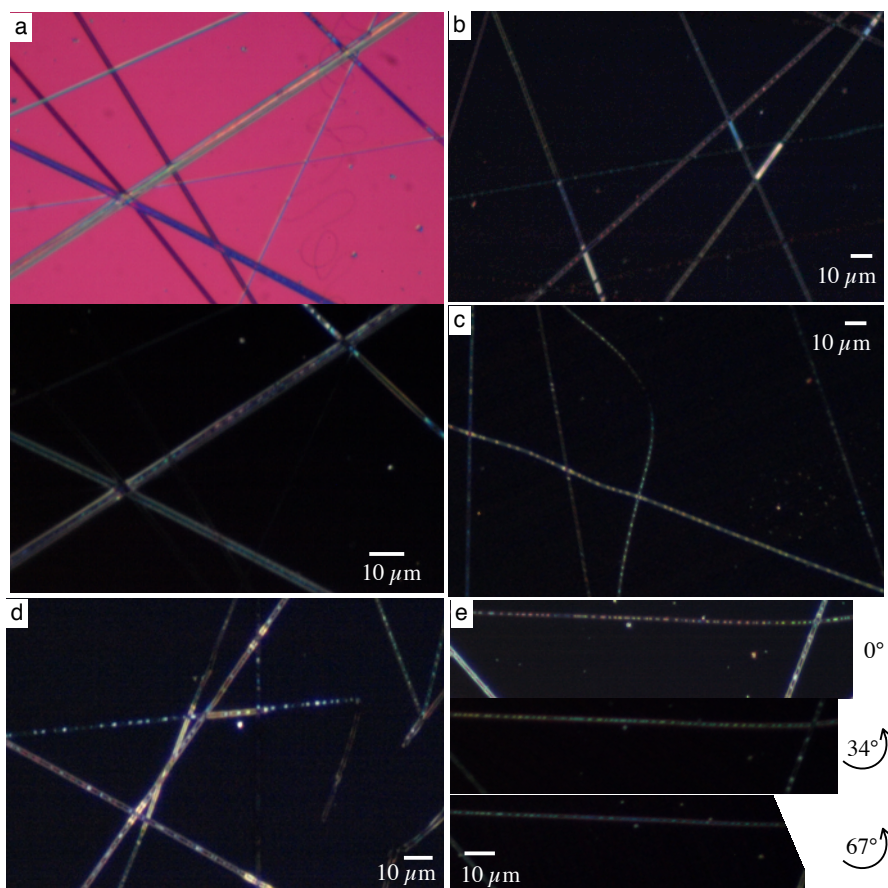
Figure 3.20: Optical microscopy images of core-sheath electrospun fibers (prepared by E. Enz) with the chiral nematic **mixture 2** in the core, pumped at 0.80 mL/h flow rate in a, d and e, 0.26 mL/h in b and 0.48 mL/h in c. The sheath in *a* is pure PVP, spun from a 15% PVP in ethanol solution, whereas it in *b* - *e* is a TiO$_2$-PVP composite. The upper photo in *a* is taken in differential interference contrast (DIC) mode, all others in polarizing microscopy mode. The crossing of fibers below and to the left of the middle in *a* is the same location as imaged by SEM in Fig. 3.10a, but turned by an angle of some -45°. In *e* the sample texture for three different fiber orientations are shown, the rotation resulting in a change in the reflected color of the liquid crystal droplets.

the final fibers could be substantially increased and the drops then adopted an elongated shape, but a fully continuous core was not reached in this case.

In our case the liquid crystalline state of the core fluid allowed us to spin fibers also with the much less viscous sheath fluid containing 12.5% PVP and no sol-gel precursor, resulting in an almost continuous filling of the fibers, cf. Fig. 3.15. The difference between these experiments and those in Fig. 3.20, as well as the observations of the Xia group clearly show that a proper matching of the viscosities of the inner and outer fluids is essential to obtain a continuous and rich filling of the fibers produced by coaxial electrospinning. If the discrepancy in elongational viscosity (for a Newtonian fluid simply three times the shear viscosity) between the inner and outer fluids is too great, the inner jet is destabilized, most likely through the Rayleigh instability acting here not at the interface air-fluid but instead outer-inner fluid. Remember that the inner and outer fluids must be immiscible in coaxial electrospinning, hence there is a substantial interfacial tension between them. Apparently, the viscosity of the outer solutions used for the fibers in Fig. 3.20 was too high to achieve continuous filling with **mixture 2**, although the filling degree was improved somewhat by increasing the flow rate, with elongated droplets being detectable in some places (not in the photos in Fig. 3.20, however). The more viscous **mixture 1** may be advantageous in this respect, although fine-tuning of its temperature during pumping to the spinneret is required before this possibility can be tested.

The cholesteric droplets in these fibers had some peculiar optical properties, seen by rotating the sample. Rather than giving an orientation independent reflected color when illuminated by linearly polarized light, as for ordinary planar-aligned cholesterics, the color (through the analyzer) changed from blue to red during the rotation process, cf. Fig. 3.20e. The origin of this phenomenon has not yet been clarified, as these fibers were produced only very recently. It seems likely that the polarization of the incoming light with respect to the director at the top of the fiber becomes important for samples as thin as these.

3.3 Outlook: what does the future hold in store for electrospinning with liquid crystals?

We are only at the very beginning of the exploration of coaxial electrospinning with liquid crystalline cores. As a first pertinent observation we might point out the remarkable stabilization of liquid crystal phases, far beyond the bulk phase sequence, by encapsulation in the thin fibers. While we have delivered the proof of concept for three different liquid crystal types there is still much fine-tuning to be done, many variations of the systems are required (PVP sheaths are for instance practical in the academic laboratory but useless for textiles due to its highly hygroscopic character), and many interesting questions have appeared. The elucidation of these questions is a stimulating challenge in the academic sense, but to a large extent also a practical necessity if one wishes to apply the functional liquid crystal fiber mats.

Moreover, there are still several liquid crystal phases to be explored inside the fibers. We are in the process of exploring electrospinning of SmC/SmC* phases and will soon begin with spinning fibers with columnar discotic liquid crystal cores. As mentioned in section 1.3.2 these liquid crystal systems offer functionalities that may be very interesting to apply in a fiber configuration. For certain, the study of such composite fibers will be a most interesting academic research topic. Further ahead, other liquid crystals, in particular systems comprising bow-shaped mesogens, will offer new challenges and certainly many new surprises.

The advantages of electrospinning for preparing liquid crystal containing fibers is foremost the very small diameter, ensuring a confinement that is sufficiently strong to affect both the phase sequence and the physical properties of the liquid crystal. For an academic research lab the

relatively low investment costs and lab space required for an electrospinning set-up, and the ease in modifying it for specific purposes, also make the technique highly attractive. In contrast, for a commercial-scale production of temperature sensing textiles based on incorporated cholesteric liquid crystal, where the fibers should not be particularly thin, electrospinning may well prove not to be the best choice. Ordinary coaxial melt spinning is probably more appropriate for this purpose. This method was employed by Masahiro Nakata *et al.* to produce polyolefin fibers containing a cholesteric liquid crystal with outer diameter in the range 80-200 μm [131]. They were extruded from the melt and further drawn after spinning for reducing the fiber diameter. While indeed much thicker than the fibers produced by electrospinning, these fibers were produced in production-realistic conditions and they could be woven into fabric sheets.

Chapter 4

# Dispersing and aligning carbon nanotubes in lyotropic liquid crystals

4.1 A very brief introduction to carbon nanotubes

Carbon nanotubes (CNTs) are cylindrical nanoparticles of extreme anisometry that can be described as graphite sheets (graphenes) rolled into seamless tubular structures. While their diameter can be on the order of 1 nm, their length is typically in the μm range and can even reach several millimeters. The thinnest CNTs are of single-wall type (SWCNTs) whereas multi-wall carbon nanotubes (MWCNTs), consisting of several concentric tubes, can reach diameters of several tens of nanometers. As illustrated in Fig. 4.1, a graphene sheet could be rolled up into an SWCNT along different directions, identified by the indices (n, m) in terms of the graphite lattice vectors $\mathbf{a}_1$ and $\mathbf{a}_2$ (cf. Fig. 4.1). The resulting tube can be either chiral or non-chiral, the latter versions being the $(n, 0)$ *zigzag* and (n, n) *armchair* geometries (the names reflecting the shape of the edge of a CNT ideally cut orthogonally to its long axis). All others are chiral with a helical atom arrangement. The specific roll-up geometry (often somewhat imprecisely referred to as the 'chirality' of the tube) and the diameter of the SWCNT are of great importance, because these factors determine the electronic properties of the nanotube [132, 133]: tubes with roll-up indices having the relation $n - m = 3l$, where l is an integer, are metallic[1] while the remainder are semiconducting, with a band gap that inversely depends on the tube diameter.

The quasi-one-dimensional structure of a defect-free tube exhibits ballistic (scattering-free) electronic transport properties, hence CNTs have generated great interest in the field of nanoscale electronics. Also heat is conducted extremely well, the thermal conductivity of MWCNTs having been experimentally measured to surpass that of diamond [133]. The mechanical properties of CNTs are likewise quite exceptional. Multi-wall CNTs can be extremely stiff and the density-normalized modulus and strength of SWCNTs are many times those of steel [133]. The hollow geometry gives them low density, thus they are highly interesting for light-weight high-strength materials, either on their own in yarns, fibers or sheets [134–136], or as filler particles in CNT-polymer composites [137]. In both these classes of large-scale CNT-based materials, metallic CNTs are often desirable, as they allow e.g. the fabrication of transparent electrodes [138] or

---

[1]More accurate is here to distinguish between metallic and quasi-metallic tubes but since the band gap of the latter is so small that it cannot be experimentally detected, it is common to include these in the metallic group.
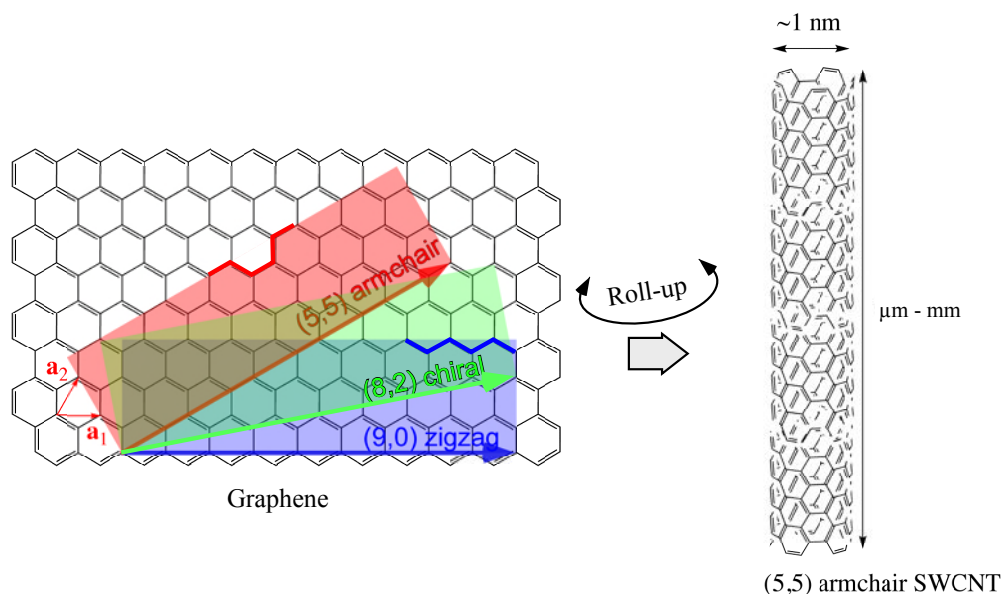
Figure 4.1: A single-wall carbon nanotube (SWCNT) can be viewed as a graphene sheet rolled up into a tube. Depending on the roll-up direction (n, m) the tube can be achiral (5,5 and 9,0 examples, the former giving the armchair tube on the right) or chiral (any direction between the achiral ones allowing closure into a seamless tube, e.g. the 8,2 example).

electromagnetic radiation shielding films [139, 140]. Among more recent trends in application-oriented carbon nanotube research can be mentioned CNT employment in pharmacology [141], ultrahydrophobic surfaces [142,143], photovoltaics [144], battery electrodes [145], sensing devices [146] or even enhancement of the display performance of liquid crystals [147].

4.1.1   Challenges in the application of carbon nanotubes

As interesting the properties of CNTs are, as difficult it is to harness them. A number of crucial post-synthesis processing steps must typically be passed in order to actually employ carbon nanotubes in a device, as schematically summarized in Fig. 4.2. Considerable progress in the field has been made during the last decade but there are still important issues to resolve, in particular since good solutions to one of the challenges may cause problems when addressing another.

Being particles with great surface area and consisting entirely of sp^2-hybridized carbon, CNTs attract each other strongly via van der Waals interactions and they therefore most often appear as disorganized bundles. Once high-quality CNTs have been synthesized[2] the large-scale aggregates that are the typical product must thus be broken up. The most common approach is to disperse the sample in an aqueous surfactant solution which is subjected to ultrasonication in order to mechanically break the aggregates, eventually yielding fully separated CNTs [148]. Reaggregation is prevented by electrostatic or steric repulsion between surfactant molecules adsorbed on the surfaces of the nanotubes. The ratio of surfactant to CNTs should however be

---

[2]Although still an important research topic, sufficiently efficient synthesis methods have by now been established to make commercially available carbon nanotubes a reality.
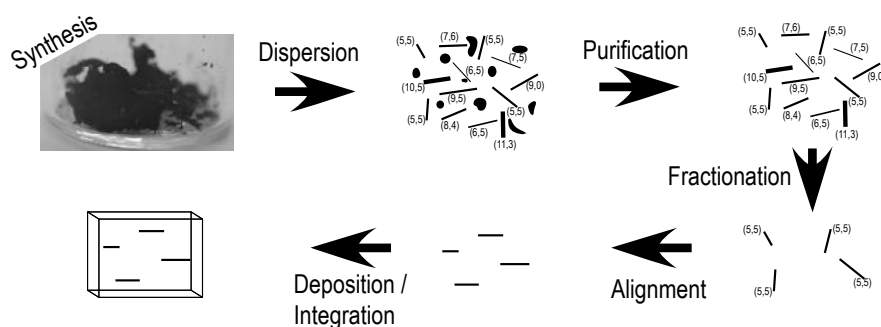
Figure 4.2: Schematic overview of the main challenges in the processing of carbon nanotubes that must be addressed in order to fully harness their unique properties in devices. Depending on the exact choice of processing scheme and the desired application some steps may be unnecessary, others may be added, and the order may also be different.

carefully tuned since otherwise depletion attraction will typically lead to substantial CNT flocculation [149,150], empty micelles in case of surplus surfactant playing the role of depletion agent, cf. section 4.4.

Alternatively, some organic solvents can be used with reasonable success if the CNT concentration is not too high [151]. A different approach is to covalently functionalize the CNTs, e.g. making them hydrophilic [152,153] or reducing them to salts for achieving truly soluble nanotubes [154]. Because of the impact on the electronic properties of the tubes [153] covalent modification is not always a good alternative, but in certain application areas or for specific purposes it has distinct advantages [155–158], most notably in the field of pharmacological uses of CNTs where hydrophilicity is imperative [159,160].

As all CNT synthesis methods yield unwanted byproducts (mainly amorphous carbon, graphite particles and metal catalyst traces) different purification methods must be employed[3]. Often also this step involves suspending the CNT sample in liquid, which is then centrifuged such that the impurities, due to their larger buoyant density, are collected in the sediment whereas well-dispersed CNTs remain in suspension. Alternatively amorphous carbon can be removed from the sample by introducing the sample in a special oven with carefully tuned high temperature, and various types of acid treatments may also play important roles in CNT purification.

Moreover, many applications of CNTs require that the tubes are strictly metallic or strictly semiconducting with a well-defined band gap. At the production stage this requirement cannot be met, since no CNT synthesis method has yet been found that allows precise control of the nanotube roll-up geometry. A raw CNT sample always contains a mixture of tube types, with different electronic properties. To solve this problem, a limited number of schemes have recently been devised for fractionating SWCNTs according to their electronic properties, allowing the removal of undesired tubes [161]. All schemes require that the CNTs be well suspended in a liquid, allowing the sample to be passed through a chromatography column or submitted to very strong acceleration in a high-power ultracentrifuge.

Efficient dispersion, purification and fractionation are criteria that in many cases are required but still not sufficient for employing CNTs. Reflecting their extreme anisometry, the physical properties of carbon nanotubes are highly anisotropic, hence the exploitation of the excellent electronic, mechanical and optical attributes to the fullest generally requires control of the tube

---

[3]The claim of 'impurity-free' CNT synthesis in some papers generally means that the amount of atoms other than carbon is small. Non-tubular carbon allotropes are normally present also in these cases.

orientation. Several schemes have been proposed to align CNTs, e.g. application of electric [162] or magnetic [163] fields, mechanical processing (shearing [164] or 'molecular combing' [165]), dispersion in liquid crystalline solvents [166] and growing the tubes with controlled direction [167, 168]. While the latter can be highly successful in terms of large-scale uniform tube orientation, the fact that the CNTs cannot be detached from the substrate without ruining their alignment prevents efficient purification and fractionation. Moreover, this solution to the alignment problem is not applicable to any of the bulk CNT synthesis methods that have been commercialized (e.g. the Hipco process), which are all substrate-free. In fact, even on an academic lab-scale, the growth of aligned tubes is far from trivial, in particular for SWCNTs. The ability to align *unsupported* CNTs is thus an important goal to strive for, key to the success of many carbon nanotube-based applications.

Field alignment certainly works, but magnetic fields of great strength are normally required (on the order of tens of Tesla), whereas electric fields act differently on different CNTs due to their varying electronic properties. Furthermore, the alignment is in both cases maintained only as long as the field is applied, hence the tubes have to be fixed onto the target substrate or in the target matrix in the presence of the field. Attempts to align CNTs via shear flow have been discouraging, orientational order parameters saturating well below S = 0.1 being reported [164]. Molecular combing is somewhat better but this method works only for very low CNT concentration and requires specific treatments of the surfaces onto which the CNTs are deposited. The liquid crystal-based alignment approach, which is the one that interests me the most, offers many advantages, as described in detail below.

In the fabrication of a device or new material based on carbon nanotubes a crucial step is the integration of the CNTs in the target environment. Reaggregation must normally be avoided and the alignment that was obtained should be maintained. Since this stage involves transferring CNTs from a suspension in a liquid which, in most cases, should not remain in the end product, neither of these requirements is trivial. The exact challenges depend much on the desired end product, the different ways of integrating the CNTs making different methods for dispersing, fractionating and aligning the tubes the preferred choice. There is no single, universally applicable 'best method' in CNT processing.

4.2   The benefits of dispersing carbon nanotubes in liquid crystals

Among the different approaches to align unsupported CNTs, I have in my research focused on the liquid crystal-based one. Liquid crystals inherently have the long-range orientational order that is such a challenge to obtain with CNTs. The research of myself and others has clearly demonstrated that this order can be transferred very well to nanotubes dispersed in them, whether of thermotropic or lyotropic type. In very general terms, the alignment mechanism can be understood as a result of the increase in free energy that CNTs *not* aligned along the director cause through their disturbance of the uniaxial orientational order of the liquid crystalline host phase, as schematically illustrated for the case of rod-shaped mesogens in Fig. 4.3.

Among the advantages of the liquid crystal-based CNT alignment concept can be mentioned:

- it works on unsupported tubes, thus being compatible with standard methods of CNT fractionation and purification,

- the achieved alignment is stable in time, requiring no external fields to maintain the alignment, provided that the alignment of the liquid crystal is controlled,

- it is non-discriminative regarding tube type, SW- as well as MWCNTs being equally well aligned and nanotube roll-up geometry having no apparent impact on the alignment efficiency,

- it works *en masse*, very large quantities of nanotubes distributed over areas that can easily reach several square centimeters being aligned simultaneously and uniformly,

- it is basically immediate: once the CNTs have been dispersed in the liquid crystal, the nanotubes will adopt any alignment imposed on the liquid crystal with very little delay.

After having aligned the nanotubes, the liquid crystal may either be solidified (e.g. via polymerization) to produce a composite material with enhanced macroscopic mechanical, electrical and/or thermal properties, or it can be removed, a necessary step in the development of most CNT-based electronic devices which are generally incompatible with the liquid crystal-based matrix. If one instead maintains the liquid crystalline state of the composite, the great response function to external forces (electric, magnetic, mechanical) of liquid crystals gives the concept a dynamic quality which may also be of much interest. Not only can we then determine the nanotube alignment over macroscopic areas by defining the director of the host in an appropriate way, but the CNTs can also be dynamically realigned at will by reorienting **n**. This concept is particularly interesting with thermotropic liquid crystals since they can be rapidly and precisely switched using electric fields.

Considering the advantages of the liquid crystal-based CNT alignment concept summarized above, the use of liquid crystals for aligning CNTs certainly appears quite attractive. It can provide us with a cheap, simple, versatile and effective means of controlling the orientation of unsupported nanotubes on macroscopic scale—if desired dynamically—and at high CNT concentration, with no fundamental restrictions on nanotube type. Of course, the concept also presents some important challenges that yet need to be resolved but the increasing international interest in research on CNT-liquid crystal composites provides a good ground for addressing these in the next few years.

4.2.1 Thermotropic or lyotropic hosts?

While both classes of liquid crystal have been used for aligning carbon nanotubes, the most successful approach so far in terms of high CNT loading without severe bundling and/or loss of alignment has been to use lyotropic hosts. This is perhaps not very surprising considering that the same surfactants that are typically used for dispersing CNTs also form lyotropic liquid crystal phases at higher concentration. In fact, the lyotropic liquid crystal alignment technique is a rather natural extension of the most successful approaches to achieve dispersion, purification and fractionation of CNTs, all based on suspension in aqueous surfactant solutions. With the implementation of the alignment step, only the integration remains in the pathway to CNT
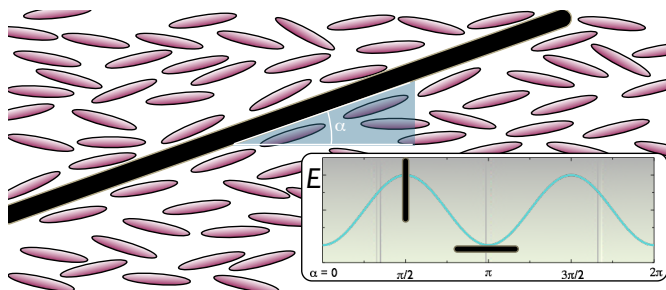
Figure 4.3: Schematic illustration of the CNT-in-LC alignment concept: the system's free energy E is minimized when the nanotubes align along the director ($\alpha = 0$, π, ...).

application, sketched in Fig. 4.2 (in Paper 14 we took the first steps towards addressing also this challenge).

Yet, when I entered this research field, all presented work on CNT alignment in liquid crystals had been done using thermotropic hosts. The dispersion of carbon nanotubes in surfactant-based lyotropic phases was an entirely unexplored area and my intention to take on this combination was awarded with a prestigious post-doc scholarship from the Knut and Alice Wallenberg Foundation, the most important non-governmental Swedish research funding institution. I carried out this work at the Universität Stuttgart in the group of Prof. Frank Gießelmann, in close collaboration with the carbon nanotube research group of Dr. Siegmar Roth at the Max-Planck-Institut für Festkörperforschung in Stuttgart, my main co-worker from this group being Dr. Giusy Scalia (at the time on leave from ENEA C.R. Portici, Italy). This was an excellent team for supporting me in this project. Dr. Scalia, who is the one who introduced me to carbon nanotubes in the first place, is one of the pioneers in studying thermotropic liquid crystal-CNT composites and her experience and input has been of critical importance for the success of our work.

Our first results on the topic in Paper 13 constituted the first demonstration of controlled CNT alignment using lyotropic liquid crystal hosts. Our later Paper 14, summarizing results obtained using a combination of cat- and anionic surfactants for building the liquid crystal–nanotube composite was also a first-of-its-kind, to the best of my knowledge still holding the world record in concentration of aligned unsupported carbon nanotubes. When opening a new line of research there will however always be new fundamental problems arising, this project being no exception. For instance, the high surfactant concentration required for obtaining a lyotropic liquid crystal phase eventually destabilizes the suspension via depletion attraction, an issue we will come back to towards the end of the chapter.

While depletion attraction is not an issue when dispersing CNTs in thermotropic liquid crystals, this materials combination is still more challenging in terms of achieving stable dispersion at reasonably high CNT loading. But, as already mentioned above, thermotropic hosts offer some interesting advantages, most notably the possibility of dynamic realignment of nanotubes. Moreover, the macroscopic alignment of thermotropics is much easier to control than with lyotropics. Actually, the realization of thermotropic liquid crystal systems heavily loaded with well-dispersed CNTs would indeed be most interesting from an applicative point of view, as it would allow a new type of guest-host display where the CNTs constitute an exceptionally stable achromatic dichroic dye (this is discussed as an interesting side issue in Paper 14). In addition, there are also indications that relatively low concentrations of CNTs may in turn be beneficial for the behavior of thermotropic nematics in standard displays [147, 169].

The main bottleneck in the further development of thermotropic liquid crystal–CNT composites is the difficulty in dispersing the nanotubes in the thermotropic host. Standard surfactants are useless for stabilizing the dispersion since both guest particles and host fluid are apolar (hydrophobic). Considering this fundamental problem and the fact that dispersion of nanotubes is never considered in the design process of thermotropic liquid crystals, most often developed with application in displays or other electrooptic devices in mind, the dispersability of carbon nanotubes in present thermotropic materials is actually surprisingly good. Nevertheless, the understanding of CNT dispersion in thermotropic liquid crystals (a very different situation from standard isotropic hosts) is still unsatisfactory and I have thus together with Dr. Scalia invested major research efforts also in this issue, resulting in important new insights that we have summarized in a manuscript that is presently in the review process. Likewise, I have together with Prof. Carsten Tschierske at the Institute of Chemistry - Organic Chemistry at the Martin-Luther-Universität Halle-Wittenberg, the practical work being done by our common doctoral student Martin Kühnast, taken on a project in synthesizing a totally new class of hybrid molecules, tailor-designed for aiding the dispersion of CNTs in standard thermotropic hosts,

i.e. taking the role of surfactants in aqueous systems. The molecules are indeed 'amphiphilic' in a certain sense, namely that one end is designed for adsorption on a CNT surface whereas the other holds a typical thermotropic mesogenic moiety. After some months of experimenting with different choices for these two units, as well as the flexible spacer that separates them, we very recently found a first series of molecules that dramatically improve the stability of carbon nanotube-in-thermotropic liquid crystal suspensions. This is a very exciting line of research that we believe can be of paramount importance for the application of CNT - thermotropic liquid crystal composites. In the interest of compactness, however, I will in this thesis limit myself to my research on lyotropic liquid crystals.

Regarding the details of how the transfer of order from liquid crystal host to nanotube guests takes place, a recent theoretical treatment by Paul van der Schoot [170] revealed that several different mechanisms may be involved. The question is actually deeper than one might at first think. Depending on the relative sizes of CNT guests and the molecules/aggregates forming the LC host phase, director field distortions, interfacial tension and/or excluded volume effects may dominate the process. The ordering mechanism in thermotropic and lyotropic hosts may thus be quite different, as a result of the different sizes of the LC building blocks.

4.3 Dispersing CNTs in lyotropic liquid crystal hosts and verifying the alignment

Because no investigations of lyotropic liquid crystal—CNT composites had been carried out before, we initially restricted our work to the simplest cases: nematic host phases and commercial purified single-wall nanotubes (the majority of our work has been performed using Hipco tubes from CNI/Unidym, USA). A number of practical questions were the first to be addressed:

- How are the nanotubes best introduced into the host phase?

- How should the transfer of orientational order of the LC onto the CNTs best be assessed?

- Which type of nematic lyotropic LC is most suitable? Which micelle shape should we strive for and what types of surfactant are the best?

- What macroscopic sample geometries are most suitable for various investigative techniques and how do we control the alignment of the lyotropic host phase in each sample type?

The answers to these questions that I found during my work are summarized in the following. If not otherwise stated, all data refer to the room temperature situation. While we have explored a large number of surfactants our four 'work horse' surfactants/co-surfactants are those in Fig. 4.4.

4.3.1 Producing lyotropic liquid crystals with well dispersed CNTs

Since sodium dodecyl sulfate (in the following abbreviated SDS) is one of the most commonly employed surfactants for carbon nanotube dispersion, and since nematic phases with rod- as well as disc-shaped micelles can be formed by aqueous SDS mixtures if we add decanol as co-surfactant [171], we started our work using SDS-based hosts. Initially we tried adding dry CNTs to a previously prepared lyotropic host phase but we quickly realized that this is an unnecessarily challenging strategy: it is very difficult to break up the macroscopic-size CNT bundles and achieve a good dispersion directly in the relatively viscous lyotropic host phase. While long-term sonication with a high-power tip sonicator might do the trick it is difficult to avoid evaporation of water in the process. We thus modified our procedure and instead started

by dispersing the CNTs in a 1%-SDS–water solution by means of high-power ultrasonication, following the standard protocol that had been formalized in the Roth group. This also allowed us to get better control of the amount of nanotubes in our samples, as we could now work with macroscopic volumes of a starting solution instead of sub-milligram amounts of dry CNTs.

After measuring up a desired volume of the starting solution in a vial, the additional SDS required for the formation of liquid crystal phases was added, followed by the small amount of decanol once all SDS had been dissolved (prior to decanol addition even the high-concentration SDS solution is isotropic). The addition of the dry surfactant and the co-surfactant are critical steps that essentially always induce a certain degree of large-scale CNT aggregation. By following an optimized practical procedure and by submitting the liquid crystalline sample to some hours of gentle sonication (in bath) a homogeneous lyotropic nematic mixture in wh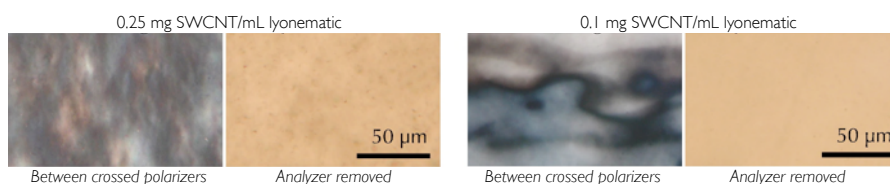ich the CNTs are well dispersed can however be achieved. Stirring may also be helpful to speed up the process, in particular when an oppositely charged surfactant is added for the liquid crystal phase formation, as will be described below. The formation of the nematic phase in the CNT-loaded mixtures showed that this is not prevented by the presence of the nanotubes, but we will see in section 4.5.1 that they at higher concentration can have a profound influence on the lyotropic phase sequence as well as other macroscopic properties. Moreover, it turned out that the lyotropic host can be very efficient in keeping the CNTs dispersed, some samples being stable, without any macroscopically visible CNT sedimentation, for more than a year.

A better picture of the dispersion quality was achieved by filling the samples into flat glass capillaries which were then investigated in the optical microscope, cf. Fig. 4.5. Bundling was now detected for this system when the CNT concentration was above 0.01 wt.-% but for lighter CNT loading no visible bundles were formed, a very satisfactory result at this stage. Of course the optical microscope cannot resolve any aggregates smaller than visible light wavelengths, so for investigating whether we have true single-tube dispersion other techniques are required. An interesting observation was that in the mixtures with too high CNT concentration, the texture of the nematic phase was much more irregular, cf. the polarizing microscopy photos in Fig. 4.5. At CNT concentrations above the limit of good dispersion, the CNTs thus seem to have a 'de-aligning' effect on the liquid crystal, i.e. the reverse effect of what we are aiming for. High-quality dispersion is thus imperative not only for the stability of the suspension, but also for the uniformity of the director orientation of the host phase. Fig. 4.5 also demonstrates well that in order to assess the dispersion quality of CNTs in a lyotropic liquid crystal one must present pictures taken *without* the analyzer (or entirely with unpolarized light). The crossed-polarizer textures contain so much structure from the variations of the liquid crystal director field that it
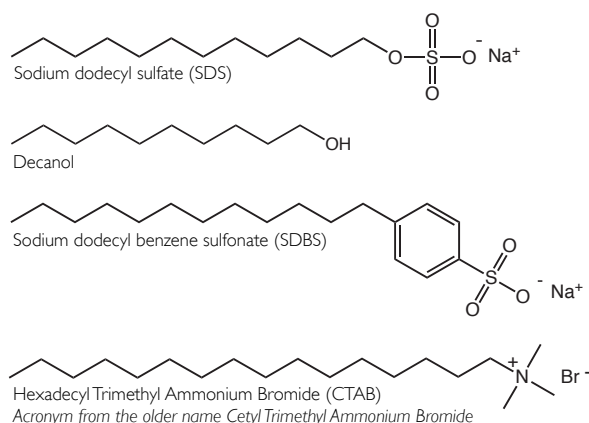
Figure 4.4: The three main surfactants used in our work, SDS, SDBS and CTAB, and the co-surfactant decanol.

0.25 mg SWCNT/mL lyonematic

0.1 mg SWCNT/mL lyonematic

50 μm

50 μm

Between crossed polarizers   *Analyzer removed*   *Between crossed polarizers*   *Analyzer removed*

Figure 4.5: Microscope images of the disc-micelle nematic lyotropic LC formed by SDS, decanol and water, loaded with SWCNTs at concentrations above (left) and below (right) the limit for sub-optical scale dispersion. From Paper 13. Copyright Wiley-VCH Verlag GmbH & Co. KGaA. Reproduced with permission.
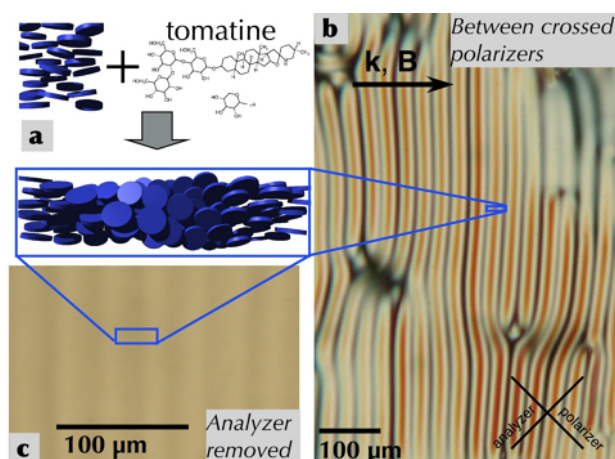
**Figure 4.6:** In Paper 13 (the source of this figure) we studied a lyotropic cholesteric phase, obtained by adding the chiral dopant tomatine (a) to the disc-micelle-forming lyotropic nematic phase composed of SDS, decanol and water, loaded with 0.003 wt.-% SWCNTs. The polarizing microscopy texture (b) shows that the cholesteric phase developed unobstructed by the CNTs and that the helix axis **k** could be aligned by appling a weak magnetic field **B**. When removing the analyzer (c) we could verify that the nanotubes remained well dispersed. (Copyright Wiley-VCH Verlag GmbH & Co. KGaA. Reproduced with permission.)

is impossible to distinguish nanotube aggregates, even when these may be quite large.

While the first successful investigations were done with a nematic host with disc-shaped micelles (Paper 13), we repeated the experiments (including the verification of alignment, described below) with a rod-micelle nematic host (the ratio decanol to SDS is slightly different), achieving very similar results, cf. Paper 12. The shape of the micelles making up the liquid crystal host phase thus seems to have little impact on the result as long as it is a nematic phase. When we in our later work prepared systems with CNTs in hexagonal columnar and lamellar lyotropic liquid crystal phases, respectively, we noticed that the former (having rod-shaped micelles of great length) worked well whereas there was always phase separation between an apparently nanotube-free liquid crystal phase and large CNT aggregates when using lamellar host phases.

Also the chiralization of the nematic host phase was possible, the CNTs remaining well dispersed and not preventing the formation of a cholesteric phase with a helical director modulation, cf. Fig. 4.6. During the work for Paper 13 we realized that the homeotropic alignment that typically arises when filling a disc-micelle lyotropic nematic into a glass capillary creates problems for the verification of the nanotube alignment. We therefore added a small amount of the chiral dopant tomatine to turn the SDS-based host phase into a cholesteric liquid crystal with a helix pitch of about 70 μm. Because the basic nematic phase is of N_D^- type (see section 1.3.2) an application of a relatively weak magnetic field will align **n** perpendicular to the field, thus the helix axis **k** is uniformly aligned along the field. With the well-defined structure that resulted we could verify the nanotube alignment using polarized Raman spectroscopy, as will be described in the following section.
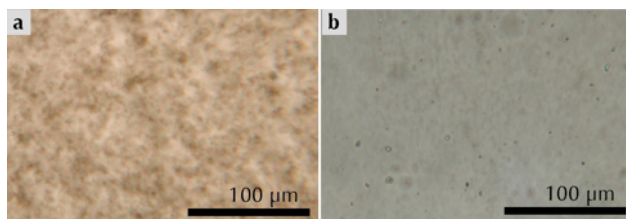
Figure 4.7: The texture of the liquid crystal formed by addition of SDS (left) and CTAB (right), respectively, to SDBS-dispersed SWCNTs. Note that the concentration in the right-hand case is four times greater than in the left-hand case (0.2 wt.-% and 0.05 wt.-%, respectively). From Paper 14. Reproduced by permission of the Royal Society of Chemistry.

After the initial successes with the SDS-based systems (the verification that the CNTs were in fact aligned along **n** in the phases is presented below) a major goal for us was to increase the CNT concentration without inducing unacceptable nanotube aggregation. This was achieved by switching from SDS to Sodium Dodecyl Benzene Sulfonate (SDBS) as surfactant for dispersing the nanotubes (SDBS has been established as one of the best surfactants for CNT dispersion [148]) and by using the oppositely charged surfactant hexadecyl trimethylammonium bromide (CTAB) for building up the liquid crystal phase. When simply trying to build up an SDS-based liquid crystal phase around SDBS-dispersed CNTs, strong aggregation was the consequence but with CTAB the aggregation was only temporary, a uniform dispersion resulting after some hours of bath sonication, cf. Fig. 4.7. This applied even at CNT concentrations as high as 0.2 wt.-%, i.e. we had increased the concentration of nanotubes by 20 times compared to the initial experiments with SDS-based nematic hosts. As will be described below this had a very visible impact on the optical properties of the phase. Equally good (in fact even slightly better) results were later on obtained with MWCNTs at the same high concentration following this concept (Paper 16). I will in section 4.4 come back to a discussion of why the combination of cat- and anionic surfactants was so much more successful.

4.3.2   Verification of CNT alignment

For verifying that the CNTs are indeed aligned by the liquid crystal host our standard technique has been polarized resonant Raman spectroscopy, first employed to study liquid crystal-CNT composites by Dr. Scalia [172]. The Raman spectra of SWCNTs contains bands of peaks peculiar to these particles, hence Raman spectroscopy can provide an unambiguous detection of the presence of single-wall CNTs. The most characteristic SWCNT band is the range of the so-called Radial Breathing Modes (RBMs), related to the curvature of the tube surface, but even some features of bands present also in other carbon allotropes, mainly the G-band, are unique to SWCNTs. Since the Raman signal from CNTs is highly dependent on the degree of parallelism between the nanotube axis and the direction of the electric field vector **E** of the exciting laser light, a Raman study as a function of light polarization directly probes the CNT orientations [173], provided that the tubes have a component in the plane perpendicular to the excitation laser beam.

The latter condition is easily met when working with a rod-micelle host phase in a flat glass capillary (Papers 12, 14 and 16), but with disc-shaped micelles (Paper 13) it was a bit of a challenge due to the typically homeotropic orientation of such a phase. This was why we chiralized the nematic phase, circumventing the problem by studying a helically modulated structure. The CNTs are then to 50% expected to be in the sample plane but never along the helix axis, since this is always perpendicular to **n**. As anticipated, the CNT Raman signal was the strongest for polarization perpendicular to the helix axis, cf. the upper row in Fig. 4.8. Moreover, the signal
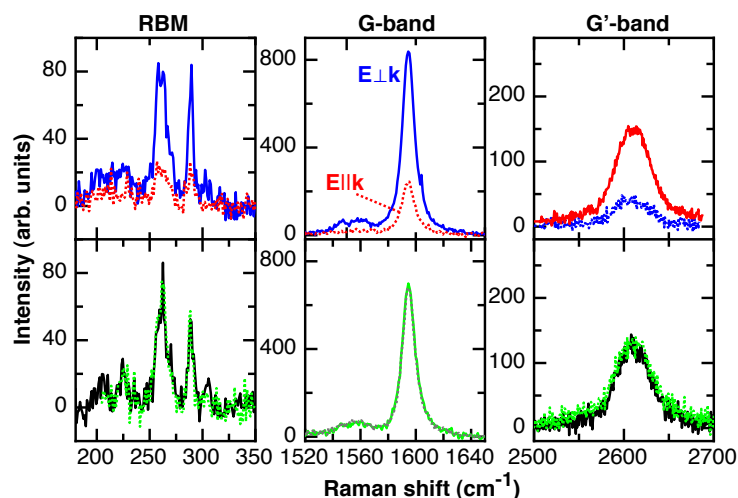
Figure 4.8: Examples of resonant Raman spectra obtained from SWCNTs in a chiral nematic SDS-based lyotropic LC host phase (top; **k** is the axis of the helical director modulation, **E** the polarization of the excitation laser light) and in a non-liquid crystalline 1% SDS-water solution (bottom). From Paper 13. (Copyright Wiley-VCH Verlag GmbH & Co. KGaA. Reproduced with permission.)

strength was essentially independent of position on the sample, demonstrating that the CNT dispersion was very uniform. To verify that the source of tube alignment was in fact the liquid crystal host we also carried out a control Raman experiment, under identical conditions, on a sample where the same type of SWCNTs were dispersed in a non-liquid crystalline standard 1% aqueous SDS solution, at the same concentration as in the liquid crystalline sample. The resulting curves, shown in the lower row of Fig. 4.8, were now essentially identical for perpendicular light polarizations, reflecting the totally random alignment of the CNTs in this host.

In order to quantify the CNT orientational order, i.e. determining the nematic order parameter S for the nanotubes, we adopted a method commonly used for determining S of nematic liquid crystals to which a dichroic dye has been added (see Paper 13 for a full description of the procedure). This yielded a value of $S \approx 0.6$, very similar to the room temperature order parameter of the SDS-decanol-water host phase [47]. In other words, the CNTs exhibited roughly the same degree of orientational order as the host that we had used.

The homeotropic alignment of the CNTs dispersed in a non-chiral disc-micelle lyotropic nematic host is difficult to prove directly, but an indirect evidence was presented in Paper 12 by comparing the Raman spectra of such a sample with one with rod-micelles and thus planar-aligned, both samples containing the same concentration of the same type of SWCNT. The nanotube G-band intensity of the planar-aligned sample depended strongly on the polarization, being maximum for polarization along **n**, whereas no polarization sensitivity was detected in the homeotropic sample, cf. Fig. 4.9. Moreover, the intensity of the response was now even lower than for the perpendicular polarization of the planar-aligned sample. The difference in intensity between the two samples, and the polarization insensitivity of the homeotropic-aligned sample, provide good indirect evidence that the nanotubes are indeed preferentially aligned perpendicular to the capillary, along **n**, in the homeotropic sample.

This study was interesting also in another respect because the planar-aligned sample had been aligned with **n** perpendicular to the filling direction by means of magnetic field application
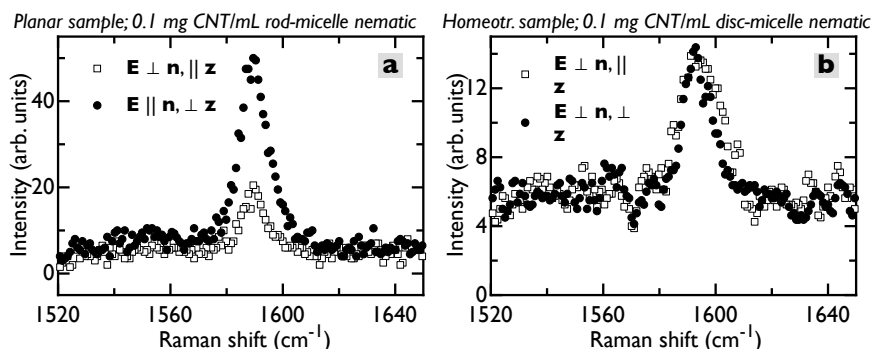
Figure 4.9: Raman spectra from a planar- and a homeotropic-aligned sample of SDS-decanol-water lyotropic nematic phases loaded with 0.01 wt.-% SWCNTs for two perpendicular polarizations **E**, in the former case parallel and perpendicular to **n**, respectively. Note the different y-axis scaling in *a* and *b*. From Paper 12. (Copyright Wiley-VCH Verlag GmbH & Co. KGaA. Reproduced with permission.)

after filling the sample. The fact that the nanotubes were aligned along and not perpendicular to **n** shows that the nanotube alignment is indeed dictated by the liquid crystal director field, not simply by flow effects during filling (had this been the case also the homeotropic sample would have shown a polarization sensitivity).

As mentioned above, our switch from SDS-based systems to the combination of SDBS-dispersed CNTs in a CTAB-based liquid crystal phase allowed a dramatically increased nanotube concentration. As usual, polarized Raman spectroscopy experiments were carried out on the samples to confirm the uniform alignment of the nanotubes, cf. Fig. 4.10. In the upper row of the figure the spectra from a 200 μm thick flat capillary filled with the suspension are shown. The liquid crystal was quite uniformly aligned simply by the shear flow during filling, with the director along the capillary axis. Consequently, a clear contrast between polarization along (blue curves) and perpendicular (red) to the capillary could be seen, showing that the nanotubes aligned along the liquid crystal director.

A quantitative analysis revealed that the contrast corresponded to an order parameter for the SWCNTs of only $S \approx 0.3$, thus substantially lower than what was found in the chiral nematic SDS-based phase with much lower CNT concentration in Paper 13. The reduced orientational order was however a result of uncontrolled averaging, reflecting simply the lesser degree of macroscopic control of the director field obtained by means of the flow during filling of the SDBS-CTAB mixture into the capillary, compared to the magnetic field-induced alignment of the cholesteric SDS-based mixture. The low value of S thus did not mean that the nanotubes were locally disordered, only that **n** was far from uniformly defined within the size of the measurement area, a circle of ≈ 10 μm diameter for the main diagrams in the upper row of Fig. 4.10. By reducing the area to a spot of 2μm diameter the diagram in the inset was obtained, yielding $S \approx 0.6$. This means that we in the catanionic system had the same degree of local CNT orientational order as in the previous system, although we here had a 20-fold increase of nanotube concentration. I will come back to the spectra in the lower row in Fig. 4.10, revealing an even higher degree of orientational order, in a moment.

The verification of CNT orientational order via polarized Raman spectroscopy was in fact not entirely necessary in this case because it turned out that the alignment in these samples could be confirmed in a much more straightforward way, even with the naked eye. By simply rotating a linear polarizer held above a sample with the lyotropic CNT suspension illuminated from below
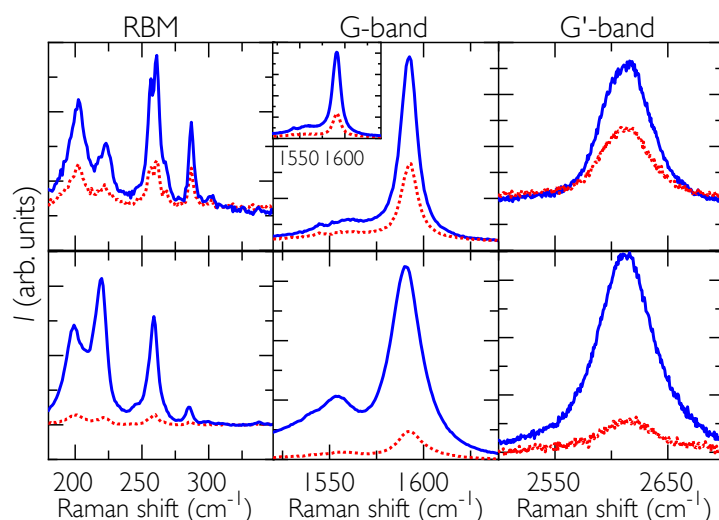
Figure 4.10: Raman spectra from the catanionic system containing 0.2 wt.-% SDBS-dispersed SWCNTs in a CTAB lyotropic liquid crystal phase. The upper row contains spectra from a capillary, decently aligned by shear flow (the inset shows spectra for a smaller beam spot). The lower row shows the spectra from the CNTs remaining after a filament of the phase was deposited on a substrate and the surfactants rinsed away. From Paper 14. Reproduced by permission of the Royal Society of Chemistry.

with unpolarized light, the sample was distinctly darker when the polarizer transmission direction was along **n** than when it was perpendicular, cf. Fig. 4.11. CNTs absorb light polarized along the nanotube axis, but not light that is polarized perpendicular. We now had such a high CNT concentration and such good alignment of the tubes, that the system effectively acted as a fluid linear polarizer. The anisotropic nanotube properties had been transferred to macroscopic scale by the liquid crystal!

This optical effect also provided a further confirmation that the CNT alignment was indeed a result of templating of the LC host phase. Fig. 4.12 shows texture micrographs taken of a sample in a capillary in which some air bubbles had formed during filling. Since an air bubble constitutes a defect in the director field (a defect of strength +1, to be precise), the liquid crystal alignment cannot be uniform around the bubble, and it can in fact exhibit a quite complex modulation. As reflected by the variations between dark and bright areas in the upper two photographs taken between crossed polarizers, such a modulation was here the case. Without the analyzer, the pattern will be invisible in a pure liquid crystal, since the liquid crystal in itself is transparent; the dark–bright modulation appears only when the birefringent sample is viewed between crossed polarizers. But when removing the analyzer in this case, the pattern was still clearly visible, although what had been bright between crossed polarizers could now be relatively dark, and vice versa. The reason is that the carbon nanotubes absorbed the light if they were aligned along the polarization of the illuminating light, but not when they were perpendicular. The fact that the pattern created by the CNTs basically mimicked the pattern seen between crossed polarizers is a further clear evidence that the carbon nanotubes align along **n**, not along the direction of flow during capillary filling. Had the latter been the case, the images without analyzer would have been uniformly dark when the capillary was along the polarization direction, and uniformly bright perpendicular, without any trace of the director modulation pattern.
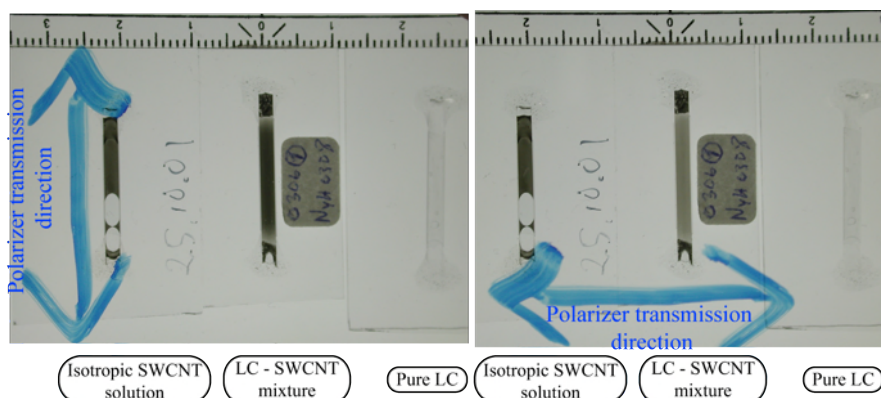
Figure 4.11: Three capillaries with different content illuminated by unpolarized light and viewed through a linear polarizer, in the left photo aligned for absorption of the polarization perpendicular to the capillaries, to the right for absorption of the parallel component. The left-most capillary contains an isotropic suspension of 0.2 wt.-% SWCNTs dispersed with SDBS and the right-most contains a CNT-free 28 wt.-% CTAB lyotropic liquid crystal phase. The appearance of both these capillaries is unaffected by the rotation of the polarizer. The middle capillary contains the combination of the two lateral capillary contents, that is the same liquid crystal phase as in the right-most sample but this time loaded with 0.2 wt.-% SDBS-dispersed SWCNTs. The director has been aligned along the capillary by flow during filling and the nanotubes are thus also aligned mainly in this direction, thus absorbing light polarized along the capillary. This is why this capillary appears darker in the left picture than in the right one.
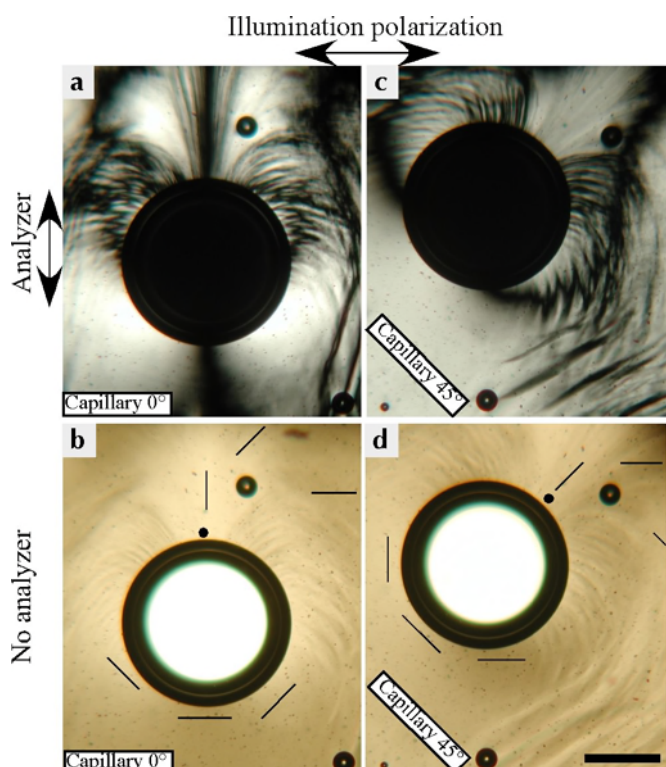
Figure 4.12: The complex director pattern around an air bubble seen between crossed polarizers (a and c) and visualized without analyzer thanks to the polarization-dependent absorption of the carbon nanotubes, everywhere aligned along the director (indicated with thin lines). The scale bar to the lower right of image d is 200 μm. From Paper 14. Reproduced by permission of the Royal Society of Chemistry.
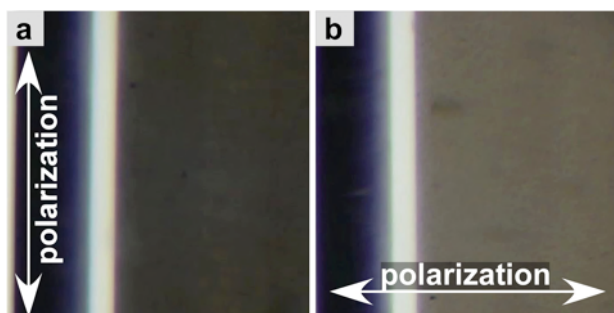
Figure 4.13: Multiwall CNTs dispersed using SDBS at a concentration of 0.2 wt.-% in a CTAB-based liquid crystal phase, aligning the tubes along the director (aligned via shear flow along the 200 μm thick capillary containing the mixture). The sample is viewed without analyzer and illuminated by light polarized along the capillary in *a* and perpendicular to it in *b*. The picture was made by Stefan Schymura and is reprinted from Paper 16. Copyright (2009), with permission from Elsevier.

The observation of linear polarizing properties of the CNT-LC mixture is interesting from applied as well as fundamental points of view (see discussion in Paper 14) but the simplicity in investigating this property also gives it great practical importance for the study of CNTs in liquid crystals. In fact, the verification of the polarizing properties has today become our standard first test of successful dispersion and alignment when characterizing a new system. A system not showing the polarizer effect need not be further characterized but rather the dispersion must be improved. Only when the nanotubes are very well dispersed do they align along **n**, and then they show the polarizer effect (provided sufficient concentration, but nowadays we almost always work with such concentrations).

While our initial experiments were conducted exclusively with SWCNTs, we later confirmed that the concept works excellently also for MWCNTs (in our case tubes from SES Research, USA, with 10-30 nm outer diameter), cf. Fig. 4.13. The fact that lyotropic LC alignment of CNTs works on such different nanotube types makes it one of the most versatile nanotube alignment approaches available.

4.4 The challenges in dispersing CNTs in high-concentration surfactant solutions

The role of the surfactant in typical isotropic aqueous CNT suspensions is first to render the nanotubes dispersible, second to counteract the van der Waals attraction of adjacent CNTs by introducing a sufficiently strong repulsive force between the nanotubes. This works excellently with dilute solutions, but with increasing surfactant content one must take the important phenomenon of *depletion attraction* into account [150, 174]. When much more surfactant is present than what is necessary for covering the CNT surfaces, the surplus surfactant molecules organize into small empty micelles. Being repelled from the CNT-containing micelles (which have the extreme 1D extension of the contained nanotube), a system with high CNT concentration has a large total excluded volume into which the CNT-free micelles cannot penetrate, an effect that decreases the entropy of the system. If two nearby CNT-containing micelles merge, they reduce the excluded volume considerably, hence an entropically driven attractive force between adjacent CNTs appears. This depletion attraction limits the amount of CNTs that can be suspended, as well as the maximum concentration of surfactant.

The combination of cat- and anionic surfactants in our current standard system actually provides a means of circumventing this important problem. Because of their different charge compared to the SDBS-wrapped CNTs, the CNT-free CTAB micelles are not repelled from the

tubes and can thus not act as depletion agents. Instead they are attracted to the tubes, effectively forming a 'buffer' of CTAB micelles that prevents close encounters of CNTs. A critical question here is of course if the SDBS really stays on the nanotube surface, instead of mixing on a molecular scale with CTAB. I believe that this is in fact to a large extent the case, the dodecyl benzene sulfonate molecules being so strongly adsorbed to the CNT surface that no appreciable molecular mixing of cat- and anionic surfactants occurred (in section 4.5.1 I will describe evidence from experiments on a reference sample without CNTs, behaving dramatically different from the CNT-containing liquid crystal, that support this conjecture). Instead a complex of cationic trimethylammonium bromide micelles surrounding each anionic CNT-containing dodecyl benzene sulfonate micelle may form, the stability of which can be attributed to the entropic gain from release of the counter ions into solution. This phenomenon has previously been observed in complexes of DNA (anionic) with cationic lipids [175]. More details on these issues can be found in Papers 14 and 15.

Obviously the ratio of cat- to anionic surfactant number plays a critical role. Together with my doctoral student Sarah Dölle I have studied the precipitates that typically form when an SDBS-CNT dispersion is destabilized by addition of cationic surfactant at the *same* molar concentration as SDBS, thus much less than what was used in the studies described above where SDBS is present only as minority surfactant. The electrostatically stabilized complexes that form under these conditions are also very interesting and some of them were found to have long-range liquid crystalline order. This is thus a liquid crystal phase formed *by* the nanotubes, rather than nanotube guests in an ordered host. The liquid crystal phases in these precipitates are however very difficult to align macroscopically and reproducibility is challenging. Moreover, the analysis of these systems is anything but trivial, hence we are only at the beginning of their study.

The fact that CNT-loaded nematic lyotropic phases could be prepared also without the combination of cat- and anionic surfactants (Papers 13 and 12) is however somewhat mysterious if one believes that depletion attraction destabilizes a CNT suspension at high surfactant concentrations blindly: according to the studies on depletion attraction in surfactant-stabilized CNT suspensions the nanotubes should have aggregated well before any liquid crystal phase formed, yet we achieved very good suspension in our lyotropic nematic and cholesteric phases formed by aqueous solutions of SDS and decanol. We therefore recently took on a more basic study of dispersion of CNTs in *isotropic* aqueous solutions of different surfactants, where the concentration of surfactant varied over a much larger range than in most studies of this kind, from near the critical micelle concentration to just below the onset of liquid crystallinity.

Figure 4.14 contains some preliminary results from this study, showing an unexpected behavior for SDS-dispersed CNTs. As first reported by Philippe Poulin and co-workers [176] SDS-dispersed CNTs aggregate quickly if the surfactant concentration is increased to around ~5%, the team drawing the conclusion that depletion attraction prevents nanotube dispersion at surfactant concentrations greater than this limit. But they did not report results for concentrations greater than 8%. It turns out, as can be clearly seen in Fig. 4.14, that the rapid aggregation takes place only within a window from ~4% to ~10%, the suspension getting more stable again at higher surfactant concentrations. Over a longer period of time (~a month) more sedimentation occurs but the general trend is maintained.

These results are of great interest for our work towards achieving diverse lyotropic systems with well-dispersed carbon nanotubes, since they show that the 'rule' that too large a surfactant concentration renders CNT suspensions unstable is somewhat too simple. While our earlier work on CNT suspension in nematic or hexagonal phases had already put this conclusion in question for the case of liquid crystalline suspensions, we now see that even isotropic CNT dispersions can contain a substantial amount of surfactant. This observation opens an alternative way towards preparing liquid crystalline CNT suspensions: the CNTs can be dispersed from the start at high
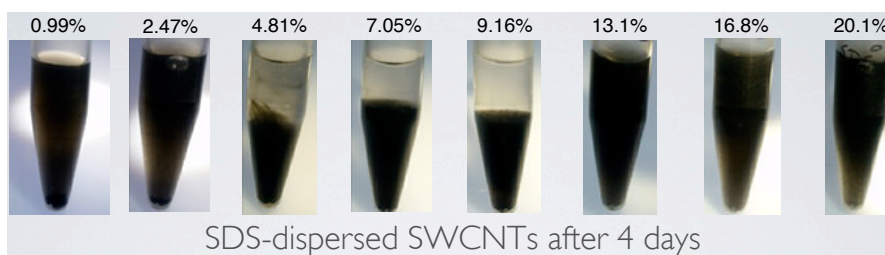
Figure 4.14: SWCNTs dispersed at 0.01 wt.-% in aqueous solutions of the surfactant sodium dodecyl sulfate (SDS) at varying concentration (courtesy of Sarah Dölle). A window between ∼4% and ∼10% concentration can be identified within which the CNT suspension rapidly becomes unstable, leading to separation between CNT-rich and CNT-poor phases. Surprisingly, the suspension becomes more stable at higher SDS concentrations.

surfactant concentration, but still below the isotropic-liquid crystal transition, and the desired liquid crystalline order can then be induced by addition of a co-surfactant such as decanol. Preliminary tests show that this route is indeed promising.

The apparent restabilization of the suspension upon going from 9% to 13% SDS concentration seen in Fig. 4.14 is however most likely mainly a kinetic effect. Our continued studies of high-surfactant-concentration CNT suspensions suggest that it is the increase in viscosity when the surfactant concentration reaches the range 15-20% that stabiizes the suspensions kinetically. Depletion attraction is still active and eventually the suspensions will collapse, but the dynamics are now so slow that we can easily work with the systems over the time scale of days to weeks, clearly sufficient to produce a liquid crystal phase. Once that has been produced, the further increased viscosity, which is moreover anisotropic, will further aid in stabilizing the suspension (still only kinetically, though), such that the stability over several months can be understood. It seems, however, that a truly stable surfactant-based lyotropic liquid crystalline CNT suspension may not be possible, at least not when using only a single ionic surfactant.

4.5 Some peculiar properties of lyotropic liquid crystals containing a high concentration of CNTs

In our initial experiments with SDS-based lyotropic hosts the maximum nanotube content before aggregation was so low that no influence on the liquid crystal properties from the nanotubes could be detected. As we succeeded in increasing the nanotube concentration to the regime where the phase acquires light polarizing properties visible by the naked eye, we also noticed a number of peculiarities of the macroscopic behavior of the system, distinctly different from the case when no CNTs were present.

4.5.1 Which liquid crystal phase did the CNT-loaded catanionic lyotropic have?

When starting the experiments on the inclusion of SDBS-dispersed CNTs in the CTAB-based liquid crystal phase the initial intention was to get a nematic phase. The phase diagram of CTAB has a small N regime close to room temperature between the isotropic and H_α phases for concentrations in the range of about 23-30 wt.-% [177]. We thus prepared our mixtures to have
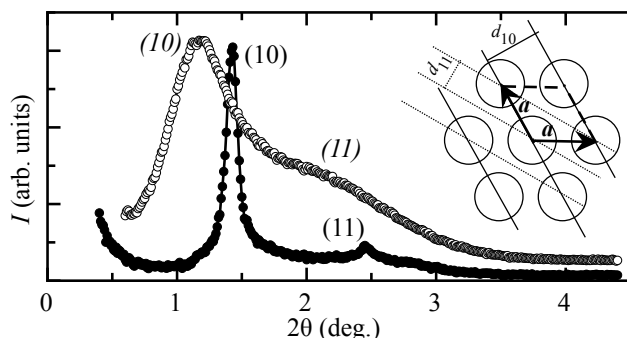
Figure 4.15: X-ray diffractograms from our original catanionic lyotropic liquid crystal mixture, containing 28 wt.-% CTAB and 1 wt.-% SDBS, with 0.2 wt.-% SWCNTs (filled symbols) and without nanotubes (empty symbols), respectively. From Paper 14 (reproduced by permission of the Royal Society of Chemistry), data obtained by Constanze Hägele.

a final CTAB concentration of 28 wt.-%, a composition that has remained our standard choice.

When placing the sample in the x-ray scattering equipment, however, the resulting diffractogram gave clear evidence that we had a hexagonal columnar phase, cf. Fig. 4.15, and we therefore described the host phase as a hexagonal one in our first paper on this system. Interestingly, when preparing the same composition of water, CTAB and SDBS but without the nanotubes, the resulting mixture was initially isotropic. Only after about a week's time did this sample become birefringent and we then investigated also this with x-ray scattering. Again a hexagonal fingerprint could be detected, albeit with extremely broad peaks, cf. Fig. 4.15, suggesting a rather short-range hexagonal order. Obviously, the nanotubes have a strong impact on the phase behavior, in this case most likely mainly in the sense that they keep the SDBS molecules adsorbed to their surface, thus preventing a molecular-scale mixing of the two surfactants. This allows the CTAB micelles to build up almost the same phase as they would have without the SDBS and nanotubes [178]. In contrast, without the nanotubes the SDBS and CTAB molecules together form mixed micelles, the shape of which apparently is far from ideal for building up a liquid crystal phase. See Paper 14 for a more detailed discussion of this issue.

In addition to the fact that previous reports had indicated a nematic phase for this concentration of CTAB, in contrast to our x-ray data, another peculiarity of our sample was that it flowed quite easily. This is not typical for a hexagonal phase which due to its two-dimensional positional order is highly viscous, more like a gel. In this respect our liquid crystalline CNT suspension indeed seemed much more like a nematic, but since the x-ray scattering had given clear evidence of a hexagonal columnar structure we initially settled with this conclusion. We note, however, that the fact that the Krafft temperature of CTAB (24°C) is slightly above room temperature complicates the issue, the liquid crystalline behavior observed at room temperature not reflecting a true equilibrium state.

Recently we have started addressing the phase sequence issue in more detail, finding that also a pristine mixture in this CTAB concentration range but without nanotubes behaves a bit out of the ordinary. Even at only 26 wt.-% CTAB the mixture is rather stiff and gel-like at room temperature, flowing only after rather strong shear above a certain threshold. Even heating to 25°C (thus above T_{Krafft}) does not dramatically change the macroscopic behavior. Only in the range 30-35° did the mixture start to flow easily without a distinct threshold, the texture then also looking more nematic-like, cf. Fig. 4.16. The 28 wt.-% mixture was obviously a bit stiffer yet.

The question is now what impact the SDBS-enveloped CNTs have on the room temperature phase of the mixture. While the hexagonal x-ray scattering pattern in Fig. 4.15 would be compatible with a gel-like phase as in Fig. 4.16a, such a state was not observed in the CNT-loaded

sample, which flows relatively easily at room temperature. In the literature one can find reports of salt addition to aqueous CTAB solutions inducing a lengthening of the rod-like micelles to the extent that they are classified as worm-like, resulting in enhanced viscoelastic behavior and shear thinning of the macroscopic phase, as well as enhancement or even induction of the nematic phase in case of a CTAB concentration similar to our systems [179,180]. Together with the CNTs we add the salt SDBS in our case and it may thus be that, although the DBS moiety is largely adsorbed to the CNT surface, the shear thinning threshold is drastically reduced. As a result we could have a phase that develops a long-range ordered hexagonal columnar phase when at rest, as in the capillary during the x-ray scattering experiment, but that easily looses the long-range correlation when subjected to shear, giving a nematic phase under dynamic conditions. This could be an explanation of the contradicting observations from x-ray scattering and viscous flow behavior.

The long time to liquid crystal phase formation and the very poor steady-state hexagonal order when SDBS was added to the CTAB phase without any nanotubes (Fig. 4.15, empty circles) corroborates the notion that SDBS addition disturbs the hexagonal structure. At the same time the strong difference to the sample with SWCNTs shows that their presence promotes long-range order. Further investigations of the impact of CNTs on the phase behavior are currently on-going in a collaboration with the group of Prof. Gießelmann at the Universität Stuttgart, the results soon to be summarized in a manuscript that will be submitted to *Soft Matter*. We have not yet carried out x-ray scattering experiments on the samples with MWCNTs (Paper 16) but it is likely that these are strictly nematic, since the diameter of these tubes is much larger than the lattice constant $a \approx 72$ Å of the hexagonal CTAB phase, as determined from the data in Fig. 4.15.

4.5.2 Filament formation in CNT liquid crystal mixtures

A further very interesting characteristic of the catanionic lyotropic CNT suspension was that thin filaments can easily be pulled from it, and these can then be deposited along selected directions (or even with curvature) on any desired substrate, cf. Fig. 4.17. Fixing the filament ends to the substrate, the water-soluble surfactant could subsequently be rinsed away, leaving behind essentially naked CNTs, very well aligned along the direction of filament deposition. This was verified with polarized Raman spectroscopy investigations of the sample, cf. the lower row of Fig. 4.10, the contrast between polarizations parallel and perpendicular to the filament deposition direction now yielding an order parameter of $S \approx 0.7$.

~20°C   ~35°C
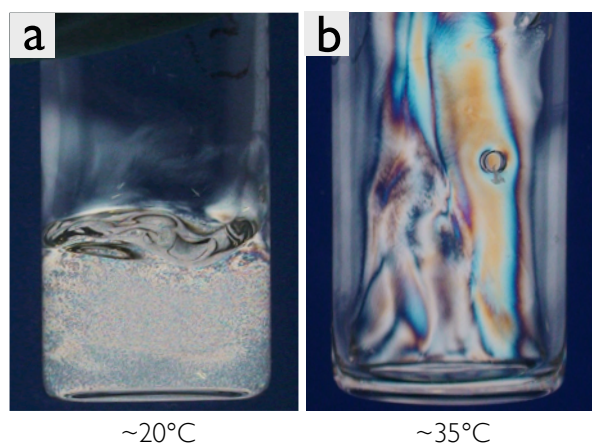
Figure 4.16: The macroscopic optical appearance between crossed polarizers of a 1 mL sample of a 26 wt.-% aqueous CTAB mixture in a horizontally placed glass vial, at room temperature (*a*) and heated to about 35°C (*b*). At room temperature the sample is like a gel whereas at the higher temperature it flows to cover the length of the vial when this is tilted.
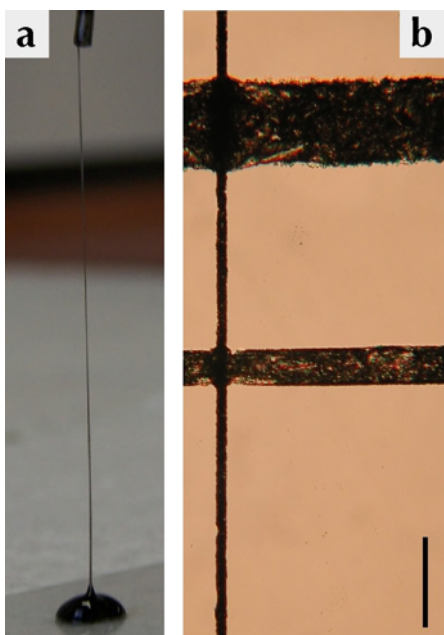
Figure 4.17: (a) Filament being drawn from the catanionic CNT—lyotropic LC composite. (b) Several such filaments deposited onto a glass substrate and then dried. In *b* the scale bar represents 200 μm, in *a* the drop diameter is about 1 cm. From Paper 14. Reproduced by permission of the Royal Society of Chemistry.

This observation is quite interesting from an applied point of view, since it opens a way of depositing the CNTs on a target substrate, retaining the uniaxial alignment, and then washing away the surfactant. Although considerable optimization is still required (in particular the removal of the surfactant without rinsing away the CNTs is a challenge) it opens a route towards usage of liquid crystal-aligned CNTs also in applications where no matrix can be tolerated. We are currently exploring different ways of optimizing the deposition, e.g. electrospinning the filaments or using a microfluidics set-up to pump the suspension at controlled rate through a tapered capillary acting as a 'pen' (preliminary results obtained with the latter technique are presented in paper 16), as well as finding a procedure that allows removal of the surfactant with minimum loss of CNTs.

The filament formation is however also very interesting from a fundamental science point of view. It is important to note that the filaments are formed neither by the pristine liquid crystal, nor by a standard isotropic nanotube suspension with the same CNT concentration. My doctoral student Stefan Schymura has recently carried out a systematic study of the filament formation phenomenon, finding that the filament formation is induced by SW- as well as MWCNTs, but they have to be very well dispersed and they must be present at a concentration above a certain threshold (empirically found to be about 0.1 wt.-%). Moreover, the suspension should be in the nematic phase range. Suspensions in the distinctly hexagonal phase range do not show filament formation, although in these cases it is of course not easy to achieve good CNT dispersion, due to the very high host phase viscosity.

The filaments can be formed simply by dipping a spatula or a capillary into a bulk sample of the lyotropic CNT suspension and then pulling it away, cf. Fig. 4.18. The beginning of the process is obviously dominated by capillary forces, a capillary bridge between the drop and the retracting spatula/capillary leading to an initial very thick thread being extended from the drop. In the next step of the process the filament reduces greatly in diameter and increases correspondingly in length. Under the right conditions a filament as long as about a meter can easily be pulled (Fig. 4.18). In contrast to the formation of the first thick thread, this next step is only seen if the above mentioned conditions on the properties of the suspension are met, hence
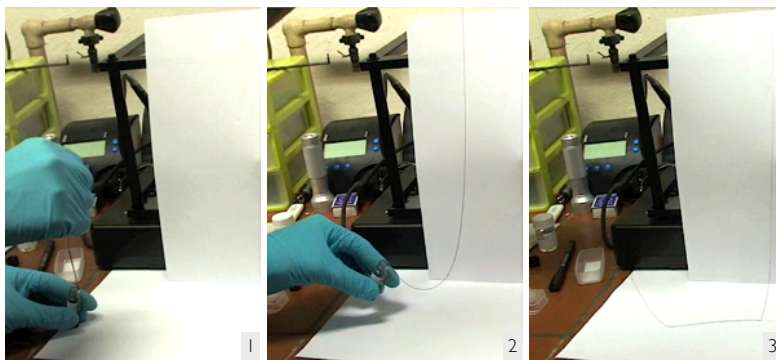
Figure 4.18: Three stages in the drawing of a very long filament from a lyotropic CNT suspension. In the third step (just before the filament broke) the two ends were held well above the top edge of the picture, the total filament length being more than a meter.

it can clearly not be a result of capillary forces alone (they do not require an anisotropic phase nor well-dispersed CNTs in the mixture).

Rather, we believe this step may be stabilized by a dynamic CNT chain formation driven by depletion attraction, which in a nematic phase is highly anisotropic [181]. It is much stronger along the director and thus, in this case, along the filament. While the nanotube concentration in the *bulk* sample is below the ridigity percolation threshold (above this threshold—around 3 wt.-%—a CNT suspension turns into a gel [182, 183]) the situation changes drastically as the more and more one-dimensional thread of liquid crystal is pulled out. The nanotubes align macroscopically along the filament and attract each other particularly strongly in this direction due to the anisotropic depletion attraction. The result would be a dynamically forming chain of CNTs that stabilizes the filament, continuously extending and thinning as the filament is pulled longer and longer. If this picture is correct, the transformation from a 3D to a quasi-1D system taking place as the filament forms would in the case of an anisotropic host fluid allow percolation at the relatively low nanotube concentration[4] of 0.1 wt.-%. These ideas are currently being further corroborated and extended with a more solid theoretical treatment with the help of Prof. Paul van der Schoot at the University of Eindhoven, a colloid theory specialist with whom I am very fortunate to collaborate. We plan to summarize the results, together with the results of a detailed study of the rheological properties (which are also very interesting), in a manuscript that we hope to submit for publication in the next month or so.

4.6   Conclusions and outlook

The work of me and my colleagues on CNT alignment by templating in lyotropic liquid crystals has shown that very good uniform orientation of unsupported nanotubes can be achieved, even at such high CNT concentrations that their physical properties become apparent to the naked eye. In this sense we have surpassed the initial expectations when I started out with this project and we have demonstrated that lyotropic liquid crystal-based nanotube alignment is a viable route that is compatible with many of the other processing steps in the development of carbon nanotube-based devices or composite materials. In terms of technological exploitation of the

---

[4]The CNT concentration in the filament may however be somewhat higher than in the bulk sample, since the large surface area of the filament promotes rapid evaporation of water from the mixture.

concept, some work with mainly engineering character remains to be done, targeting optimized routes for polymerization of the composite or for the removal of surfactants without removing the CNTs or ruining their alignment. Together with colleagues in the United States and Sweden who have shown interest in these issues and have expertise that very well complements mine, my students and I are currently pursuing research in this direction.

Also the quality of the nanotube dispersion in the liquid crystal host phases is generally satisfactory, although sub-optical scale imaging of the systems are yet lacking. Unfortunately, it is far from trivial to obtain such data. The only technique I know of that could *in principle* image the CNT liquid crystal composites *directly* is cryogenic electron microscopy (cryo-TEM). I have been communicating for some time with Prof. Oren Regev at the Ben-Gurion University in Beer-Sheva, Israel, an expert in cryo-TEM with experience in imaging surfactant-dispersed CNTs [184], about investigating our samples with this technique. He informed me, however, that our surfactant concentrations are far too high, since a maximum of 10-15% surfactant can be tolerated for cryo-TEM imaging to work out.

An alternative approach is to use freeze-fracture electron microscopy (FF-TEM), where a replica of the surface of a sample that has been fractured after vitrification is imaged. During a short stay in 2006 in the group of Prof. Noel Clark (probably today's leading expert in FF-TEM study of liquid crystals [185, 186]), University Colorado at Boulder, USA. These preliminary experiments, carried out with the help of Dr. Michael-Scott Heberling, showed the difficulties to work with suspensions with low concentrations of SWCNTs. It was almost impossible to distinguish the nanotubes in the resulting images. With the catanionic samples holding a much higher concentration of CNTs we might be more successful, so it could be a good time for a new attempt in this direction.

In sections 4.4 and 4.5 the issues in focus contain much interesting soft matter physical chemistry, and some of them are also important from an applied point of view. Much work remains to be done, however, of experimental as well as analytical/theoretical character, and the conclusions will very likely need to be adjusted in various degrees.

The formation of catanionically complexed liquid crystal phases *by* the nanotubes, in the precipitates that form when an isotropic aqueous surfactant suspension of CNTs is destabilized by addition of an equimolar amount of the oppositely charged surfactant, is a very interesting alternative route that we have only begun to explore. Apart from being a fascinating example of self-organization in soft matter it may well turn out to be highly useful as a means of producing new organized nanostructures e.g. in the field of metamaterials. Most of the surfactant combinations did however not produce long-range ordered phases and the reasons for the different behavior are far from being understood. This is thus an interesting topic for future development.

We are slightly further in understanding the filament formation process, such that we now have a model for what is going on and a protocol for how to achieve the filaments, allowing us to explore this phenomenon for the controlled deposition of liquid crystal-aligned nanotubes. Nevertheless, also this topic requires further research efforts, as some aspects of our model need the deeper theoretical insight given through our collaboration with Prof. van der Schoot.

Chapter 5

Summary and general outlook

I would here like to summarize the general scope of my research and the overall conclusions that can be drawn from the three, seemingly quite different, research topics that I have described in this thesis. My main aim when writing it has been to provide some inspiring examples of how liquid crystal research can be both fundamentally intriguing and highly applicable, well beyond the limited domain of liquid crystal displays. A drawback of the success of LCDs is in fact that many people tend to connect liquid crystals solely with these devices, forgetting how much more these fascinating ordered fluids have to offer. I sincerely hope that the reader of this thesis will not have such a limited view of liquid crystals (at least not at the end of the process) and I would be very glad if some ideas for interesting new research thrusts have arisen while reading.

Being intermediate between solids and liquids, requiring knowledge and tools from physics as well as chemistry for their analysis, and having great relevance in technology as well as biology, liquid crystals are inherently interdisciplinary. It is then quite natural to study them from an interdisciplinary point of view, an open attitude towards combinations with other materials being highly rewarding. In this thesis I have presented three aspects of modern liquid crystal research, embracing this open-minded interdisciplinary attitude, one chapter dealing with liquid crystal phases on their own, another with liquid crystals inside solid materials, and a third with solid materials inside liquid crystals. Very different questions arise in the study of each topic but the unique properties that come with the combination of long-range order and fluidity that liquid crystals offer constitute the common basis for all this research.

When a single chiral smectic compound can exhibit no less than six different thermodynamically stable phases *between* the solid and the liquid state (sections 2.2 and 2.4) it becomes strikingly clear how insufficient the old school teacher's wisdom of 'the three states of matter' is. Liquid crystals do not give one but a whole series of additional states to be considered. The subtle change of switching between syn- and anticlinic director ordering provides a very strong change in physical properties of the chiral smectic-C-type phases where these terms are applied. As discussed in sections 2.1-2.3, a spontaneous polarization appears and this can be modulated in a variety of ways depending on the overall structure of the phase, the influence of external fields or interfaces playing very important roles. A good grasp of the meanings of ferro- and antiferroelectricity is then helpful if not required for correctly interpreting the behavior of these systems (section 2.5).

If a single liquid crystal is not complex enough then mixing of smartly selected mesogens certainly makes life more interesting, as shown in section 2.6, chirality being an important spice in the recipe. An organic chemist can instead vary the mesogen structure, for instance connecting two mesogenic units in a dimer as in BMHBOP-8. As demonstrated in section 2.7 the result is as fascinating as it is complex, the conformational freedom provided by a central spacer unit leading to entirely new phenomena.

But the study of chiral smectics constitutes but an example of the complexity that liquid

crystalline organization may give rise to and the richness in physical properties that one may see as a result of this self-assembly process. When switching to discotic liquid crystals, forming nematic, columnar or even (in rare cases) smectic phases, entirely different properties arise, of particular interest for photovoltaics and organic electronics [187–189]. In fact, also this class of liquid crystal can exhibit ferro- and antiferroelectricity when chiral [190]. For chiral smectics as well as chiral or non-chiral discotics it will be very interesting to see how they behave when encapsulated in thin fibers, conveniently produced via coaxial electrospinning. My research so far on calamitic nematics and on one achiral smectic confined in the core of such fibers (section 3.2) has clearly shown that a dramatic extension of the liquid crystal phase temperature range may result and that the director alignment along the fiber is very robust.

The optical properties of short-pitch cholesterics in electrospun fibers are both fascinating and potentially useful (section 3.2.5). The most commonly achieved configuration with helix perpendicular to the fiber axis gives distinct selective reflection although the liquid crystalline cylinder inside the fiber may have a diameter that is no greater than a single pitch of the helix. Much remains to be done in optimizing the spinning process and the fluids involved, such that continuous cylindrical filling rather than a distribution of liquid crystal droplets inside the fiber can be ensured. For applying the functional fibers it will also be important to find convenient polymer-solvent combinations for the outer fluid, such that textiles can be produced that are stable against the typical environment in which they will be used.

The requirement on immiscibility between inner and outer fluids during coaxial electrospinning limits the choice of outer polymer solutions as long as we have thermotropic liquid crystal in the core, so in this respect a switch to water-based lyotropic liquid crystals can be very interesting. These will hardly mix with non-polar solvent solutions of useful polymers like polystyrene, polycarbonate or poly(methyl methacrylate). The study of this materials combination in electrospinning remains to be done, and for this my experience in using lyotropic liquid crystals in combination with carbon nanotubes will certainly be useful.

Although at first surprising, considering the expected problems of depletion attraction when having such large surfactant concentration as required for producing a lyotropic liquid crystal phase (section 4.4), carbon nanotubes can be very well dispersed in this ordered fluid host, as shown in section 4.3.1. As may be expected, the choice of surfactants plays an important role for the result, the combination of cat- and anionic surfactants for CNT dispersion and liquid crystal phase formation, respectively, being particularly rewarding. With such a system we achieved such high CNT concentration and degree of tube alignment that the liquid crystal turned into a fluid polarizer (Figs. 4.11 - 4.12) and at the same time the mechanical properties of the phase were influenced in quite peculiar ways. A very subtle balance between nematic and hexagonal order was detected (section 4.5.1), as was the formation of thin filaments with very well aligned CNTs (section 4.5.2).

The filament formation is not just a phenomenon that can easily fascinate a physical chemist with interest in soft matter, it is also highly useful since it may provide a way of depositing the aligned carbon nanotubes on a target substrate. The fact that the lyotropic liquid crystal-based alignment works for any type of carbon nanotube, single- as well as multiwall (Fig. 4.11 and 4.13, respectively) makes it one of the most versatile alignment techniques available for unsupported carbon nanotubes. Another beautiful aspect of the approach is that it is perfectly compatible with all purification and fractionation schemes devised for CNTs, hence it has great potential for future device and materials development involving carbon nanotubes.

However, there is no need to restrict the research to *carbon* nanotubes. I am presently involved in the European research network COINAPO, devoted to the study of inorganic nanotubes in polymers, and here I am applying my expertise to liquid crystal-based alignment of an entirely new class of nanotubes and nanowires [191–193]. Either a low-molar mass liquid crystal (thermotropic or lyotropic) can provide the nanotube alignment prior to polymerization, or a liquid crystalline polymer may be used as the host matrix, although the dispersion will probably be a challenge when following the latter approach. In any case, there is much interesting research yet

to be done when combining liquid crystals with different types of nanotubes and -wires.

I have in this thesis chosen not to describe my work on carbon nanotubes in thermotropic liquid crystal hosts, partially in the interest of compactness, partially because this is research largely initiated and driven by my colleague Dr. Giusy Scalia. I would like to stress, however, that also this liquid crystal class holds great potential for combination with a variety of nanotubes or other nanoscale particles, in many respects perfectly complementing lyotropics. I urge the interested reader to learn more about this work in the articles of myself, Dr. Scalia and many other researchers around the world (several references are provided in Paper 15).

While each of the three topics that I discussed in this thesis still holds many interesting mysteries and challenges for the future, I have no intention to limit myself to these topics. Liquid crystals have so much more to offer, behaving differently and offering other possibilities when studied in different geometries or in combination with other materials. My most recent research interest is microfluidics with liquid crystals, where I concentrate foremost on the production of liquid crystalline shells using the coaxial capillary microfluidics set-up devised in David Weitz' group at Harvard [194]. His team already produced the first nematic shells using this technique [195], demonstrating that the shell morphology is of great interest for studying liquid crystals. Somewhat earlier theoretical work of David Nelson [196] also suggests that the shells may provide a means of developing colloidal crystals with diamond symmetry, expected to have most attractive optical properties but being very difficult to achieve with ordinary colloidal particles.

In my research in this field I explore not only the nematic but also smectic phases, and both chiral and non-chiral phases will be used. I believe the resulting structures will be of considerable interest for realizing Nelson's theoretically predicted colloid structures, but they may also shed light on phenomena occurring in vesicles formed by aqueous suspension of some synthetic phospholipids (as well as in certain biological systems) where the L_α-$L_{\beta'}$ phase transition plays a central role [197]. The liquid crystalline shells produced in our microfluidics set-up are in a sense thermotropic liquid crystal vesicles and they can thus be very interesting as model systems for these and other phenomena occurring in biology-related liquid crystalline systems.

I end this thesis with a beautiful photo (Fig. 5.1) taken by my doctoral student Hsin-Ling Liang. She is the one working on the liquid crystal microfluidics topic, the production of smectic shells and their study being one of the main foci. The photo shows a rather large shell, roughly 350 μm in diameter, formed by an achiral SmC phase. A deep look into this 'liquid crystal ball' may well reveal much information about my future research.
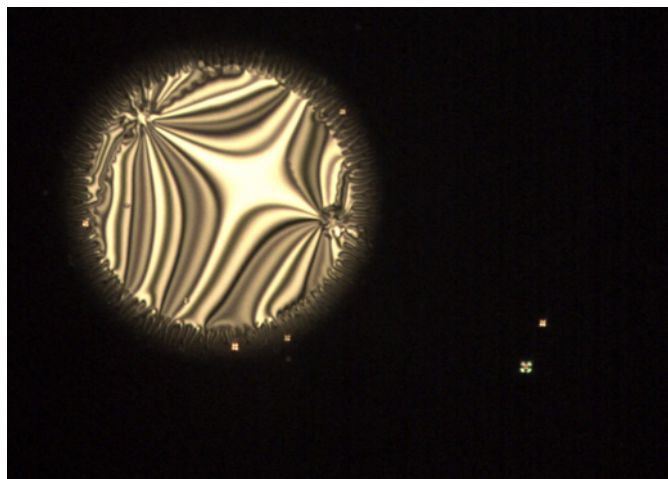
Figure 5.1: A shell of achiral SmC, containing and dispersed in an aqueous surfactant solution, produced by coaxial capillary microfluidics. Courtesy of Ms. Hsin-Ling Liang.

Bibliography

[1] Timothy J. Sluckin, David A. Dunmur and Horst Stegemeyer. *Crystals that flow: Classic papers from the history of liquid crystals* (Taylor and Francis, London, 2004).

[2] P. Boonbrahm and Alfred Saupe. 'Critical-behavior of uniaxial biaxial nematic phase-transitions in amphiphilic systems'. *J. Chem. Phys.*, **81** (4), pp. 2076–2081 (1984).

[3] L. J. Yu and Alfred Saupe. 'Observation of a biaxial nematic phase in potassium laurate-1-decanol-water mixtures'. *Phys. Rev. Lett.*, **45** (12), pp. 1000–1003 (1980).

[4] M. Lehmann, C. Kohn, Horst Kresse and Z. Vakhovskaya. 'Synthesis and properties of oxadiazole based V-shaped, shape persistent nematogens'. *Chem. Commun.*, (15), pp. 1768–1770 (2008).

[5] T. Kato, N. Mizoshita and K. Kishimoto. 'Functional liquid-crystalline assemblies: Self-organized soft materials'. *Angew. Chem. (Int. Ed.)*, **45** (1), pp. 38–68 (2006).

[6] Rudolf Pummerer and Ludwig Seligsberger. 'Über 4.4-Derivate des Sexiphenyls und Quaterphenyls'. *Ber. deutsch. chem. Ges.*, **64**, pp. 2477–2486 (1931).

[7] D. Chandler. 'Interfaces and the driving force of hydrophobic assembly'. *Nature*, **437** (7059), pp. 640–647 (2005).

[8] D. Fennell Evans and Håkan Wennerström. *The Colloidal Domain: Where Physics, Chemistry, Biology, and Technology Meet (Advances in Interfacial Engineering)* (Wiley-VCH, 1999).

[9] Z. Dogic and Seth Fraden. 'Ordered phases of filamentous viruses'. *Curr. Opin. Colloid Interface Sci.*, **11** (1), pp. 47–55 (2006).

[10] M. C. Mourad, J. E. Wijnhoven, D. D. Van't Zand, David van der Beek and Henk N. W. Lekkerkerker. 'Gelation versus liquid crystal phase transitions in suspensions of plate-like particles.' *Philos. Transact. A Math. Phys. Eng. Sci.*, **364** (1847), pp. 2807–2816 (2006).

[11] S. Badaire, Cecile Zakri, M. Maugey, A. Derre, J. N. Barisci, G. Wallace and Philippe Poulin. 'Liquid crystals of DNA-stabilized carbon nanotubes'. *Adv. Mater.*, **17** (13), p. 1673 (2005).

[12] W. H. Song, Iain A. Kinloch and Alan H. Windle. 'Nematic liquid crystallinity of multiwall carbon nanotubes'. *Science*, **302** (5649), pp. 1363–1363 (2003).

[13] John Lydon. 'Chromonic mesophases'. *Curr. Opin. Colloid Interface Sci.*, **8** (6), pp. 480–490 (2004).

[14] Peter J. Collings and Michael Hird. *Introduction to liquid crystals* (The Liquid Crystal Books Series Taylor & Francis, London, 1997).

[15] Sabine Laschat, Angelika Baro, Nelli Steinke, Frank Giesselmann, Constanze Hägele, Giusy Scalia, Roxana Judele, Elisabeth Kapatsina, Sven Sauer, Alina Schreivogel and Martin Tosoni. 'Discotic Liquid Crystals: From Tailor-Made Synthesis to Plastic Electronics'. *Angew. Chem. (Int. Ed.)*, **46** (26), pp. 4832–4887 (2007).

[16] Xiao Hong Cheng, Malay Kumar Das, Sigmar Diele and Carsten Tschierske. 'Novel liquid-crystalline phases with layerlike organization'. *Angew. Chem.*, **114** (21), pp. 4203 – 4207 (2002).

[17] Carsten Tschierske. 'Micro-segregation, molecular shape and molecular topology partners for the design of liquid crystalline materials with complex mesophase morphologies'. *J. Mater. Chem.*, **11** (11), pp. 2647–2671 (2001).

[18] Pierre-Gilles de Gennes and Jacques Prost. *The physics of liquid crystals* (Clarendon Press, Oxford, UK, 1993).

[19] Jan P. F. Lagerwall. *Phase characterization of polar liquid crystals using dielectric spectroscopy* (Chalmers University of Technology, Department of Microelectronics & Nanoscience, Liquid Crystal Physics (freely available for download at www.lcsoftmatter.com), Göteborg, Sweden, 2000).

[20] Philip W. Anderson. *Basic Notions Of Condensed Matter Physics (Advanced Book Classics)* (Westview Press, 1997).

[21] Jeffrey Goldstone, Abdus Salam and Steven Weinberg. 'Broken symmetries'. *Physical Review*, **127** (3), pp. 965 – 970 (1962).

[22] Sven T. Lagerwall. *Ferroelectric and antiferroelectric liquid crystals* (Wiley-VCH, Weinheim, 1999).

[23] G. S. Smith, E. B. Sirota, C. R. Safinya and Noel A. Clark. 'Structure of the L_β phases in a hydrated phosphatidylcholine multimembrane'. *Phys. Rev. Lett.*, **60** (9), pp. 813–816 (1988).

[24] Dietrich Demus, John W. Goodby, George Gray, H.-W. Spiess and Volkmar Vill (eds.). *Handbook of liquid crystals* (Wiley-VCH, Weinheim, 1998).

[25] M. Barón. 'Definitions of basic terms relating to low-molar-mass and polymer liquid crystals'. *Pure Appl. Chem.*, **73** (5), pp. 845–895 (2001).

[26] Antonio M. Figueiredo Neto and Silvio R. A. Salinas. *The Physics of Lyotropic Liquid Crystals: Phase Transitions and Structural Properties (Monographs on the Physics and Chemistry of Materials)* (Oxford University Press, USA, 2005).

[27] Peter P. Crooker and H. S. Kitzerow. 'Blue phases'. *Condensed Matter News*, **1** (3), pp. 6–10 (1992).

[28] Peter P. Crooker. 'The blue phases - a review of experiments'. *Liq. Cryst.*, **5** (3), pp. 751–775 (1989).

[29] Heinz S. Kitzerow. 'Blue phases at work!' *ChemPhysChem*, **7** (1), pp. 63–66 (2006).

[30] Ingo Dierking. *Textures of liquid crystals* (Wiley-VCH, Weinheim, 2003).

[31] H Kikuchi, M Yokota, Y Hisakado, H Yang and T Kajiyama. 'Polymer-stabilized liquid crystal blue phases'. *Nat. Mater.*, **1** (1), pp. 64–68 (2002).

[32] Lev M. Blinov, S. A. Davidyan, A. G. Petrov, A. T. Todorov and S. V. Yablonskii. 'Manifestation of ferroelectricity in a lyotropic liquid-crystal with a chiral impurity - a structural analog of a biological membrane'. *Jetp Letters*, **48** (5), pp. 285–288 (1988).

[33] A. G. Petrov, A. T. Todorov, B. Bonev, Lev M. Blinov, S. V. Yablonski, D. B. Fubachyus and N. Tvetkova. 'Manifestations of ferroelectricity in lyotropics with chiral additives: Biomembranes' analogs'. *Ferroelectrics*, **114**, pp. 415 – 427 (1991).

[34] P. Das, J. Xu, J. Roy and N. Chakrabarti. 'Liquid crystal polymorphism in f-actin: Optical microscopic and rotatory dispersion studies'. *J. Chem. Phys.*, **111** (17), pp. 8240–8250 (1999).

[35] S. W. Lee, B. M. Wood and Angela M. Belcher. 'Chiral smectic C structures of virus-based films'. *Langmuir*, **19** (5), pp. 1592–1598 (2003).

[36] John Harden, Nicholas Diorio, G. Petrov, Alexander and Antal Jakli. 'Chirality of lipids makes fluid lamellar phases piezoelectric'. *Phys. Rev. E*, **79** (1), p. 011 701 (2009).

[37] R. A. Reddy and Carsten Tschierske. 'Bent-core liquid crystals: polar order, superstructural chirality and spontaneous desymmetrisation in soft matter systems'. *J. Mater. Chem.*, **16** (10), pp. 907–961 (2006).

[38] Hideo Takezoe and Y. Takanishi. 'Bent-core liquid crystals: Their mysterious and attractive world'. *Jpn J Appl Phys 1*, **45** (2A), pp. 597–625 (2006).

[39] Gerhard Pelzl, Siegmar Diele and Wolfgang Weissflog. 'Banana-shaped compounds - a new field of liquid crystals'. *Adv. Mater.*, **11** (9), pp. 707–724 (1999).

[40] Darren R. Link, G. Natale, R. Shao, Joseph E. Maclennan, Noel A. Clark, Eva Körblova and David M. Walba. 'Spontaneous formation of macroscopic chiral domains in a fluid smectic phase of achiral molecules'. *Science*, **278** (5345), pp. 1924–1927 (1997).

[41] Hans Sawade, I. D. Olenik, Daniel Krüerke and Gerd Heppke. 'Chirality in discotic lyomesophases'. *Mol. Cryst. Liq. Cryst.*, **367**, pp. 529–536 (2001).

[42] Daniel Krüerke. *Experimentelle untersuchungen nematischer und cholesterischer phasen diskotischer flüssigkristalle*. Ph.D. thesis, TU Berlin, Berlin, Germany (1999).

[43] K. Praefcke, B. Kohne, K. Gutbier, N. Johnen and D. Singer. 'Syntheses and unusual mesophase sequences of hydrocarbons of a novel type of non-calamitic liquid-crystal'. *Liq. Cryst.*, **5** (1), pp. 233–249 (1989).

[44] P. H. Hermans and P. Platzek. *Kolloid Z.*, **88**, p. 68 (1939).

[45] V. Tsvetkov. *Acta Physiochim. (ussr)*, **16**, pp. 132–147 (1942).

[46] P. O. Quist, B. Halle and I. Furo. 'Nuclear-spin relaxation in a hexagonal lyotropic liquid-crystal'. *J. Chem. Phys.*, **95** (9), pp. 6945–6961 (1991).

[47] T. Beica, R. Moldovan, M. Tintaru, I. Enache and S. Frunza. 'Measurements of optical anisotropy of a calamitic lyotropic liquid crystal'. *Cryst. Res. Technol.*, **39** (2), pp. 151–156 (2004).

[48] H. Johannesson, I. Furo and B. Halle. 'Orientational order and micelle size in the nematic phase of the cesium pentadecafluorooctanoate-water system from the anisotropic self-diffusion of water'. *Phys. Rev. E*, **53** (5), pp. 4904–4917 (1996).

[49] N. Boden, J. Clements, K. A. Dawson, K. W. Jolley and D. Parker. 'Universal nature of the nematic-to-isotropic transition in solutions of discotic micelles'. *Phys. Rev. Lett.*, **66** (22), pp. 2883–2886 (1991).

[50] J. P. Mcclymer and Mortimer M. Labes. 'Simultaneous measurement of guest and host ordering in a nematic lyophase via fluorescence spectroscopy'. *Mol. Cryst. Liq. Cryst.*, **195**, pp. 39–44 (1991).

[51] Michael Krueger and Frank Giesselmann. 'Dielectric spectroscopy of 'de vries' type smectic A* - C* transitions'. *Phys. Rev. E*, **71** (4), p. 041 704 (2005).

[52] A. A. Sonin. *Freely Suspended Liquid Crystalline Films* (Wiley, 1999).

[53] G. S. Smith, E. B. Sirota, C. R. Safinya, R. J. Plano and Noel A. Clark. 'X-ray Structural Studies of Freely Suspended Ordered Hydrated DMPC Multimembrane Films'. *J. Chem. Phys.*, **92** (7), pp. 4519–4529 (1990).

[54] Ralf Stannarius, C. Cramer and H. Schuring. 'Self-supporting smectic bubbles (vol 350, pg 297, 2000)'. *Mol. Cryst. Liq. Cryst.*, **350**, pp. 297–305 (2000).

[55] Ralf Stannarius and C. Cramer. 'Self-supporting bubbles of thermotropic smectic liquid crystals'. *Europhys. Lett.*, **42** (1), pp. 43–48 (1998).

[56] Igor Musevic, Miha Skarabot, U Tkalec, M Ravnik and S Zumer. 'Two-dimensional nematic colloidal crystals self-assembled by topological defects'. *Science*, **313** (5789), pp. 954–958 (2006).

[57] E. B. Preistley and P. J. Wojtowicz. *Introduction to Liquid Crystals* (Plenum Pub Corp, 1976).

[58] Robert B. Meyer, L. Liebert, L. Strzelecki and Patrick Keller. 'Ferroelectric liquid crystals'. *J. Phys. (Paris) Lett.*, **36** (3), pp. L69–71 (1975).

[59] M. E. Lines and a. M. Glass. *Principles and applications of ferroelectrics and related materials* (Clarendon Press, Oxford, 1977).

[60] Noel A. Clark and Sven T. Lagerwall. 'Submicrosecond bistable electro-optic switching in liquid crystals'. *Appl. Phys. Lett.*, **36** (11), pp. 899–901 (1980).

[61] Jan P. F. Lagerwall. 'Demonstration of the antiferroelectric aspect of the helical superstructures in SmC*, SmC$_\alpha$* and SmC$_a$* liquid crystals'. *Phys. Rev. E*, **71**, p. 051 703 (2005).

[62] Jan P. F. Lagerwall and Frank Giesselmann. 'The experimental study of phases and phase transitions in antiferroelectric liquid crystals'. In Wojciech Kuczynski (ed.), 'Chiral Liquid Crystals', pp. 147–184 (Polish Academy of Sciences, Poznan, Poland, 2005).

[63] S. Garoff and Robert B. Meyer. 'Electroclinic effect at the A-C phase change in a chiral smectic liquid crystal'. *Phys. Rev. Lett.*, **38** (15), pp. 848–851 (1977).

[64] Frank Giesselmann. *Smectic A-C phase transitions in liquid crystals* (Habilitation thesis, Clausthal University of Technology, Clausthal-Zellerfeld, 1997).

[65] Atsuo Fukuda, Yoichi Takanishi, Tadaaki Isozaki, K. Ishikawa and Hideo Takezoe. 'Antiferroelectric chiral smectic liquid crystals (feature article)'. *J. Mater. Chem.*, **4** (7), pp. 997–1016 (1994).

[66] Per Rudquist, Jan P. F. Lagerwall, Johann G. Meier, K. D'havé and Sven T. Lagerwall. 'Tilt plane orientation in antiferroelectric liquid crystal cells and the origin of the pretransitional effect'. *Phys. Rev. E*, **66**, p. 061 708 (2002).

[67] E. Gorecka, D. Pociecha, M. Cepic, B. Zeks and R. Dabrowski. 'Enantiomeric excess dependence of the phase diagram of antiferroelectric liquid crystals'. *Phys. Rev. E*, **65**, p. 061 703 (2002).

[68] Jan P. F. Lagerwall, Per Rudquist, Sven T. Lagerwall and Frank Giesselmann. 'On the phase sequence of antiferroelectric liquid crystals and its relation to orientational and translational order'. *Liq. Cryst.*, **30** (4), pp. 399 – 414 (2003).

[69] Carsten Tschierske. 'Liquid crystal engineering - new complex mesophase structures and their relations to polymer morphologies, nanoscale patterning and crystal engineering'. *Chem. Soc. Rev.*, **36** (12), pp. 1930–1970 (2007).

[70] D Lingwood and K Simons. 'Lipid rafts as a membrane-organizing principle.' *Science*, **327** (5961), pp. 46–50 (2010).

[71] Pg Degennes. 'Electrostatic buckling of chiral lipid bilayers'. *C. R. Acad. Sci.*, **304** (7), pp. 259–263 (1987).

[72] J. F. Cooley. *US Patent*, **USA** (1902).

[73] W. J. Morton. *US Patent*, **USA** (1902).

[74] Anton Formhals. 'Process and apparatus for preparing artificial threads' (1934).

[75] DH Reneker and AL Yarin. 'Electrospinning jets and polymer nanofibers'. *Polymer*, **49** (10), pp. 2387–2425 (2008).

[76] JH Yu, SV Fridrikh and GC Rutledge. 'The role of elasticity in the formation of electrospun fibers'. *Polymer*, **47** (13), pp. 4789–4797 (2006).

[77] K Arayanarakul, N Choktaweesap, D Aht-ong, C Meechaisue and P Supaphol. 'Effects of poly(ethylene glycol), inorganic salt, sodium dodecyl sulfate, and solvent system on electrospinning of poly(ethylene oxide)'. *Macromol. Mater. Eng.*, **291** (6), pp. 581–591 (2006).

[78] SR Bhattarai, N Bhattarai, HK Yi, PH Hwang, DI Cha and HY Kim. 'Novel biodegradable electrospun membrane: scaffold for tissue engineering'. *Biomaterials*, **25** (13), pp. 2595–2602 (2004).

[79] D Li, YL Wang and YN Xia. 'Electrospinning of polymeric and ceramic nanofibers as uniaxially aligned arrays'. *Nano. Lett.*, **3** (8), pp. 1167–1171 (2003).

[80] D Li, YL Wang and YN Xia. 'Electrospinning nanofibers as uniaxially aligned arrays and layer-by-layer stacked films'. *Adv. Mater.*, **16** (4), pp. 361–366 (2004).

[81] Jt Mccann, D Li and Yn Xia. 'Electrospinning of nanofibers with core-sheath, hollow, or porous structures'. *J. Mater. Chem.*, **15** (7), pp. 735–738 (2005).

[82] Jt Mccann, M Marquez and Yn Xia. 'Melt coaxial electrospinning: A versatile method for the encapsulation of solid materials and fabrication of phase change nanofibers'. *Nano. Lett.*, **6** (12), pp. 2868–2872 (2006).

[83] Eva Enz, Ute Baumeister and Jan Lagerwall. 'Coaxial electrospinning of liquid crystal-containing poly(vinyl pyrrolidone) microfibers'. *Beilstein Journal of Organic Chemistry*, **5** (58) (2009).

[84] Jan P. F. Lagerwall, J. T. McCann, Eric Formo, Giusy Scalia and Younan Xia. 'Coaxial electrospinning of microfibres with liquid crystal in the core'. *Chem. Commun.*, (42), pp. 5420–5422 (2008).

[85] W Salalha, J Kuhn, Y Dror and E Zussman. 'Encapsulation of bacteria and viruses in electrospun nanofibres'. *Nanotechnology*, **17** (18), pp. 4675–4681 (2006).

[86] CX Zhang, XY Yuan, LL Wu, Y Han and J Sheng. 'Study on morphology of electrospun poly(vinyl alcohol) mats'. *Eur. Polym. J.*, **41** (3), pp. 423–432 (2005).

[87] Z Jun, HQ Hou, JH Wendorff and A Greiner. 'Poly(vinyl alcohol) nanofibres by electrospinning: influence of molecular weight on fibre shape'. *E-POLYMERS*, p. 038 (2005).

[88] N Li, XH Qin, EL Yang and SY Wang. 'Effect on instability section of PVA electrospinning nanofibers by adding LiCl'. *Mater. Lett.*, **62** (8-9), pp. 1345–1348 (2008).

[89] N Li, XH Qin, L Lin and SY Wang. 'The Effects of Spinning Conditions on the Morphology of Electrospun Jet and Nonwoven Membrane'. *Polym. Eng. Sci.*, **48** (12), pp. 2362–2366 (2008).

[90] D He, B Hu, QF Yao, K Wang and SH Yu. 'Large-scale synthesis of flexible free-standing SERS substrates with high sensitivity: electrospun PVA nanofibers embedded with controlled alignment of silver nanoparticles.' *ACS Nano*, **3** (12), pp. 3993–4002 (2009).

[91] Haizhu Sun, Hao Zhang, Junhu Zhang, Haotong Wei, Jie Ju, Minjie Li and Bai Yang. 'White-light emission nanofibers obtained from assembling aqueous single-colored CdTe NCs into a PPV precursor and PVA matrix'. *J. Mater. Chem.*, **19** (37), pp. 6740–6744 (2009).

[92] B Sundaray, V Subramanian, TS Natarajan, RZ Xiang, CC Chang and WS Fann. 'Electrospinning of continuous aligned polymer fibers'. *Appl. Phys. Lett.*, **84** (7), pp. 1222–1224 (2004).

[93] S Megelski, JS Stephens, DB Chase and JF Rabolt. 'Micro- and nanostructured surface morphology on electrospun polymer fibers'. *Macromolecules*, **35** (22), pp. 8456–8466 (2002).

[94] R Sen, B Zhao, D Perea, ME Itkis, H Hu, J Love, E Bekyarova and RC Haddon. 'Preparation of single-walled carbon nanotube reinforced polystyrene and polyurethane nanofibers and membranes by electrospinning'. *Nano. Lett.*, **4** (3), pp. 459–464 (2004).

[95] CL Casper, JS Stephens, NG Tassi, DB Chase and JF Rabolt. 'Controlling surface morphology of electrospun polystyrene fibers: Effect of humidity and molecular weight in the electrospinning process'. *Macromolecules*, **37** (2), pp. 573–578 (2004).

[96] SG Wang, YX Li, J Bai, QB Yang, Y Song and CQ Zhang. 'Characterization and photoluminescence studies of CdTe nanoparticles before and after transfer from liquid phase to polystyrene'. *B Mater Sci*, **32** (5), pp. 487–491 (2009).

[97] G Eda and S Shivkumar. 'Bead-to-fiber transition in electrospun polystyrene'. *J. Appl. Polym. Sci.*, **106** (1), pp. 475–487 (2007).

[98] G Eda, J Liu and S Shivkumar. 'Flight path of electrospun polystyrene solutions: Effects of molecular weight and concentration'. *Mater. Lett.*, **61** (7), pp. 1451–1455 (2007).

[99] RVN Krishnappa, K Desai and CM Sung. 'Morphological study of electrospun polycarbonates as a function of the solvent and processing voltage'. *J. Mater. Sci.*, **38** (11), pp. 2357–2365 (2003).

[100] GM Kim, GH Michler and P Pötschke. 'Deformation processes of ultrahigh porous multiwalled carbon nanotubes/polycarbonate composite fibers prepared by electrospinning'. *Polymer*, **46** (18), pp. 7346–7351 (2005).

[101] SC Moon and RJ Farris. 'The morphology, mechanical properties, and flammability of aligned electrospun polycarbonate (PC) nanofibers'. *Polym. Eng. Sci.*, **48** (9), pp. 1848–1854 (2008).

[102] JT McCann, M Marquez and YN Xia. 'Highly porous fibers by electrospinning into a cryogenic liquid'. *J. Am. Chem. Soc.*, **128** (5), pp. 1436–1437 (2006).

[103] J Liu, ZR Yue and H Fong. 'Continuous Nanoscale Carbon Fibers with Superior Mechanical Strength'. *Small*, **5** (5), pp. 536–542 (2009).

[104] Eun Ju Ra, Tae Hyung Kim, Woo Jong Yu, Kay Hyeok An and Young Hee Lee. 'Ultra-micropore formation in PAN/camphor-based carbon nanofiber paper'. *Chem. Commun.*, **46** (8), pp. 1320–1322 (2010).

[105] C Lai, QH Guo, XF Wu, DH Reneker and H Hou. 'Growth of carbon nanostructures on carbonized electrospun nanofibers with palladium nanoparticles'. *Nanotechnology*, **19** (19), p. 195 303 (2008).

[106] QH Zhang, ZJ Chang, MF Zhu, XM Mo and DJ Chen. 'Electrospun carbon nanotube composite nanofibres with uniaxially aligned arrays'. *Nanotechnology*, **18** (11), p. 115 611 (2007).

[107] A Bianco, G Iardino, A Manuelli, C Bertarelli and G Zerbi. 'Strong orientation of polymer chains and small photochromic molecules in polyamide 6 electrospun fibers'. *ChemPhysChem*, **8** (4), pp. 510–514 (2007).

[108] C Mit-uppatham, M Nithitanakul and P Supaphol. 'Ultrafine electrospun polyamide-6 fibers: Effect of solution conditions on morphology and average fiber diameter'. *Macromol. Chem. Phys.*, **205** (17), pp. 2327–2338 (2004).

[109] R Dersch, Tq Liu, Ak Schaper, a Greiner and Jh Wendorff. 'Electrospun nanofibers: Internal structure and intrinsic orientation'. *J. Polym. Sci. A*, **41** (4), pp. 545–553 (2003).

[110] YF Yao, ZZ Gu, JZ Zhang, C Pan, YY Zhang and HM Wei. 'Fiber-oriented liquid crystal polarizers based on anisotropic electrospinning'. *Adv. Mater.*, **19** (21), p. 3707 (2007).

[111] XM Sui and HD Wagner. 'Tough Nanocomposites: The Role of Carbon Nanotube Type'. *Nano. Lett.*, **9** (4), pp. 1423–1426 (2009).

[112] AV Bazilevsky, AL Yarin and CM Megaridis. 'Co-electrospinning of core-shell fibers using a single-nozzle technique'. *Langmuir*, **23** (5), pp. 2311–2314 (2007).

[113] Dh Reneker, Al Yarin, H Fong and S Koombhongse. 'Bending instability of electrically charged liquid jets of polymer solutions in electrospinning'. *J. Appl. Phys.*, **87** (9), pp. 4531–4547 (2000).

[114] A Greiner and JH Wendorff. 'Electrospinning: A fascinating method for the preparation of ultrathin fibres'. *Angew. Chem. (Int. Ed.)*, **46** (30), pp. 5670–5703 (2007).

[115] P Katta, M Alessandro, RD Ramsier and GG Chase. 'Continuous electrospinning of aligned polymer nanofibers onto a wire drum collector'. *Nano. Lett.*, **4** (11), pp. 2215–2218 (2004).

[116] LS Carnell, EJ Siochi, NM Holloway, RM Stephens and C. 'Aligned Mats from Electrospun Single Fibers'. *Macromolecules*, **41**, pp. 5345–5349 (2008).

[117] Hao Yan, Luqi Liu and Zhong Zhang. 'Alignment of electrospun nanofibers using dielectric materials'. *Appl. Phys. Lett.*, **95** (14), p. 143 114 (2009).

[118] D Li and Yn Xia. 'Direct fabrication of composite and ceramic hollow nanofibers by electrospinning'. *Nano. Lett.*, **4** (5), pp. 933–938 (2004).

[119] Zc Sun, E Zussman, Al Yarin, Jh Wendorff and a Greiner. 'Compound core-shell polymer nanofibers by co-electrospinning'. *Adv. Mater.*, **15** (22), p. 1929 (2003).

[120] Dh Reneker and I Chun. 'Nanometre diameter fibres of polymer, produced by electrospinning'. *Nanotechnology*, **7** (3), pp. 216–223 (1996).

[121] S Koombhongse, WX Liu and DH Reneker. 'Flat polymer ribbons and other shapes by electrospinning'. *J. Polym. Sci. B*, **39** (21), pp. 2598–2606 (2001).

[122] Per Rudquist, Jan P. F. Lagerwall, M. Buivydas, F. Gouda, Sven T. Lagerwall, Noel A. Clark, Joseph E. Maclennan, R. F. Shao, D. Coleman, Sebastien Bardon, Tommaso Bellini, Darren R. Link, Giorgio Natale, Mathew A. Glaser, David M. Walba, Michael D. Wand and X. H. Chen. 'The case of thresholdless antiferroelectricity: Polarization-stabilized twisted smc* liquid crystals give v-shaped electro-optic response'. *J. Mater. Chem.*, **9** (6), pp. 1257–1261 (1999).

[123] GS Iannacchione, GP Crawford, S Qian, JW Doane and D Finotello. 'Nematic ordering in highly restrictive Vycor glass'. *Phys. Rev. E*, **53** (3), pp. 2402–2411 (1996).

[124] Jan P. F. Lagerwall, Deven D. Parghi, Daniel Krüerke, Fathi Gouda and Pontus Jägemalm. 'Phases, phase transitions and confinement effects in a series of antiferroelectric liquid crystals'. *Liq. Cryst.*, **29** (2), pp. 163–178 (2002).

[125] RL Leheny, S Park, RJ Birgeneau, JL Gallani, CW Garland and GS Iannacchione. 'Smectic ordering in liquid-crystal-aerosil dispersions. I. X-ray scattering'. *Phys. Rev. E*, **67** (1), p. 011 708 (2003).

[126] T Jin, B Zalar, a Lebar, M Vilfan, S Zumer and D Finotello. 'Anchoring and structural transitions as a function of molecular length in confined liquid crystals'. *Eur. Phys. J. E*, **16**, pp. 159–165 (2005).

[127] M Steinhart, S Zimmermann, P Goring, AK Schaper, U Gosele, C Weder and JH Wendorff. 'Liquid crystalline nanowires in porous alumina: Geometric confinement versus influence of pore walls'. *Nano. Lett.*, **5** (3), pp. 429–434 (2005).

[128] Da Winterbottom, R Narayanaswamy and Im Raimundo. 'Cholesteric liquid crystals for detection of organic vapours'. *Sensors and Actuators B-chemical*, **90** (1-3), pp. 52–57 (2003).

[129] Fl Dickert, a Haunschild and P Hofmann. 'Cholesteric liquid-crystals for solvent vapor detection - elimination of cross-sensitivity by band shape-analysis and pattern-recognition'. *Fresenius J. Anal. Chem.*, **350** (10-11), pp. 577–581 (1994).

[130] HS Kitzerow, B Liu, F Xu and PP Crooker. 'Effect of chirality on liquid crystals in capillary tubes with parallel and perpendicular anchoring'. *Phys. Rev. E*, **54** (1), pp. 568–575 (1996).

[131] M Nakata, M Sato, Y Matsuo, S Maeda and S Hayashi. 'Hollow fibers containing various display elements: A novel structure for electronic paper'. *J. SID*, **14** (8), pp. 723–727 (2006).

[132] R. Saito, Mildred S. Dresselhaus and Gene Dresselhaus. *Physical properties of carbon nanotubes* (Imperial College Press, UK, 1998).

[133] Ray H. Baughman, A. A. Zakhidov and W. A. de Heer. 'Carbon nanotubes - the route toward applications'. *Science*, **297** (5582), pp. 787–792 (2002).

[134] M. Zhang, K. R. Atkinson and Ray H. Baughman. 'Multifunctional carbon nanotube yarns by downsizing an ancient technology'. *Science*, **306** (5700), pp. 1358–1361 (2004).

[135] Mei Zhang, Shaoli Fang, Anvar A. Zakhidov, Sergey B. Lee, Ali E. Aliev, Christopher D. Williams, Ken R. Atkinson and Ray H. Baughman. 'Strong, transparent, multifunctional, carbon nanotube sheets'. *Science*, **309**, pp. 1215–1219 (2005).

[136] K. Koziol, J. Vilatela, A. Moisala, M. Motta, P. Cunniff, M. Sennett and Alan H. Windle. 'High-performance carbon nanotube fiber.' *Science*, **318** (5858), pp. 1892–1895 (2007).

[137] M. Moniruzzaman and K. L. Winey. 'Polymer nanocomposites containing carbon nanotubes'. *Macromolecules*, **39** (16), pp. 5194–5205 (2006).

[138] A. D. Pasquier, H. E. Unalan, A. Kanwal, S. Miller and M. Chhowalla. 'Conducting and transparent single-wall carbon nanotube electrodes for polymer-fullerene solar cells'. *Appl. Phys. Lett.*, **87** (20), p. 203 511 (2005).

[139] J. M. Thomassin, X. Lou, C. Pagnoulle, A. Saib, L. Bednarz, I. Huynen, R. Jerome and C. Detrembleur. 'Multiwalled carbon Nanotube/Poly(epsilon-caprolactone) nanocomposites with exceptional electromagnetic interference shielding properties'. *J. Phys. Chem. C*, **111** (30), pp. 11 186–11 192 (2007).

[140] N. Li, Y. Huang, F. Du, X. B. He, X. Lin, H. J. Gao, Y. F. Ma, F. F. Li, Y. S. Chen and P. C. Eklund. 'Electromagnetic interference (EMI) shielding of single-walled carbon nanotube epoxy composites'. *Nano. Lett.*, **6** (6), pp. 1141–1145 (2006).

[141] R. Singh, D. Pantarotto, L. Lacerda, G. Pastorin, C. Klumpp, M. Prato, A. Bianco and K. Kostarelos. 'Tissue biodistribution and blood clearance rates of intravenously administered carbon nanotube radiotracers'. *Proc. Natl. Acad. Sci. USA*, **103** (9), pp. 3357–3362 (2006).

[142] H. Liu, J. Zhai and L. Jiang. 'Wetting and anti-wetting on aligned carbon nanotube films'. *Soft Matter*, **2** (10), pp. 811–821 (2006).

[143] K. K. S. Lau, J. Bico, K. B. K. Teo, M. Chhowalla, G. A. J. Amaratunga, W. I. Milne, G. H. Mckinley and K. K. Gleason. 'Superhydrophobic carbon nanotube forests'. *Nano. Lett.*, **3** (12), pp. 1701–1705 (2003).

[144] R. A. Hatton, A. J. Miller and S. R. P. Silva. 'Carbon nanotubes: a multi-functional material for organic optoelectronics'. *J. Mater. Chem.*, **18** (11), pp. 1183–1192 (2008).

[145] FF Cao, YG Guo, SF Zheng, XL Wu, LY Jiang and RR and. Bi. *Symbiotic Coaxial Nanocables: Facile Synthesis and an Efficient and Elegant.*, volume 22 (2010).

[146] C. Stampfer, T. Helbling, Dirk Obergfell, B. Schoberle, M. K. Tripp, A. Jungen, Siegmar Roth, V. M. Bright and C. Hierold. 'Fabrication of single-walled carbon-nanotube-based pressure sensors'. *Nano. Lett.*, **6** (2), pp. 233–237 (2006).

[147] H. Qi and Torsten Hegmann. 'Impact of nanoscale particles and carbon nanotubes on current and future generations of liquid crystal displays'. *J. Mater. Chem.*, **18** (28), pp. 3288–3294 (2008).

[148] M. F. Islam, E. Rojas, D. M. Bergey, A. T. Johnson and A. G. Yodh. 'High weight fraction surfactant solubilization of single-wall carbon nanotubes in water'. *Nano. Lett.*, **3** (2), pp. 269–273 (2003).

[149] J. M. Bonard, T. Stora, J. P. Salvetat, F. Maier, T. Stöckli, C. Duschl, L. Forro, W. A. Deheer and A. Chatelain. 'Purification and size-selection of carbon nanotubes'. *Adv. Mater.*, **9** (10), pp. 827–831 (1997).

[150] Cecile Zakri and Philippe Poulin. 'Phase behavior of nanotube suspensions: From attraction induced percolation to liquid crystalline phases'. *J. Mater. Chem.*, **16** (42), pp. 4095–4098 (2006).

[151] Silvia Giordani, S. D. Bergin, V. Nicolosi, S. Lebedkin, M. M. Kappes, Werner J. Blau and Jonathan N. Coleman. 'Debundling of single-walled nanotubes by dilution: Observation of large populations of individual nanotubes in amide solvent dispersions'. *J. Phys. Chem. B*, **110** (32), pp. 15 708–15 718 (2006).

[152] Y. P. Sun, W. Huang, Y. Lin, K. Fu, A. Kitaygorodskiy, L. A. Riddle, Y. J. Yu and David L. Carroll. 'Soluble Dendron-Functionalized Carbon Nanotubes: Preparation, Characterization, and Properties'. *Chem. Mater.*, **13** (9), pp. 2864–2869 (2001).

[153] D. Tasis, N. Tagmatarchis, V. Georgakilas and Maurizio Prato. 'Soluble carbon nanotubes'. *Chem. -Eur. J.*, **9** (17), pp. 4001–4008 (2003).

[154] Alain Penicaud, Philippe Poulin, A. Derre, Eric Anglaret and P. Petit. 'Spontaneous dissolution of a single-wall carbon nanotube salt'. *J. Am. Chem. Soc.*, **127** (1), pp. 8–9 (2005).

[155] J. Cabana and R. Martel. 'Probing the reversibility of sidewall functionalization using carbon nanotube transistors'. *J. Am. Chem. Soc.*, **129** (8), pp. 2244–+ (2007).

[156] Stéphane Campidelli, C. Sooambar, E. L. Diz, C. Ehli, Dirk M. Guldi and Maurizio Prato. 'Dendrimer-functionalized single-wall carbon nanotubes: Synthesis, characterization, and photoinduced electron transfer'. *J. Am. Chem. Soc.*, **128** (38), pp. 12 544–12 552 (2006).

[157] Dirk M. Guldi, G. M. A. Rahman, F. Zerbetto and Maurizio Prato. 'Carbon nanotubes in electron donor-acceptor nanocomposites'. *Accounts Chem. Res.*, **38** (11), pp. 871–878 (2005).

[158] X. F. Guo, J. P. Small, J. E. Klare, Y. L. Wang, M. S. Purewal, I. W. Tam, B. H. Hong, R. Caldwell, L. M. Huang, S. O'Brien, J. M. Yan, R. Breslow, S. J. Wind, J. Hone, P. Kim and Colin Nuckolls. 'Covalently bridging gaps in single-walled carbon nanotubes with conducting molecules'. *Science*, **311** (5759), pp. 356–359 (2006).

[159] Kostas Kostarelos, L. Lacerda, G. Pastorin, W. Wu, S. Wieckowski, J. Luangsivilay, S. Godefroy, D. Pantarotto, J. P. Briand, S. Muller, Maurizio Prato and Alberto Bianco. 'Cellular uptake of functionalized carbon nanotubes is independent of functional group and cell type'. *Nat. Nanotechnol.*, **2** (2), pp. 108–113 (2007).

[160] D. Pantarotto, J. P. Briand, Maurizio Prato and Alberto Bianco. 'Translocation of bioactive peptides across cell membranes by carbon nanotubes'. *Chem. Commun.*, (1), pp. 16–17 (2004).

[161] Mark C. Hersam. 'Progress towards monodisperse single-walled carbon nanotubes'. *Nat. Nanotechnol.*, **3** (7), pp. 387–394 (2008).

[162] Ralf Krupke, F. Hennrich, H. von Lohneysen and M. M. Kappes. 'Separation of metallic from semiconducting single-walled carbon nanotubes'. *Science*, **301** (5631), pp. 344–347 (2003).

[163] Jack E. Fischer, W. Zhou, J. Vavro, C. Llaguno, C. Guthy, R. Haggenmueller, M. J. Casavant, D. E. Walters and Richard E. Smalley. 'Magnetically aligned single wall carbon nanotube films: Preferred orientation and anisotropic transport properties'. *J. Appl. Phys.*, **93** (4), pp. 2157–2163 (2003).

[164] H Wang, G. T. Christopherson, Z. Y. Xu, L. Porcar, D. L. Ho, D. Fry and E. K. Hobbie. 'Shear-sans study of single-walled carbon nanotube suspensions'. *Chem. Phys. Lett.*, **416** (1-3), pp. 182–186 (2005).

[165] S. Gerdes, T. Ondarcuhu, S. Cholet and C. Joachim. 'Combing a carbon nanotube on a flat metal-insulator-metal nanojunction'. *Europhys. Lett.*, **48** (3), pp. 292–298 (1999).

[166] Jan P. F. Lagerwall and Giusy Scalia. 'Carbon nanotubes in liquid crystals (Feature article)'. *J. Mater. Chem.*, **18** (25), pp. 2890–2898 (2008).

[167] A. Ismach and Ernesto Joselevich. 'Orthogonal self-assembly of carbon nanotube crossbar architectures by simultaneous graphoepitaxy and field-directed growth'. *Nano. Lett.*, **6** (8), pp. 1706–1710 (2006).

[168] K. Hata, D. N. Futaba, K. Mizuno, T. Namai, M. Yumura and S. Iijima. 'Water-assisted highly efficient synthesis of impurity-free single-walled carbon nanotubes'. *Science*, **306** (5700), pp. 1362–1364 (2004).

[169] Muklesur Rahman and Wei Lee. 'Scientific duo of carbon nanotubes and nematic liquid crystals'. *J. Phys. D-Appl. Phys.*, **42** (6), p. 063 001 (2009).

[170] P van der Schoot, V Popa-Nita and S Kralj. 'Alignment of carbon nanotubes in nematic liquid crystals'. *J. Phys. Chem. B*, **112** (15), pp. 4512–4518 (2008).

[171] L. Q. Amaral and M. E. Marcondes Helene. 'Nematic domain in the sodium lauryl sulfate water decanol system'. *J. Phys. Chem.*, **92** (21), pp. 6094–6098 (1988).

[172] Giusy Scalia, Miroslav Haluska, Ursula Dettlaff-Weglikowska, Frank Giesselmann and Siegmar Roth. 'Polarized Raman spectroscopy study of SWCNT orientational order in an aligning liquid crystalline matrix'. *AIP Conf. Proc.*, **786**, pp. 114–117 (2005).

[173] Gs Duesberg, I Loa, M Burghard, K Syassen and S Roth. 'Polarized raman spectroscopy on isolated single-wall carbon nanotubes'. *Phys. Rev. Lett.*, **85** (25), pp. 5436–5439 (2000).

[174] D. Marenduzzo, K. Finan and P. R. Cook. 'The depletion attraction: An underappreciated force driving cellular organization.' *J. Cell Biol.*, **175** (5), pp. 681–686 (2006).

[175] Jo Rädler, I Koltover, T Salditt and Cr Safinya. 'Structure of DNA-cationic liposome complexes: DNA intercalation in multilamellar membranes in distinct interhelical packing regimes'. *Science*, **275** (5301), pp. 810–814 (1997).

[176] B Vigolo, a Penicaud, C Coulon, C Sauder, R Pailler, C Journet, P Bernier and P Poulin. 'Macroscopic fibers and ribbons of oriented carbon nanotubes'. *Science*, **290** (5495), pp. 1331–1334 (2000).

[177] G. Hertel and H. Hoffmann. 'Lyotropic nematic phases of double chain surfactants'. *Progr. Colloid Polym. Sci.*, **76**, pp. 123–131 (1988).

[178] X Auvray, T Perche, C Petipas, R Anthore, Mj Marti, I Rico and A. Lattes. 'Influence of solvent headgroup interactions on the formation of lyotropic liquid-crystal phases of surfactants in water and nonaqueous protic and aprotic-solvents'. *Langmuir*, **8** (11), pp. 2671–2679 (1992).

[179] R Krishnaswamy, SK Ghosh, S Lakshmanan, VA Raghunathan and AK Sood. 'Phase behavior of concentrated aqueous solutions of cetyltrimethylammonium bromide (CTAB) and sodium hydroxy naphthoate (SHN)'. *Langmuir*, **21** (23), pp. 10 439–10 443 (2005).

[180] L Coppola, R Gianferri, I Nicotera, C Oliviero and Ga Ranieri. 'Structural changes in CTAB/H2O mixtures using a rheological approach'. *Phys. Chem. Chem. Phys.*, **6** (9), pp. 2364–2372 (2004).

[181] P van der Schoot. 'Self-assembly of globular particles in a nematic dispersion of colloidal rods'. *J. Chem. Phys.*, **117** (8), pp. 3537–3540 (2002).

[182] La Hough, Mf Islam, B Hammouda, Ag Yodh and Pa Heiney. 'Structure of semidilute single-wall carbon nanotube suspensions and gels'. *Nano. Lett.*, **6** (2), pp. 313–317 (2006).

[183] La Hough, Mf Islam, Pa Janmey and Ag Yodh. 'Viscoelasticity of single wall carbon nanotube suspensions'. *Phys. Rev. Lett.*, **93** (16), p. 168 102 (2004).

[184] E Nativ-Roth, R Yerushalmi-Rozen and O Regev. 'Phase behavior and shear alignment in SWNT-surfactant dispersions'. *Small*, **4** (9), pp. 1459–1467 (2008).

[185] L. E. Hough, H. T. Jung, D. Krueerke, M. S. Heberling, M. Nakata, C. D. Jones, D. Chen, D. R. Link, J. Zasadzinski, G. Heppke, J. P. Rabe, W. Stocker, E. Koerblova, D. M. Walba, M. A. Glaser and N. A. Clark. 'Helical Nanofilament Phases'. *Science*, **325** (5939), pp. 456–460 (2009).

[186] L. E. Hough, M. Spannuth, M. Nakata, D. A. Coleman, C. D. Jones, G. Dantlgraber, C. Tschierske, J. Watanabe, E. Koerblova, D. M. Walba, J. E. Maclennan, M. A. Glaser and N. A. Clark. 'Chiral Isotropic Liquids from Achiral Molecules'. *Science*, **325** (5939), pp. 452–456 (2009).

[187] Xinliang Feng, Valentina Marcon, Wojciech Pisula, Michael Ryan Hansen, James Kirkpatrick, Ferdinand Grozema, Denis Andrienko, Kurt Kremer and Klaus Muellen. 'Towards high charge-carrier mobilities by rational design of the shape and periphery of discotics'. *Nat. Mater.*, **8** (5), pp. 421–426 (2009).

[188] Michael Ryan Hansen, Tobias Schnitzler, Wojciech Pisula, Robert Graf, Klaus Muellen and Hans Wolfgang Spiess. 'Cooperative Molecular Motion within a Self-Assembled Liquid-Crystalline Molecular Wire: The Case of a TEG-Substituted Perylenediimide Disc'. *Angew. Chem. (Int. Ed.)*, **48** (25), pp. 4621–4624 (2009).

[189] Wojciech Pisula, Matthias Zorn, Ji Young Chang, Klaus Muellen and Rudolf Zentel. 'Liquid Crystalline Ordering and Charge Transport in Semiconducting Materials'. *Macromol. Rapid Commun.*, **30** (14), pp. 1179–1202 (2009).

[190] D Kruerke, P Rudquist, ST Lagerwall, H Sawade and G Heppke. 'Ferroelectric switching of chiral discotic lyomesophases'. *Ferroelectrics*, **243** (1-4), pp. 207–+ (2000).

[191] MI Ploscaru, SJ Kokalj, M Uplaznik, D Vengust, D Turk, A Mrzel and D Mihailovic. 'Mo6S9-xIx nanowire recognitive molecular-scale connectivity'. *Nano. Lett.*, **7** (6), pp. 1445–1448 (2007).

[192] A Zimina, S Eisebitt, M Freiwald, S Cramm, W Eberhardt, A Mrzel and D Mihailovic. 'Electronic structure of subnanometer diameter MOS2-I-x nanotubes'. *Nano. Lett.*, **4** (9), pp. 1749–1753 (2004).

[193] M Remskar, A Mrzel, Z Skraba, A Jesih, M Ceh, J Demsar, P Stadelmann, F Levy and D Mihailovic. 'Self-assembly of subnanometer-diameter single-wall MoS2 nanotubes'. *Science*, **292** (5516), pp. 479–481 (2001).

[194] Rhutesh K. Sharh, Ho Cheung Shum, Amy C. Rowat, Daeyeon Lee, Jeremy J. Agresti, Andrew S. Utada, Liang-Yin Chu, Jin-Woong Kim, Alberto Fernandez-Nieves, Carlos J. Martinez and David A. Weitz. 'Designer emulsions using microfluidics'. *Materials Today*, **11** (4), pp. 18–27 (2008).

[195] A. Fernandez-Nieves, V. Vitelli, A.S. Utada, Darren R. Link, M. Marquez, D. R. Nelson and David A. Weitz. 'Novel defect structures in nematic liquid crystal shells'. *Phys. Rev. Lett.*, **99** (15), p. 157 801 (2007).

[196] DR Nelson. 'Toward a tetravalent chemistry of colloids'. *Nano. Lett.*, **2** (10), pp. 1125–1129 (2002).

[197] Jv Selinger, Ms Spector and Jm Schnur. 'Theory of self-assembled tubules and helical ribbons'. *J. Phys. Chem. B*, **105** (30), pp. 7157–7169 (2001).

Appendix A

Papers on which this thesis is based

Papers related to Chapter 2

In chronological order:

1. *A chameleon chiral polar liquid crystal:*
   Rod-shaped when nematic, bent-shaped when smectic
   J.P.F. Lagerwall, F. Giesselmann, M.D. Wand, and D.M. Walba, *Chem. Mater.*, **16**, *19*,
   pp. 3606-3615 (2004)

2. *Chiral smectic C subphases induced by mixing a bistereogenic*
   antiferroelectric liquid crystal with a non-chiral liquid crystal
   J.P.F. Lagerwall, F. Giesselmann, S. Rauch, G. Heppke, P. Rudquist, and S. Lagerwall,
   Ferroelectrics, **315**, pp. 221-230 (2005)

3. *Generation of frustrated liquid crystal phases by mixing an achiral N–SmC mesogen with*
   an antiferroelectric chiral smectic liquid crystal
   J.P.F. Lagerwall, F. Giesselmann, C. Selbmann, S. Rauch, and G. Heppke, *J. Chem. Phys.*,
   122, *14*, 144906 (2005)

4. *Frustration between syn- and anticlinicity in mixtures of*
   chiral and non-chiral tilted smectic-C-type liquid crystals
   J.P.F. Lagerwall, G. Heppke, and F. Giesselmann, *Eur. Phys. J. E*, **18**, *1*, pp. 113-121
   (2005)

5. *Demonstration of the antiferroelectric aspect of the*
   helical superstructures in SmC^*, SmC_α^* and SmC_a^* liquid crystals
   J.P.F. Lagerwall, *Phys. Rev. E*, **71**, 051703 (2005)

6. *Current topics in smectic liquid crystal research* (Review article)
   J.P.F. Lagerwall, and F. Giesselmann, *ChemPhysChem*, **7**, *1*, pp. 20-45 (2006)

7. *On the change in helix handedness at transitions between the*
   $Sm-C^*$ and $Sm-C_a^*$ phases in chiral smectic liquid crystals
   J.P.F. Lagerwall, F. Giesselmann, and M.A. Osipov, *Liq. Cryst.*, **33**, *6*, pp. 625-633 (2006)

8. *Antiferroelectric liquid crystals with induced intermediate polar phases*
   and the effects of doping with carbon nanotubes

J.P.F. Lagerwall, R. Dabrowski, and G. Scalia, *J. Non-Cryst. Solids*, **353**, *47-51*, pp. 4411-4417 (2007)

9. *On the balance between syn- and anticlinicity in smectic phases*
   formed by achiral hockey-stick mesogens with and without chiral dopants
   E. Enz, S. Findeisen-Tandel, R. Dabrowski, F. Giesselmann, W. Weissflog, U. Baumeister, and J. Lagerwall, *J. Mater. Chem.*, **19**, *19*, pp. 2950-2957 (2009)

Papers related to Chapter 3

In chronological order:

10. *Coaxial electrospinning of microfibres with liquid crystal in the core*
    J.P.F. Lagerwall, J.T. McCann, E. Formo, G. Scalia, and Y. Xia, *Chem. Commun.*, *42*, pp. 5420-5422 (2008)

11. *Coaxial electrospinning of liquid crystal-containing poly(vinyl pyrrolidone) microfibers*
    E. Enz, U. Baumeister, and J. Lagerwall, *Beilstein J. Org. Chem.*, **5**, *58*, doi: 10.3762/bjoc.5.58 (2009)

Papers related to Chapter 4

In chronological order:

12. *Simultaneous alignment and dispersion of carbon nanotubes with lyotropic liquid crystals*
    J.P.F. Lagerwall, G. Scalia, M. Haluska, U. Dettlaff-Weglikowska, S. Roth, and F. Giesselmann, *Phys. Stat. Sol. (b)*, **243**, *13*, pp. 3046-3049 (2006)

13. *Nanotube alignment using lyotropic liquid crystals*
    J.P.F. Lagerwall, G. Scalia, M. Haluska, U. Dettlaff-Weglikowska, S. Roth, and F. Giesselmann, *Adv. Mater.*, **19**, *3*, pp. 359-364 (2007)

14. *Spontaneous macroscopic carbon nanotube alignment via colloidal suspension in hexagonal columnar lyotropic liquid crystals*
    G. Scalia, C. von Bühler, C. Hägele, S. Roth, F. Giesselmann, and J.P.F. Lagerwall, *Soft Matter*, **4**, *3*, pp. 570-576 (2008)

15. *Carbon nanotubes in liquid crystals* (Feature article)
    J.P.F. Lagerwall, and G. Scalia, *J. Mater. Chem.*, **18**, *25*, pp. 2890-2898 (2008)

16. *Macroscopic-scale carbon nanotube alignment via self-assembly in lyotropic liquid crystals*
    S. Schymura, E. Enz, S. Roth, G. Scalia, and J.P.F. Lagerwall, *Synth. Met.*, **159**, pp. 2177-2179 (2009)

Condensed Curriculum Vitae

Name[1]	Jan Peter Felix Lagerwall
Address	Robert-Franz-Ring 7, 06108 Halle, Germany
Date of birth	28. May 1970
Place of birth	Göteborg, Sweden
Marital status	Married

04/2010	Application for the opening of the habilitation process at the Martin-Luther-Universität Halle-Wittenberg, Naturwissenschaftliche Fakultät II
Since 09/2007	Junior research group leader, Institute of Chemistry - Physical Chemistry, Martin Luther University Halle-Wittenberg
05.04.2007	Awarded the Docent title at Chalmers University of Technology, Department of Physics, Göteborg, Sweden
07/2003 - 08/2007	Post-doctoral researcher at Universität Stuttgart, Germany, Institute of Physical Chemistry (funded by scholarships from the Alexander von Humboldt Foundation and the Knut & Alice Wallenbergs Stiftelse)
01-05/2003	Post-doctoral researcher at Technische Universität Berlin, Germany, Institute of Physical and Theoretical Chemistry
10-12/2002	Post-doctoral researcher at University of Colorado at Boulder, USA, Physics department
10/1997 - 05/2002	Graduate education, Chalmers University of Technology, Göteborg, Sweden, Department of Physics. Ph.D. Thesis (08.05.2002): *Structures and Properties of the Chiral Smectic C Liquid Crystal Phases—Ferro- and Antiferroelectricity in Soft Matter* Lic. Thesis (18.02.2000): *Phase Characterization of Polar Liquid Crystals Using Dielectric Spectroscopy*
09/1994 - 06/1995	Courses at humanistic faculties (philosophy, religion and history of economics), Göteborgs universitet, Sweden
09/1991 - 04/1997	Undergraduate education in engineering physics, Chalmers University of Technology, Göteborg, Sweden

---

[1]Note that the Dr. title is not part of the name for Swedish citizens.

Erklärung

Hiermit erkläre ich an Eides statt, dass ich die vorliegende Arbeit selbständig und ohne fremde Hilfe verfasst, andere als die angegebenen Quellen und Hilfsmittel nicht benutzt und die den benutzten Werken wörtlich oder inhaltlich entnommenen Stellen als solche kenntlich gemacht wurden.

Die Arbeit wurde nur an der Naturwissenschaftlichen Fakultät II der Martin-Luther-Universität Halle-Wittenberg vorgelegt.

Jan Lagerwall

Halle (Saale), im April 2010